Scattering Amplitude Calculations at Two Loops

Dhimiter D. Canko

This dissertation is submitted for the degree of
Doctor of Philosophy

Athens 2024

PhD Advisory Committee:

- Costas G. Papadopoulos (Supervisor) – Researcher A', NCSR "Demokritos"

- Nikolaos Tetradis – Professor, NKUA

- Vassilis C. Spanos – Associate Professor, NKUA

NATIONAL AND KAPODISTRIAN UNIVERSITY OF ATHENS
DEPARTMENT OF PHYSICS
NUCLEAR AND PARTICLE PHYSICS SECTION
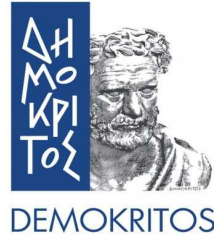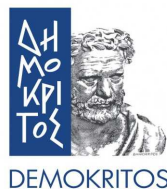
NATIONAL CENTER FOR SCIENTIFIC RESEARCH "DEMOKRITOS"
INSTITUTE OF NUCLEAR AND PARTICLE PHYSICS

Scattering Amplitude Calculations at Two Loops

Dhimiter D. Canko

This dissertation is submitted for the degree of *Doctor of Philosophy*

Athens 2024

PhD Advisory Committee:

- Costas G. Papadopoulos (Supervisor) – Researcher A', NCSR "Demokritos"

- Nikolaos Tetradis – Professor, NKUA

- Vassilis C. Spanos – Associate Professor, NKUA

PhD Defence Committee:

- Costas G. Papadopoulos (Supervisor) – Researcher A', NCSR "Demokritos"

- Nikolaos Tetradis – Professor, NKUA

- Vassilis C. Spanos – Associate Professor, NKUA

- Fotios Diakonos – Professor, NKUA

- Ioannis Papadimitriou – Assistant Professor, NKUA

- Tiziano Peraro – Associate Professor, UniBo

- Lorenzo Tancredi – Assistant Professor, TUM

Dedicated to my family

Abstract

Despite the groundbreaking discovery of Higgs boson and the thus far successful interpretation of experimental data received by the Large Hadron Collider (LHC) at Cern, the Standard Model of Particle Physics (SM) still remains inadequate in providing a compelling explanation for various cosmological and not only issues, such as the origin of dark matter, dark energy, matter-antimatter asymmetry, and the incorporation of Quantum Gravity and neutrino oscillations. These challenges indicate that SM shall be considered as an effective theory valid at low energies and underscore the importance of extending it. To gain insights into what lies beyond SM we need to push its limits and explore potential inconsistencies with highly accurate experimental data obtained from the high luminosity LHC and upcoming colliders. Hence, it has become essential to generate theoretical predictions with equally high precision for multi-particle scattering processes, especially those involving Quantum Chromodynamics (QCD). These theoretical predictions are conducted within the framework of perturbative Quantum Field Theory, wherein the scattering cross section is computed through a series expansion based on the coupling constants of the relevant theory. The initial term of this expansion represents the leading-order prediction (LO), followed by the subsequent next-to-leading-order (NLO) prediction, further extended to the next-to-next-to-leading-order (NNLO) prediction, continued by the next-to-next-to-next-to-leading-order (N3LO) prediction, and so forth.

Currently, the forefront of these computations reaches NNLO for processes involving five particles and N3LO for those involving four particles. Within this thesis we tackle these two frontiers in a two-fold manner. Concerning the NNLO computations, we upgrade the `HELAC` framework so that to be able to construct generic two-loop QCD scattering amplitudes using a mixed approach between Dyson-Schwinger recursion and Feynman graphs generation. Regarding the N3LO corrections, we compute all the three-loop $2 \to 2$ planar Feynman integral families (plus some non-planar ones) with massless internal propagators and one massive external particle, relevant to processes like $e^+e^- \to \gamma^* \to 3$ jets, $pp \to Z+$ jet and $pp \to H+$ jet. Both our approaches contribute to the virtual part of the corrections.

The structure of this thesis is divided into two main parts. The first part, consisting of the first three chapters, represents a brief introduction to the currently employed techniques and methods for the production of precise theoretical predictions for collider physics phenomenology. More specifically, the first chapter of this part serves as an introduction to fundamental aspects of SM and QCD, delving into how theoretical estimations are crafted for cross sections predicted from collision experiments. The second chapter is dedicated to multi-loop scattering amplitudes discussing their basic properties, such as unitarity cuts and integration-by-parts identities, their construction at Tree-level and One-loop using the recursive approach implemented in `HELAC`, and their computation, focusing on the one-loop amplitude reduction paradigm, especially the Ossola-Papadopoulos-Pittau (OPP) method, which resulted in the automation of NLO computations. The third chapter delves into the concept of Feynman Integrals, examining their characteristics and parametric representations, while also introducing the main technique currently utilized for their computation, meaning the method of differential equations and a variant of it, the simplified differential equations approach.

In the second part, consisting of the forth and fifth chapters, we present in detail our results for the `HELAC` two-loop upgrade and the computation of the three-loop 4-point Feynman integral families. Particularly, in the fourth we outline the algorithm for the construction of two-loop scattering amplitudes encoded in `HELAC-2LOOP`, providing a comprehensive rationale for each procedural aspect, and using as illustration a schematic example of a two-loop contribution to the scattering amplitude of the process $gg \rightarrow gg$. Furthermore, results concerning the construction of two-loop scattering amplitudes for various processes are presented and discussed. In the fifth chapter we provide details for the analytic computation in terms of real-valued multiple poly-logarithm (for both Euclidean and physical kinematics) of the ladder-box and the two tennis-court Feynman integral families, crucial for leading color $2 \rightarrow 2$ scattering processes involving one massive external particle and massless particles circulating in the loops, using the simplified differential equations approach. Moreover, we present also the analytic computation of two non-planar families relevant for the same scattering process but for full-color predictions, employing the standard differential equation method. Finally, in the last chapter we conclude, discussing on the importance of our results and possible extensions and next steps on the same direction.

Acknowledgements

First and foremost, I would like to express my deepest gratitude to my supervisor, Dr. Costas Papadopoulos, for his guidance, expertise, and unwavering support throughout my Ph.D. journey. His mentorship and encouragement have been instrumental in shaping my research and academic development. I am truly grateful for introducing me to the exciting topic of particle physics phenomenology, and for giving me the opportunity to interact with the international scientific community through conferences, schools, workshops, and collaborations.

I am immensely grateful to my colleague and friend Dr. Nikolaos Syrrakos for his valuable professional collaboration on numerous projects and for fruitful discussions concerning physics and not only, which significantly enhanced my overall Ph.D. experience, making it more enjoyable and fulfilling. Furthermore, I would like to especially thank my collaborators and friends, Dr. Giuseppe Bevilacqua and Dr. Aris Spourdalakis, for very insightful discussions concerning physics, programming, and other topics. Additionally, I wish to thank Dr. Ioannis Gialamas, Prof. Adam Kardos, Dr. George Kodaxis, Dr. Vasily Sotnikov and Prof. Lorenzo Tancredi for our very nice collaboration and communication during the last few years.

I'm most grateful to Prof. Tiziano Peraro who give me the opportunity to continue my scientific journey within his group, and for steadfast support and understanding as I embarked on the postdoc journey while concurrently completing my PhD. Moreover, I am thankful to my new colleagues in Bologna, Dr. Matteo Becchetti, Dr. Vsevolod Chestnov and Mattia Pozzolli, for their support, friendship and enjoyable collaboration, during the last months of my Ph.D..

Moreover, I would like to extend my heartfelt appreciation to my professors at the National and Kapodistrian Univesity of Athens (NKUA), standing out Prof. Nikolaos Tetradis (my BSc and MSc thesis advisor), Prof. Vassilis Spanos, Prof. Athanasios Lahanas, Prof. Fotios Diakonos, Prof. George Diamandis, Prof. Alexandros Karanikas, Prof. Theodosis Christodoulakis and Prof. Vassilis Georgalas, whose knowledge, expertise, and passion have greatly enriched my educational experience. Their teaching of several topics of theoretical and mathematical physics has inspired me to strive for intellectual growth and pursue new avenues of knowledge through conducting research in theoretical particle physics. I would like to especially thank the members of the Ph.D. advisory committee from NKUA, meaning Prof. Vassilis Spanos and Prof. Nikolaos Tetradis, for their kind assistance and support whenever I needed them.

I would like to express my gratitude to my dear friends (Anastasia, Aris, Aristides, Costas, Dimitris, Dimitra, Elisavet, Entzy, Eugenia, Giannis, Gilho, Giorgos, Marialena, Nina, Panos, Panagiotis, and Vasilis) for their unwavering support, understanding, and encouragement. Their companionship, shared experiences, and intellectual discussions have provided solace and inspiration during the challenging phases of my research. Their friendship has enriched my life in countless ways, and I am grateful for their presence in my academic journey.

Last but not least, my heartfelt thanks go to my parents, Dhimiter and Blerta, and my beloved twin brother, Aleksander, for their unconditional love, endless support and continuous encouragement. I am grateful for their sacrifices, unwavering belief in me, and understanding throughout my academic journey. They have been the foundation of my achievements and without them nothing would have been possible.

x

Contents

Preface

This thesis gathers some of the main results I have obtained during my Ph.D. studies, for the *Doctorate Degree in Physical Sciences*, from July 2018 to May 2024. These studies have been performed at the National Center of Scientific Research "Demokritos" and the National and Kapodistrian University of Athens, under the supervision of Dr. Costas. G. Papadopoulos.

The thesis is organized as follows:

- Chapter 1 serves as an introduction to the Standard Model of Particle Physics and the theoretical framework (Quantum ChromoDynamics) for the estimation of observable quantities derived from collision experiments.

- Chapter 2 provides a concise overview of the concept of multi-loop scattering amplitudes and the methodologies employed for their calculation.

- Chapter 3 delves into an exploration of Feynman integrals, examining their underlying significance, identities, and computation methods.

- Chapter 4, based on the conference proceedings [1–3], gives a comprehensive presentation of the algorithm used for the construction of two-loop scattering amplitudes by `HELAC-2LOOP`, an in-development package aiming at the automation of two-loop scattering amplitude calculations.

- Chapter 5, based on the articles [4–7], presents the analytical computation of the three ladder-box (one planar and two non-planar) and two tennis-court Feynman integral families, which are relevant for the computation of three-loop $2 \to 2$ scattering processes that involve one massive external particle and massless particles in the loops.

Additional papers and conference proceedings:

Over the past six years, I have been involved in various research projects, some of which led to the publication of the articles [8, 9]. However, as these projects did not align with the main focus of this thesis, they have not been included in the present work. Furthermore, I have presented part of my work related to this thesis at several international conferences, including the *XXVII Cracow Epiphany Conference, RADCOR–Loopfest-2021, HEP-2021, CORFU-2021, HP2-2022* and *RADCOR-2023*. As a result, the proceedings [1–3, 5, 10] based on these presentations have been published.

Author: Dhimiter D. Canko
Student ID: 2017540

Περίληψη

Παρά την ανακάλυψη του μποζονίου Higgs και τη μέχρι στιγμής επιτυχημένη επεξήγηση των πειραματικών δεδομένων που λαμβάνονται στον Large Hadron Collider (LHC) του CERN, το Καθιερωμένο Πρότυπο της Σωματιδιακής Φυσικής (ΚΠ) εξακολουθεί να είναι ανεπαρκές ως προς την παροχή μιας πειστικής ερμηνίας για διάφορα κοσμολογικά και όχι μόνο ζητήματα, όπως η προέλευση της σκοτεινής ύλης και της σκοτεινής ενέργειας, η ασυμμετρία μεταξύ ύλης και αντιύλης στο παρατηρούμενο σύμπαν, και η αδυναμία ενσωμάτωσης σε αυτό της Κβαντικής Βαρύτητας και των ταλαντώσεων των νετρίνων. Οι προκλήσεις αυτές υποδεικνύουν ότι το ΚΠ θα πρέπει να θεωρείται μια αποτελεσματική θεωρία η οποία ισχύει σε χαμηλές ενέργειες, και υπογραμμίζουν την αναγκαιότητα επέκτασής της. Για να αποκτήσουμε γνώσεις σχετικά με το τι βρίσκεται πέρα από το ΚΠ πρέπει να εξετάσουμε λεπτομερώς τα όριά της θεωρίας αυτής και να διερευνήσουμε πιθανές ασυνέπειες μεταξύ των θεωρητικών προβλέψεων της και τα πειραματικά δεδομένα υψηλής ακρίβειας που λαμβάνονται και θα ληφθούν από τον LHC υψηλής φωτεινότητας και μελλοντικούς επιταχυντές. Ως εκ τούτου, είναι απαραίτητο να πραγματοποιηθούν, στα πλαίσια του ΚΠ, θεωρητικές προβλέψεις υψηλής ακρίβεια για διάφορες διαδικασίες σκέδασης που περιλαμβάνουν πολλά σωματίδια, ιδίως για εκείνες στις οποίες υπερισχύει η επίδραση της Κβαντικής Χρωμοδυναμικής (QCD). Τέτοιου είδους προβλέψεις πραγματοποιούνται στο πλαίσιο της διαταρακτικής Κβαντικής Θεωρίας Πεδίου, όπου η ενεργός διατομή σκέδασης υπολογίζεται μέσω ενός αναπτύγματος ως προς τις σταθερές σύζευξης της σχετικής θεωρίας. Ο πρώτος όρος του αναπτύγματος αυτού αντιπροσωπεύει την πρόβλεψη πρώτης τάξης (LO), ακολουθούμενη από την πρόβλεψη δεύτερης τάξης (NLO), η οποία με την σειρά της ακολουθείται απο την πρόβλεψη τρίτης τάξης (NNLO), η οποία συνεχίζεται από την πρόβλεψη τέταρτης τάξης (N3LO), και ούτω καθεξής.

Επί του παρόντος, η αιχμή αυτών των υπολογισμών βρίσκεται στην NNLO τάξη για διεργασίες σκέδασης που περιλαμβάνουν πέντε σωματίδια, και στην N3LO τάξη για εκείνες που περιλαμβάνουν τέσσερα σωματίδια. Στο πλαίσιο αυτής της διατριβής αντιμετωπίζουμε αυτά τα δύο προβλήματα αιχμής με διττό τρόπο. Όσον αφορά τους υπολογισμούς NNLO τάξης, αναβαθμίζουμε το πακέτο HELAC έτσι ώστε να κατασκευάζει πλάτη σκέδασης δύο βρόχων για QCD διεργασίες, χρησιμοποιώντας μια μικτή προσέγγιση μεταξύ Dyson-Schwinger αναδρομής και δημιουργίας γραφημάτων Feynman. Όσον αφορά τις N3LO διορθώσεις, υπολογίζουμε όλες τις οικογένειες επίπεδων ολοκληρωμάτων Feynman τριών βρόχων (καθώς και μερικές μη επίπεδες οικογένειες) για $2 \rightarrow 2$ διαδικασίες σκέδασης με άμαζους εσωτερικούς διαδότες στους βρόχους και ένα έμμαζο εξωτερικό σωματίδιο. Τα ολοκληρώματα αυτά είναι απαραίτητα για την μελέτη διεργασίων όπως οι $e^+ e^- \rightarrow \gamma^* \rightarrow 3\,\text{jets}$, $pp \rightarrow Z + \text{jet}$ και $pp \rightarrow H + \text{jet}$. Και τα δύο αποτελέσματά μας συνεισφέρουν στο εικονικό (virtual) μέρος των διορθώσεων.

Η δομή της παρούσας διατριβής χωρίζεται σε δύο κύρια μέρη. Το πρώτο μέρος, που συγκροτείται απο τα τρία πρώτα κεφάλαια, αποτελεί μια σύντομη εισαγωγή στις τεχνικές και τις μεθόδους που χρησιμοποιούνται σήμερα για την παραγωγή υψηλής ακρίβειας θεωρητικών προβλέψεων για φαινομενολογία σχετιζόμενη με τους επιταχυντές σωματιδίων.

Πιο συγκεκριμένα, το πρώτο κεφάλαιο αυτού του μέρους χρησιμεύει ως μια εισαγωγή σε θεμελιώδεις πτυχές του ΚΠ και της QCD, εμβαθύνοντας στον τρόπο με τον οποίο δημιουργούνται θεωρητικές εκτιμήσεις για τις ενεργές διατομές που μετρούνται από τα σύγχρονα πειράματα σύγκρουσης σωματιδίων. Το δεύτερο κεφάλαιο είναι αφιερωμένο στα πλάτη σκέδασης πολλαπλών βρόχων, συζητώντας τις βασικές ιδιότητές τους, όπως τα unitarity cuts και οι ταυτότητες που προκύπτουν από κατά παράγοντες ολοκλήρωσης, την κατασκευή τους σε επίπεδο δέντρου και ενός βρόχου χρησιμοποιώντας την αναδρομική προσέγγιση που εφαρμόζεται στο HELAC, και τον υπολογισμό τους, εστιάζοντας στο παράδειγμα της αναγωγής του πλάτους σκέδασης ενός βρόχου σε βασικά ολοκληρώματα στο integrand level, και ειδικότερα στη μέθοδο Ossola-Papadopoulos-Pittau (OPP), η οποία οδήγησε στην αυτοματοποίηση των NLO υπολογισμών. Το τρίτο κεφάλαιο εμβαθύνει στην έννοια των ολοκληρωμάτων Feynman, εξετάζοντας τα χαρακτηριστικά τους και τις παραμετρικές αναπαραστάσεις τους, ενώ παράλληλα παρουσιάζει την κύρια τεχνική που χρησιμοποιείται σήμερα για τον υπολογισμό τους, δηλαδή τη μέθοδο των διαφορικών εξισώσεων, καθώς και μια παραλλαγή της, την προσέγγιση των απλοποιημένων διαφορικών εξισώσεων (SDE approach).

Στο δεύτερο μέρος, που αποτελείται από το τέταρτο και το πέμπτο κεφάλαιο, παρουσιάζουμε λεπτομερώς τα αποτελέσματά μας για την αναβάθμιση του HELAC και τον υπολογισμό των οικογενειών ολοκληρωμάτων Feynman τριών βρόχων και με τέσσερα εξωτερικά σωματίδια. Ειδικότερα, στο τέταρτο κεφάλαιο περιγράφουμε τον αλγόριθμο για την κατασκευή των πλατών σκέδασης δύο βρόχων που είναι κωδικοποιημένος στο πακέτο HELAC-2LOOP, παρέχοντας μια περιεκτική αιτιολόγηση για κάθε αλγοριθμική πτυχή, και χρησιμοποιώντας για καλύτερη κατανόηση ένα σχηματικό παράδειγμα μιας συνεισφοράς δύο βρόχων στο πλάτος σκέδασης της διαδικασίας $gg \rightarrow gg$. Επιπλέον, παρουσιάζονται και συζητούνται αποτελέσματα σχετικά με την κατασκευή πλατών σκέδασης δύο βρόχων για διάφορες διεργασίες. Προχωρώντας στο πέμπτο κεφάλαιο, παρέχουμε λεπτομέρειες για τον αναλυτικό υπολογισμό σε όρους real-valued πολλαπλών πολυλογαρίθμων (τόσο για την ευκλείδεια όσο και για τη φυσική κινηματική του προβήματος σκέδασης τεσσάρων σωματιδίων, ένα εκ' των όποιων είναι έμμαζο) των οικογενειών ολοκληρωμάτων Feynman, ladder-box και (δυο) tennis-courts, οι οποίες συνεισφέρουν στις leading color $2 \rightarrow 2$ διεργασίες σκέδασης που περιλαμβάνουν ένα έμμαζο εξωτερικό σωματίδιο και άμαζα σωματίδια στους βρόχους, χρησιμοποιώντας την προσέγγιση των απλοποιημένων διαφορικών εξισώσεων. Επιπλέον, παρουσιάζουμε τον αναλυτικό υπολογισμό δύο μη επίπεδων οικογενειών που σχετίζονται με την ίδια διαδικασία σκέδασης, αλλά για προβλέψεις πλήρους χρώματος (full color), χρησιμοποιώντας την τυπική μέθοδο διαφορικών εξισώσεων. Τέλος, στο τελευταίο κεφάλαιο συζητάμε τη σημασία των αποτελεσμάτων μας, τις πιθανές επεκτάσεις και τα επόμενα βήματα που μπορούν να ακολουθηθούν προς την ίδια κατεύθυνση.

Chapter 1

Standard Model and Observables

In this chapter, we introduce some basic concepts of the Standard Model of Particle Physics, focusing on Quantum ChromoDynamics, and we describe how theoretical estimations can be made for observable quantities obtained from collision experiments, such as the Large Hadron Collider at CERN. This chapter is based on standard Quantum Field Theory and Standard Model textbooks and reviews [11–17], and we refer therein for more details.

1.1   Introduction to Standard Model

Particle physics serves as the fundamental cornerstone of our understanding of the universe, aiming to unravel the enigmas surrounding elementary particles and their interactions. Nowadays, our best understanding of nature's fundamental elements and interactions comes from the *Standard Model of Particle Physics* (SM), successfully describing three (*Electromagnetic*, *Weak*, and *Strong*) of the total four fundamental forces[1]. SM is a quantum field theory where the elementary particles arise from the quantization of their respective fields, and its dynamics are described by a Lagrangian density obeying the gauge symmetry groups

$$SU(3)_C \times U(1)_Y \times SU(2)_L \xrightarrow{\text{EW Symmetry Breaking}} SU(3)_C \times U(1)_Q,$$

where the subscripts C, Y, L, and Q refer to color, hypercharge, left-handed chirality, and electric charge. $SU(3)_C$ is the color symmetry of *Quantum ChromoDynamics* (QCD) and is realized as an exact symmetry of nature. $U(1)_Y \times SU(2)_L$ is linked to the theory of Electroweak (EW) interactions and is spontaneously broken, via the Higgs mechanism, to $U(1)_Q$ which describes the Weak and Electromagnetic interactions we observe today, through *Quantum ElectroDynamics* (QED). The Electroweak symmetry breaking occurs after the Big Bang when the universe cools down and the Higgs boson acquires a non-zero vacuum expectation value. This mechanism is of high importance as it maintains the gauge invariance of the SM Lagrangian density while at the same time generating masses for the massive particles of SM. The fundamental particle content of SM consists of: 1) the *interacting matter*, formed by twelve fermionic particles (bearing spin 1/2) accompanied by their anti-particles, 2) the *mediators of forces*, composed of four bosonic (bearing spin 1) particles, and 3) the scalar (spinless) *Higgs boson*, H.

---

[1]The quantization and incorporation of *Gravity* within the SM is an open question, while a plethora of gravitational phenomena is described through a geometrical interpretation of Gravity, the *General Relativity*.

Flavor	*Charge*	*Mass*	$2I_3$	C	S	T	B	Y_W	I_W^3
u (u_L, u_R)	$+2/3$	$2.16^{+0.49}_{-0.26}$ MeV	1	0	0	0	0	$(1/3, 4/3)$	$(1/2, 0)$
d (d_L, d_R)	$-1/3$	$4.67^{+0.48}_{-0.17}$ MeV	-1	0	0	0	0	$(1/3, -2/3)$	$(-1/2, 0)$
c (c_L, c_R)	$+2/3$	1.27 ± 0.02 GeV	0	1	0	0	0	$(1/3, 4/3)$	$(1/2, 0)$
s (s_L, s_R)	$-1/3$	$93.4^{+8.6}_{-3.4}$ MeV	0	0	-1	0	0	$(1/3, -2/3)$	$(-1/2, 0)$
t (t_L, t_R)	$+2/3$	172.69 ± 0.3 GeV	0	0	0	1	0	$(1/3, 4/3)$	$(1/2, 0)$
b (b_L, b_R)	$-1/3$	$4.18^{+0.03}_{-0.02}$ GeV	0	0	0	0	-1	$(1/3, -2/3)$	$(-1/2, 0)$

Table 1.1: SM quarks. Charges are proportional to positron's charge.

The fermionic constituents of matter are separated into six *quarks* and six *leptons*, independently grouped into three generations according to their flavor[2]. The first generation of quarks contains *up* (*u*) and *down* (*d*) bearing *isospin* (I_3), the second consists of *charm* (*c*) and *strange* (*s*) carrying the quantum numbers of *charm* (*C*) and *strangeness* (*S*), respectively, and the third includes *top* (*t*) and *bottom* (*b*) bearing *bottomness* (*B*) and *topness* (*T*), respectively. The first generation of leptons contains *electron* (e^-) and its neutrino (ν_e), the second consists of *muon* (μ) and its neutrino ν_μ, and the third includes *tau* (τ) and its neutrino (ν_τ). To each lepton type a lepton number (L_e, L_μ, L_τ) is associated. The anti-particles are denoted with an over-line, named inserting the prefix anti- to the name of the particle[3] and have the same quantum numbers but with opposite sign. In Tables 1.1 and 1.2 we quote the SM fermions (quarks and leptons, respectively) with their EW quantum numbers and masses. Therein, with I_W^3 we denote the third component of weak isospin ($SU(2)_L$ charge), and with Y_W the weak hypercharge defined via the relation

$$Q = I_W^3 + \frac{Y_W}{2}, \tag{1.1}$$

and choosen so that the electric charge (Q) to be in agreement with the experimental predictions. Concerning the mediators of forces, Strong interactions are induced by the massless *gluon* (*g*), Weak interactions by the massive $W^\pm$ and Z bosons, and Electormagnetic ones by the massless photon (γ). We collect these bosons and the Higgs one together with their EW quantum numbers and masses in Table 1.3.

Quarks carry mass, charge, flavor (weak charge), and color, interacting thus through Electroweak and Strong interactions. On the other side, leptons e^-, μ and τ, carry mass, charge, and flavor thus being "blind" to Strong interactions, while their neutrinos being massless[4] and neutral, interact only weakly. According to the classification of Eugene Wigner for the irreducible representations of the Poincare group [18], each spin 1/2 fermion comes in two different states of *chirality*, the *left-handed* (*L*) and the

---

[2]Experimentally the existence of three generations is well-proven but the reason why is still unknown.

[3]Except for electron's anti-particle, which is denoted as e^+ and is named positron.

[4]Although within the SM neutrinos can not acquire mass, the existence of neutrino oscillations foreshadow that they carry a small mass, the effect of which is insignificant for collider physics.

Flavor	*Charge*	*Mass*	L_e	L_μ	L_τ	Y_W	I_W^3
e (e_L, e_R)	-1	0.51099895 MeV	1	0	0	$(-1, -2)$	$(-1/2, 0)$
ν_e (ν_e^L)	0	< 225 eV	1	0	0	(-1)	$(1/2)$
μ (μ_L, μ_R)	-1	105.6583755 MeV	0	1	0	$(-1, -2)$	$(-1/2, 0)$
ν_μ (ν_μ^L)	0	< 0.19 MeV	0	1	0	(-1)	$(1/2)$
τ (τ_L, τ_R)	-1	1776.86 ± 0.12 MeV	0	0	1	$(-1, -2)$	$(-1/2, 0)$
ν_τ (ν_τ^L)	0	< 18.2 MeV	0	0	1	(-1)	$(1/2)$

Table 1.2: SM leptons. Charges are proportional to positron's charge and the error estimations for the masses of e and μ are $\pm 15 \times 10^{-11}$ and ± 0.0000023, respectively, not noted above for space convenience.

Flavor	*Charge*	*Mass*	Y_W	I_W^3
g	0	0	0	0
$W^\pm$	± 1	80.377 ± 0.012 GeV	0	± 1
Z	0	91.1876 ± 0.0021 GeV	0	0
γ	0	$< 10^{-18}$ eV	0	0
H	0	125.25 ± 0.17 GeV	1	$-1/2$

Table 1.3: SM bosons. Charges are proportional to positron's charge

right-handed (R). For massless fermions chirality coincides with *helicity*, defined as the projection of spin onto the direction of the momentum. The left-handed fermions transform as $SU(2)$ doublets

$$\begin{pmatrix} u_L \\ d_L \end{pmatrix}, \begin{pmatrix} c_L \\ s_L \end{pmatrix}, \begin{pmatrix} t_L \\ b_L \end{pmatrix}, \begin{pmatrix} e_L \\ \nu_e^L \end{pmatrix}, \begin{pmatrix} \mu_L \\ \nu_\mu^L \end{pmatrix}, \begin{pmatrix} \tau_L \\ \nu_\tau^L \end{pmatrix},$$

and the right-handed fermions as singlets. For neutrinos, it is assumed, and observed so far, that only left-handed chirality ones exist, along with right-handed anti-neutrinos. Massive spin 1 bosons, like $W^\pm$ and Z, come in three different polarization states (one longitudinal and two transverse), while massless gauge bosons, like gluon and photon, have only two polarization states (two transverse).

As interested in QCD perturbative corrections within this thesis, in the following we will focus on the Quantum Chromodynamics sector of the SM. For a complete discussion[5] of the Lagrangian density of the SM and its Feynman rules, we refer to the analytic source [19].

---

[5]Meaning, including the EW interactions.

1.2   Quantum Chromodynamics

1.2.1   Lagrangian and Feynman Rules

In SM the Strong interactions between quarks and gluons are described via a non-abelian gauge theory known as QCD[6]. QCD is obeying the $SU(N_c)$ symmetry group, with $N_c = 3$ being the number of colors (*red, green, blue*). This group contains $N_c^2 - 1 = 8$ generators, t_{ij}^a, being 3×3 traceless hermitian matrices. The indices enumerating the rows and columns of these matrices ($i, j = 1, ..., 3$) are called *fundamental indices*, while the indices enumerating the generators ($a = 1, ..., 8$) are referred to as *adjoint indices*. Gluons live in the adjoint representation of the symmetry group, having thus 8 colors, while quarks live in the fundamental, having thus 3 colors. The generators of $SU(N_c)$ satisfy the commutation relation

$$[t^a, t^b] = i f^{abc} t_c \Rightarrow f^{abc} = -\frac{i}{T_R} \mathrm{Tr}([t^a, t^b] t^c), \tag{1.2}$$

where f^{abc} are the fully anti-symmetric structure constants of $SU(N_c)$ and $\mathrm{Tr}(t^a t^b) = T_R \delta^{ab}$ with $T_R = 1/2$. Some useful relations for computing expressions containing products of t_{ij}^a matrices and f_{abc} constants, the so-called color algebra of $SU(N_c)$, are

$$\sum_{a=1}^{8} t_{ij}^a t_{kl}^a = T_R \left(\delta_{jk} \delta_{il} - \frac{1}{N_c} \delta_{ij} \delta_{kl} \right) \quad \text{(Fierz Identity)}, \tag{1.3}$$

$$\sum_{a=1}^{8} t_{ij}^a t_{jk}^a = \frac{N_c^2 - 1}{2 N_c} \delta_{ik}, \tag{1.4}$$

$$\sum_{c,d=1}^{8} f^{acd} f^{bcd} = N_c \delta^{ab}. \tag{1.5}$$

The Lagrangian density of QCD remains invariant under local gauge transformations of the form $U(x) = e^{i t^a \theta^a(x)}$, and is made up of three different terms

$$\mathcal{L}_{\text{QCD}} = \mathcal{L}_{\text{Classic}} + \mathcal{L}_{\text{GF}} + \mathcal{L}_{\text{Ghost}}. \tag{1.6}$$

The first term is the classical Lagrangian density consisting of a Yang-Mills and a fermionic part, while the other two terms are necessary for the proper quantization of the theory. Using the notation ψ_q^i ($\bar{\psi}_q^i = \gamma^0 \psi_q^{i\dagger}$) for the quark (anti-quark) field with flavor q and fundamental index i, and A_μ^a for the gluon gauge field with adjoint index a, $\mathcal{L}_{\text{Classic}}$ can be written in the following form

$$\mathcal{L}_{\text{Classic}} = -\frac{1}{4} F_{\mu\nu}^a F_a^{\mu\nu} + \sum_{q=1}^{N_f} \bar{\psi}_q^i (\slashed{D}_{ij} - \delta_{ij} m_q) \psi_q^j, \tag{1.7}$$

where m_q are the masses of the quarks induced by the Higgs mechanism and N_f ($N_f = 6$) the number of quark flavors. Usually in high-energy collisions, all the quarks are assumed to be massless, except for the top quark. Starting from Eq. (1.7) and

---

[6]The gauge charges are called colors and thus the underlying gauge theory is baptized Quantum ChromoDynamics.

applied as notation from here on, summation over dummy indices is assumed and Feynman's slash notation ($\gamma^\mu p_\mu = \not{p}$) is used, with γ^μ the Dirac gamma matrices. The field strength tensor, $F^\alpha_{\mu\nu}$, and the covariant derivative, D^μ_{ij}, are defined by the relations

$$F^a_{\mu\nu} = \partial_\mu A^a_\nu - \partial_\mu A^a_\nu + g_s f^{abc} A^b_\mu A^c_\nu, \tag{1.8}$$

$$D^\mu_{ij} = \delta_{ij}\partial^\mu - ig_s t^a_{ij} A^\mu_a, \tag{1.9}$$

with g_s the coupling constant of the strong interactions, which is often expressed in terms of the dimensionless parameter

$$a_s = \frac{g_s^2}{4\pi}. \tag{1.10}$$

The non-abelian group structure of $SU(N_c)$ results in the introduction of the last term in the definition of $F^a_{\mu\nu}$, which implies that gluons interact with themselves. The interactions between quarks and gluons show up from the second term of the covariant derivative.

The classical Lagrangian density contains degenerate field configurations which are equivalent up to gauge transformations, causing the construction of the gluon propagator impossible due to non-invertibility of the gluon field bilinear operator. This issue can be solved by following a gauge fixing procedure, which results in adding the last two terms of eq. (1.6) in $\mathcal{L}_{\text{Classic}}$ in order to allow for a consistent quantization of the theory. For the gauge fixing term, $\mathcal{L}_{\text{GF}}$, the most common choice (many gauge choices are possible) is a *covariant gauge* (R_ξ gauge) of the form

$$\mathcal{L}_{\text{GF}} = -\frac{1}{2\xi}(\partial_\mu A^\mu_a)(\partial^\nu A^a_\nu), \tag{1.11}$$

where ξ is an arbitrary parameter (*Lagrange multiplier*) the choice of which specifies the gauge fixing. The most typical choices for ξ are the *Feynman-'t Hooft gauge*, where $\xi = 1$, and the *Landau gauge*, where $\xi \to 0$. In the following chapters we will use the *Feynman-'t Hooft gauge*.

Although the gauge fixing allows for a proper definition of gluon propagator it comes with a price: it introduces unphysical degrees of freedom, by allowing the propagation of longitudinal and time-like polarization gluon states. These unwanted degrees of freedom are canceled by the Faddeev-Popov Lagrangian density [20]

$$\mathcal{L}_{\text{Ghost}} = (\partial^\mu \bar{c}_a)(\delta^{ab}\partial_\mu - g_s f^{abc} A^\mu_c)c_b, \tag{1.12}$$

which introduces ghost (c^a) and anti-ghost ($\bar{c}^a$) fields. Ghosts are colored (living in the adjoint representation) complex anti-commuting scalars, therefore violating the spin-statistics theorem. Being unphysical by construction, ghosts do not correspond to real particles and never appear as external states in scattering amplitudes, but only as virtual particles in closed loops.

Having all the pieces of the QCD Lagrangian density in place we can now read the QCD Feynman rules. From the bilinear terms we read the propagators and from the terms containing three or four fields (interactions) the vertices. We collect the QCD Feynman rules for propagators and vertices in Figure 1.1, using straight lines for quarks, curly lines for gluons, and dashed lines for ghosts. Supplementary to these

$$\mathcal{P} = \delta_{ji} \frac{i(\not{k} + m_q)}{k^2 - m_q^2 + i\epsilon}$$

$$\Pi_{\mu\nu} = i\delta_{ab} \left(\frac{-g_{\mu\nu}}{k^2 + i\epsilon} + (1 - \xi) \frac{k_\mu k_\nu}{(k^2 + i\epsilon)^2} \right)$$

$$\Pi = \frac{i\delta_{ab}}{k^2 + i\epsilon}$$

$$V_{ggg}^{\mu\nu\rho} = g_s f^{abc} \left[g^{\mu\nu}(p_1 - p_2)^\rho + g^{\nu\rho}(p_2 - p_3)^\mu + g^{\rho\mu}(p_3 - p_1)^\nu \right]$$

$$V_{gggg}^{\mu\nu\rho\sigma} = -ig_s^2 \left[f^{xab} f^{xcd}(g^{\mu\rho} g^{\nu\sigma} - g^{\mu\sigma} g^{\nu\rho}) \right.$$
$$+ f^{xac} f^{xdb}(g^{\mu\sigma} g^{\rho\nu} - g^{\mu\nu} g^{\rho\sigma})$$
$$\left. + f^{xad} f^{xbc}(g^{\mu\nu} g^{\rho\sigma} - g^{\mu\rho} g^{\nu\sigma}) \right]$$

$$V_{gq\bar{q}}^{\mu} = ig_s \gamma^\mu t_{ij}^a$$

$$V_{gc\bar{c}}^{\mu} = g_s f^{abc} p_1^\mu$$
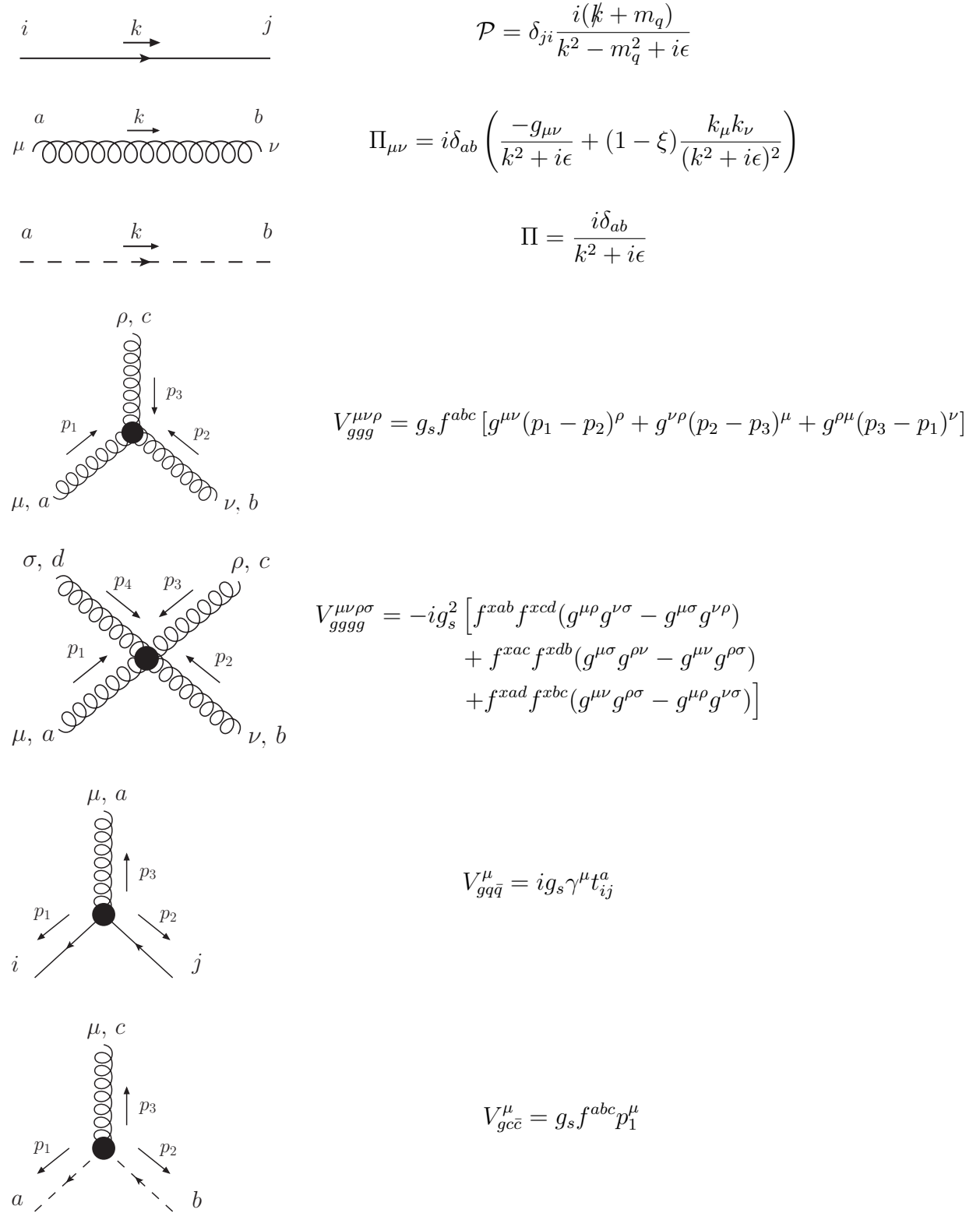
Figure 1.1: QCD Feyynman rules, in R_ξ gauge, for propagators and vertices. The $+i\epsilon$ prescription, introduced in the denominator of the propagators, is used to fix the contour over which the integration in the complex k_0 plane should be made. In all the vertices momentum conservation is implied, meaning that for the 3-vertices we have $p_1^\mu + p_2^\mu + p_3^\mu = 0$, and for the 4-vertex $p_1^\mu + p_2^\mu + p_3^\mu + p_4^\mu = 0$.

rules, for the computation of Feynman diagrams we need to apply also the following ones

- For each loop multiply with $d^d k/(2\pi)^d$ and integrate over the loop momentum k, where with d we represent the number of space-time dimensions. As we will discuss later, in general $d \neq 4$.

- Multiply with (-1) for each fermionic and ghost loop.

- Multiply each diagram with a symmetry factor that accounts for all equivalent permutations of internal or external legs.

and multiply with the wave functions (Dirac's spinor $u^\lambda(p)$ and $v^\lambda(p)$) or polarisation vectors ($\epsilon_\mu^\lambda(p)$) for incoming and outgoing particles

- Incoming quark (fermion): $u^\lambda(p)$.

- Outgoing quark (fermion): $\bar{u}^\lambda(p)$.

- Incoming anti-quark (anti-fermion): $\bar{v}^\lambda(p)$.

- Outgoing anti-quark (anti-fermion): $v^\lambda(p)$.

- Incoming gluon (or photon): $\epsilon_\mu^\lambda(p)$.

- Outgoing gluon (or photon): $\epsilon_\mu^\lambda(p)^*$.

where λ takes into account the chirality of fermions (anti-fermions) and the polarization of gluon (photon). Feynman rules are a powerful computational tool for theoretical calculation of observable quantities for collider physics as they are used for the construction of Feynman diagrams. The later are used for the computation of scattering amplitudes (matrix elements), which are equal to the sum over all the Feynman diagrams contributing to a process at hand.

1.2.2 Regularization and Renormalization

In QCD computations, tree-order calculations (where no loops at the loop momenta appear) of matrix elements are not accurate enough to match the experimental precision of current colliding experiments, thus the need for computing higher-order corrections containing loop integrals becomes apparent. However, the integration over the whole possible momentum space of the loop momenta gives rise to two kinds of divergences: the *Infra-Red* (IR) and *Ultra-Violet* (UV) divergences. IR divergences arise when the loop momentum becomes *soft* ($k^\mu \to 0$) or *collinear* to the momentum of an external massless particle, while UV ones show up in the large loop momentum region ($k^\mu \to \infty$). The fact that the observable quantities are finite means that these divergences cancel, leaving behind a finite part. In order to manipulate and cancel the divergences we need a regulator to quantify them.

While many different regularization schemes have been studied the most successful one seems to be *Dimensional Regularization* (DR) [21, 22], which regularizes both UV and IR divergences at the same time and preserves both Lorentz and gauge invariance. In DR, the divergences are regularized by analytically continuing the space-time

dimensions from 4 to $d = 4 - 2\varepsilon$, and appear in the limit $\varepsilon \to 0$ as poles in ε (the regulator of DR). The integration measure changes too in DR as

$$\int \prod_{i=1}^{L} \frac{d^4 k_i}{(2\pi)^4} \to \bar{\mu}^{(4-d)L} \int \prod_{i=1}^{L} \frac{d^d k_i}{(2\pi)^d} \, , \tag{1.13}$$

where L is the number of independent loop momenta, and $\bar{\mu}$ is an arbitrary mass scale introduced to preserve the dimensions of the coupling constants and the loop integral. The algebra is also extended to $d-$dimensions, implying for instance $\delta^{ij}\delta_{ij} = d$. The $d-$dimensional integrals behave identically to their 4-dimensional counterparts, thus fulfilling the standard laws (axioms) of integration [23]

$$1) \ \text{Linearity:} \int d^d k \, (a f(k) + b g(k)) = a \int d^d k \, f(k) + b \int d^d k \, g(k) \, ,$$

$$2) \ \text{Scaling:} \int d^d k \, f(\mu k) = \mu^{-d} \int d^d k \, f(k) \, , \tag{1.14}$$

$$3) \ \text{Translation Invariance:} \int d^d k \, f(k + p) = \int d^d k \, f(k) \, ,$$

and have the properties

$$1) \ \text{Interchange of Integrations:} \int d^d k_1 \int d^d k_2 \, f(k_1, k_2) = \int d^d k_2 \int d^d k_1 \, f(k_1, k_2) \, ,$$

$$2) \ \text{Scaleless Integrals Vanish:} \int d^d k \, \left(k^{-2}\right)^a = 0 \, , \tag{1.15}$$

$$3) \ \text{Total derivatives Vanish within Integrals:} \int d^d k \, \frac{\partial}{\partial k^\mu} f(k) = 0 \, .$$

The second property is derived from the second axiom. The third property can be considered as a consequence of translation invariance in $k-$space and as we will see in the next chapters it gives rise to a set of identities that is of high importance for phenomenological calculations. Having quantified UV and IR divergences we can see now how we can systematically remove them from theoretical computations of observables.

Concerning UV divergences, the cancellation is done following a so-called *Renormalization* procedure, where a redefinition in the parameters (fields, masses, coupling constants) of the Lagrangian density is applied. This is reasonable by realizing that the *bare* parameters, introduced to $\mathcal{L}_{\text{QCD}}$ in the previous subsection, do not directly correspond to physical parameters, due to loop corrections. Within a renormalization procedure, the *bare* parameters are rewritten in terms of *renormalized* ones as

$$m_q = Z_m m_q^r, \quad g_s = \mu^\varepsilon \sqrt{Z_g} g_s^r, \quad \psi = \sqrt{Z_\psi} \psi^r, \quad A_\mu^a = \sqrt{Z_A} A_\mu^{a,r}, \quad c_a = \sqrt{Z_c} c_a^r, \tag{1.16}$$

where $Z_i = 1 + \delta_i$ are *renormalization factors* containing a divergent part, δ_i, which is computed order by order in perturbation theory for sake of canceling the UV divergences at each order. Thus we have

$$\delta_i = \sum_{l=0}^{\infty} \left(\frac{a_s^r}{4\pi}\right)^l \delta_{i,l}, \tag{1.17}$$

with l the number of loops, $a_s^r = (g_s^r)^2/4\pi$, and $\delta_{i,0} = 0$, meaning that at the leading order, where no loops and UV divergences exist, the bare parameters correspond to the physical ones. The redefinition of the parameters of $\mathcal{L}_{\text{QCD}}$ results into a redefinition of $\mathcal{L}_{\text{QCD}}$ itself in the following way[7]

$$\mathcal{L}_{\text{QCD}}(g_s, m_q, \psi_q, A_\mu^a, c_a) \to \mathcal{L}_{\text{QCD}}(\mu, g_s^r, m_q^r, \psi_q^r, A_\mu^{a,r}, c_a^r) + \mathcal{L}_{CT}(\mu, \delta_i, \ldots, c_a^r). \quad (1.18)$$

The first term in the rhs of Eq. (1.18) is the same as the one in Eq. (1.6) with the only difference being that the bare parameters have been replaced by the renormalized ones. Thus the Feynman Rules read from this part are identical to the ones mentioned in the previous subsection[8]. The second term in the rhs of Eq. (1.18), $\mathcal{L}_{\text{CT}}$, contains new terms (consisting of the divergent parts δ_i) that cancel the UV divergences implied by the integration of the loop momenta. These terms are so-called *counter-terms* and generate additional Feynman rules, which depend on the order of perturbation theory.

In Eq. (1.16) beside the renormalization factors, we have also introduced an arbitrary mass scale, the renormalization scale μ, aiming to keep the strong coupling constant dimensionless. There is freedom in the definition of μ resulting in the existence of different *renormalization schemes*. The most famous one is the *modified minimal subtraction scheme* ($\overline{MS}$), in which μ is related to $\bar{\mu}$ of Eq. (1.13) via the relation

$$\mu^2 = 4\pi e^{-\gamma_E} \bar{\mu}^2, \quad (1.19)$$

with $\gamma_E = 0.5772156649$ the Euler-Mascheroni constant. At the end of the day, physical observables should not depend on the choice of the renormalization scheme. This is expressed via the *Renormalization Group Equations* (RGE) which relates the value of a parameter in a chosen renormalization scale with the value of the same parameter in another scale. The RGE of a_s^r leads to the so-called *running of the strong coupling*, expressed by the equation

$$\mu^2 \frac{\partial a_s^r}{\partial \mu^2} = \beta(a_s^r) = -\sum_{n=0}^{\infty} \left(\beta_n \frac{a_s^r}{4\pi}\right)^{n+2}, \quad (1.20)$$

where $\beta(a_s^r)$ is the QCD β-function, which is computed perturbatively on a_s^r and is known up to five loops (β_4) [24–28]. At one-loop the solution of (1.20) results to

$$a_s^r(\mu^2) = \frac{a_s^r(\mu_0^2)}{1 + \beta_0 a_s^r(\mu_0^2) \ln(\mu^2/\mu_0^2)} \quad \text{with} \quad \beta_0 = \frac{11 N_c - 2 n_f}{3}. \quad (1.21)$$

Here μ_0 is an initial renormalization scale, and β_0 is computed for the coupling of an effective theory in which n_f of the quark flavors are considered light ($m_q \ll \mu$) and the remaining heavier quark flavors decouple from the theory.

From Eq. (1.21) follows that for $n_f \leq 16$ ($N_C = 6$) the sign of β_0 is positive and therefore $a_s^r(\mu^2)$ decreases for large value of μ^2. This means that at large scales (high energies) QCD acts as a weak theory and quarks and gluons can be treated as if they were free particles, a phenomenon called *asymptotic freedom*, which has been

---

[7]The gauge fixing parameter, ξ, is also renormalized in terms of the renormalization factor of the gauge field, as $\xi = Z_A \xi^r$, in order for Eq. (1.11) to not produce counter-terms.

[8]Of course again the bare parameters should be replaced by the renormalized ones.
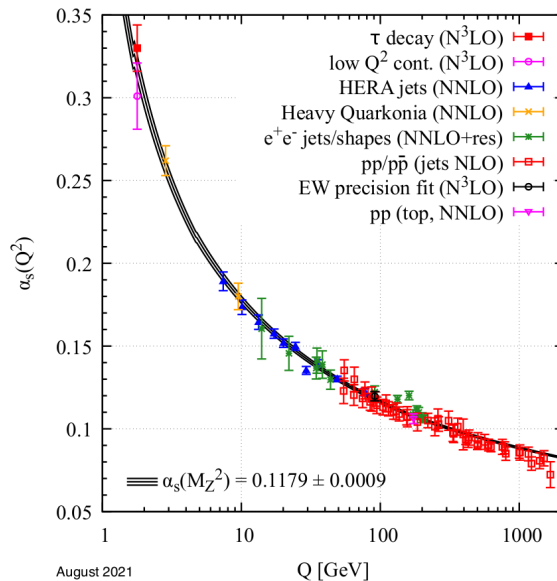
Figure 1.2: Running of the strong coupling as a function of the energy scale ($a_s(Q^2) \equiv a_s^r(\mu^2)$ and $Q \equiv \mu$). Colored error bars correspond to different experimental measurements, while the solid black line accounts for the theoretical prediction. The world average value for the strong coupling at the energy scale equal to the mass of Z boson is $a_s^r(M_Z^2) = 0,1179 \pm 0.0009$. Figure taken from [15].

confirmed experimentally[9] (see Figure 1.2). A consequence of asymptotic freedom is that at high energies QCD can be treated perturbatively using a_s^r as the expansion parameter, allowing for very accurate computations of scattering observables of QCD processes. This is not anymore the case at low energies ($\Lambda_{\text{QCD}} \approx 250$ MeV), where a_s^r becomes sufficiently large (stronger interaction) and the perturbative approach breaks. At these energies, quarks and gluons can not be observed as free particles but exist only as bound states in the form of colorless hadrons, a phenomenon called *color confinement*. Hadrons consist of mesons, composed of an equal number of valence quarks and anti-quarks, and baryons containing an odd number of valence quarks (at least three).

Regarding IR singularities, these have a different physical interpretation from the UV ones, and thus a different way of treatment. These are canceled at the level of physical observables thus we are going to discuss their resolution in the next section, after having introduced first the notion of cross sections.

1.3   Precision Calculations and Observables

Particle collisions form the main way of experimentally testing the validity of SM and exploring the physics beyond it. These are happening within huge circular infrastructures called *particle colliders*, where one or more beams of particles are accelerated in order to collide, resulting in a scattering event. The colliding particles must be charged, as they are accelerated through electromagnetic fields, each time they go around the

---

[9]Asymptotic freedom is a property of non-abelian field theories, QED is not asymptotically free.

cycle[10]. The outcome (particles) of a scattering event is recorded through detectors surrounding the collider, and through the application of 4-momentum conservation to find missing 4-momenta of weakly interacting particles (such as neutrinos) that can not be detected by the detector. The records of the scattering events are collected and analyzed by our experimental colleagues, resulting in scattering observables. The most robust and straightforward observable that can be measured by colliding experiments is the cross section.

1.3.1 Cross sections

The cross section is a quantity measuring the probability of a scattering event taking place, and depends on the properties of the colliding beams, meaning their particle content, size, and intensities. For the definition of the cross section, consider two colliding bunches of different types of particles, N_a and N_b, with a common transverse area, say A. Then the cross section of a particular scattering event is related to the above-stated quantities and the total number of times this event occurred, N_{event}, via the relation

$$\sigma \equiv \frac{A N_{\text{event}}}{N_a N_b}. \tag{1.22}$$

From Eq. (1.22) we understand that the unit of the cross section is m^2, but for historical reasons the barn ($1b = 10^{-28} m^2$) is used instead. In real-life experiments, we don't deal with the number of colliding particles and their common transverse area but with the flux of colliding beams. The properties of the flux, such as how the particles are distributed within the beams, are taken into account by the so-called luminosity, $L(t)$, which is an experimentally measurable quantity. In terms of luminosity, the cross section of a scattering event is computed via the formula

$$\sigma = \frac{N_{\text{event}}}{\int_0^T dt \, L(t)}, \tag{1.23}$$

where $\int_0^T dt \, L(t)$ is the *integrated luminosity* (measured in b^{-1}) and T the operation time of the collider. Another useful observable quantity is the *differential cross section* which gives information not only about the total number of scattering events but also about the scattering angle or the energy bin of the outgoing particles.

Cross sections can be computed theoretically within the context of Quantum Field Theory (QFT), a combination of Quantum Mechanics and Special Relativity. Within this framework, differential probabilities are given by the modulus squared of inner products of Hilbert states. Having this in mind and focusing on the scattering process, consider an incoming state described by two distinct wave packets of well-separated single-particle states, concentrated about the momenta p_1 and p_2, respectively, constructed in the remote past ($t_i \to -\infty$) and freely evolving since then. Let's denote this incoming state as $|i; t_i\rangle \equiv |p_1, p_2, Q_1, Q_2; t_i\rangle$, where Q_1 and Q_2 symbolize the quantum numbers that the two particles can bear, such as helicities. As time elapses the wave functions of these states overlap, and the particles start interacting and scatter into some final states. Assuming that the duration of the interaction is finite, in the

---

[10]Due to *synchroton radiation* ($\sim 1/r^2$) radiated by charged accelerated particles, modern colliders are constructed with a large circumference in order for the beam to reach high energies.

distant future $(t_f \rightarrow \infty)$ the final states will again be freely evolving wave packets of n single-particle states, let's denote them $\langle f; t_f| \equiv \langle p_3, ..., p_n, Q_3, ..., Q_n; t_f|$. The incoming and the final states are related via time translation and the overlap of the two states defines the *scattering matrix* ($S-$matrix)

$$\langle f| S |i\rangle = \lim_{\substack{t_i \rightarrow -\infty \\ t_f \rightarrow \infty}} \langle f; t_f| U(t_f, t_i) |i; t_i\rangle, \tag{1.24}$$

where $U(t_f, t_i)$ is the unitary time-evolution operator given in the *interaction picture*, by the expression

$$U(t_f, t_i) = \mathbb{T}\left[e^{\int_{t_i}^{t_f} dt H_I(t)}\right], \tag{1.25}$$

with H_I being the interaction part of the Hamiltonian describing the theory at hand, $H = H_0 + H_I$ (H_0 being the free field part), and $\mathbb{T}$ is the time-order operator.

In order to incorporate a non-interacting theory and the fact that even if the theory at hand contains interactions there is always a possibility that the incoming states simply miss one another, the $S-$matrix is rewritten in terms of the *transfer matrix* ($T-$matrix)

$$S = \mathbf{1} + iT, \tag{1.26}$$

which encodes the probability of a given state from the far past evolving into one other (different) state in the far future. By factoring out a δ function reflecting the 4-momentum conservation from the $T-$matrix we define the *scattering amplitude*

$$\langle f| iT |i\rangle = (2\pi)^4 \delta^{(4)}((p_1 + p_2 - \sum_{j=3}^{n} p_j) \times i\mathcal{M}(p_1, p_2 \rightarrow p_3, \ldots, p_n). \tag{1.27}$$

When the interaction Hamiltonian is small allowing for a perturbative expansion to be applied in Eq. (1.25), as is the case in QCD, the scattering amplitude $\mathcal{M}$ can be computed in perturbation theory using Feynman diagrams and Feynman rules, such as the ones we have seen in the previous section. From the scattering amplitude square, the cross section is computed using the relation

$$d\sigma = \frac{1}{4E_1 E_2 |u_1 - u_2|} d\Phi^{(n-2)} |\mathcal{M}(p_1, p_2 \rightarrow p_3, \ldots, p_n)|^2, \tag{1.28}$$

where $|u_1 - u_2|$ is the relative velocity of the colliding beams as viewed from the laboratory frame and

$$d\Phi^{(n-2)} = \prod_{j=3}^{n} \left(\frac{d^3 p_j}{(2\pi)^3} \frac{1}{2E_j}\right) (2\pi)^4 \delta^{(4)}((p_1 + p_2 - \sum_{j=3}^{n} p_j), \tag{1.29}$$

is the Lorentz invariant phase space of the final state particles. Above with E_j we denote the energy corresponding to the 4-momentum p_j^μ. Eq. (1.28) is the master formula for making theoretical predictions of cross sections when the colliding beams are constituted by elementary particles (such as $e^+ e^-$ collisions). If in the incoming states, we have composite objects such as hadrons, we need in addition to take into account information about their structure. This is the case of Large Hadron Collider (LHC), where the colliding beams consist of protons.

Having introduced the concept of cross section we can now discuss the remedy of IR divergences. In the previous section we saw that one source of IR singularities in perturbative computations is the integration over loop momenta that become soft or collinear to the momenta of massless external particles (virtual divergences), but it turns out this is not the only case. IR divergences also appear in cross sections due to the emission of additional unresolved particles (real-emission divergences), resulting from phase space integrations (Eq. (1.29)) over a soft or collinear region of the momenta of the additional particles. Within SM, the Kinoshita-Lee-Nauenberg (KLN) theorem [29, 30] ensures that real-emission and virtual IR divergences cancel each other leading to a finite result for the cross section, only after summing order by order in perturbation theory. Thus IR divergences arising from loop integrations are canceled from IR divergences arising from fewer loops but extra unresolved particles in the final state. From a physical standpoint, this means that a scattering process containing n particles cannot be distinguished from a process with $n + X$ particles where the X cannot be resolved, making sense also experimentally as the detectors cannot observe particles of very small momenta nor can distinguish particles radiated in the same direction, due to finite resolution.

1.3.2 Perturbative QCD

As already mentioned, Eq. (1.28) needs to be revised in order to describe scattering processes that include colliding hadrons. In order to make predictions about their interactions we need information about their elementary particle structure (long-range effect). According to the *QCD-improved parton model*, hadrons are composed of a cloud of partons (quarks and gluons) [31], where partons are constantly emitted and absorbed. In high-energy collisions of hadrons, the interactions and the scattering happens at the level of partons (short-range effect), which are carrying a fraction of hadron's momentum. At this scale, partons are asymptotically free, and the coupling constant is small enough so that the scattering amplitudes can be computed perturbatively.

A very important theorem that allows for the computation of QCD observables is the *factorization theorem* [32–34]. This theorem states that long-range and short-range effects can be separated at high energies[11], and the differential cross section for the scattering of two initial hadrons (h_1, h_2), with momenta (p_1, p_2) and center of mass energy $s = (p_1 + p_2)^2$, to some final state f is given by the expression

$$
\begin{aligned}
d\sigma_{h_1 h_2 \to f} = \sum_{i,j=q,\bar{q},g} \int_0^1 dx_1 \int_0^1 dx_2\, \mathcal{F}_{i/h_1}(x_1, \mu_F) \mathcal{F}_{j/h_2}(x_2, \mu_F)\, d\hat{\sigma}_{ij \to f} \\
+ \mathcal{O}\left(\Lambda_{\text{QCD}}/s\right),
\end{aligned}
\tag{1.30}
$$

where $\mathcal{F}_{i/h_1}$ and $\mathcal{F}_{j/h_2}$ are the *parton distribution functions* (PDFs) and $d\hat{\sigma}_{ij \to f}$ the *hard-scattering cross section* for the production of the final state f from the interaction of two partons i and j with momenta $x_1 p_1$ and $x_2 p_2$, respectively. PDFs encode the partonic composition of hadrons and can be interpreted as the number density of a specific type of parton (i) inside a fast-moving hadron (h_1), that carries a fraction (x_1) of hadron's momentum (p_1). They cannot be computed perturbatively and need to be extrapolated from experimental data, but since the structure of hadrons does not

---

[11]The interference terms are suppressed Λ_{QCD}.

depend on the considered process of an experiment, they are *universal*. This means that one can determine PDFs using data from a suitable process and then use them for making predictions for other processes.

Similarly to the parameters of the QCD Lagragnian density, the PDFs are also renormalized in terms of an factorization scale μ_F, in order to absorb divergences induced by soft and collinear emissions of partons in the initial state. The evolution of PDFs between different μ_F scales is obtained perturbatively by the (RGE-like) Dokshitzer-Gribov-Lipatov-Altarelli-Parisi (DGLAP) equations [35–37]. DGLAP equations are a $(2n_f + 1)-$dimensional matrix equation in the space of quarks, anti-quarks and gluons, and for the proton case they read

$$
\frac{\partial}{\partial \ln \mu_F^2} \begin{pmatrix} \mathcal{F}_{q_i}(x, \mu_F^2) \\ \mathcal{F}_g(x, \mu_F^2) \end{pmatrix} = \sum_{q_j, \bar{q}_j} \int_x^1 \frac{dz}{z} \begin{pmatrix} P_{q_i \to q_j}(z, a_s^r(\mu_F^2)) & P_{q_i \to g}(z, a_s^r(\mu_F^2)) \\ P_{g \to q_j}(z, a_s^r(\mu_F^2)) & P_{g \to g}(z, a_s^r(\mu_F^2)) \end{pmatrix} \begin{pmatrix} \mathcal{F}_{q_i}(x/z, \mu_F^2) \\ \mathcal{F}_g(x/z, \mu_F^2) \end{pmatrix},
$$

with $P_{i \to j}(z, a_s^r(\mu_F^2))$ being the splitting functions computed in a series expansion on $a_s^r(\mu_F^2)$

$$
P_{i \to j}(z, a_s^r(\mu_F^2)) = \sum_{i_1 = 1}^n \left(\frac{a_s^r(\mu_F^2)}{2\pi} \right)^{i_1} P_{i \to j}^{(i_1)}(z),
$$

and are known up to third order in the series expansion [38, 39].

The hard-scattering cross section $d\hat{\sigma}_{ij \to f} \equiv d\hat{\sigma}_{ij \to f}(x_1 p_1, x_2 p_2, \mu, \mu_F)$ depends both in the factorization scale μ_F and the renormalization scale μ, it is process dependent and it is thus considered the main ingredient for connecting experiments and theory. As already stated, $d\hat{\sigma}_{ij \to f}$ can be computed perturbatively within a series expansion in powers of a_s^R. Normalizing this expansion in terms of the powers of a_s^r of the first term of the expansion we have

$$
d\hat{\sigma}_{ij \to f} = d\hat{\sigma}_{ij \to f}^{\mathrm{LO}} + \left(\frac{a_s^r}{2\pi} \right) d\hat{\sigma}_{ij \to f}^{\mathrm{NLO}} + \left(\frac{a_s^r}{2\pi} \right)^2 d\hat{\sigma}_{ij \to f}^{\mathrm{NNLO}} + \left(\frac{a_s^r}{2\pi} \right)^3 d\hat{\sigma}_{ij \to f}^{\mathrm{N^3LO}} + \mathcal{O}\left((a_s^r)^4 \right), \quad (1.31)
$$

where LO stands for Leading Order, NLO for Next-to-Leading Order, NNLO for Next-to-Next-to-Leading Order and N³LO for Next-to-Next-to-Next-to-Leading Order. We have on purpose written the above expansion till N³LO because in the next chapters we will deal with QCD corrections up to this order. Let us mention here that if we could compute the pertutbative expansions on a_s^r to all-orders the scale dependence on μ and μ_F would vanish. But because this is not the case, usually, μ_F and μ are chosen so that $\mu_F = \mu = \mu_0$ or varied from $\mu_0/2$ to $2\mu_0$, where μ_0 is a chosen mass scale such as m_t, m_H, etc.

Focusing on the NNLO contribution to the hard-scattering cross section, in agreement with what we have seen in the previous subsection, this receives contributions from three different sources

1. The *virtual corrections*, which contain the interference term of two-loop Feynman graphs with tree-level ones and the one-loop squared Feynman graphs.

2. The *mixed real−virtual corrections*, which contain one-loop Feynman graphs with an extra particle, which can become unresolved.

3. The *doubly−real corrections*, which contain tree-level Feynman graphs with two extra particles, which can become unresolved.

Each of these contributions is individually divergent[12], and the divergences cancel in the sum leaving behind a finite result for the cross section

$$
\begin{aligned}
d\hat{\sigma}_{ij\to f}^{NNLO} \sim \int d\Phi^{(n)} \left|\mathcal{M}_{n+2}^{(0)}\right|^2 + 2\int d\Phi^{(n-1)}\mathrm{Re}\left[\mathcal{M}_{n+1}^{(1)}(\mathcal{M}_{n+1}^{(0)})^*\right] \\
+ \int d\Phi^{(n-2)} \left|\mathcal{M}_n^{(1)}\right|^2 + 2\int d\Phi^{(n-2)}\mathrm{Re}\left[\mathcal{M}_n^{(2)}(\mathcal{M}_n^{(0)})^*\right],
\end{aligned}
\tag{1.32}
$$

where $n-2$ is the number of particles in the final state f, and $\mathcal{M}_n^{(L)} \equiv \mathcal{M}^{(L)}(p_1, p_2 \to p_3, \ldots, p_n)$ is the $L-$loop and $n-$particle scattering amplitude. The approximate symbol is used above due to not including the energy and velocity terms of Eq. (1.28). Within this thesis we will focus on the construction and computation (at the integrand-level?) of the two-loop amplitude, $\mathcal{M}_n^{(2)}$, while we will also discuss the computation of three-loop Feynman integrals for relevant three-loop amplitudes.

We comment here that in order to make theoretical predictions for cross sections of processes containing partons in the hard-scattering final state, one needs to further take into account non-perturbative information about the evolution of these partons into physical states that are observable by the detector. The final state evolution contains of several process-independent ingredients (similarly to PDFs), such as the further emission of extra partons from the final state partons (*parton showers*), the combination of the partons into hadrons (*hadronization*) and the use of *jet algorithms*. Jets are collimated cones of hadrons (and other particles) produced by the hadronization of partons, and their accurate definition depends on the jet algorithm used for their identification from the signals of an event.

---

[12]Due to IR divergences, as the UV ones have been removed by renormalization.

Chapter 2

Scattering Amplitudes

In this chapter, we briefly discuss the procedure followed for the computation of scattering amplitudes. We start by stating some important properties of scattering amplitudes, continue with their recursive construction using Dyson-Schwinger equations, and finally close with the techniques that led to the automation of one-loop amplitude calculations and a quotation of the currently applied methods on the multi-loop frontier.

2.1   Introduction and Properties

Being the fundamental link between theoretical models and experimental observables, scattering amplitudes are at the core of phenomenological predictions. As already discussed in the previous chapter, scattering amplitudes are computed within a perturbative expansion around the coupling constants of the theory at hand. For the case of QCD, the expansion is done around the strong coupling constant, a_s^r

$$\mathcal{M}_n = (a_s^r)^t \sum_{l=0}^{L} (a_s^r)^l \, \mathcal{M}_n^{(l)}, \tag{2.1}$$

where n is the number of particles involved in the scattering, l is the order of the expansion, and t is the power of a_s^r at the leading order. At each order of the expansion, the scattering amplitude of a process at hand is equal to the sum of the Feynman graphs contributing to this process at the specific order. In the following, we will assume that l is equal to the number of loops, but this is not always the case[1]. Thus at the leading order the amplitude is equal to the sum of tree-level graphs, at NLO is equal to the sum of one-loop graphs, at NNLO is equal to the sum of two-loop graphs, and so on.

For avoiding redundant computations in QCD, it is convenient to apply a *color decomposition* in the scattering amplitudes. Any l-loop n-particle QCD scattering amplitude can be decomposed into a color factor and a kinematic-dependent part

$$\mathcal{M}_n^{(l)} = \sum_F c_F^{(l)} \mathcal{A}_{n,F}^{(l)} \tag{2.2}$$

where $c_F^{(l)}$ is the color factor of the color-stripped amplitude, $\mathcal{A}_{n,F}^{(l)}$, which can be constructed using color-stripped Feynman rules and contains information regarding kinematics. For the computation of color factors, there exist different *color representations*

---

[1]For processes where tree-level graphs do not exist, like the case of $gg \rightarrow HHH$, the leading order term corresponds to the sum of one-loop graphs.

(color basis) with the most famous one being the *fundamental representation*, where the color factors are expressed in terms of traces of the $SU(3)$ generators t_{ij}^a (see subsection 1.2.1) [40]. Within this thesis, we are going to use the *color-flow (color-connection) representation* [41–43], which we will present in Section 2.2.

A color-stripped l-loop scattering amplitude with n external particles can be written as[2]

$$\mathcal{A}_n^{(l)} = \int \left(\prod_{i=1}^{l} \frac{d^d k_i}{(2\pi)^d} \mu^{4-d} \right) A_n^{(l)}, \tag{2.3}$$

with $\{k\}$ being the loop momenta and $A_n^{(l)}$ being the amplitude integrand. In general, $A_n^{(l)}$ has the following form

$$A_n^{(l)} = \sum_{I \subseteq T} \frac{N_I\left(\{k\}, \{p\}, \gamma^\mu, \{\epsilon^\mu\}\right)}{\prod_{j \in I} D_j^{a_j}\left(\{k\}, \{p\}, m_j\right)}, \tag{2.4}$$

where T is the set containing all the l-loop graph topologies of the process at hand, N_I is the topology numerator depending on invariant contractions of gamma matrices, polarization vectors, and momenta (N_I is a scalar quantity), and $a_j > 0$ are integer exponents of the inverse loop propagators

$$D_j = q_j^2 - m_j^2 + i\epsilon, \tag{2.5}$$

with m_j being the masses of the virtual loop particles, $+i\epsilon$ being the usual prescription, and q_j being a combination from the set of loop and external ($\{p\}$) momenta

$$q_j = \sum_{i=1}^{l} b_i^{(j)} k_i + \sum_{i=1}^{n-1} b_i'^{(j)} p_i, \qquad \text{with} \qquad b_i^{(j)}, b_i'^{(j)} = 0, \pm 1. \tag{2.6}$$

The integrand numerators, as the inverse loop propagators, are polynomials in the components of the loop momenta. The d-dimensional loop momenta can be decomposed into a 4-dimensional ($\bar{k}_i$) and an ε-dimensional part (k_i^*)

$$k_i = \bar{k}_i + k_i^* \qquad \text{with} \qquad k_i \cdot k_j = \bar{k}_i \cdot \bar{k}_j + \mu_{ij}, \tag{2.7}$$

where $\mu_{ij} = \mu_{ji} = k_i^* \cdot k_j^*$. Therefore $A_n^{(l)}$ is a rational function of

$$n_l = 4l + \frac{l(l+1)}{2}, \tag{2.8}$$

independent loop coordinates, and can only depend on n_l loop scalar products (let's denote them $\{z_1, \ldots, z_{n_l}\}$)

$$
\begin{aligned}
&1) k_i \cdot k_j, &\rightarrow&\quad \#_z = l(l+1)/2 \\
&2) k_i \cdot p_j, &\rightarrow&\quad \#_z = \min[4, n-1] \times l \\
&3) k_i \cdot t_j, &\rightarrow&\quad \#_z = (4 - \min[4, n-1]) \times l
\end{aligned}
$$

---

[2]Here we concentrate on amplitudes containing loops. For tree-level amplitudes, there do not exist loop momenta and integrations over them. Hence the subsequent analysis does not concern them. From here on, we omit the index F for convenience.

where t_j are vectors orthogonal to the external momenta, meaning $p_i \cdot t_j = 0$, originating from polarization vectors. From the above expression, we see that for $n \geq 5$ we have $t_j = 0$, as expected since the external momenta span the 4-dimensional space. For a topology I with n_I propagators, n_I of the loop scalar products can be expressed as linear combinations of inverse propagators. These are called *reducible scalar products*, and if they appear in the numerator they can cancel propagators from the denominator resulting in topologies with fewer propagators. The rest of the loop scalar products that can not be written in terms of the propagators of the topology (being $n_{ir} = n_l - n_I$ in number) are called *irreducible scalar products*, let us denote them $\{\bar{z}_1^{(I)}, \ldots, \bar{z}_{n_{ir}}^{(I)}\}$. If $n_I > n_l$ then the propagators of the topology I are not independent and the topology is reducible to topologies with fewer propagators.

The observation above together with the constraint on the powers of loop momenta that we can have on the numerator of a topology (n_{th}^I), imposed by the UV structure of the theory at hand, indicates that the numerators can have the following form

$$N_I\left(\{k\}, \{p\}, \gamma^\mu, \{\epsilon^\mu\}\right) = \sum_{i_1, \ldots, i_{n_{ir}}=0}^{n_{th}^I} C_{i_1, \ldots, i_{n_{ir}}}^{(I)} \left(\bar{z}_1^{(I)}\right)^{i_1} \cdots \left(\bar{z}_{n_{ir}}^{(I)}\right)^{i_{n_{ir}}}, \qquad (2.9)$$

with the coefficients being rational functions of the dimensional regulator and the scalar products of external momenta, $C_{i_1, \ldots, i_{n_l}}^{(I)} \equiv C_{i_1, \ldots, i_{n_l}}^{(I)}\left(\{p_i \cdot p_j\}, \varepsilon\right)$. Thus in the end, the color-stripped l-loop amplitude can be written as a sum of process-independent scalar integrals of loop momenta, the so-called *Feynman integrals*, multiplied by some rational coefficients depending on the process at hand

$$\mathcal{A}_n^{(l)} = \sum_{I \subseteq T} \left(\sum_{i_1, \ldots, i_{n_{ir}}=0}^{n_{th}^I} C_{i_1, \ldots, i_{n_{ir}}}^{(I)} \int \left[\prod_{i=1}^{l} \frac{d^d k_i}{(2\pi)^d} \mu^{4-d}\right] \frac{\left(\bar{z}_1^{(I)}\right)^{i_1} \cdots \left(\bar{z}_{n_{ir}}^{(I)}\right)^{i_{n_{ir}}}}{\prod_{j \in I} D_j^{a_j}(\{k\}, \{p\}, m_j)}\right). \qquad (2.10)$$

We need to comment here that the Feynman integrals appearing in the rhs of the above expression should not be confused with the integral expressions resulting from the application of the Feynman rules to the Feynman diagrams of QCD. Feynman integrals do not obey the Feynman rules of Figure 1.1 but to them can be assigned Feynman graphs, where the vertices are equal to one and do not depend on the number or kind of particle that they contain (e.g. we can have six particles in a vertex) but the momentum must be conserved on them, and the inverse propagators have the form of Eq. (2.5). We will discuss more about Feynman integrals in the next Chapter.

The complexity of the computation of scattering amplitudes grows very fast with the number of loops and their kinematics, which depend on the number of external particles and internal[3] or external (different or not) masses. The kinematic complexity of a scattering amplitude can be quantified in terms of its independent kinematic invariant scales (*Mandelstam variables*)

$$n_{scales} = n_p + n_m - 1. \qquad (2.11)$$

Let's shortly describe the terms on the rhs of the above expression. Assuming that all the external momenta are incoming (or equivalently outgoing), n_p corresponds to the

---

[3]Meaning masses included in the propagators.

number of momentum invariants

$$s_{ij} = s_{ji} = (p_i + p_j)^2, \tag{2.12}$$

resulted by the contractions of different and independent momenta, meaning the total number of s_{ij} with $i < j$ and $j < n$,

$$n_p = (n-1)(n-2)/2. \tag{2.13}$$

This holds true only for $n \leq 5$ because, in a 4-dimensional vector space, it is not possible to have more than 4 independent vectors. n_m is the number of different internal and external masses, and -1 is a result of the momentum conservation which imposes the following constrain

$$\sum_{i<j<n} s_{ij} = \sum_k m_k^2, \tag{2.14}$$

on the momentum invariants and masses of the external particles. For example, consider the amplitudes of a 4-particle and a 5-particle scattering with one external massive particle and no massive intermediate particles. In the first case we have $n_p = 3$, $n_m = 1$ and thus $n_{scales} = 3$, while in the second we have $n_p = 6$, $n_m = 1$ and thus $n_{scales} = 6$. In order to fully specify the kinematics, in addition to the independent Mandelstam variables one needs also a pseudo-scalar[4] invariant [44], defined usually as

$$\mathrm{tr}_5 = 4i\varepsilon_{\mu_1\mu_2\mu_3\mu_4} p_1^{\mu_1} p_2^{\mu_2} p_3^{\mu_3} p_4^{\mu_4}, \tag{2.15}$$

with $\varepsilon_{\mu_1\mu_2\mu_3\mu_4}$ being the 4-dimensional Levi-Civita symbol, and $\mathrm{tr}_5 = 0$ for $n < 5$.

2.1.1   Unitarity Cuts and Generalized Unitarity Cuts

In sections 1.2 and 1.3 we revealed an unexpected property of the scattering amplitudes beyond tree-level: they diverge. Therein we discussed the origin of the (UV and IR) divergences, as well as, their resolution in order to obtain finite results for physical observables. Another important property of the scattering amplitudes is the appearance of branch cut singularities when the loop particles can be produced as real particles, meaning when the loop particles go on-shell. This follows from probability conservation in the scattering process, which corresponds to the *unitarity of the $S-$matrix*

$$SS^\dagger = \mathbf{1} \xrightarrow{(1.26)} i(T^\dagger - T) = TT^\dagger. \tag{2.16}$$

We remind that the completeness relation of the identity matrix in the Fock space reads

$$\mathbf{1} = \sum_{\{x\},n_x \geq 0} \int d\Phi^{n_x} \ket{\{x\}} \bra{\{x\}} \tag{2.17}$$

with $\ket{\{x\}}$ denoting an n_x-particle state where the particles can be of different kinds and bear different quantum numbers, and thus the sum runs both on the n_x and $\{x\}$ meaning that we sum in all the particle species of the model and their quantum numbers. Sandwiching Eq. (2.16) between an initial state $\ket{i}$ and a final state $\bra{f}$ and

---

[4]Pseudo-scalar is a quantity that behaves like a scalar, except that it changes sign under a parity inversion $(p^0, \vec{p}) \to (p^0, -\vec{p})$.

using Eq. (2.17) we obtain

$$2\text{Im}\left(\mathcal{M}_{i\to f}\right) = \sum_{\{x\},n_x\geq 0}\int d\Phi^{n_x}(2\pi)^4\delta^{(4)}(p_i - p_{\{n_x\}})\mathcal{M}_{\{x\}\to f}\mathcal{M}^*_{i\to\{x\}}, \qquad (2.18)$$

which is known as the *optical theorem*, that relates the imaginary part of an amplitude to the product of two amplitudes integrated over all intermediate particle states. Expanding the amplitudes of Eq. (2.18) in coupling constants, we observe that the imaginary part of a multi-loop amplitude is given by the product of lower loop amplitudes, implying thus relations between terms of different order in the perturbative expansion.

Considering now the amplitude as an analytic function of some complex[5] kinematic invariants, s, it can be shown [44] that its imaginary part is related to its discontinuity when s crosses the real axis

$$\text{Disc}\left(\mathcal{M}_{i\to f}(s)\right) = \lim_{\epsilon\to 0}\left(\mathcal{M}_{i\to f}(s + i\epsilon) - \mathcal{M}_{i\to f}(s - i\epsilon)\right) = 2i\text{Im}\left(\mathcal{M}_{i\to f}(s)\right). \qquad (2.19)$$

Thus the imaginary part of a scattering amplitude is proportional to its discontinuity across the branch cut of interest. For real momenta, the discontinuities of a scattering amplitude are sourced by the $+i\epsilon$ prescription (see Feynman rules in Figure 1.1) when a loop propagator goes on-shell ($k^2 = m^2$ in the following equation). In that case, the discontinuity of an amplitude in a given kinematical channel is computed by cutting the loop propagators in that channel and using Cutkosky's rule [45]

$$\frac{1}{k^2 - m^2 + i\epsilon} \to 2\pi i \times \delta(k^2 - m^2)\theta(k^0) \quad\text{with}\quad \theta(k^0) = \begin{cases} 1, & k^0 \geq 0 \\ 0, & k^0 < 0 \end{cases}. \qquad (2.20)$$

Due to being related to the unitarity of $S-$matrix, these types of cuts are called *unitarity cuts*. By allowing for the loop momenta to be complex we can take even more cuts beyond the ones prescribed by unitarity (multi-channel cuts). These cuts are called generalized unitarity cuts [46, 47] and are computed by deforming the integration contour around the poles of the cut propagators and using the residue theorem.

2.1.2 Integration-By-Parts Identities

In Eq. (2.10) we saw that the scattering amplitudes containing loops can be represented as a sum of Feynman integrals. However, the increment in the number of loops results in a huge augmentation in the number of Feynman diagrams, and thus an enormous increase in the number of Feynman integrals needed to be computed for the determination of the scattering amplitude. Hopefully, it turns out that not all the Feynman integrals of a scattering amplitude are independent due to the existence of relations between them, emerging by the vanishing of total derivatives in dimensional regularization (third property of Eq. (1.15)). These relations are called *integration-by-part identities* (IBPs) [48, 49], are linear in the Feynman integrals with the coefficients being rational functions of the external kinematic invariants and the dimensional regulator,

---

[5]This is an unphysical generalization because for physical processes we have real momenta that correspond to real invariants.

and have the following form

$$\int \left(\prod_{i=1}^{l} \frac{d^d k_i}{(2\pi)^d} \right) \frac{\partial}{\partial k_b^\mu} \left(u_b^\mu \frac{\bar{z}_1^{i_1} \cdots \bar{z}_{n_{ir}}^{i_{n_{ir}}}}{\prod_j D_j^{a_j}} \right) = 0, \qquad (2.21)$$

where the vector u_b^μ can be any linear combination of the external or loop momenta with rational coefficients depending on loop or kinematic scalar products. IBP identities can be used to reduce the Feynman integrals of a scattering amplitude to a finite basis of independent integrals [50], the so-called *master integrals*. Another set of identities that produces linear relation between Feynman Integrals are the Lorentz-invariance (LI) identities [51]

$$\sum_{j_1=1}^{n-1} \left(p_{j_1}^\mu \frac{\partial}{\partial p_{j_1,\nu}} - p_{j_1}^\nu \frac{\partial}{\partial p_{j_1,\mu}} \right) \left(\int \left(\prod_{i=1}^{l} \frac{d^d k_i}{(2\pi)^d} \right) \frac{\bar{z}_1^{i_1} \cdots \bar{z}_{n_{ir}}^{i_{n_{ir}}}}{\prod_j D_j^{a_j}} = \right) 0. \qquad (2.22)$$

LI identities are proved to be linear combinations of IBP identities [52], but can help convergence in solving the linear system of equations produced by IBPs. For a detailed discussion of IBP and LI identities, we refer the interested reader to [53].

The most famous technique for solving the system of IBP identities and determining a set of master integrals is *Laporta's algorithm* [54]. Within this algorithm, the integrals are assigned a weight according to their complexity, with the simpler integrals, defined as the ones that have fewer propagators or irreducible scalar products, obtaining the lower weight. Then for the provided integrals IBP and LI identities are generated and solved using Gaussian elimination, expressing higher-weight integrals in terms of lower-weight ones. The integrals that remain undetermined from this procedure are chosen to be the master integrals. The choice of master integrals is not unique, as one can provide a lower index for specific integrals in this procedure, and a convenient choice may help a lot in the reduction procedure [55, 56] or in their computation, as we will see in the next Chapter. There exist several publicly-available automated packages that implement Laporta's algorithm, such as `AIR` [57], `FIRE` [58], `LiteRed` [59], `KIRA` [60], `REDUZE` [61], `Azurite` [62], `NeatIBP` [63] etc.

In general, solving IBP identities for problems with many scales and loops is a bottleneck, and so far impossible in many cases. This is because IBPs produce a large number of linear equations to be solved, with huge expressions appearing in their coefficients. For this reason, many strategies [64–75] have been proposed in the last years in order to improve several aspects of Laporta's algorithm and facilitate in many cases the reduction, while also new methods for reducing to a set of master integrals by completely skipping the IBP reduction are under investigation [76–80]. Of these strategies, the one that has been proven to be the most efficient and has been adopted from most of the last versions of the automated packages stated above is the IBP reduction using constant numbers, and especially finite fields, for the variables of the coefficients of the equations (integrals are kept symbolic) and reconstruction of their analytic form in the final expressions [66, 68]. This method avoids numerically the intermediate large expressions and reconstructs the final results which are much simpler, and is perfectly suited for IBP coefficients which are always rational numbers of kinematic invariants and ε. The cost to be paid for using this method is that one should repeat the computation for different values of the variables in order to reconstruct the analytic form

of the final expressions. For implementing complex numerical algorithms over finite fields and reconstructing multivariate rational functions, the package `FiniteFlow` [70] is publicly available.

2.1.3 Computational Procedure

Having in mind the things stated in the previous subsections let's summarize here the procedure needed to be followed for the computation of a *l*-loop scattering amplitude with *n* external particles. In general, one should follow three non-trivial steps

1. Construct the scattering amplitude for the process at hand by using Feynman rules to generate the contributing diagrams or to apply a Dyson-Schwinger recursion

$$\mathcal{M}_n^{(l)} = \sum_F c_F^{(l)} \int \left(\prod_{i=1}^l \frac{d^d k_i}{(2\pi)^d} \mu^{4-d} \right) \sum_{I \subseteq T} \frac{N_{I,F}\left(\{k\}, \{p\}, \gamma^\mu, \{\epsilon^\mu\}\right)}{\prod_{j \in I} D_j^{a_j}(\{k\}, \{p\}, m_j)}. \tag{2.23}$$

2. Reduce at the integrand or/and integral level the scattering amplitude into a set of master integrals, determining the rational coefficients of the reduction

$$\mathcal{M}_n^{(l)} = \sum_F c_F^{(l)} \left(\sum_{i'} \tilde{c}_{i',F}^{(l)}\left(\{p_i \cdot p_j\}, \{m\}, \varepsilon\right) F_{i',F}^{(l)}\left(\{p_i \cdot p_j\}, \{m\}, \varepsilon\right) \right). \tag{2.24}$$

3. Compute the master integrals using numerical or analytical methods.

For the computation of tree-level amplitudes, the first step is sufficient.

Regarding the first of the above-mentioned steps, the generation of the contributing Feynman diagrams can be done using automated packages like `QGRAF` [81] or `FeynArts` [82], and the manipulation of the expressions for the construction of the amplitude is possible through frameworks such as `FORM` [83], `FeynCalc` [84, 85] and `FormCalc` [86]. The Dyson-Schwinger recursion has been applied at tree-level within `HELAC` [42, 87], and at one-loop within `HELAC-1LOOP` [88] and `Recola` [89, 90] in a hybrid approach together with graph topologies (blob-topologies). More details of this approach will be given in section 2.3. A similar hybrid approach we have developed within `HELAC-2LOOP` [3], which we are going to discuss in Chapter 4.

In Section 2.4 we will review the second of the aforementioned steps. Within this section, we will start discussing the well-known one-loop techniques that led to the automation of NLO computations, focusing on the *Ossola-Papadopoulos-Pittau* (OPP) method [91, 92], and then we will summarize the currently used methods for multi-loop amplitude reductions. The third step is the main topic of Chapter 3, and some novel results concerning three-loop master integrals are going to be presented in Chapter 5.

2.2 Color-Flow Representation

In the *color-flow representation* [41–43] the eight-component gluon field, A_μ^a, is traded for a $N_c \times N_c$ (= 9) traceless matrix, $(A_\mu)_{ij}$, by multiplying and contracting, over the

adjoint index a, with the corresponding $\sqrt{2}t_{ij}^a$ matrix

$$(A_\mu)_{ij} = \sqrt{2}A_\mu^a t_{ij}^a. \tag{2.25}$$

Thus gluons (and ghosts) bear a pair of color (fundamental) and anti-color (anti-fundamental) indices (i,j), while quarks have only a color index $(i,0)$[6]. The contraction of Eq. (2.25) is applied for every gluon of the scattering amplitude leading to a simplified color factor, being equal to a product of Kronecker delta functions carrying fundamental and anti-fundamental indices of the external particles. This form of the color factor holds true for amplitudes of any kind of external particles, leading to a unified approach for any process. More specifically, if a l-loop n-particle scattering amplitude consists of n_g gluons, $n_{q\bar{q}}$ quarks and $n_{q\bar{q}}$ anti-quarks, then it bears $k = n_g + n_{q\bar{q}}$ color lines (indices) and can be decomposed as

$$\mathcal{M}_n^{(l)} = \sum_{\sigma}^{k!} \delta_{j_1}^{i_{\sigma_1}} \delta_{j_2}^{i_{\sigma_2}} \cdots \delta_{j_k}^{i_{\sigma_k}} \mathcal{A}_{n,\sigma}^{(l)}, \tag{2.26}$$

where the sum is running over all the possible permutations σ_i of the set $\{1,2,3,\ldots,k\}$, $k!$ in total. In the above expression, we have chosen to keep fixed the order of anti-color indices and permute the color ones, but without altering the result one could do the opposite. Let us comment here that, in the definition of $\mathcal{A}_{n,\sigma}^{(l)}$ there are included some coefficients which are polynomials on N_c, the form of which we will see with an example in Chapter 4. For a better understanding of the notation in Eq. (2.26), we give below the form of three color factors

$$1)\delta_{j_1}^{i_1}\delta_{j_2}^{i_2}\cdots\delta_{j_k}^{i_k}, \quad 2)\delta_{j_1}^{i_2}\delta_{j_2}^{i_1}\cdots\delta_{j_k}^{i_k} \quad \text{and} \quad 3)\delta_{j_1}^{i_k}\delta_{j_2}^{i_1}\cdots\delta_{j_k}^{i_2}. \tag{2.27}$$

The (color-summed) interference term of two scattering amplitudes, coming in general from different orders of the expansion, is given by

$$\mathcal{M}_n^{(l)}(\mathcal{M}_n^{(l')})^* = \sum_{\sigma\sigma'} \mathcal{A}_{n,\sigma}^{(l)} \mathcal{C}_{\sigma\sigma'} (\mathcal{A}_{n,\sigma'}^{(l')})^*, \tag{2.28}$$

with the color matrix, $\mathcal{C}_{\sigma\sigma'}$, having the very simple form

$$\mathcal{C}_{\sigma\sigma'} = \delta_{j_1}^{i_{\sigma_1}} \delta_{j_2}^{i_{\sigma_2}} \cdots \delta_{j_k}^{i_{\sigma_k}} \delta_{i_{\sigma_1'}}^{j_1} \delta_{i_{\sigma_2'}}^{j_2} \cdots \delta_{i_{\sigma_k'}}^{j_k} = \delta_{i_{\sigma_1'}}^{i_{\sigma_1}} \delta_{i_{\sigma_2'}}^{i_{\sigma_2}} \cdots \delta_{i_{\sigma_k'}}^{i_{\sigma_k}} = N_c^{m(\sigma,\sigma')}, \tag{2.29}$$

where $1 \le m(\sigma,\sigma') \le k$ counts the number of common cycles of the two permutations (σ,σ'). The color structure of the color-flow representation shows how the color flows in the real physical process and reflects the fact that the color remains unchanged on an uninterrupted color line. An advantage of this representation is the fact that it is very well-suited for the recursive construction of the scattering amplitude using Dyson-Schwinger Equations.

The Feynman rules for the construction of scattering amplitudes in the color-flow representation are obtained by contracting with $\sqrt{2}t_{ij}^a$ matrices for each gluon/ghost the QCD Feynman rules that we presented in subsection 1.2.1. Doing so, the gluon propagator takes the following form

---

[6]Anti-quarks have only an anti-color index $(0,j)$, and colorless particles have $(0,0)$.
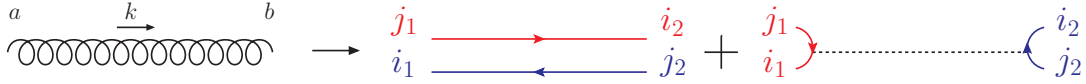
$$\Pi_{\mu\nu} = i \left(\delta^{i_2}_{j_1} \delta^{i_1}_{j_2} - \frac{1}{N_c} \delta^{i_1}_{j_1} \delta^{i_2}_{j_2} \right) \left(\frac{-g_{\mu\nu}}{k^2 + i\epsilon} + \frac{(1 - \xi) k_\mu k_\nu}{(k^2 + i\epsilon)^2} \right),$$

and thus it has two different color flows. The $SU(N)$ gluon is separated into a $U(N)$ gluon (first flow) and an unphysical $U(1)$ gluon (second flow). The second flow does not transfer color (neutral), and couples only to gluons interactions with quarks, due to the anti-symmetry of the three-gluon, four-gluon, and anti-ghost-ghost-gluon vertices. The quark propagator remains unchanged, while the ghost propagator becomes

$$\Pi = \frac{i \delta^{i_2}_{j_1} \delta^{i_1}_{j_2}}{k^2 + i\epsilon},$$

having only one color flow[7]. The three-gluon vertex, the anti-ghost-ghost-gluon vertex, and the anti-quark-quark-gluon vertex have two color flows each

$$V^{\mu\nu\rho}_{ggg} = i \frac{g_s}{\sqrt{2}} \left(\delta^{i_2}_{j_1} \delta^{i_3}_{j_2} \delta^{i_1}_{j_3} - \delta^{i_3}_{j_1} \delta^{i_1}_{j_2} \delta^{i_2}_{j_3} \right) \left[g^{\mu\nu} (p_1 - p_2)^\rho + g^{\nu\rho} (p_2 - p_3)^\mu + g^{\rho\mu} (p_3 - p_1)^\nu \right],$$

---

[7]One could argue here that, an extra neutral flow should exist for the ghost propagator. From the mathematical point of view, due to the contraction with the t^a_{ij} matrices, this is correct but the interaction vertices of the ghost fields do not allow for such a propagator to couple to any field of the theory. That's why we keep only the color flow that transfers color.

$$V_{gc\bar{c}}^{\mu} = i\frac{g_s}{\sqrt{2}} \left(\delta_{j_1}^{i_2}\delta_{j_2}^{i_3}\delta_{j_3}^{i_1} - \delta_{j_1}^{i_3}\delta_{j_2}^{i_1}\delta_{j_3}^{i_2} \right) p_1^{\mu},$$
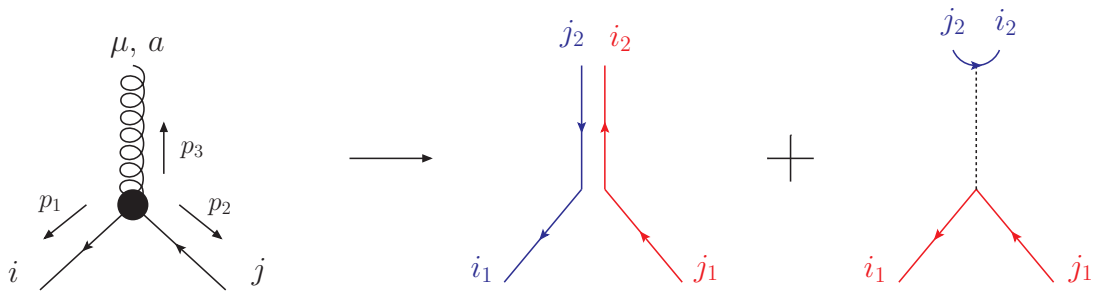
$$V_{gq\bar{q}}^{\mu} = i\frac{g_s}{\sqrt{2}} \left(\delta_{j_1}^{i_2}\delta_{j_2}^{i_1} - \frac{1}{N_c}\delta_{j_1}^{i_1}\delta_{j_2}^{i_2} \right) \gamma^{\mu},$$

while the four-gluon vertex consists of six color flows
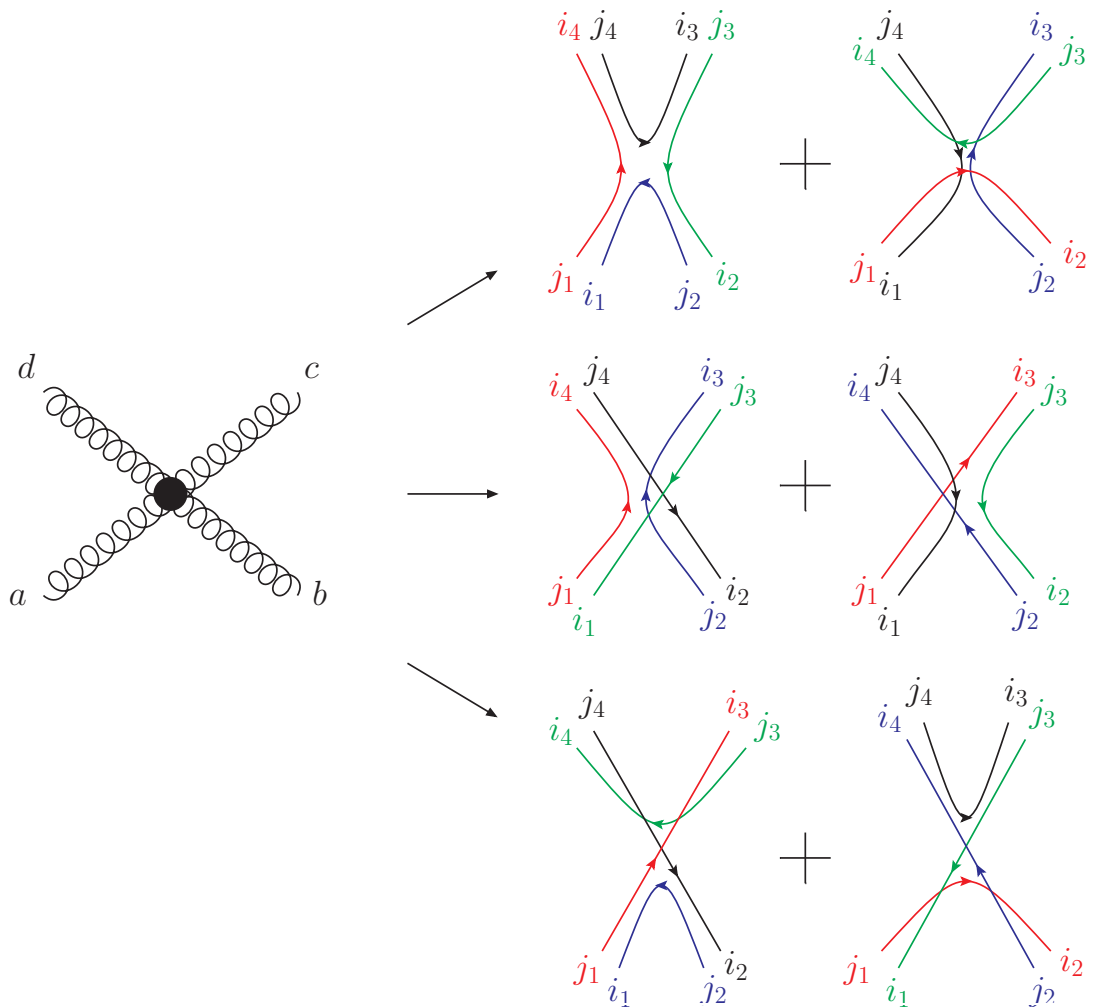
$$V_{gggg}^{\mu\nu\rho\sigma} = i\frac{g_s^2}{2} \left[\left(\delta_{j_1}^{i_4}\delta_{j_2}^{i_1}\delta_{j_3}^{i_2}\delta_{j_4}^{i_3} + \delta_{j_1}^{i_2}\delta_{j_2}^{i_3}\delta_{j_3}^{i_4}\delta_{j_4}^{i_1} \right) \left(2g^{\mu\rho}g^{\nu\sigma} - g^{\mu\sigma}g^{\nu\rho} - g^{\mu\nu}g^{\rho\sigma} \right) \right.$$
$$+ \left(\delta_{j_1}^{i_4}\delta_{j_2}^{i_3}\delta_{j_3}^{i_1}\delta_{j_4}^{i_2} + \delta_{j_1}^{i_3}\delta_{j_2}^{i_4}\delta_{j_3}^{i_2}\delta_{j_4}^{i_1} \right) \left(2g^{\mu\nu}g^{\rho\sigma} - g^{\mu\rho}g^{\nu\sigma} - g^{\mu\sigma}g^{\nu\rho} \right)$$
$$\left. + \left(\delta_{j_1}^{i_3}\delta_{j_2}^{i_1}\delta_{j_3}^{i_4}\delta_{j_4}^{i_2} + \delta_{j_1}^{i_2}\delta_{j_2}^{i_4}\delta_{j_3}^{i_1}\delta_{j_4}^{i_3} \right) \left(2g^{\mu\sigma}g^{\nu\rho} - g^{\mu\nu}g^{\rho\sigma} - g^{\mu\rho}g^{\nu\sigma} \right) \right].$$

2.3 Dyson-Schwinger Recursion in `HELAC`

2.3.1 The Tree-level case

At tree-level, the computational cost for evaluating scattering amplitudes grows very fast with the number of external particles when using the standard Feynman diagram representation for the scattering amplitudes. An alternative way for computing scattering amplitudes that reduces the computational cost is using recursive algorithms based on the Dyson-Schwinger equations [93–95]. These equations express recursively an n-point Green's function in terms of 1-, 2-, ..., $(n-1)$-point functions, are valid to all orders in perturbation theory, and contain complete information about the fields and their interactions, regardless of the number of external particles.

The first package to follow this alternate approach was `HELAC` [42, 87], which uses off-shell sub-amplitudes (currents) as building blocks for the recursion, reorganized to minimize the amount of computation that needs to be repeated. The calculation is organized by decomposing the scattering amplitude in color-stripped amplitudes using the color-flow representation and constructing the color-stripped amplitude for each term of the color basis (configuration). Let's briefly describe the algorithm implemented in `HELAC`. Consider, within the SM, a scattering process containing n external particles, all taken to be incoming, with momenta $p_1, p_2, \ldots, p_n$. The off-shell sub-amplitude $J(f, P, \{\delta\})$ constructed by a subset $I \subset \{1, \ldots, n\}$ of the external particles, and describing a particle bearing flavor f, color $\{\delta\}$ and momentum P^μ,

$$P^\mu = \sum_{i \in I} p_i^\mu, \tag{2.30}$$

is defined as the sum of all Feynman sub-diagrams that combine the particles of I in order to produce the particle at hand

$$J(f, P, \{\delta\}) = I \; \begin{matrix} \vdots \\ \vdots \end{matrix} \; \bullet \!\!\!-\!\!\!- \; {}^P \qquad . \tag{2.31}$$
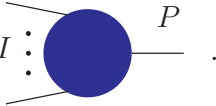
In Eq. (2.31), the blue blob is a visual representation of all potential sub-diagrams. If the Feynman rules do not allow for the particles from the set I to generate the particle at hand, the sub-amplitude $J(f, P, \{\delta\})$ vanishes. Although omitted within the above notation, the sub-amplitude can contain open (not contracted) Lorentz indices in the case that it describes a boson field, thus in general we can write

$$J(f, P, \{\delta\}) = \begin{cases} \Psi(P)\delta_{i'}^i, & \text{for a fermion field} \\ \bar{\Psi}(P)\delta_j^{j'}, & \text{for an anti-fermion field} \\ A^\mu(P)\delta_{j'}^i, \delta_j^{i'}, & \text{for a boson field} \end{cases} \tag{2.32}$$

with the color structure omitted for colorless particles. If the set I contains only one of the external particles then the sub-amplitude is equal to the wave function of that particle, meaning

$$\Psi(p_i) = \begin{cases} u^\lambda(p_i), & \text{for } p_i^0 \geq 0 \\ v^\lambda(-p_i), & \text{for } p_i^0 \leq 0 \end{cases}, \qquad \bar{\Psi}(p_i) = \begin{cases} \bar{u}^\lambda(p_i), & \text{for } p_i^0 \geq 0 \\ \bar{v}^\lambda(-p_i), & \text{for } p_i^0 \leq 0 \end{cases},$$

$$\text{and} \qquad A^\mu(p_i) = \begin{cases} \epsilon_\lambda^\mu(p_i), & \text{for } p_i^0 \geq 0 \\ \epsilon_\lambda^\mu(-p_i)^*, & \text{for } p_i^0 \leq 0 \end{cases} \qquad \text{with} \qquad \lambda = \pm 1, 0. \tag{2.33}$$

Note that here $p_i^0 \leq 0$ means that the particle is in practice outgoing, as the outgoing momenta are turned into incoming by the transformation $p_i \to -p_i$. Internally in `HELAC`, all calculations are performed in the light-cone representation of four-vectors, using the chiral representation for the Dirac matrices, and the explicit form of the wave functions used therein can be found in the appendix of [42].

Within the SM, where the fundamental particles can interact only through three- and four-vertices, the Dyson-Schwinger equations for recursively constructing the sub-amplitude $J(f, P, \{\delta\})$ take the following general form
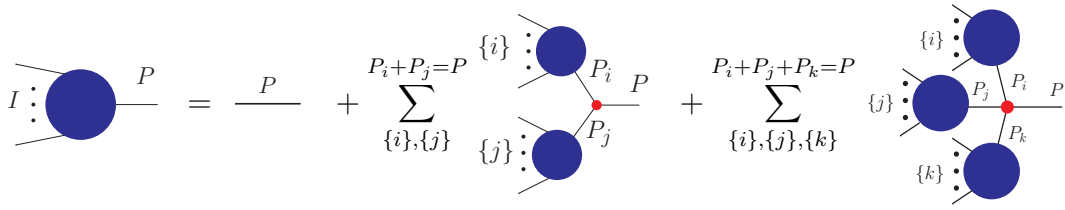
$$J(f, P, \{\delta\}) = \sum_{i=1}^{n} \delta_{Pp_i} J(p_i, f_i, \{\delta_i\})$$

$$+ \sum_{\{i\},\{j\},\{\delta\}}^{P_i+P_j=P} V_3 \Pi'(P) J(f_i, P_i, \{\delta_i\}) J(f_j, P_j, \{\delta_j\}) \epsilon(P_i, P_j) \tag{2.34}$$

$$+ \sum_{\{i\},\{j\},\{k\},\{\delta\}}^{P_i+P_j+P_k=P} V_4 \Pi'(P) J(f_i, P_i, \{\delta_i\}) J(f_j, P_j, \{\delta_j\}) J(f_k, P_k, \{\delta_k\}) \epsilon(P_i, P_j + P_k)$$

In this context, the first term corresponds to the case where the set I contains only one of the external particles. The second term sums over all possible ways[8] of splitting, via a three-vertex, the particles of the set I into two subsets of particles $\{i\}$ and $\{j\}$, where the two subsets are again split into more subsets in all possible ways using three- and four-vertices, with this procedure going on till arriving at subsets containing only one of the external particles. The third term sums over all possible ways of splitting, via a four-vertex, the particles of the set I into three subsets $\{i\}$, $\{j\}$ and $\{k\}$, each one of which is again split into all possible ways using three- and four-vertices till arriving at subsets consisting only one of the external particles. In the equation above, V_3 and V_4 denote any three- and four-vertex of the SM, respectively,

---

[8]Taking into account all possible color connections.

and $\Pi'(P)$ corresponds to the propagator of the sub-amplitude $J(f, P, \{\delta\})$ that is split, and $J(f_i, P_i, \{\delta_i\})$, $J(f_j, P_j, \{\delta_j\})$ and $J(f_k, P_k, \{\delta_k\})$ are the sub-amplitudes of the subsets $\{i\}$, $\{j\}$ and $\{k\}$, respectively. For QCD processes, within `HELAC`, the vertices and propagators defined in Section 2.2 are used. The symbol $\epsilon(P_i, P_j)$ is a sign factor taking the values ± 1, which considers the anti-symmetry of the sub-amplitude when two identical fermions are interchanged.

A very convenient notion, that dictates a natural path on the recursive construction of sub-amplitudes, is that of the level of a sub-amplitude, l_b. The level of a sub-amplitude is defined as the number of external particles that are included in it. In this notion, the external particles can be viewed as level-1 sub-amplitudes, and the recursive construction goes as follows: one starts by using level-1 sub-amplitudes in order to compute the level-2 ones applying Eq. (2.34), then applying the same equations computes level-3 sub-amplitudes from the level-2 and level-1 ones, and so on up to the level of the sub-amplitude at hand. This procedure is more efficient than computing Feynman diagrams since it avoids the repeated computation of identical parts that contribute to different diagrams because each sub-amplitude is computed only once.

The last sub-amplitude of the recursion is the one carrying $n - 1$ of the external particles and is constructed in such a way that to correspond to the n-th particle[9], let us denote this particle with the subscript i. This sub-amplitude is unique, and its propagator $\Pi'(-p_i)$ is removed by the expression in Eq. (2.34), due to its momentum being on-shell[10]. Thus we will denote this "amputated" sub-amplitude with the subscript 0. Then the total color-stripped amplitude can be constructed by multiplying this sub-amplitude with the wave function of the particle (field) i

$$
\mathcal{A}_n^{(0)} = J_0(f_i, -p_i, \{\delta\}) J(f_i, p_i, \{\delta\}) =
\begin{cases}
A_0^\mu(-p_i) A_\mu(p_i), & \text{for boson} \\
\bar{\Psi}_0(-p_i) \Psi(p_i), & \text{for fermion} \\
\bar{\Psi}(p_i) \Psi_0(-p_i), & \text{for anti-fermion}
\end{cases}
. \quad (2.35)
$$

For solving the recursive Dyson-Schwinger equations a binary representation is used for the external particles [96], where the $i-$th particle acquires the unique integer ID, $id_i = 2^{i-1}$. In this framework, the momentum of a sub-amplitude (Eq. (2.30)) is assigned a binary vector $\vec{m} = \{\tilde{m}_1, \ldots, \tilde{m}_n\}$, with its components being equal to 0 or 1 in such a manner that

$$
P^\mu = \sum_{i=1}^n \tilde{m}_i p_i^\mu \quad (2.36)
$$

and the sub-amplitude itself receives a unique integer ID, defined as the sum of all the ids of the external particles that is constructed by

$$
m = \sum_{i=1}^n 2^{i-1} \tilde{m}_i \quad \text{with} \quad 0 \leq m \leq 2^n - 1. \quad (2.37)
$$

---

[9]Any of the external particles can be chosen as the n-th particle, which is the endpoint of the recursion.

[10]Only the propagator of the last step of the recursion is removed. All the other propagators produced in previous steps of the recursion are obviously kept explicitly.

For example, for $n = 6$ the external particles and the sub-amplitude with momentum $p_{235}^\mu = p_2^\mu + p_3^\mu + p_5^\mu$ are interpreted by the IDs

$$\{1, 2, 3, 4, 5, 6\} \rightarrow \{1, 2, 4, 8, 16, 32\} \qquad \text{and} \qquad J(f, p_{235}, \{\delta\}) \rightarrow J(f, 22, \{\delta\}). \quad (2.38)$$

In the same context, the level of the sub-amplitude can be defined by the following expression

$$l_b = \sum_{i=1}^{n} \tilde{m}_i, \quad (2.39)$$

and the sign factor $\epsilon(P_{i_1}, P_{i_2}) \rightarrow \epsilon(m_{i_1}, m_{i_2})$ via the equation

$$\epsilon(m_{i_1}, m_{i_2}) = (-1)^{\chi(m_{i_1}, m_{i_2})} \qquad \text{with} \qquad \chi(m_{i_1}, m_{i_2}) = \sum_{i=n}^{2} \hat{m}_{i_1 i} \left(\sum_{j=1}^{i-1} \hat{m}_{i_2 j} \right), \quad (2.40)$$

where hated components are set to 0 if the corresponding external particle is a boson.

Within `HELAC`, particle 1 is always chosen as the endpoint of the recursion. This results in all sub-amplitudes to obtain ID values from the set of even integers between 2 and $2^n - 2$. Furthermore, the color-stripped amplitude is always computed by

$$\mathcal{A}_n^{(0)} = J_0(f_1, 2^n - 2, \{\delta\}) J(f_1, 1, \{\delta\}). \quad (2.41)$$

The computation of the amplitude happens in two phases. In the first phase, called *initialization phase*, the program builds a *skeleton* of the color-stripped amplitude for each color configuration, meaning it constructs recursively all the relevant sub-amplitudes that contribute to the process at hand and stores the information in a file. In the second phase, called *computation phase*, the program numerically calculates the amplitude for each provided phase space point, summed over all possible chirality configurations of the external particles[11].

2.3.2   The One-loop case

At one-loop level, there do not exist programs that implement an algorithm that uses direct Dyson-Schwinger recursion for the construction of a scattering amplitude. This mainly happens due to the fact that for computing a one-loop amplitude it is optimal to collect contributions that contain the same loop-assignment structure and reduce them, at the integrand level, to the corresponding master integrals. This is difficult to be combined with a direct Dyson-Schwinger recursion, as the latter would in general combine in a single configuration different Feynman diagrams with different loop-assignment structures. For this reason, a hybrid approach between Feynman diagrams and Dyson-Schwinger recursion is applied by `HELAC-1LOOP` [88, 97] in order to construct the 4-dimensional part of the numerators that contribute to a one-loop scattering amplitude. The main idea of the algorithm is that an $n-$particle one-loop diagram, keeping information about its loop structure, can be uniquely corresponded to an $(n + 2)$-particle tree-level diagram, where the latter can be constructed using `HELAC`. Let us mention here that, `HELAC-1LOOP` is a completely automated framework for the calculation of one-loop n-particle scattering amplitudes, but in this subsection,

---

[11]Or for a specific chirality configuration if specified otherwise.
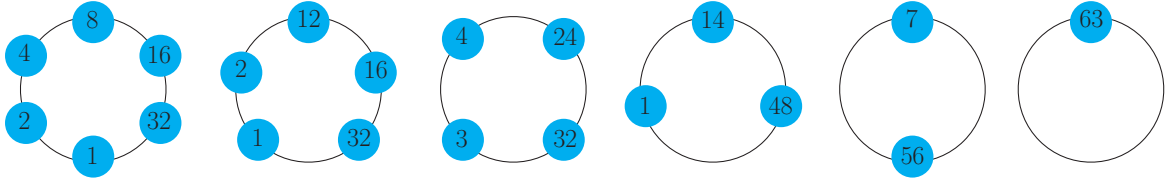
Figure 2.1: Some inequivalent topologies for n = 6. From left to right, we have depicted the topologies $\{1, 2, 4, 8, 16, 32\}$, $\{1, 2, 12, 16, 32\}$, $\{3, 4, 24, 32\}$, $\{1, 14, 48\}$, $\{7, 56\}$ and $\{63\}$. The rest of the topologies that are not depicted here are topologically (in terms of the number of blobs) the same as these ones, meaning they are hexagon-, pentagon-, box-, triangle-, bubble-, and tadpole-topologies, but have a different assignment on the external particles coming on the blobs.

because we haven't yet discussed the OPP method used internally for the reduction of the numerators into master integrals, we focus only on the algorithmic approach used therein for the construction of the numerators that contribute to a given amplitude (initialization phase).

Having as input the number (n) and the flavor $(f_i, \ldots, f_n)$ of the external particles, together with the allowed flavors for the loop particles, `HELAC-1LOOP` generates all possible color configurations of the external particles and constructs for each of them the numerators that contribute to the color-stripped amplitudes, storing color-wised the information in the skeleton. In the first step of the construction of the color-stripped amplitudes, `HELAC-1LOOP` generates all topologically inequivalent partitions of the external particles into all possible number of sets (*blobs*) attached to the loop, the so-called one-loop *blob-topologies*. A *blob* is interpreted as the sum of all possible tree-level sub-amplitudes that can be constructed including the external particles that are contained in the ID number defining the blob, and its level is equal to the number of particles that it consists of. In practice, this means that blobs are constructed by a Dyson-Schwinger recursion like the one applied at tree-level. Blobs can contain propagators but they do not depend on the loop momentum. Thus a blob-topology is actually a sum of Feynman graphs with the same loop-assignment structure. For a better understanding of the concept of blobs, consider as an example the following level-4 blob, constructed from the particles $\{1, 2, 4, 8\}$ (the black line corresponds to the loop line where the blob is attached)
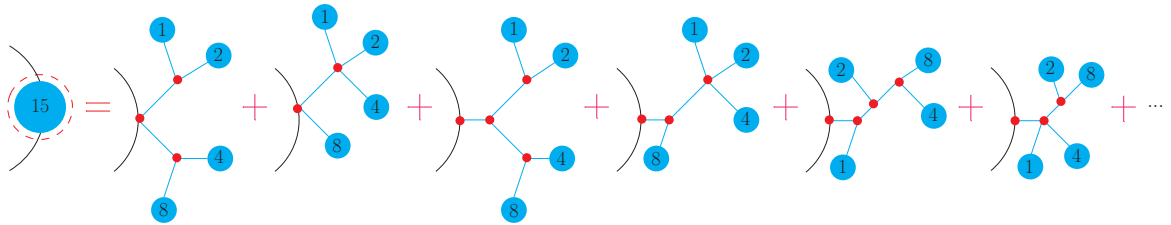
The dots count for the extra sub-amplitudes coming from all inequivalent permutations of the external particles in the 6 depicted sub-graphs. In this example, the total number of sub-amplitudes taken as one contribution from the level-4 blob is 26, of which, 3 are of the first, 4 are of the second, 3 are of the third, 4 are of the fourth, 12 are of the fifth, and 3 are of the sixth sub-graph type.
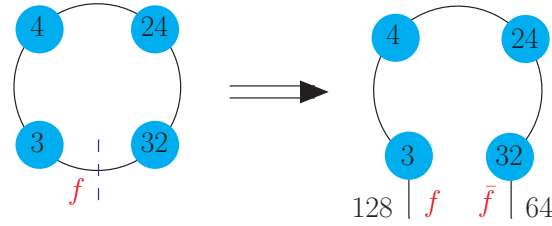
Figure 2.2: Cutting a propagator from the one-loop amplitude with n external particles results to a $(n+2)$-particle tree-level amplitude, which can be calculated by `HELAC`. The two cut particles have flavors $\bar{f}$ and f, respectively, and obtain the usual `HELAC` notation, meaning 2^n and $2^{(n+1)}$, respectively.

Concerning the one-loop blob-topologies, in an n-particle process there will contribute topologies with $n, n-1, n-2, \ldots, 1$ blobs attached on the loop. For a better understanding and visualization of the one-loop blob-topologies we quote in Figure 2.1 a typical collection of possible contributions to a 6-particle process. By convention in `HELAC-1LOOP`, the loop momentum in blob-topologies flows counterclockwise, and the propagator bearing momentum $\bar{k}^2$ (with $\bar{k}$ denoting the 4-dimensional part of the loop momentum) is the one between the blob that contains the particle 1 and the last blob. As the last blob is defined the first blob encountered after the blob that contains the particle 1, moving counterclockwise on the loop, e.g. in the hexagonal topology of Figure 2.1, the last blob is the one with ID number 32. Thus the numbering of the blobs in the blob-topologies always starts from the blob containing the particle 1 and continues following a clockwise flow on the loop, as we can see in the examples of Figure 2.1.

After the generation of the blob-topologies, the loop-particles of each topology are dressed with flavor and color, in all possible ways, using SM Feynman rules and the color-flow representation[12]. In this way, all the configurations that contribute to the partial amplitudes are constructed. This procedure is equivalent to drawing all one-loop Feynman diagrams and then collecting them in sub-classes that are characterized by a common loop-assignment structure. For the construction of each numerator, the corresponding configuration is cut on the propagator that connects the last blob and the blob containing the particle 1. The two extra external particles arising from the cut, obtain the number IDs 2^n and 2^{n+1}, respectively, and their flavor is defined by the flavor of the cut loop-particle, f, with the particle 2^{n+1} bearing flavor f and the particle 2^n bearing flavor $\bar{f}$ (see Figure 2.2). The cut also results in the addition, to the existing color connection, of two more color lines if the cut-propagator is a gluon/ghost or one more color line if it is a quark/anti-quark, with the extra lines corresponding to the two extra particles. Afterward, the color connection of the cut configuration is relabeled accordingly by tracking again the flow of color (see [97]).

Having created an $n+2$ tree-level configuration with a specified flavor and color for the $n+2$ particles, and with fixed loop-assignment structure and flavors for the loop-particles, `HELAC-1LOOP` constructs and stores as a sequence of sub-amplitudes all the information needed for the computation of the corresponding numerator. The sequence of sub-amplitudes respects the loop-assignment structure of the configuration, meaning

---

[12]The one-loop color dressing is done by tracking at each vertex the flow of color. For more details, we refer to [97].

that it starts from the particle 2^n and combines it with the last blob in order to create the next sub-amplitude that describes the corresponding loop-particle. Then, the latter sub-amplitude is subsequently combined with the next blob (penultimate) in order to create the sub-amplitude of the corresponding loop-particle, and this procedure goes on till arriving at the (first) blob which is combined (except for the particle 1) with the previous sub-amplitude and the particle 2^{n+1}, in such a way that the particle 1 to be always the last particle of the recursion. At each step, Dyson-Schwinger recursion is applied to the blobs, creating sub-amplitudes containing only external particles.

For a given set of momenta (including the loop momentum[13]) and polarizations of the external particles (including the cut-particles), a numerator is computed by multiplying the last sub-amplitude of the recursion, identified by the ID number $2^{n+2} - 2$, with the wave function of the particle 1. This is part of the computation phase of `HELAC-1LOOP`, where also the reduction to master integrals and the actual computation of the scattering amplitude is done. For the computation of the last sub-amplitude, no denominators are used for the sub-amplitudes of the internal loop propagators, and the wave functions for the two extra particles are suitably chosen in such a way that the contraction originally contained in the loop is reproduced. Working in the Feynman gauge, the wave functions of fermions $(\nu^{(i)}(p), \bar{\nu}^{(i)}(p))$ and gauge bosons $(e^\mu_{(i)})$ for the two extra particles are defined so that to satisfy the following relations

$$\sum_{i=1}^{2} \bar{\nu}^{(i)}(p)\nu^{(i)}(p) = \not{p} + m \quad \text{and} \quad \sum_{i=1}^{4} e^\mu_{(i)} e^\nu_{(i)} = g^{\mu\nu}. \tag{2.42}$$

Ghost particles are also included in this procedure, and in that case, the sum should be equal to 1. Thus for computing the 4-dimensional part of a one-loop n-particle numerator using the `HELAC-1LOOP` algorithm, we need to take a sum of four (two) [one] tree-level $(n + 2)$-particle amplitudes, which differ only on the wave functions of the extra two gluons (quarks/anti-quarks) [ghosts] resulted by the cut propagator, with the latter being defined for each term of the sum so that Eq. (2.42) to be fulfilled. This is taken into account in the computation phase.

Within the initialization phase of `HELAC-1LOOP`, in the skeleton beside the construction and storage of the one-loop 4-dimensional numerators that contribute to the process at hand, there are also constructed and stored, using the tree-level Dyson-Schwinger recursion algorithm, the UV and R_2 counter-terms. The UV counter-terms, as discussed in Subsection 1.2.2, are necessary in order to renormalize the one-loop scattering amplitude. The R_2 counter-terms are needed for the computation of the rational part of the amplitude resulting from the explicit ε-dimensional part of the numerators, and these can be produced using appropriate Feynman rules within a tree-like computation [99–102].

---

[13]In `HELAC-1LOOP` the value of the loop-momentum is specified by `CutTools` [98], which is reducing the numerator into a set of master integrals using the OPP method. The cut-particle 2^n acquires momentum $\bar{k}$ and the cut-particle 2^{n+1} acquires momentum $-\bar{k}$.

2.4   Amplitude Reduction

2.4.1   The One-loop Paradigm

According to our notation established in Eqs. (2.3)-(2.4), the general form of a one-loop n-particle color-stripped amplitude is

$$\mathcal{A}_n^{(1)} = \int \frac{\mu^{(4-d)} d^d k}{(2\pi)^d} \, A_n^{(1)} = \sum_{I \subseteq T} \int \frac{\mu^{(4-d)} d^d k}{(2\pi)^d} \frac{N_I(k, p_1, ..., p_{n-1}, \gamma^\mu, \{\epsilon^\mu\})}{\prod_{j \in I} D_j}, \qquad (2.43)$$

with the inverse propagator defined as in Eq. (2.5) but for $k_j \to k$, due to having only one loop momentum. A surprisingly long time ago [103–107], as a consequence of Lorentz invariance it was proven that, for $d \to 4$ any one-loop scattering amplitude can be cast into the following form

$$\begin{aligned}
\mathcal{A}_n^{(1)} = &\sum_{i_0 < i_1 < i_2 < i_3} d(i_0, i_1, i_2, i_3) \, F_{i_0 i_1 i_2 i_3} + \sum_{i_0 < i_1 < i_2} c(i_0, i_1, i_2) \, F_{i_0 i_1 i_2} \\
&+ \sum_{i_0 < i_1} b(i_0, i_1) \, F_{i_0 i_1} + \sum_{i_0} a(i_0) \, F_{i_0} + R + \mathcal{O}(\varepsilon)
\end{aligned} \qquad (2.44)$$

where $F_{i_0 i_1 i_2 i_3}$ (*boxes*), $F_{i_0 i_1 i_2}$ (*triangles*), $F_{i_0 i_1}$ (*bubbles*), and F_{i_0} (*tadpoles*) refer to the well-known scalar one-loop master integrals [108–111] with four, three, two, and one external particles, respectively,

$$F_{i_0 \ldots i_{n-1}} = \int \frac{d^d k}{(2\pi)^d} \frac{1}{D_{i_0} D_{i_1} \ldots D_{i_{n-1}}}. \qquad (2.45)$$

In expression (2.44) the coefficients of the master integrals are rational functions of the external momenta, polarization vectors, and masses and are independent of the dimensional regulator. Of the same form but with extra ε dependence is the so-called *rational part* [46, 112] of the amplitude, denoted above as R. The rest of the amplitude can be computed using generalized unitarity cuts and is thus called *cut-constructible part* [46, 47, 112–116]. We comment here that in Eq. (2.44) the ε dependence of the amplitude comes from the master integrals and R.

For the reduction to the set of scalar one-loop master integrals, several methods can be applied besides the standard Passarino-Veltman reduction [106, 117, 118]. Some of them are applied at the *integral level*, like the IBP reduction [48, 49] and the (generalized) unitarity cut method [46, 47, 112–116, 119, 120]. The most successful ones that led to the automation of one-loop amplitude reduction are the ones applied at the *integrand level*. Such methods are the *OPP method* [91, 92], the *4-dimensional numerical unitarity*[14] [122], the *d-dimensional numerical unitarity* [123–125], etc [126, 127]. Within the methods of [123–127] the reduction happens at d-dimensions, meaning that the integrand is constructed in $d-$dimensions working with tree-amplitudes in higher dimensions[15], and the expression in Eq. (2.44) is modified such that the rational part

---

[14]This method in practice applies an OPP approach to the reduction of the amplitude but as a basis for the decomposition of the loop momentum is using the van Neerven-Vermaseren basis [107] instead of the basis used within OPP [91, 121].

[15]For these computations the wave functions, polarization vectors, and Clifford algebra, are extended in higher dimensions.

is included in the extra master integrals and the coefficients of the reduction

$$
\mathcal{A}_n^{(1)} = \sum_{i_0 < i_1 < i_2 < i_3 < i_4} e^*_{i_0 i_1 i_2 i_3 i_4} F_{i_0 i_1 i_2 i_3 i_4} + \sum_{i_0 < i_1 < i_2 < i_3} d^*_{i_0 i_1 i_2 i_3} F_{i_0 i_1 i_2 i_3}
$$
$$
+ \sum_{i_0 < i_1 < i_2} c^*_{i_0 i_1 i_2} F_{i_0 i_1 i_2} + \sum_{i_0 < i_1} b^*_{i_0 i_1} F_{i_0 i_1} + \sum_{i_0} a^*_{i_0} F_{i_0} + \mathcal{O}(\varepsilon). \tag{2.46}
$$

The difference between the relations (2.44) and (2.46) is that in the latter, master integrals with five external particles (pentagons) are also included while the rational terms are excluded, and the coefficients of the master integrals depend now on the dimensional regulator.

Let's focus now on the OPP method. The main idea of this method is that the 4-dimensional part of any one-loop numerator is decomposed as

$$
\bar{N}_I(\bar{k}) = \sum_{i_0 < i_1 < i_2 < i_3}^{I} \left[d(i_0, i_1, i_2, i_3) + \tilde{d}(\bar{k}, i_0, i_1, i_2, i_3) \right] \prod_{i \neq i_0, i_1, i_2, i_3}^{I} \bar{D}_i
$$
$$
+ \sum_{i_0 < i_1 < i_2}^{I} \left[c(i_0, i_1, i_2) + \tilde{c}(\bar{k}, i_0, i_1, i_2) \right] \prod_{i \neq i_0, i_1, i_2}^{I} \bar{D}_i
$$
$$
+ \sum_{i_0 < i_1}^{I} \left[b(i_0, i_1) + \tilde{b}(\bar{k}, i_0, i_1) \right] \prod_{i \neq i_0, i_1}^{I} \bar{D}_i
$$
$$
+ \sum_{i_0}^{I} \left[a(i_0) + \tilde{a}(\bar{k}, i_0) \right] \prod_{i \neq i_0}^{I} \bar{D}_i, \tag{2.47}
$$

where with a bar we denote the quantities living in 4 dimensions. In this expression the coefficients $d(i_0, i_1, i_2, i_3)$, $c(i_0, i_1, i_2)$, $b(i_0, i_1)$ and $a(i_0)$ are the same with the ones appearing in Eq. (2.44), while the tilted coefficients (which are still $\bar{k}$-depended) vanish upon integration on $d^d k$ and are known as *spurious terms*. The explicit form of the spurious terms was proven in [91] by decomposing $\bar{k}$ into a basis of massless momenta

$$
\bar{k}^\mu = -p_0^\mu + \frac{(\bar{k}+p_0)\cdot \ell_2}{(\ell_1 \cdot \ell_2)} \ell_1^\mu + \frac{(\bar{k}+p_0)\cdot \ell_1}{(\ell_1 \cdot \ell_2)} \ell_2^\mu - \frac{(\bar{k}+p_0)\cdot \ell_4}{4(\ell_1 \cdot \ell_2)} \ell_3^\mu - \frac{(\bar{k}+p_0)\cdot \ell_3}{4(\ell_1 \cdot \ell_2)} \ell_4^\mu, \tag{2.48}
$$

where for a symmetric treatment of the inverse propagators a non-vanishing momentum p_0^μ is introduced (this does not change the result due to translation invariance, see Eq. (1.14)), and the momenta $\{\ell_1, \ell_2, \ell_3, \ell_4\}$ are defined via the relations

$$
\ell_1^\mu = \frac{K_1^\mu - a_1 K_2^\mu}{1 - a_1 a_2}, \quad \ell_2^\mu = \frac{K_2^\mu - a_2 K_1^\mu}{1 - a_1 a_2}, \quad \ell_3^\mu = \bar{u}_-(\ell_1)\gamma^\mu u_-(\ell_2), \quad \ell_4^\mu = \bar{u}_-(\ell_2)\gamma^\mu u_-(\ell_1),
$$

with

$$
K_i^\mu = p_i^\mu - p_0^\mu, \quad a_i = K_i^2/\gamma, \quad \text{and} \quad \gamma = 2(\ell_1 \cdot \ell_2) = K_1 \cdot K_2 \pm \sqrt{(K_1 \cdot K_2)^2 - K_1^2 K_2^2}.
$$

In the definition of γ, the minus (plus) sign is used when $p_1 \cdot p_2 > 0$ ($p_1 \cdot p_2 < 0$). As we see, the first two elements of the basis (ℓ_1, ℓ_2) are linear combinations of two external momenta of the sub-diagram identified by the considered set of inverse propagators, and the rest two (ℓ_3, ℓ_4) are chosen to be orthogonal to them by using spinor techniques.

If the sub-diagram has less than two independent external momenta, ℓ_2 or/and ℓ_1 are substituted by arbitrary reference vectors. Without giving exact expressions for their form (one can find them in [91]) we state that for each term of the sums in Eq. (2.47) the spurious terms $\tilde{a}(\bar{k}, i_0)$ are composed of four terms, $\tilde{b}(\bar{k}, i_0, i_1)$ from eight, $\tilde{c}(\bar{k}, i_0, i_1, i_2)$ from six, and $\tilde{d}(\bar{k}, i_0, i_1, i_2, i_3)$ from one. For example, in the case of a 6-point one-loop scattering amplitude where 56 master integrals contribute to its computation there exist $56 \times (19 + 4) = 1288$ unknown coefficients (spurious and not) in the decomposition of Eq. (2.47).

The existence of the decomposition of Eq. (2.47) implies that the problem of computing a one-loop amplitude is reduced to the algebraic problem of determining the coefficients of the master integrals and spurious terms, plus the calculation of the rational part of the amplitude. Within OPP, the coefficients are determined by solving iteratively systems of equations, by evaluating the LHS and the RHS of Eq. (2.47) at values of $\bar{k}$ that are solutions of

$$\bar{D}_i(\bar{k}) = 0, \text{ for } i = 0, ..., M - 1, \text{ and } M = 4, ..., 1. \tag{2.49}$$

Using a top-down approach (from more to fewer propagators) the system of equations becomes triangular, namely one starts with the determination of the coefficients $\{d(i_0, i_1, i_2, i_3), \tilde{d}(\bar{k}, i_0, i_1, i_2, i_3)\}$ by finding two solutions of the loop momentum that satisfy $D_{i_0} = D_{i_1} = D_{i_2} = D_{i_3} = 0$. For these solutions, all the other coefficients do not appear in the system of equations. Then having determined $\{d(i_0, i_1, i_2, i_3), \tilde{d}(\bar{k}, i_0, i_1, i_2, i_3)\}$, one continues for the determination of $\{c(i_0, i_1, i_2), \tilde{c}(\bar{k}, i_0, i_1, i_2)\}$ by finding seven loop momenta that satisfy $D_{i_0} = D_{i_1} = D_{i_2} = 0$. At this step the coefficients $\{b(i_0, i_1), \tilde{b}(\bar{k}, i_0, i_1), a(i_0), \tilde{a}(\bar{k}, i_0)\}$ do not appear in the system of equations and $\{d(i_0, i_1, i_2, i_3), \tilde{d}(\bar{k}, i_0, i_1, i_2, i_3)\}$ are not considered anymore unknowns. This procedure ends up with the determination of $\{a(i_0), \tilde{a}(\bar{k}, i_0)\}$[16].

Within the OPP reduction framework, the rational terms of the amplitude come from two sources of different origin [91, 99], which is to say

$$R = R_1 + R_2. \tag{2.50}$$

The first source denoted, as R_1, originates from the mismatch in the cancellation of the $d-$dimensional denominators of Eq. (2.43) with the 4-dimensional ones of Eq. (2.47). This mismatch is compensated by introducing in the coefficients of Eq. (2.47) a $\mu_{11} = (k^*)^2$ dependence (k^* being the ε-dimensional part of the loop momentum) through the mass shift

$$m_i^2 \to m_i^2 - \mu_{11}. \tag{2.51}$$

Due to vanishing because of Lorentz invariance, the spurious terms remain spurious under this change, while for the coefficients b, c, one can prove that change as

$$\begin{aligned} b(i_0, i_1; \mu^2) &= b(i_0, i_1) + \mu_{11} b^{(2)}(i_0, i_1) \\ c(i_0, i_1, i_2; \mu^2) &= c(i_0, i_1, i_2) + \mu_{11} c^{(2)}(i_0, i_1, i_2). \end{aligned} \tag{2.52}$$

---

[16]In practice for the determination of $a(i_0)$ one needs only two (not five) solutions of loop momenta. Also when working with an amplitude where the particles that appear in the loop are massless, the tadpole coefficients do not need to be computed at all, and for computing $b(i_0, i_1)$ one needs four instead of nine solutions.

Furthermore, by using Eq. (2.51) in Eq. (2.47) its first line in d-dimensions takes the form

$$\mathcal{D}^{(n)}(\bar{k}^2, \mu_{11}) \equiv \sum_{i_0 < i_1 < i_2 < i_3}^{n-1} \left[d(i_0, i_1, i_2, i_3; \mu_{11}) + \tilde{d}(\bar{k}, i_0, i_1, i_2, i_3; \mu_{11}) \right] \prod_{i \neq i_0, i_1, i_2, i_3}^{n-1} D_i, \tag{2.53}$$

and the following expansion holds true

$$\mathcal{D}^{(n)}(\bar{k}^2, \mu_{11}) = \sum_{j=2}^{n} \mu_{11}^{j-2} d^{(2j-4)}(\bar{k}), \tag{2.54}$$

where the last coefficient is independent of $\bar{k}$, namely $d^{(2n-4)}(\bar{k}) \equiv d^{(2n-4)}$. For the calculation of the μ_{11} parts of the coefficients, once the 4-dimensional coefficients have been determined, one simply redoes the fits for different values of μ_{11}. Finally, the R_1 term is computed via the following expression

$$R_1 = \frac{d^{(2n-4)}}{(2\pi)^4} R_{1,1} + \sum_{i_0 < i_1 < i_2}^{n-1} \frac{c^{(2)}(i_0, i_1, i_2)}{(2\pi)^4} R_{1,2} + \sum_{i_0 < i_1}^{m-1} \frac{b^{(2)}(i_0, i_1)}{(2\pi)^4} R_{1,3} \tag{2.55}$$

where $R_{1,1}$, $R_{1,2}$ and $R_{1,3}$ are the following extra integrals

$$\begin{aligned}
R_{1,1} &\equiv \int d^d k \frac{\mu_{11}^2}{D_{i_0} D_{i_1} D_{i_2} D_{i_3}} = -\frac{i\pi^2}{6} + \mathcal{O}(\varepsilon) \\
R_{1,2} &\equiv \int d^d k \frac{\mu_{11}}{D_{i_0} D_{i_1} D_{i_2}} = -\frac{i\pi^2}{2} + \mathcal{O}(\varepsilon) \\
R_{1,3} &\equiv \int d^d k \frac{\mu_{11}}{D_{i_0} D_{i_1}} = -\frac{i\pi^2}{2} \left(m_{i_0}^2 + m_{i_1}^2 - \frac{(p_{i_0} - p_{i_1})^2}{3} \right) + \mathcal{O}(\varepsilon)
\end{aligned} \tag{2.56}$$

generated by the μ_{11} dependence of the OPP coefficients. The OPP reduction, meaning the computation of the OPP coefficients of Eq. (2.47) and the R_1 rational term of Eq. (2.55), is automated within `CutTools` [98], where a specific choice for the solutions of the loop momenta that satisfy Eq. (2.49) is chosen according to [91].

Concerning the second source of rational terms, denoted as R_2 in (2.50), this term originates from the explicit dependence of the numerator on ε. Given a numerator, one can recognize the R_2 term by performing the algebraic manipulations in d dimensions and isolating the terms depending on ε[17]

$$N_I(k) = \bar{N}_I(\bar{k}) + N_I^*(\bar{k}, \mu_{11}, \varepsilon) \tag{2.57}$$

resulting from the ε components of

$$\begin{aligned}
k_\mu &= \bar{k}_\mu + k_\mu^* \\
\gamma_\mu &= \bar{\gamma}_\mu + \gamma_\mu^* \\
g_{\mu\nu} &= \bar{g}_{\mu\nu} + g_{\mu\nu}^*
\end{aligned} \tag{2.58}$$

---

[17] With a star we denote ε-dimensional part of an expression.

R_2 is then defined via the following equation in the 't Hooft-Veltman (HV) scheme

$$R_2 = \int \frac{d^d k}{(2\pi)^4} \frac{N_I^*(\bar{k}, \mu_{11}, \varepsilon)}{\prod_{j \in I} D_j}. \tag{2.59}$$

A practical way to compute R_2 is determining appropriate tree-level Feynman rules (effective vertices like counter-terms) by computing, using Eq. (2.58), the R_2 part coming from all possible one-particle irreducible amplitudes of the theory at hand, up to four external legs. The fact that four external legs are enough to account for the R_2 is guaranteed by the UV nature of the rational terms [128]. The tree-level Feynman rules for the computation of the R_2 term in QCD and SM can be found in [99–102].

The OPP method together with the other methods quoted at the beginning of this subsection, led to the, once and for all, solution of the problem of amplitude reduction at one-loop level and thus the calculation of scattering amplitudes and cross sections for many processes at NLO (*NLO revolution*). By now several highly automated packages such as `HELAC-NLO` [88], `Recola` [89, 90], `MadGraph5_AMC@NLO` [129, 130], `OpenLoops` [131, 132], `GoSam` [133, 134] and other public or private tools exist for the computation of one-loop scattering amplitudes within the SM.

2.4.2 Multi-loop Techniques

Due to increased complexity, the reduction of any multi-loop scattering amplitude into a set of master integrals is currently not automated as in the one-loop case. Although not automated, much progress has been done in the last years leading to the computation of many two- and three-loop scattering amplitudes, where the current frontier stands at four- and five-particle processes, respectively [135, 136]. The methods used for these computations can be categorized into two categories according to the level of the amplitude at which the reduction happens.

In the first category, the reduction happens at the *integral level*, using IBP identities [48, 49, 54]. Notwithstanding that the concept of this method is clear, the computational cost of solving IBP identities increases very fast with the multiplicity of the amplitude making the reduction for processes with five and more particles impossible without the use of computer clusters with many cores and high capacity of RAM memory. For this reason, many methods have been developed in order to facilitate the solution or generation of the IBP identities or to optimize the form of the amplitude before the reduction [65, 66, 68–75, 137–140]. The reduction at the integral level has produced in last years several state-of-the-art results for two-loop (see [141–157]) and three-loop (see [158–163]) scattering amplitudes.

In the second category the reduction happens at the *integrand level*, where the scattering amplitude is decomposed into a basis of master integrands, that integrate to master integrals, and surface terms, that integrate to zero [164]. The basis is constructed case by case according to the process at hand, and the coefficients of the decomposition are computed using a generalization of the one-loop d-dimensional generalized numerical unitarity [164–166]. This method has been applied for the numerical and analytical computation of frontier scattering amplitudes up to two-loops [166–175], and is implemented (for specific processes and kinematic regions) in a publicly available package, called `Caravel` [176].

It is worth mentioning also that in recent years, progress has been made towards the extension at two-loops of the one-loop methods applied for the 4-dimensional integrand reduction into tensor integrals [177], and towards the computation of the rational terms originating by the explicit ε-dependence of the two-loop numerators [178–180].

Chapter 3

Feynman Integrals

In this chapter we review the concept of Feynman Integrals, considering their basic properties and two of their parametric representations. Furthermore, we tackle the computation of Feynman Integrals using the method of differential equations and a variant of it, the simplified differential equations approach. For a more in-depth discussion, we refer the interested reader to standard textbooks and reviews [181–186].

3.1 Introduction to Feynman Integrals

As we have seen in the previous chapter, the task of computing a scattering amplitude includes the calculation of scalar *Feynman integrals* (FIs). To each FI one can associate a *Feynman graph* (and vice-versa), defined as a directed and connected graph constructed by external half-edges (external legs), and internal edges (propagators), connected via vertices that respect momentum conservation and that do not have a limitation on the number of edges that can connect. Each independent cycle of the graph is called a loop and it introduces an arbitrary loop momentum. The external legs bear momenta being linear combinations of the momenta of the external particles of the process at hand, with the total momentum of the external legs to be conserved. The propagators are assigned a mass and a momentum that is a linear combination of external and loop momenta.

For the calculation of FIs, it is convenient to group them into *integral families* according to the topology of the loop Feynman diagrams and the kinematics of the process at hand. Roughly speaking, the *integral family* is the set of all the FIs with a given propagator structure, allowing for arbitrary integer powers of the propagators. This includes also cases with fewer propagators, i.e. sub-graphs, when the integer powers are equal to zero. More specifically, an *integral family* of FIs with L loops and $E + 1$ external legs (E independent momenta p_j[1]) associated to a Feynman graph with n_{top} propagators, is defined through the relation

$$G_{\alpha_1 \ldots \alpha_N}(s, \varepsilon) = \int \left(\prod_{j=1}^{L} e^{\gamma_E \varepsilon} \frac{d^d k_j}{i \pi^{d/2}} \right) \frac{\prod_{j=n_{top}+1}^{N} D_j^{-\alpha_j} (\{k\}, \{p\}, m_j)}{\prod_{j=1}^{n_{top}} D_j^{\alpha_j} (\{k\}, \{p\}, m_j)} , \qquad (3.1)$$

---

[1]Considering a scattering process with n external particles, $E = \min(4, n-1)$ of them are independent due to four-momentum conservation and the 4-dimensional nature of space-time.

where $s = \{s_{ij}\} \cup \{m^2\}$ is the set of kinematic invariant scales of the family, as these are defined in section 1.1,

$$s_{ij} = s_{ji} = (p_i + p_j)^2 \text{ with } j > i, \text{ and } \{m^2\} : \text{set of internal/external masses}, \quad (3.2)$$

α_j are arbitrary integers of which $\alpha_{n_{top}+1}, \ldots, \alpha_N$ are non-positive, and N is the number of scalar products containing loop momenta (i.e. $k_i \cdot k_j$ and $k_i \cdot p_j$),

$$N = \frac{L(L+1)}{2} + L \cdot E, \quad (3.3)$$

and is equal to the number of linear independent propagators of the family, which are of the form[2] (similar to Eqs. (2.5) and (2.6))

$$D_j = \left(\sum_{i=1}^{L} b_i^{(j)} k_i + \sum_{i=1}^{n-1} b_i'^{(j)} p_i \right)^2 - m_j^2 + i\epsilon, \quad \text{with} \quad b_i^{(j)}, b_i'^{(j)} = 0, \pm 1. \quad (3.4)$$

Starting from $L > 1$, there exists a set of propagators ($N - n_{top}$ in the number) coming from *irreducible scalar products*, meaning scalar products of loop momenta that can not be expressed as a linear combination of the n_{top} propagators of the family[3]. These propagators are usually called *auxiliary propagators* and can appear only to the numerator of a FI, thus their corresponding integer powers are non-positive. The auxiliary propagators are not uniquely fixed, but they are constrained only by the requirement that together with the n_{top} propagators they form a linearly independent basis, in terms of which can be expressed all the scalar products involving loop momenta.

As we have already discussed in the previous chapters, in order to regularize IR and UV divergences, FIs are defined and computed within the scheme of dimensional regularization (DR), where we have $d = 4 - 2\varepsilon$ space-time dimensions (1 time dimension and $d - 1$ space dimensions). In this framework, assuming that all the propagators are quadratic, $G_{\alpha_1 \ldots \alpha_N}$ is a homogeneous function of external momenta and internal masses of degree $\deg = L \cdot d - 2 \sum_{i=1}^{N} \alpha_i$, and satisfy the scaling relation

$$G_{\alpha_1 \ldots \alpha_N}(s \cdot \lambda, \varepsilon) = \lambda^{\deg/2} G_{\alpha_1 \ldots \alpha_N}(s, \varepsilon). \quad (3.5)$$

Within DR, if a FI is scaleless it vanishes. Moreover, it can be shown that a FI can have at most poles of multiplicity $2l$ in the complex $\varepsilon-$plane, but no branch cuts, i.e. it is a meromorphic function of ε. This is a very important property of FIs as it allows us to write a Laurent expansion around (the point of interest) $\varepsilon = 0$

$$G_{\alpha_1 \ldots \alpha_N}(s, \varepsilon) = \sum_{i \geq i_0} \varepsilon^i G_{\alpha_1 \ldots \alpha_N}^{(i)}(s), \quad (3.6)$$

and focus our interest on the determination of the coefficients of the expansion. If $i_0 < 0$ then $G_{\alpha_1 \ldots \alpha_N}$ is divergent in 4 dimensions.

---

[2]In the following, we will not write the dependence of the propagators on the $+i\epsilon$ prescription explicitly anymore, except for the cases where it is important for our discussion.

[3]Let us comment here that the definition of irreducible scalar products in this chapter does not include the scalar products of loop momenta with four-vectors transverse to the external momenta (defined in chapter 2). In fact, these kinds of scalar products do not exist at the integral level as they integrate to zero.

Although an integral family contains an infinite number of FIs, the IBP identities (discussed in subsection 2.1.2) imply the existence of a finite basis of independent integrals, the *master integrals* (MIs) of the family. There exists a freedom in the choice of this basis, and any FI of the family can be expressed as a linear combination of MIs with some algebraic coefficients of the kinematic invariant scales and ε. A useful notion for the organization of FIs is this of the *integral sector*, defined as any possible set T of the n_{top} propagators of the family. In general, one integral family has $2^{n_{\text{top}}}$ sectors but due to IBP relations and symmetry relations, only some of them contain integrals contributing to the MIs of the family. The sector containing all the n_{top} propagators is called *top-sector* while all the other sectors, which have fewer propagators are called *lower-sectors.*

3.2 Representations of Feynman Integrals

Except for the straightforward form of FIs in the momentum-space (Eq. (3.1)), which is directly connected with the concept of Feynman graphs, other alternative representations of FIs exist. Each of them is optimal for the evaluation or the study of different properties of the FIs. For the purposes of this thesis, we will focus on two parametric representations, the *Feynman* and the *Baikov representation.*

3.2.1 Feynman Representation

The Feynman representation of FIs is obtained by trading the integration over the loop momenta with integrations over the so-called *Feynman parameters*, x_j [186–188]. Assuming the case where the FI doesn't contain auxiliary propagators, this happens by first converting the product of propagators into sums using *Feynman's trick*[4]

$$\prod_{j=1}^{n} \frac{1}{D_j^{\alpha_j}} = \frac{\Gamma(\alpha)}{\prod_{j=1}^{n} \Gamma(\alpha_j)} \int_0^\infty \left(\prod_{j=1}^{n} dx_j\, x_j^{\alpha_j-1} \right) \frac{\delta\left(1 - \sum_{j=1}^n x_j\right)}{\left(\sum_{j=1}^n x_j D_j\right)^{\alpha}} \quad \text{with} \quad \alpha \equiv \sum_{j=1}^{n} \alpha_j, \quad (3.7)$$

The sum of propagators appearing in the denominator above can be expressed as

$$\sum_{j=1}^{n} x_j D_j = \sum_{r,s=1}^{l} M_{rs} k_r \cdot k_s - 2 \sum_{r=1}^{l} k_s \cdot Q_r + J + i\epsilon \qquad (3.8)$$

with M an $L \times L$ matrix with scalar entries and Q a L-component vector with four-vectors as entries. Then, one can perform the integrations over the loop momenta using shifts for each loop momentum and translation invariance of d-dimensional integrals (Eq. (1.14)). This procedure leads to the following form for a FI with n propagators (where none of them is auxiliary)

$$G = (-1)^{\alpha} e^{L\gamma_E \varepsilon} \frac{\Gamma(\alpha - Ld/2)}{\prod_{j=1}^{n} \Gamma(\alpha_j)} \int_0^\infty \left(\prod_{j=1}^{n} dx_j\, x_j^{\alpha_j-1} \right) \delta\left(1 - \sum_{j=1}^{n} x_j \right) \frac{\mathcal{U}^{\alpha-(L+1)d/2}}{\mathcal{F}^{\alpha-Ld/2}}, \quad (3.9)$$

---

[4]Although broadly known as Feynman's trick it was actually Schwinger the one who invented it.

where $\mathcal{U}$ and $\mathcal{F}$ are given by the expressions

$$\mathcal{U} = \det(M) \quad \text{and} \quad \mathcal{F} = \mathcal{U} \times \left(QM^{-1}Q - J - i\varepsilon\right), \tag{3.10}$$

and are known as the *first* and *second Symanzik polynomial*, respectively. $\mathcal{U}$ is a homogeneous polynomial in Feynman parameters of degree l, it is linear in each x_j, and each of its monomials has $+1$ as coefficient. Thus the first Symanzik polynomial does not vanish inside the integration region, except maybe on its boundary. The second Symanzik polynomial is a homogeneous polynomial in x_j's of degree $L+1$, and contains also kinematic invariants beside Feynman parameters. $\mathcal{F}$ can vanish within the integration region as the coefficients of its monomials do not have all of them the same sign, resulting in divergences after integration. The location of these singularities can be found from the Landau equations [44, 189]. Requiring the invariants appearing in the monomials of $\mathcal{F}$ to be such that all the monomials have the same sign, defines the *Euclidean region* of a FI, where all the external invariants $(p_i + \cdots + p_j)^2 \leq 0$ and all the internal masses are positive. In the Euclidean region, the FI is free of branch cuts and evaluates to real numbers. For a family of FIs, the Euclidean region is defined via the $\mathcal{F}$ polynomial of the top sector (the integral with n_{top} propagators).

In order to generalize Eq. (3.9) so that to include auxiliary propagators one needs to compute the derivative instead of the integral for the corresponding Feynman parameters [190, 191]. For us to be consistent with the notation of the previous section, let us assume dealing with a FI with n_{top} propagators and $N - n_{\text{top}}$ auxiliary propagators, $G_{\alpha_1 \ldots \alpha_N}$. Then, keeping the same definition for the Symanzik polynomials but including to them also the auxiliary propagators (taking the sum in Eq (3.7) till N), the Feynman representation of $G_{\alpha_1 \ldots \alpha_N}$ reads

$$
\begin{aligned}
G_{\alpha_1 \ldots \alpha_N} =& (-1)^{\bar{\alpha}} e^{L\gamma_E \varepsilon} \frac{\Gamma(\alpha - Ld/2)}{\prod_{j=1}^{n_{\text{top}}} \Gamma(\alpha_j)} \int_0^\infty \left(\prod_{j=1}^{n_{\text{top}}} dx_j\, x_j^{\alpha_j - 1} \right) \delta\left(1 - \sum_{j=1}^{n_{\text{top}}} x_j \right) \\
& \times \left(\left[\prod_{j=n_{\text{top}}+1}^{N} \frac{\partial^{\alpha_j}}{\partial x_j^{\alpha_j}} \right] \frac{\mathcal{U}^{\alpha - (L+1)d/2}}{\mathcal{F}^{\alpha - Ld/2}} \right) \Bigg|_{x_{\text{top}+1} = \cdots = x_N = 0},
\end{aligned}
\tag{3.11}
$$

where

$$\bar{\alpha} = \sum_{j=1}^{n_{\text{top}}} \alpha_j \quad \text{and} \quad \alpha = \sum_{j=1}^{N} \alpha_j. \tag{3.12}$$

A beneficial property of the delta function appearing in Eqs. (3.9)-(3.11) is that, according to Cheng-Wu theorem[5] [192], one can choose not to keep all the Feynman parameters appearing in its argument but only a subset of them and the result of the integration to be the same. This means that one can do the following trade

$$\delta\left(1 - \sum_{j=1}^{n} x_j\right) \longrightarrow \delta\left(1 - \sum_{j=1}^{n} a_j x_j\right), \tag{3.13}$$

with $a_j \geq 0$ and at least one $a_j \neq 0$.

---

[5]This hold true for all the functions satisfying $\int dx_j f(\{x_j\}) = \int dx_j' f(\{x_j'\})$, for $x_j' = cx_j$, with c being a constant.

The Feynman representation is the most widely used parametric representation of FIs, as it has been applied for both analytic and numerical computations. The analytic computations are obtained by direct integration over Feynman parameters (see for example [193–197]), where the package `HyperInt` [195] can be used to facilitate the integrations whenever possible. Let us mention that the integrations in the Feynman parameters are not always doable and this has led to the development of other methods for the analytic computation of FIs, such as the method of differential equations that we are going to discuss in the next section. For the numerical computations the method of *sector decomposition* [128, 198] is used, where the integration region is decomposed into sectors with simple singularity structure, the integrals are expanded on ε and the integration of their finite coefficients is done numerically. The method of sector decomposition is implemented within the public codes `pySecDec` [199, 200] and `FIESTA` [201]. Although these packages are able to provide high precision results for several multi-loop and multi-scale FIs in the Euclidean region, this is not the case of phase-space points for kinematic regions of physical interest from the scattering point of view (*physical regions*), which are relevant for phenomenological applications.

Another important application of Feynman's representation for the modern computation of FIs, through the method of differential equations, is its adaption for the determination of boundary conditions of MIs to asymptotic limits, using the method of *expansion by regions* [202–207]. The core principle of this method is that one can compute the asymptotic value of a FI to a limit where some of its variables are small, by partitioning the space of loop momenta into distinct regions, Taylor expanding the integrand within each region with respect to the variables that are deemed to be small (in that particular region), and performing the integrations of the expanded integrand across the entire domain of loop momenta. The scaleless integrals generated by this procedure should be set to zero. This corresponds to the application of expansion by regions in the standard momentum representation of FIs. The same method can be applied in the Feynman representation, where the regions are specified by the scaling of the Feynman parameters in terms of the powers of the small variables. A geometric approach for the identification of the regions that contribute to an asymptotic limit of a FI, together with the Feynman parametric form of the integral in each region was first formulated in [204] and implemented in the `MATHEMATICA` script `asy.m`. The last version of `asy.m` is shipped along with `FIESTA` [201], while also another public implementation is included in the last version of `pySecDec` [200, 208].

3.2.2 Baikov Representation

In the Baikov representation of FIs [45, 209, 210], the integration over the loop momenta is traded for integrations over the propagators (including the auxiliary ones) of the integral. For obtaining the Baikov representation, let us denote as $\tilde{q}_i = k_i$ with $i = 1, \ldots, L$ the loop momenta, $\tilde{q}_{L+i} = p_i$ with $i = 1, \ldots, E$ the independent external momenta, $M = L + E$ and $\tilde{s}_{ij} = \tilde{q}_i \cdot \tilde{q}_j$. Using these definitions we can write the propagators D_α in the general form

$$D_\alpha = \sum_{i=1}^{L} \sum_{j=i}^{M} A_\alpha^{ij} \tilde{s}_{ij} + f_\alpha = \sum_{i=1}^{L} \sum_{j=i}^{L} A_\alpha^{ij} k_i \cdot k_j + \sum_{i=1}^{L} \sum_{j=L+1}^{M} A_\alpha^{ij} k_i \cdot p_{j-L} + f_\alpha \,, \qquad (3.14)$$

where f_α is a function depending on external kinematics and internal masses, A_α^{ij} is a matrix associated with the topology of the graph and whose elements are taken from the set $\{-2, -1, 0, 1, 2\}$, and $\alpha = 1, \ldots, N$. The pair (ij) in A_α^{ij} can be seen as a single index which has N different values as $i = 1, \ldots, L$ and $j = i, \ldots, M$ [211], and hence we can view A_α^{ij} as a $N \times N$ matrix. Using this we can solve the last equation for $\tilde{s}_{ij}$

$$\tilde{s}_{ij} = \sum_{\alpha=1}^{N} A_{ij}^{\alpha}(D_\alpha - f_\alpha), \qquad (3.15)$$

with A_{ij}^{α} the inverse matrix of A_α^{ij}.

We start deriving the Baikov representation by first writing a FI as an integral in the scalar products $\tilde{s}_{ij}$. Starting from the innermost integral we write $k_1^\mu = k_{1\parallel}^\mu + k_{1\perp}^\mu$, with $k_{1\parallel}^\mu$ the projection of k_1^μ on the hyperplane spanned by the momenta $k_2^\mu, \ldots, k_L^\mu, p_1^\mu, \ldots, p_E^\mu$ ($M - 1$ components) and $k_{1\perp}^\mu$ the transverse component to this hyperplane. Then we continue writing $k_2^\mu = k_{2\parallel}^\mu + k_{2\perp}^\mu$, where $k_{2\parallel}^\mu$ is the projection of k_2^μ on the hyperplane spanned by $k_3^\mu, \ldots, k_L^\mu, p_1^\mu, \ldots, p_E^\mu$ ($M - 2$ components) and $k_{2\perp}^\mu$ is the transverse component to this hyperplane, and so on for the rest loop momenta. Therefore for the integration measure of Eq. (3.1) we can write

$$d^d k_1 d^d k_2 \ldots d^d k_L = d^{M-1} k_{1\parallel} d^{d-M+1} k_{1\perp} d^{M-2} k_{2\parallel} d^{d-M+2} k_{2\perp} \ldots d^{M-L} k_{L\parallel} d^{d-M+L} k_{L\perp}. \qquad (3.16)$$

For each loop momentum projection $k_{l\parallel}^\mu$ we can write

$$k_{l\parallel}^\mu = \alpha_i^{(l)} \tilde{q}_i^\mu \Rightarrow k_{l\parallel} \cdot \tilde{q}_j = \alpha_i^{(l)} \tilde{q}_i \cdot \tilde{q}_j = \alpha_i^{(l)} \tilde{s}_{ij} \Rightarrow \alpha_i^{(l)} = \zeta_{lj} \tilde{s}_{ij}^{-1} \quad \text{for} \quad i, j > l, \qquad (3.17)$$

with $\zeta_{lj} = k_{l\parallel} \cdot \tilde{q}_j = \tilde{s}_{lj}$ and $j = l + 1, \ldots, M$[6]. For the innermost loop momentum, we want to make a change of integration variables from $d^{M-1} k_{1\parallel}$ to $d\tilde{s}_{12} d\tilde{s}_{13} \ldots d\tilde{s}_{1M}$. From vector analysis, we know that under a change of integration variables, the integration measure of $k_{1\parallel}^\mu$ transforms as

$$d^{M-1} k_{1\parallel} = \left| \det \left(\frac{\partial k_{1\parallel}^\mu}{\partial \tilde{s}_{1i}} \right) \right| d\tilde{s}_{12} d\tilde{s}_{13} \ldots d\tilde{s}_{1M} \quad \text{with} \quad i = 2, \ldots, M, \qquad (3.18)$$

where for the Jacobian determinant from Eq. (3.17) we have

$$\left| \det \left(\frac{\partial k_{1\parallel}^\mu}{\partial \tilde{s}_{1i}} \right) \right| = \det(\tilde{s}_{ij}^{-1} \tilde{q}_i^\mu) = (\det(\tilde{s}_{ij}))^{-1} \det(\tilde{q}_i^\mu) = \frac{1}{\sqrt{\mathbb{G}(\tilde{q}_2, \ldots, \tilde{q}_n)}}, \qquad (3.19)$$

with $\mathbb{G}(\tilde{q}_1, \ldots, \tilde{q}_n) = \det(\tilde{q}_i \cdot \tilde{q}_j)$ for $i, j = 1, \ldots, M$ the Gram determinant (from the geometrical point of view, $\mathbb{G}^{1/2}(\tilde{q}_1, \ldots, \tilde{q}_n)$ is the volume of the parallelogram formed by $\tilde{q}_1, \ldots, \tilde{q}_n$), and where above we used that

$$(\det(\tilde{q}_i^\mu))^2 = \det(\tilde{q}_i^\mu) \det(\tilde{q}_{j\mu}) = \det(\tilde{q}_i^\mu \tilde{q}_{j\mu}) = \mathbb{G} \Rightarrow \det(\tilde{q}_i^\mu) = \mathbb{G}^{1/2}(\tilde{q}_2, \ldots, \tilde{q}_n). \qquad (3.20)$$

The same procedure can be followed to change the integration variables of all the loop momentum projections $k_{l\parallel}$ to their corresponding scalar products. Thus for the volume

---

[6]This results from $\zeta_{lj} = k_{l\parallel} \cdot \tilde{q}_j = (k_l - k_{l\perp}) \cdot \tilde{q}_j \xrightarrow{j > l} \zeta_{lj} = k_l \cdot \tilde{q}_j = \tilde{s}_{lj}$.

elements $d^{M-i}k_{i\parallel}$ we obtain

$$
\begin{aligned}
d^{M-1}k_{1\parallel} &= \frac{d\tilde{s}_{12}d\tilde{s}_{13}\ldots d\tilde{s}_{1M}}{\mathbb{G}^{1/2}(k_2,\ldots,k_L,p_1,\ldots,p_E)}\,, \\[4pt]
d^{M-2}k_{2\parallel} &= \frac{d\tilde{s}_{23}d\tilde{s}_{24}\ldots d\tilde{s}_{2M}}{\mathbb{G}^{1/2}(k_3,\ldots,k_L,p_1,\ldots,p_E)}\,, \\
&\vdots \\
d^{M-L}k_{L\parallel} &= \frac{d\tilde{s}_{LL+1}d\tilde{s}_{LL+2}\ldots d\tilde{s}_{LM}}{\mathbb{G}^{1/2}(p_1,\ldots,p_E)}\,.
\end{aligned}
\tag{3.21}
$$

Concerning the volume elements of the transverse components $k_{l\perp}^\mu$, noticing that the integrand of Eq. (3.1) depends on the orthogonal directions only through $k_{l\perp}^2$, allows us to integrate over the angular part of the orthogonal space resulting to

$$
d^n k_{l\perp} = \frac{1}{2}\Omega_n k_{l\perp}^{n-2}dk_{l\perp}^2\,,
\tag{3.22}
$$

with $\Omega_n = 2\pi^{n/2}/\Gamma(n/2)$ the $n-$dimensional solid angle. Also, using the equation $\tilde{s}_{ll} \equiv k_{ll}^2 = k_{l\parallel}^2 + k_{l\perp}^2$ we can make the replacement $dk_{l\perp}^2 = ds_{ll}$. Geometrically, $k_{l\perp}$ can be seen as the height of the parallelogram with the base formed by $k_{l+1},\ldots,k_L,p_1,\ldots,p_E$ and the extra vector k_l^μ, which is equal to the volume of the whole parallelogram divided by the area of its base. Therefore we have

$$
\begin{aligned}
d^{d-M+1}k_{1\perp} &= \frac{1}{2}\Omega_{d-M+1}\left(\frac{\mathbb{G}(k_1,\ldots,k_L,p_1,\ldots,p_E)}{\mathbb{G}(k_2,\ldots,k_L,p_1,\ldots,p_E)}\right)^{(d-M-1)/2} d\tilde{s}_{11}\,, \\[4pt]
d^{d-M+2}k_{2\perp} &= \frac{1}{2}\Omega_{d-M+2}\left(\frac{\mathbb{G}(k_2,\ldots,k_L,p_1,\ldots,p_E)}{\mathbb{G}(k_3,\ldots,k_L,p_1,\ldots,p_E)}\right)^{(d-M)/2} d\tilde{s}_{22}\,, \\
&\vdots \\
d^{d-M+L}k_{L\perp} &= \frac{1}{2}\Omega_{d-M+L}\left(\frac{\mathbb{G}(k_L,p_1,\ldots,p_E)}{\mathbb{G}(p_1,\ldots,p_E)}\right)^{(d-M+L-2)/2} d\tilde{s}_{LL}\,.
\end{aligned}
\tag{3.23}
$$

Replacing Eqs. (3.21) and (3.23) in the relation of the integration measurement, Eq. (3.16), all the Gram determinants except from $\mathbb{G}(k_1,\ldots,k_L,p_1,\ldots,p_E)$ and $\mathbb{G}(p_1,\ldots,p_E)$ cancel each other out, and the FI takes the form

$$
G_{\alpha_1\ldots\alpha_N} = \frac{e^{L\gamma_E\varepsilon}\pi^{-\frac{L(L-1)}{4}-\frac{LE}{2}}}{\prod_{i=1}^L \Gamma\left(\frac{d-M+i}{2}\right)}\mathbb{G}(p_1,\ldots,p_E)^{\frac{E+1-d}{2}}\int\prod_{i=1}^L\prod_{j=i}^M d\tilde{s}_{ij}\,\frac{\mathbb{G}(k_1,\ldots,k_L,p_1,\ldots,p_E)^{\frac{d-M-1}{2}}}{D_1^{\alpha_1}\ldots D_N^{\alpha_N}}
$$

Finally, using Eq. (3.15) we change the integration variables from $\tilde{s}_{ij}$'s to the propagators $x_\alpha = D_\alpha$ (*Baikov variables*). The Jacobian of this transformation is equal to $\det(A_{ij}^\alpha)$ and hence we obtain the following form for the (full) Baikov representation of a FI

$$
G_{\alpha_1\ldots\alpha_N} = \frac{e^{L\gamma_E\varepsilon}C_N^L}{[G(p_1,\ldots,p_E)]^{\frac{d-E-1}{2}}}\int\frac{dx_1\ldots dx_N}{x_1^{\alpha_1}\ldots x_N^{\alpha_N}}\left[P_N^L(x_1-f_1,\ldots,x_N-f_N)\right]^{\frac{d-M-1}{2}}
\tag{3.24}
$$

with

$$C_N^L = \frac{\pi^{-\frac{L(L-1)}{4}-\frac{LE}{2}}}{\prod_{i=1}^{L}\Gamma\left(\frac{d-M+i}{2}\right)}\det(A_{ij}^\alpha),\tag{3.25}$$

and

$$P_N^L(x_1-f_1,\ldots,x_N-f_N) = G(k_1,\ldots,k_L,p_1,\ldots,p_E)\big|_{\tilde{s}_{ij}=\sum_{\alpha=1}^{N}A_{ij}^\alpha(x_\alpha-f_\alpha)\,\&\,\tilde{s}_{ji}=\tilde{s}_{ij}}.\tag{3.26}$$

The integration region in the Baikov variables has a complicated shape and is usually defined by the assumption (see [212] for a nice discussion of the integration limits)

$$P_N^L(x_1-f_1,...,x_N-f_N)\geq 0,\tag{3.27}$$

which means that the Baikov polynomial vanishes in the boundaries.

An alternative form of the Baikov representation, known as *loop-by-loop*, was presented in [213]. This form results by instead of projecting one loop momentum k_i to the rest loop momenta $\{k_j\}$ with $j>i$ and all the (E in total) external momenta as done in the full Baikov approach, by projecting each loop momentum k_i over the space spanned by its "external" momenta, where the definition of "external" momenta of k_i, in general, contains a subset of the E external momenta and possibly a subset of the loop momenta $\{k_j\}$ with $j>i$. Therefore the application of the loop-by-loop approach will result in a Baikov representation with fewer Baikov variables than following the standard (full) Baikov approach. For obtaining the (full or loop-by-loop) Baikov representation of a FI the publicly available `Mathematica` script `Baikov.m`, from [213], can be used.

The Baikov representation of FIs has attracted much interest during the last years, due to its very natural definition of cuts in d-dimensions. The $n-$cut of a FI in Baikov representation is defined as follows [213]

$$G_{\alpha_1,\ldots,\alpha_N}^{n\times cut}\equiv\frac{e^{L\gamma_E\varepsilon}C_N^L}{G^{(d-E-1)/2}}\left(\prod_{a=n+1}^{N}\int dx_a\right)\left(\prod_{c=1}^{n}\oint_{x_c=0}dx_c\right)\frac{(P_N^L)^{(d-M-1)/2}}{x_1^{\alpha_1}\ldots x_N^{\alpha_N}},\tag{3.28}$$

where the Baikov variables $\{x_a : a = 1,\ldots,N\}$ have been divided into two subsets, containing n cut propagators, to whom we have replaced the integrals in the corresponding Baikov variable with contour integrals around zero, and $(N-n)$ uncut ones. This definition of cuts differs from the definition of the unitarity cuts that we saw in the previous Chapter, due to the lack of the θ-function of energy. Computing the maximal cut (we cannot cut the auxiliary propagators) of a FI can give information for its leading singularities and the class of functions that appear in the un-cut FI. Moreover, the Baikov representation has found application also in the integral reduction into MIs, through its use for the generation of syzygy equations [62–65, 67, 214–216] and its adaption for the method of intersection numbers [76–80].

3.3   Feynman Integral Computations

As already discussed in the previous section, FIs can be possibly computed using their parametric representations. Nevertheless, their increased complexity when many loops and many scales are involved drives (in many cases) their analytic computation through

direct integrations impossible, and their numerical calculation, through the method of sector decomposition, insufficient in terms of precision for the physical regions of phenomenological interest. The bottlenecks of these methods are detoured in the modern way of computing FIs through the method of *differential equations* (DE) [51, 217–220], where the integrals are usually computed analytically in the Euclidean region and afterward they are extended in the physical regions using proper analytic continuation techniques. In this section, we will give a brief introduction to the DE method and to a variant of it, known as *simplified differential equations* approach (SDE) [221].

3.3.1 Differential Equations Method and their Canonical Form

The DE method is applied within the concept of integral families and computes the MIs, and thus (through IBP) all the integrals of the family. Let us denote the MIs as $G_i(s, \varepsilon)$, with $i = 1, \ldots I$, I the number of MIs and $\mathbf{G} \equiv \{G_1, \ldots G_I\}$ a chosen basis. The DE method relies on the fact that the MIs are functions of external momenta and internal masses and hence we can differentiate them with respect to the kinematic invariants, $s = \{s_{ij}\} \cup \{m^2\}$. The differentiation of the MIs results in a combination of FIs with different propagator exponents, which belong to the same family, and therefore using IBP relations can be re-expressed in terms of the MIs. This procedure gives rise to a linear system of differential equations for the MIs of the form[7]

$$\frac{\partial}{\partial s_k} G_i(s, \varepsilon) = A_{s_k}^{ij}(s, \varepsilon) G_j(s, \varepsilon) \Rightarrow \partial_{s_k} \mathbf{G} = \mathbf{A}_{s_k} \mathbf{G} \tag{3.29}$$

where $s_k \in s$, and $\mathbf{A}_{s_k}$ are the partial derivative matrices. One can solve this system of DEs in a Laurent expansion around $\varepsilon = 0$ after first finding appropriate boundary conditions for the MI, which can be done using asymptotic expansion by regions [202–207] or by imposing the regularity of MIs at the pseudo-thresholds of the DE (*regularity conditions* [222, 223]) or using other methods [224, 225]. The MIs of each sector receive contributions to their DE only from lower sectors, thus the system of DEs can be solved in a bottom-up approach. From the possibility of interchanging the order of taking partial derivatives of a function, we find that $\mathbf{A}_{s_k}$ satisfy the (Schwarz) integrability condition

$$\partial_{s_1} \mathbf{A}_{s_2} - \partial_{s_2} \mathbf{A}_{s_1} = \mathbf{A}_{s_2} \mathbf{A}_{s_1} - \mathbf{A}_{s_1} \mathbf{A}_{s_2}, \tag{3.30}$$

the verification of which is a standard cross-check that the DEs were derived correctly. In order to take derivatives with respect to the external kinematical invariants, one needs to replace them with derivatives with respect to the external momenta[8], using the relations [51, 220, 226]

$$\frac{\partial}{\partial (p_i \cdot p_j)} \mathbf{G} = \tilde{\mathbb{G}}_{kj}^{-1} \left(p_k \cdot \frac{\partial}{\partial p_i} \right) \mathbf{G} \quad \text{and} \quad \frac{\partial}{\partial (p_i^2)} \mathbf{G} = \frac{1}{2} \tilde{\mathbb{G}}_{ki}^{-1} \left(p_k \cdot \frac{\partial}{\partial p_i} \right) \mathbf{G}, \tag{3.31}$$

with $\tilde{\mathbb{G}}_{kj} = p_i \cdot p_j$ the gram matrix and $\tilde{\mathbb{G}}_{kj}^{-1}$ its inverse.

---

[7]Summation over repeated indices is assumed.

[8]The derivatives with respect to internal masses do not need to be changed as these masses appear explicitly in the propagators and do not correlate to the external kinematics.

As mentioned previously, the basis of MIs is not unique and therefore one can make a change to the basis of the following form

$$\mathbf{G} \to \mathbf{G}' = \mathbf{T}\,\mathbf{G}. \tag{3.32}$$

Under this transformation, it is easy to see that the partial derivative matrices change as

$$\mathbf{A}_{s_k} \to \mathbf{A}'_{s_k} = \mathbf{T}\,\mathbf{A}_{s_k}\,\mathbf{T}^{-1} + \mathbf{T}\partial_{s_k}\mathbf{T}^{-1}. \tag{3.33}$$

A groundbreaking idea that has led to numerous computations of FIs during the last years, is that of the *canonical form of differential equations*, introduced in [227]. According to this idea, for a suitable choice of basis of MIs[9] (suitable choice of $\mathbf{T}$) the DE can obtain the form

$$\frac{\partial}{\partial s_k}\mathbf{G}'(s,\varepsilon) = \varepsilon\mathbf{A}'_{s_k}(s)\mathbf{G}'(s,\varepsilon) \tag{3.34}$$

where ε has been factorized out of the partial derivative matrices and hence this DE can be solved iteratively in ε. Moreover, in this case, the integrability condition becomes

$$\partial_{s_1}\mathbf{A}'_{s_2} - \partial_{s_2}\mathbf{A}'_{s_1} = \mathbf{A}'_{s_2}\mathbf{A}'_{s_1} - \mathbf{A}'_{s_1}\mathbf{A}'_{s_2} = 0. \tag{3.35}$$

In [227] it was conjectured that, in order to obtain a DE of canonical form, the basis of MIs should be chosen such that it contains only functions with *uniform degree of transcendentality* (UT). The transcendentality of a function f, $\mathcal{T}(f)$, is defined as the number of iterated integrations needed to define the function f, and the transcendentality of a product of functions is equal to the sum of their transcendentalities, meaning $\mathcal{T}(f_1 f_2) = \mathcal{T}(f_1) + \mathcal{T}(f_2)$. The algebraic factors have degree zero ($\mathcal{T}(\text{Algebraic Factors}) = 0$) and within the framework of DR, ε is assigned $\mathcal{T}(\varepsilon) = -1$. For example,

$$\mathcal{T}\left(\log(x)\right) = 1, \quad \text{and} \quad \mathcal{T}(Li_n) = \mathcal{T}(\pi^n) = \mathcal{T}(\zeta(n)) = n. \tag{3.36}$$

In addition, if a function is UT and its transcendentality is reduced by one degree by taking a derivative, meaning $\mathcal{T}(\partial f) = \mathcal{T}(f) - 1$, then this function is called *pure* [227]. This implies that the coefficients of the transcendental functions in f cannot be anything more than pure numbers, because if they were algebraic coefficients, upon differentiation would generate additional terms with transcendentality equal to $\mathcal{T}(f)$.

In the case where all the MIs of the family are expressible in terms of multiple poly-logarithms[10] [228, 229], given a *pure basis* of MIs results in a canonical DE of the form

$$d\mathbf{G}' = \varepsilon\sum_a \mathbf{M}^a d\log(W_a(s))\mathbf{G}', \tag{3.37}$$

which is ε-factorized and the partial derivative matrices have been replaced by a sum of residue matrices, $\mathbf{M}^a$, containing only rational numbers as elements. $W_a(s)$ are known as the *letters* of the DE, and their set $\{W_a\}$ forms the so-called *alphabet*. The letters can include square roots of the kinematic invariants and in order to obtain a *Fuchsian* form for the canonical DE one needs to rationalize these square roots. Despite

---

[9]In general, as a MI can be chosen a combination of FIs. In the following, we may use the terminology basis elements when referring to MIs.

[10]This is the case for all the families that we will study within this thesis.

the fact that an algorithmic approach for rationalizing square roots was proposed in [230] and implemented in the package `RationalizeRoots` [231], in general, the task of rationalization is not always feasible. For example, the alphabet of the massless two-loop five-leg families with one off-shell leg contains a number of square roots where all of them can not be simultaneously rationalized [225, 232].

In [227, 233] it was conjectured that FIs with constant leading singularities tend to be pure. Although there doesn't exist a general method for obtaining a pure basis of MIs (or even proving its existence) for any given family of FIs, there exist several different methods and public packages the combination of which can lead to a canonical DE of the form of Eq. (3.37). Some of these methods, such as the *Magnus exponential method* [234], the method proposed in [235], *Lee's algorithm* (implemented in `epsilon` [236], `Fuchsia` [237] and `Libra` [238]), *Meyer's algorithm* (utilized in `CANONICA` [239]) and the algorithm implemented in `Initial` [240] (which has as a starting point a pure MI on the top sector), perform transformations on the DEs in order to bring them into a canonical form. Other methods rely on the construction of MIs with constant leading singularities, such as the construction of *d*log integrands implemented in `DlogBasis` [241] using a four-dimensional analysis or the Baikov representation [242, 243], or (for multi-loop problems) performing a loop-by-loop analysis for the leading singularities using lower loop pure combinations of MIs as building blocks [244, 245]. Moreover, a method utilizing the intersection theory was recently proposed in [246, 247], while also other intuitive approaches exist [225, 232].

For complex integral families with many legs, scales, loops, and massive particles running on them, the augmentation of the difficulty of finding a canonical DE (Eq. (3.34)), the problem of rationalization of the square roots appearing in the alphabet of the DEs, or in the definition of the pure basis elements, and the extension of the functional space of the solution to functions beyond the multiple poly-logarithms (whose numerical evaluation is well established), stands the analytical solution of their corresponding DEs in some cases not efficient (or impossible). In order to surpass these problems, in the last years there have been developed some numerical methods for solving DEs[11]. The most noticables of them are the *multi-dimensional series expansion method* [248] implemented in `DiffExp` [249] and `SeaSyde` [250], and the *auxiliary mass flow method* [251–253] implemented in `AMFlow` [254]. In the latter, an auxiliary mass term, η, is introduced in some propagators of the studied family, and a DE is constructed with respect to η, fixing the kinematic invariants, s, to a specific phase-space point. The DE is solved using numerical methods [255, 256] for $\eta \to i0^-$ using boundary conditions at $\eta \to \infty$, which can be computed iteratively. The last feature makes this method a systematic and efficient way for computing MIs, with its only bottleneck being the IBP reduction for the construction of the DE in η.

3.3.2 Multiple (Goncharov) Poly-Logarithms

As it has been demonstrated in the previous subsection through the canonical form of DE, the occurrence of iterated integrals is inherent in the DEs that FIs satisfy. *Multiple poly-logarithms*, also known as *Goncharov poly-logarithms* (GPLs), can be considered the most notable (and most studied) class of iterated integrals that emerge

---

[11]These methods are usually called *semi-numerical* in order to be distinguished from the numerical methods that do not utilize the DE method.

from computations involving FIs. GPLs can be defined recursively, for $n \geq 0$, via the iterated integral [228, 229]

$$\mathcal{G}(a_1, \ldots, a_n; z) = \int_0^z \frac{dt}{t - a_1} \mathcal{G}(a_2, \ldots, a_n; t) \quad \text{with} \quad \mathcal{G}(z) \equiv \mathcal{G}(; z) = 1, \qquad (3.38)$$

where a_i (letters) and z (argument) are complex variables. The vector $\vec{a} = (a_1, \ldots, a_n)$ is called the *vector of singularities* (alphabet) of the GPL, and its length n is called the *weight* of the GPL, corresponding to the number of logarithmic integrations in Eq. (3.38). In the relation above, for $a_n = 0$ the integral is divergent and needs to be regularised. This is usually done by including the following special definition in the definition of GPLs

$$\mathcal{G}(\vec{0}_n; z) = \frac{1}{n!} \log^n(z) \quad \text{with} \quad \vec{0}_n = (\overbrace{0, \cdots, 0}^{n \text{ terms}}). \qquad (3.39)$$

Although there doesn't exist proof for that, GPLs are generally considered to be transcendental functions. The definition through the relations (3.38)-(3.39) shows that GPLs define a general class of functions that include the well-known logarithm and classical poly-logarithm as special cases

$$\mathcal{G}(\vec{a}_n; z) = \frac{1}{n!} \log^n \left(1 - \frac{z}{a}\right) \quad \text{and} \quad \mathcal{G}(\vec{0}_{n-1}, a; z) = -\text{Li}_n \left(\frac{z}{a}\right), \quad \text{with} \quad \vec{a}_n = (\overbrace{a, \cdots, a}^{n \text{ terms}}).$$

If the rightmost index (a_n), of the vector $\vec{a}$ is not equal to zero (these GPLs are called GPLs without trailing zeros), then the GPL remains unchanged when all its arguments are scaled by a complex number k (except zero)

$$\mathcal{G}(k\vec{a}; kz) = \mathcal{G}(\vec{a}; z) \qquad (3.40)$$

If $a_i/z \notin (0, 1)$, GPLs are real-valued functions. As can be seen from Eq. (3.38), GPLs are not well defined whenever any of $a_1, \ldots, a_n$ lies precisely along the integration path that is the straight line in complex space connecting the origin and its argument z, i.e. if $a_i/z \in (0, 1)$. There is a discontinuity whenever a_i crosses this straight line and this exactly defines all the branch cuts of the GPLs. Therefore whenever $a_i/z \in (0, 1)$, GPLs become complex-valued functions and an infinitesimal imaginary perturbation in z (or equivalently in a_i because of Eq. (3.40)) is required such as to make the GPLs well-defined and correctly capture their imaginary part [257, 258].

An important property of GPLs is that they satisfy a *graded shuffle algebra* [184, 259, 260]. This means that a product of GPLs with weight n_1 and n_2 can be expressed as a sum of GPLs with weight $n_1 + n_2$ (*shuffle product*)

$$\mathcal{G}(a_1, \ldots, a_{n_1}; z)\mathcal{G}(a_{n_1+1}, \ldots, a_{n_1+n_2}; z) = \sum_{\sigma \in \Sigma(n_1, n_2)} \mathcal{G}(a_{\sigma(1)}, \ldots, a_{\sigma(n_1+n_2)}; z), \quad (3.41)$$

where $\Sigma(n_1, n_2)$ denotes the set of all shuffles of $n_1 + n_2$. The fact that the shuffle algebra is graded means that the product of Eq. (3.41) preserves the weight of the GPLs, while at the same time preserving the ordering inside the vectors $(a_1, \ldots, a_{n_1})$

and $(a_{n_1+1}, \ldots, a_{n_1+n_2})$. As an example consider the following product

$$\mathcal{G}(a_1, a_2; z)\mathcal{G}(a_3, a_4; z) = \mathcal{G}(a_1, a_2, a_3, a_4; z) + \mathcal{G}(a_1, a_3, a_2, a_4; z) + \mathcal{G}(a_1, a_3, a_4, a_2; z)$$
$$+ \mathcal{G}(a_3, a_1, a_2, a_4; z) + \mathcal{G}(a_3, a_1, a_4, a_2; z) + \mathcal{G}(a_3, a_4, a_1, a_2; z).$$

The shuffle product can be also used to remove trailing zeros from GPLs, apart from objects of the form $G(\vec{0}_n; z)$. For example,

$$\mathcal{G}(0, a, 0, 0, z) = \mathcal{G}(0, 0, z)\mathcal{G}(0, a, z) - 2\mathcal{G}(0, z)\mathcal{G}(0, 0, a, z) + 3\mathcal{G}(0, 0, 0, a, z).$$

The numerical evaluation of GPLs has been intensively studied and fast algorithms exist nowadays [257], which have been implemented in `GiNaC` [257, 261] (a computer algebra program based on `C++`) and `HandyG` [262] (a `Fortran`-based package). Let us mention that, when one needs to add a small imaginary part to the kinematic variables for the analytic continuation to regions where GPLs are complex-valued the computation may be more time-consuming, while also the efficiency of the evaluation depends on the requested precision. Moreover for the manipulation of GPLs, using the properties described in this subsection and much more (see [184, 186, 259, 260] for more properties and details), the `Mathematica` package `PolyLogTools` [263] exist, alongside with the `Maple` package `HyperInt` [195].

In the integral families studied within this thesis, we are not going to face special functions beyond GPLs. Let us comment though that there is a wide range of FIs where such functions appear and that for the study and understanding of these functions, a lot of effort has been put in by the community, during the last years. For a nice review of this topic, we refer to [264].

3.3.3 Simplified Differential Equations Approach

The *simplified differential equations approach* (SDE) [221] is a variant of the standard DE method, applicable when at least one of the external momenta is off-shell, where for a given integral family a system of DEs with respect to one variable only is derived[12], in a systematic and simplified way. Consider a family with $E + 1$ external momenta, and let us define the *degree of off-shellness* of this family, n_{off}, as the number of off-shell external momenta. Then within this approach, the external momenta are parametrized in terms of a dimensionless parameter x and a set of $E + 1$ momenta with a degree of off-shellness $n_{\text{off}} - 1$, in such a way that to capture the degree of off-shellness of the initial external momenta. For example, having a set of 5 external momenta

$$\{q_1, q_2, q_3, q_4, q_5\} \quad \text{with} \quad q_1^2 = m^2 \quad \text{and} \quad q_2^2 = \cdots = q_5^2 = 0,$$

one possible SDE-parametrization, in terms of $\{x, p_1, p_2, p_3, p_4, p_5\}$ with $p_1^2 = \cdots = p_5^2 = 0$, is the following[13] [9]

$$q_1 \to p_{123} - xp_{12}, \quad q_2 \to p_4, \quad q_3 \to -p_{1234}, \quad q_4 \to xp_1, \quad \text{and} \quad q_5 \to xp_2,$$

---

[12]And not with respect to all the kinematic invariants of the problem as in the standard approach.
[13]We use the notation $p_{i\ldots j} = p_i + \cdots + p_j$.

where the off-shellness of q_1 is captured due to the fact that $(p_{123} - xp_{12})^2 \neq 0$. The parameterization is not unique (x could be introduced to less or more than two of the external momenta above[14]) and different parametrizations are optimal for different problems. For example, in combining the SDE approach with a pure basis of MIs containing square roots, the rationalization of these square roots with respect to x is something that one needs to take into account in order to choose a viable parametrization.

Having introduced x in the propagators of the family through the SDE-parametrization, the MIs depend now explicitly on x, and we can take derivatives of them with respect to x and derive a system of DE on x using IBP relations

$$\frac{\partial}{\partial x}\mathbf{G}(S, x, \varepsilon) = \mathbf{A}(S, x, \varepsilon)\mathbf{G}(S, x, \varepsilon), \tag{3.42}$$

where $S = \{S_{ij}\} \cup \{m^2\}$[15] is the set of kinematic invariants and masses created by the external momenta of the SDE parametrization (the ones with degree of off-shellness $n_{\text{off}} - 1$) and the independent propagator masses. In order to solve Eq. (3.42) one has to compute the boundary conditions of the MIs at $x \to 0$[16]. Some of the advantages of this method compared to the standard DEs method are the followings:

- The easier derivation of a system of DEs, due to the fact that from the differentiation with respect only to x fewer FIs are produced for reduction to MIs, compared to the standard approach.

- The need of solving only one system of DEs, and not a system of DEs for each kinematic variable.

- The rationalization of square roots with respect to x, for some cases where in the standard approach the rationalization with respect to all the variables is not possible, leading to analytic solutions in terms of GPLs [9, 267].

- When a pure basis of MIs is provided and an analytic reduction is a bottleneck, a semi-numerical reduction can be applied by putting prime numbers to all the invariants except x, and afterward determining the letters of the DE using other methods (such as the study of maximally cut DEs).

- By taking the $x \to 1$ limit (which we will see later) one can obtain also the solution for the MIs of the same family but with one external off-shell momentum less.

The combination of the SDE approach with the method of the canonical form of DEs leads to an algorithmic way of computing multi-loop and multi-scale integral families. Assuming studying an integral family for which we have a pure basis of MIs, let us denote it $\mathbf{g}$, Eq. (3.42) takes the form

$$\frac{\partial}{\partial x}\mathbf{g} = \epsilon \left(\sum_{i=1}^{l_{\text{max}}} \frac{\mathbf{M}_i}{x - l_i} \right) \mathbf{g}, \tag{3.43}$$

---

[14]As momenta where x has been introduced we count only the ones where the momentum is parametrized as xp_i. In this example we have only two such momenta, $q_4 \to xp_1$ and $q_5 \to xp_2$.

[15]($S_{ij} = (p_i^{\text{SDE}} + p_j^{\text{SDE}})^2$ with $j > i$.

[16]See [221, 265, 266] for methods of computing boundaries when SDE is not applied in a canonical DE.

where the purely numerical matrices $\mathbf{M}_i$ correspond to each individual letter $l_i = l_i(S)$[17], and $l_{\max}$ is the size of the alphabet. The above system of DEs can be solved iteratively in a Laurent expansion around $\varepsilon = 0$, finding appropriate boundary conditions for the MIs. The solution depends on the power of ε where the series expansion is truncated, and in general, has the following form (assuming summation over dummy indices)

$$
\begin{aligned}
\mathbf{g} =& \epsilon^0 \mathbf{b}_0^{(0)} + \epsilon \left(\mathcal{G}_i \mathbf{M}_i \mathbf{b}_0^{(0)} + \mathbf{b}_0^{(1)} \right) + \epsilon^2 \left(\mathcal{G}_{ij} \mathbf{M}_i \mathbf{M}_j \mathbf{b}_0^{(0)} + \mathcal{G}_i \mathbf{M}_i \mathbf{b}_0^{(1)} + \mathbf{b}_0^{(2)} \right) \\
&+ \epsilon^3 \left(\mathcal{G}_{ijk} \mathbf{M}_i \mathbf{M}_j \mathbf{M}_k \mathbf{b}_0^{(0)} + \mathcal{G}_{ij} \mathbf{M}_i \mathbf{M}_j \mathbf{b}_0^{(1)} + \mathcal{G}_i \mathbf{M}_i \mathbf{b}_0^{(2)} + \mathbf{b}_0^{(3)} \right) \\
&+ \epsilon^4 \left(\mathcal{G}_{ijkl} \mathbf{M}_i \mathbf{M}_j \mathbf{M}_k \mathbf{M}_l \mathbf{b}_0^{(0)} + \mathcal{G}_{ijk} \mathbf{M}_i \mathbf{M}_j \mathbf{M}_k \mathbf{b}_0^{(1)} + \mathcal{G}_{ij} \mathbf{M}_i \mathbf{M}_j \mathbf{b}_0^{(2)} \right. \\
&\left. + \mathcal{G}_i \mathbf{M}_i \mathbf{b}_0^{(3)} + \mathbf{b}_0^{(4)} \right) + \mathcal{O}(\varepsilon^5)
\end{aligned}
\tag{3.44}
$$

where $\mathbf{b}_0^{(i)}$ are the boundaries in the limit $x \to 0$, of the pure basis elements expanded around $\varepsilon = 0$, with i indicating the corresponding weight. $\mathbf{b}_0^{(i)}$ consist of $\zeta(i)$, logarithms and GPLs of weight i which have as arguments rational functions of the kinematic invariants S. The notation $\mathcal{G}_{ijkl} \equiv \mathcal{G}(l_i, l_j, l_k, l_l; x)$ for the GPLs is used above for space convenience. The solution is normalized so that each coefficient of ε^k is multiplied with GPLs of transcendental weight k, and the pure basis elements have a uniform degree of transcendentality equal to zero. For problems with L loops, we need to obtain a solution for up to order ε^{2L}, while the extension of Eq. (3.44) to higher orders is trivial.

In practical applications, it is common before starting to compute all the boundary conditions of an integral family one by one, first to look at the existing literature for integral sectors that are shared with other families[18] which have been already calculated and their results are accessible. If this is the case, then the boundary conditions for these integral sectors can be obtained from the pre-computed results. The rest of the boundary conditions can be computed using the *resummation matrix method* [4, 9], which utilizes the residue matrix of the letter $l_1 = 0$, $\mathbf{M}_1$, together with some input from the method of expansion by regions. Let us briefly describe now how this method works. Taking the limit $x \to 0$ to the canonical DE of Eq. (3.43) results in

$$
\frac{\partial}{\partial x} \mathbf{g}_0 = \epsilon \frac{\mathbf{M}_1}{x} \mathbf{g}_0 + \mathcal{O}(x^0),
\tag{3.45}
$$

the solution of which is ($\mathbf{b} = \sum_{i=0}^k \varepsilon^i \mathbf{b}_0^{(i)}$)

$$
\mathbf{g}_0 = e^{\varepsilon \mathbf{M}_1 \log(x)} \mathbf{b}.
\tag{3.46}
$$

Because $\mathbf{M}_1$ is a square matrix we can always find its Jordan decomposition, $\mathbf{M}_1 = \mathbf{S} \mathbf{D} \mathbf{S}^{-1}$, which allows us to write Eq. (3.46) as

$$
\mathbf{g}_0 = \mathbf{R}_0 \mathbf{b} \quad \text{with} \quad \mathbf{R}_0 = \mathbf{S} e^{\varepsilon \mathbf{D} \log(x)} \mathbf{S}^{-1},
\tag{3.47}
$$

---

[17]Here we use a different definition for the letters, which in the standard notation would have been defined as $x - l_i$. This different notation is directly connected with the notation of letters in the GPLs.

[18]For example, the non-planar double-box families share many integral sectors with the planar ones.

where $\mathbf{R}_0$ is the *resummation matrix at $x = 0$*, which correctly resums all the $\log(x)$ dependence of the basis element. In the most general case, $\mathbf{R}_0$ is of the form

$$\mathbf{R}_0 = \sum_i^{n_{\max}} x^{n_i \varepsilon} \left(\mathbf{R}_{0i} + \sum_j^{j_{\max}} \varepsilon^j \log^j(x) \mathbf{R}_{0i0}^{(j)} \right), \tag{3.48}$$

with $\mathbf{R}_{0i}$ and $\mathbf{R}_{0i0}^{(j)}$ being matrices of rational numbers, n_i being the eigenvalues of the matrix $\mathbf{D}$, and $n_{\max}$ being the total number of eigenvalues. The logarithmic terms in $\mathbf{R}$ appear when the matrix $\mathbf{D}$ is non-diagonal, and $j_{\max}$ depends on the position of the non-zero elements on the right of the diagonal.

On the other hand, we can use IBP reduction to express the pure basis elements ($\mathbf{g}$) in terms of a set of MIs ($\mathbf{G}$) through the relation

$$\mathbf{g} = \mathbf{T}\mathbf{G}. \tag{3.49}$$

In $\mathbf{G}$ we can apply expansion by region methods [202–207] in order to obtain information for their asymptotic behavior. In this way, for each MI (G_i) in the asymptotic limit $x \to 0$ we obtain a sum over region-integrals

$$G_i^{x\to 0} = \sum_j x^{b_j + a_j \varepsilon} G_{i,\text{region}}^{(b_j + a_j \varepsilon)}, \tag{3.50}$$

where a_j and b_j are integer numbers indicating the contributing regions ($x^{b_j + a_j}$) to G_i when $x \to 0$, and $G_{i,\text{region}}^{(b_j + a_j \varepsilon)}$ is the form that G_i obtains in the corresponding region (region-integral). All these can be computed using public codes such as `FIESTA` [201] and `pySecDec` [200]. Combining Eqs. (3.47), (3.49) and (3.50), we obtain the following powerful formula, which allows for the determination of all the boundaries at $x \to 0$

$$\mathbf{R}_0 \mathbf{b} = \lim_{x\to 0} \mathbf{T}\mathbf{G}\big|_{\mathcal{O}\left(x^{0 + a_j \varepsilon} \right)}, \tag{3.51}$$

where in the rhs we expand around $x = 0$, keeping terms only of order $x^{0 + a_j \epsilon}$ (leading regions), which are the only ones captured from the resummation matrix[19]. It is important to observe here that the lhs of Eq. (3.51) comprises pure functions with coefficients that are rational numbers (there is no dependence on the kinematic variables S). Therefore the same should hold true for the rhs, and thus we can determine the $\mathbf{T}$ matrix using IBP identities where we keep analytical the dependence on the variables x and ε, while we use (prime) numbers for the kinematic variables S. Let's call this way of computing the $\mathbf{T}$ matrix semi-numerical. For complicated problems where the analytic IBP reduction is non-trivial, this technique leads to a significant reduction in complexity and CPU time.

Concerning the determination of the boundaries using Eq. (3.51), first of all, when the lhs contains logarithmic terms since such terms do not appear in the rhs we put the coefficient of these terms to zero

$$\mathbf{R}_{0i0}^{(j)} \mathbf{b} = 0, \quad \text{for} \quad i = 1, \dots, n_{\max} \text{ and } j = 1, \dots j_{\max}. \tag{3.52}$$

---

[19]The resummation matrix method is "blind" in the sub-leading regions.

The last equation gives rise to a set of linear relations among elements of the array $\mathbf{b}$. Additionally, from powers of $x^{n_i \epsilon}$ that appear only on the lhs of Eq. (3.51), more linear relations are produced by vanishing their coefficients

$$\mathbf{R}_{0i}\mathbf{b} = 0, \quad \text{for} \quad n_i \neq a_j. \tag{3.53}$$

The relations obtained from Eqs. (3.52) and (3.53) are linear relations between the boundary conditions of different pure basis elements with rational numbers as coefficients, and therefore we shall call them *pure relations*. These relations contribute to determining a substantial portion of the components of the boundary array $\mathbf{b}$, and in some cases all of them. Finally, the application of this procedure (known boundaries from other families plus pure relations) may leave some elements of $\mathbf{b}$ undetermined, for the calculation of which one can use again Eq. (3.51) after computing first the region-integrals of Eq. (3.50) that contribute to them. In this case, if the $\mathbf{T}$ matrix has been computed semi-numerically then when implementing the region-integrals in Eq. (3.50) it is necessary to replace the rational factors of their transcendental functions with the same numerical values of S for which the $\mathbf{T}$ matrix was evaluated. Let us mention here that, for problems where this approach leads to a large number of region-integrals to be computed, one can apply the expansion by regions directly to the pure basis elements of which the boundary condition has not been determined [268]. This may significantly reduce the number of region-integrals to be computed while at the same time overpassing the need for an IBP reduction of the basis elements.

As we have already commented, one extra feature of the SDE approach is that by taking the limit of x approaching 1 in the solution, we can easily derive the solution for the same family involving one external massive momentum less (the one the off-shellness of which we captured with the introduction of x). This is again done utilizing the resummation matrix method but this time at $x = 1$ and making some further manipulations. More specifically, we start by rewriting the solution of Eq. (3.44) as an expansion in $\log(1-x)$ [266]

$$\mathbf{g} = \sum_{n \geq 0} \epsilon^n \sum_{i=0}^{n} \frac{1}{i!} \mathbf{c}_i^{(n)} \log^i(1-x), \tag{3.54}$$

with the coefficients $\mathbf{c}_i^{(n)}$ being finite in the limit $x \to 1$. This form is obtained by transporting the letter $l_2 = 1$ of all the GPLs to the right by employing shuffle properties. Having done this, we define the regular part of $\mathbf{g}$ at $x = 1$ as

$$\mathbf{g}_{\text{reg}} = \sum_{n \geq 0} \epsilon^n \mathbf{c}_0^{(n)}. \tag{3.55}$$

and through it, the truncated part of $\mathbf{g}$ by setting $x = 1$ to the regular part [266]

$$\mathbf{g}_{\text{trunc}} = \mathbf{g}_{\text{reg}}\big|_{x=1}. \tag{3.56}$$

In the next step, from the residue matrix of the letter $l_2 = 1$, $\mathbf{M}_2$, we define the resummation matrix at $x = 1$, following exactly the same procedure as we did for the resummation matrix at $x = 0$, meaning

$$\mathbf{R}_1 = \mathbf{S}_1 e^{\epsilon \mathbf{D}_1 \log(1-x)} \mathbf{S}_1^{-1} \quad \text{with} \quad \mathbf{M}_1 = \mathbf{S}_1 \mathbf{D}_1 \mathbf{S}_1^{-1}. \tag{3.57}$$

$\mathbf{R}_1$ contains terms of the form $(1 - x)^{a_i \epsilon}$, where a_i represents the eigenvalues of $\mathbf{M}_1$. Setting these terms to zero, we obtain the following purely numerical matrix

$$\mathbf{R}_{10} = \mathbf{R}_1 \big|_{(1-x)^{a_i \epsilon} \to 0} . \tag{3.58}$$

Then we determine the limit $x \to 1$ of Eq. (3.44) by the acting with the above matrix on the truncated part of the bases elements

$$\mathbf{g}_{x \to 1} = \mathbf{R}_{10} \mathbf{g}_{\text{trunc}} \tag{3.59}$$

The family with one off-shell external momentum less, the solution of which we obtain by Eq. (3.59), has always a fewer number of MIs ($N_{n_{\text{off}}-1}$), than the one we started from ($N_{n_{\text{off}}}$). Thus as a last step, one needs to distinguish from the $N_{n_{\text{off}}}$ basis elements $\mathbf{g}_{x \to 1}$, $N_{n_{\text{off}}-1}$ of them that are independent and can be chosen as basis elements of the family with the reduced (by one) degree of off-shellness. This can be done using IBP identities, but before doing so one can take advantage of an intriguing characteristic of $\mathbf{R}_{10}$, which simplifies the IBP reduction procedure or even skips it. Remarkably, $\mathbf{R}_{10}$ is an *idempotent matrix* and thus possesses the following properties

1. $\mathbf{R}_{10} = \mathbf{R}_{10}^2$.

2. $\text{Trace}\big(\mathbf{R}_{10}\big) = \text{Rank}\big(\mathbf{R}_{10}\big)$.

3. It is singular (except if it is equal to the identity matrix $\mathbf{I}$).

4. Its eigenvalues are either 0 or 1.

5. The matrix $\mathbf{I} - \mathbf{R}_{10}$ is also idempotent.

By multiplying Eq. (3.59) from the left with $\mathbf{R}_{10}$, the first of these properties, implies

$$\mathbf{R}_{10} \mathbf{g}_{x \to 1} = \mathbf{R}_{10}^2 \mathbf{g}_{\text{trunc}} = \mathbf{R}_{10} \mathbf{g}_{\text{trunc}} \Rightarrow \mathbf{R}_{10} \mathbf{g}_{x \to 1} = \mathbf{g}_{x \to 1}. \tag{3.60}$$

Solving this relation as an equation for each row provides us with the means to determine linearly independent basis elements for the family with $N_{n_{\text{off}}-1}$ MIs. It is important to comment here though that, the outcome of this method, as it concerns the number of linearly independent basis elements that are identified, depends on the choice of the SDE-parametrization. Our findings thus far indicate that the selection of a parametrization where x is introduced to two of the external momenta is the most optimal for applying this method, as in all the studied cases has resulted in a number of linearly independent basis elements that matched the $N_{n_{\text{off}}-1}$ MIs, skipping in this way the IBP reduction. This correspondence can also be confirmed by calculating the rank of $\mathbf{R}_{10}$, which should be equal to $N_{n_{\text{off}}} - N_{n_{\text{off}}-1}$ in order for the IBP reduction to be skipped.

Chapter 4

Two-Loop Amplitude Construction using `HELAC`

In this chapter, we present in detail the algorithm for the construction of two-loop scattering amplitudes within `HELAC-2LOOP` (initialization phase), an under-construction package for automated computations of two-loop scattering amplitudes. More specifically, we will start by stretching the basic steps of the algorithm and after that, we will focus on its new features with respect to the existing `HELAC` framework, explaining the logic behind each step[1]. Furthermore, we provide a concrete schematic example of the construction of a two-loop numerator to the amplitude of a specific process, and present/discuss our results for the construction of the two-loop amplitudes of several processes. This chapter is based on novel work presented in the conference proceedings [1–3].

4.1 Introduction to the Algorithm

Similar to the one-loop case, the computation of a scattering amplitude at the two-loop level involves gathering Feynman diagrams according to their loop-assignment structure, in order for the reduction to master integrals to be facilitated. For this reason, as in `HELAC-1LOOP` [88, 97], we follow a hybrid approach between Feynman diagrams and Dyson-Schwinger recursion for the construction of scattering amplitudes within `HELAC-2LOOP`. Our algorithm is based on the observation that any n-particle two-loop topology can be consistently matched to an $(n+2)$-particle one-loop topology, allowing for the application of the algorithm developed in `HELAC-1LOOP` after making some appropriate modifications. In this section, we will provide a brief overview of the steps involved in this algorithm, which are also summarized schematically in Figure 4.1. In Subsequent sections, we will delve into some of these steps in more detail and present a concrete example to illustrate how the algorithm works in practice.

For a given process at hand, described by a specific number of external particles, n, and their flavors, $\{f_1, \ldots, f_n\}$, one starts by choosing one of the three master blob-topologies that exist at two loops, denoted as *theta-*, *infinity-* and *dumbbell-topologies*. Of course, all three of them are eventually taken into account for the correct computation of all the numerator contributions to the scattering amplitude. Then, this step is followed by the production of all potential flavors that can be acquired by the first set

---

[1]In some cases, it may seem that we depth into too many details as it regards the algorithm but this is done in order for this chapter to be a reference for future users who want to get involved with `HELAC-2LOOP`.

of *cut-particles*, meaning the $n+1$ (f_{n+1}) and $n+2$ ($f_{n+2} = \bar{f}_{n+1}$) particles described by the binary numbers 2^n and 2^{n+1}, respectively. In the next step for each flavor combination of the $n+2$ particles, one generates all the possible $(n+2)$-particle color-states[2] in the color-flow representation, $(n_g + n_{q\bar{q}})!$ in total[3]. After that for every $(n+2)$-particle color-state we generate all the independent two-loop n-particle blob-topologies belonging to the chosen master blob-topology. These topologies are subsequently cut and uniquely corresponded to $(n+2)$-particle one-loop blob-topologies[4], which are dressed with all feasible flavors and colors allowed by SM Feynman rules and color conservation.

Afterward, the constructed one-loop configurations are cut resulting in tree-level configurations with $n+4$ particles. The second set of cut-particles arising from the last cut obtains the usual binary numbering, meaning 2^{n+2} for the $n+3$ particle and 2^{n+3} for the $n+4$ one, and their flavor is defined by the flavor of the cut loop-particle, f_{loop}, with the $n+3$ particle bearing flavor $f_{n+3} = \bar{f}_{\text{loop}}$ and the $n+4$ one bearing flavor $f_{n+4} = f_{\text{loop}}$. The cutting process also introduces additional color lines to the existing color connection, leading from an $(n+2)$-particle color-state to an $n+4$ one. If the cut-propagator is a gluon/ghost, two more color lines are added, while if it is a quark/anti-quark, only one more color line is added, with the extra color lines corresponding to the two extra particles. After the introduction of the extra color lines, the color and anti-color indices of all the particles are appropriately reassigned according to the flow of color before the cut (see [88, 97]).

In the next step, for every $(n+4)$-particle tree-level configuration a sequence of sub-amplitudes is constructed, which respects the loop-assignment structure of the configuration. This means that one starts from the particle 2^{n+2} and combines it with the last blob[5] in order to create the next sub-amplitude that describes the corresponding loop-particle. Then, the latter sub-amplitude is subsequently combined with the next blob (penultimate) in order to create the sub-amplitude of the corresponding loop-particle, and this procedure goes on till arriving at the (first) blob which is combined (except for particle 1) with the previous sub-amplitude and the particle 2^{n+3}, in such a way that the particle 1 to be always the last particle of the recursion. At every point of this procedure, Dyson-Schwinger recursion is applied to the higher-level blobs that contain only external particles (i.e. binary numbers from the set $\{2, \ldots, 2^{n-1}\}$), creating extra sub-amplitudes contributing to the configuration. The careful reader will have by now observed that this step of the algorithm is exactly the same as the one applied in the one-loop case, which we discussed in subsection 2.3.2[6]. The only new feature that differs with respect to the one-loop case is that, when the first cut is done, information about the structure of the cut loop-line is explicitly kept, and when one arrives at the blob containing the particle 2^{n+1}, this information is used in order to create the sub-amplitudes corresponding to the loop-particles of this loop-line.

Subsequently, for each configuration, the projection of the $(n+4)$-particle color-state

---

[2]As a color-state here we define a combination of Kronecker's deltas like the ones in Eq. (2.27).

[3]Assuming that in the $n+2$ particles are included n_g gluons and $n_{q\bar{q}}$ sets of quarks and anti-quarks.

[4]At this point the external one-loop process is fixed as we have specific flavors and colors for the $n+2$ particles.

[5]Same as in `HELAC-1LOOP`, the last blob of the configuration corresponds to the first one encountered moving counterclockwise (on the one-loop blob-topology) from the blob containing the particle 1.

[6]With the replacements $2^n \to 2^{n+2}$ and $2^{n+1} \to 2^{n+3}$.
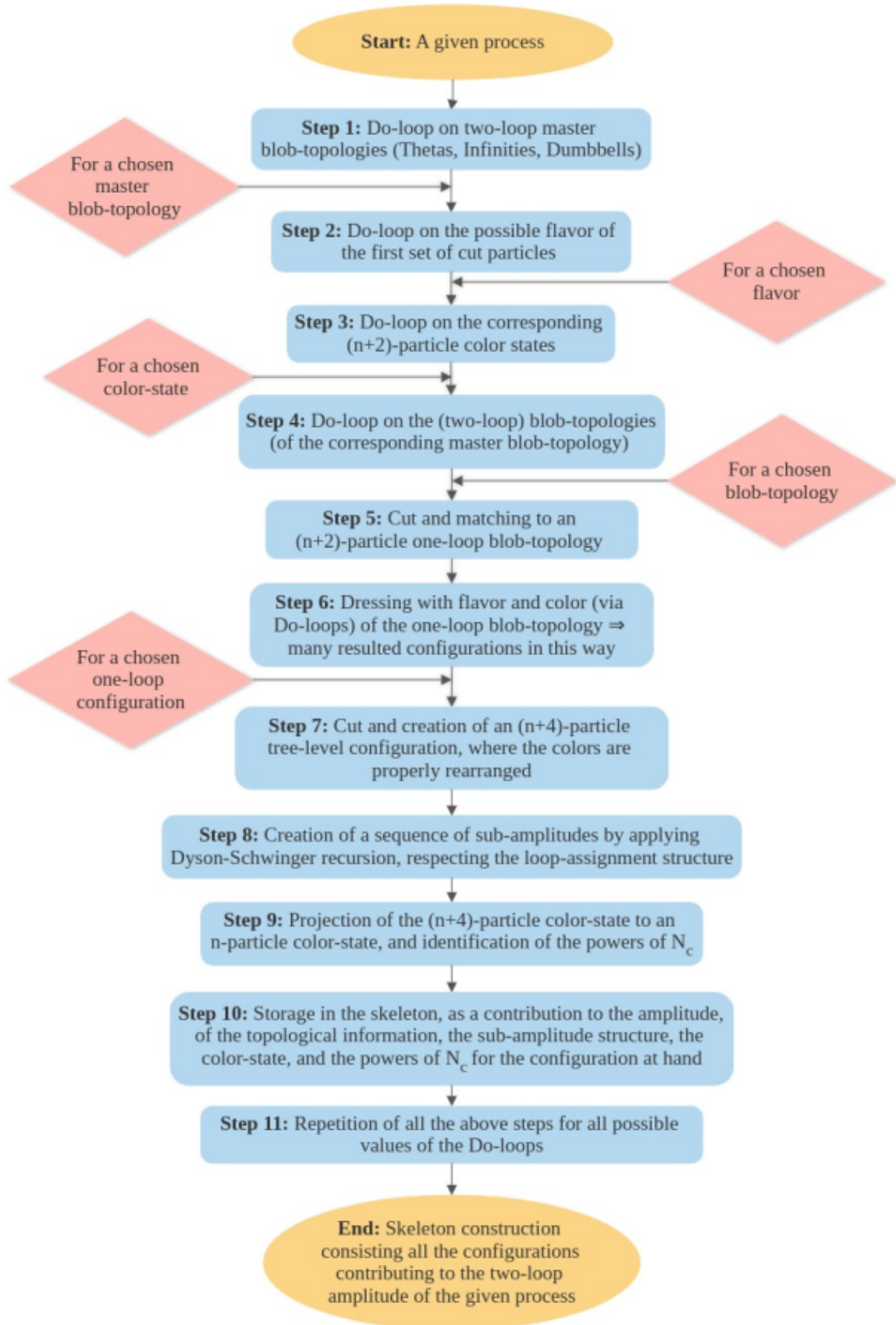
Figure 4.1: A schematic summary of the algorithm implemented in `HELAC-2LOOP`, for the construction of two-loop scattering amplitudes.
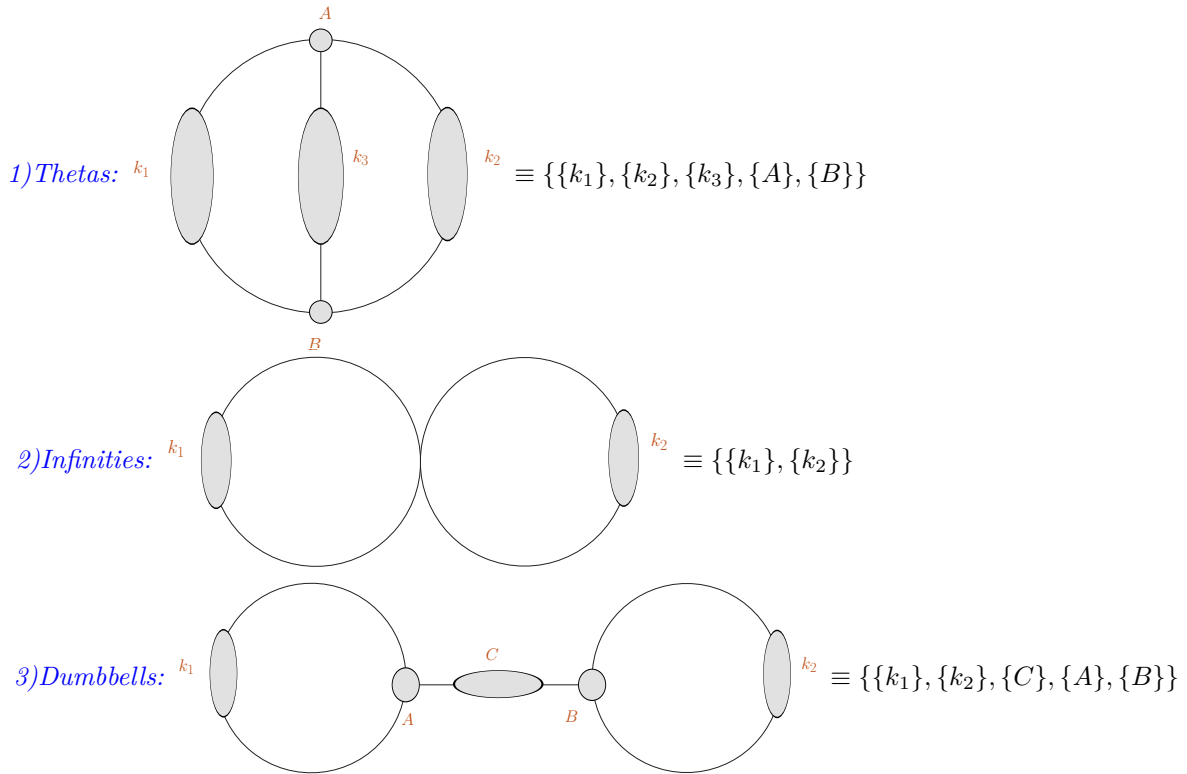
Figure 4.2: The three master blob-topologies contributing to two-loop scattering amplitudes. The sub-lists represent the incoming blobs to the corresponding loop-lines (k_1, k_2, k_3), the internal line (C), and the vertex points (A, B). We observe that *theta-topologies* are genuinely two-loop topologies, while *infinities* and *dumbbells* correspond to one-loop squared topologies.

to an n-particle color-state[7] and the identification of the powers of N_c coming from this projection are done. The projection happens through the contraction of the $(n + 4)$-particle color-state with the Kronecker delta functions $\delta_{i_{n+2}}^{j_{n+1}} \delta_{i_{n+1}}^{j_{n+2}} \delta_{i_{n+4}}^{j_{n+3}} \delta_{i_{n+3}}^{j_{n+4}}$, which in practice apply the constraint that the color (anti-color) index of the one cut-particle should be equal to the anti-color (color) index of the other cut-particle of the same set of cut-particles. In the last step, for every configuration, the topological information, together with the sub-amplitude structure, the n-particle color-state, and the powers of N_c, are stored in the skeleton.

The execution of the above-described algorithm, concludes the initialization phase of `HELAC-2LOOP` and results in the completion of the skeleton, which contains all the configurations contributing to the two-loop scattering amplitude of the process at hand. Aimed at the study of QCD corrections, the current implementation works and has been validated for processes containing only (massless) quarks, ghosts, and gluons running within the loops, and for up to five external particles. Although not tested, after some small modifications concerning the capacity of some arrays, the implementation should work, without taking into account possible efficiency and memory constraints of the used machine, for any number of external particles.

---

[7]This projection is unequivocal in the sense that each $(n + 4)$-particle color-state is projected to one only n-particle color-state, but obviously different $(n + 4)$-particle color-states could be projected to the same n-particle color-state.

4.2   Blob-Topology Generation

As we already mentioned, at two loops the scattering amplitude receives contributions from three different graph topologies, which according to their shape we name *theta*, *infinity*, and *dumbbell*. Within the `HELAC` framework, this means that we need to construct the corresponding three master blob-topologies which we describe via a list representation as depicted in Figure 4.2. As can be seen from this figure, for the *theta-* and the *dumbbell-topologies* we use a five-list format, with the sub-lists $\{k_1\}, \ldots, \{k_3\}, \{C\}$ describing the blobs attached to the momentum-lines $k_1, \ldots, k_3, C$, respectively, and with the sub-lists $\{A\}, \{B\}$ expressing the blobs attached to the vertices A and B. For the *infinity-topologies* we use a two-list format, with each sub-list $\{k_1\}, \{k_2\}$ containing the blobs attached to the corresponding loop-line. We comment here that due to the fact that in the SM there exist only three-particle and four-particle vertices, it is not possible for blobs to be attached in the vertex of the infinity-topologies where the loop-lines k_1 and k_2 are connected. In Figure 4.3 we quote some examples of two-loop blob-topologies for underlining the notation and the interpretation of the used list representation.

For obtaining the two-loop blob-topologies we have created two generators, one implemented in `Mathematica` (named `BlobMod`) and one implemented in `FORTRAN` (named `GENTOOLS`), each of which is using a different approach for the generation of the blob-topologies. More specifically

- `BlobMod` starts by putting external particles (level-1 blobs) in the sub-lists, taking into account all possible combinations. In this way, all the high-sector topologies are created and represented by lists of sub-lists. Then in order to create the lower-sector topologies, if there exist lists containing sub-lists with two or more blobs within a sub-list, it takes for every list all the possible combinations of summing at most two neighboring blobs of the same sub-list[8]. This step is repeated till arriving at topologies where at most one blob is included in their sub-lists (lowest-sector topologies). In all the steps of the generation, an ordering on the size of sub-lists together with graph symmetries, are applied for the removal of identical topologies.

- `GENTOOLS` generates the blob-topologies exactly in the opposite way of `BlobMod`, meaning that it starts by putting higher-level blobs in the sub-lists in all possible ways and then takes all possible splittings of them into lower-level blobs till it arrives at topologies consisting only of level-1 blobs (high-sector topologies). In order to avoid double countings and remove identical blob-topologies, an ordering is kept on the size of the sub-lists, and graph symmetries are also applied.

Graphs are symmetric in combined or individual mirror transformations on the vertical[9] and the horizontal axis. Remarkably, all the symmetries of the graphs can be translated into symmetries of the lists using one or both of the following two actions

1. Swap of two sub-lists, e.g. $\{\{k_1\}, \{k_2\}\} \to \{\{k_2\}, \{k_1\}\}$.

2. Reversion of the elements of a sub-list, e.g. $\{1, 2, 4\} \to \{4, 2, 1\}$.

---

[8]Vertices $\{A\}$ and $\{B\}$ can receive at most one blob, of any level though.

[9]For the *theta-topologies*, this symmetry is interpreted as symmetry under the interchange of the three loop lines.
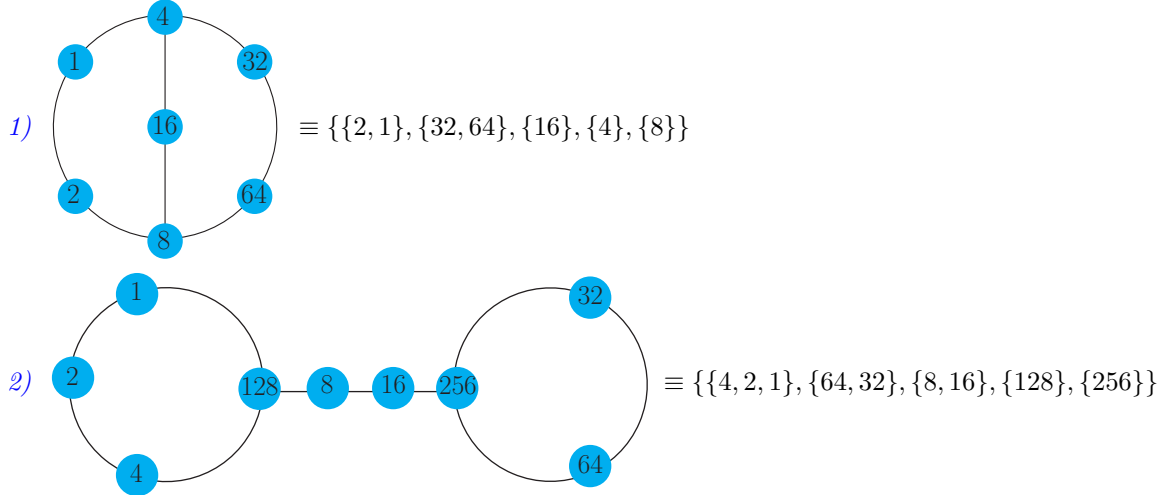
Figure 4.3: In *theta-topologies* the blobs in the sub-lists $\{k_1\}$ and $\{k_3\}$ are listed starting from the point B and ending at A, while in $\{k_2\}$ starting from A and ending at B. In *infinity-* and *dumbbell-topologies* the blobs in $\{k_1\}$ and $\{k_2\}$ are listed using a bottom-up approach, and the blobs in $\{C\}$ (dumbbells only) are listed starting from the point A and ending at B.

In particular, using these actions, the graph symmetries of the *theta-topologies* can be expressed as[10]

$$
\begin{aligned}
\{\{k_1\}, \{k_2\}, \{k_3\}, \{A\}, \{B\}\} &= \{R[\{k_1\}], R[\{k_2\}], R[\{k_3\}], \{B\}, \{A\}\} \\
&= \{R[\{k_1\}], R[\{k_3\}], R[\{k_2\}], \{B\}, \{A\}\} \\
&= \{R[\{k_2\}], R[\{k_1\}], R[\{k_3\}], \{B\}, \{A\}\} \\
&= \{R[\{k_2\}], R[\{k_3\}], R[\{k_1\}], \{B\}, \{A\}\} \\
&= \{R[\{k_3\}], R[\{k_1\}], R[\{k_2\}], \{B\}, \{A\}\} \\
&= \{R[\{k_3\}], R[\{k_2\}], R[\{k_1\}], \{B\}, \{A\}\}, \qquad (4.1) \\
&= \{\{k_1\}, \{k_3\}, \{k_2\}, \{A\}, \{B\}\} \\
&= \{\{k_2\}, \{k_1\}, \{k_3\}, \{A\}, \{B\}\} \\
&= \{\{k_2\}, \{k_3\}, \{k_1\}, \{A\}, \{B\}\} \\
&= \{\{k_3\}, \{k_1\}, \{k_2\}, \{A\}, \{B\}\} \\
&= \{\{k_3\}, \{k_2\}, \{k_1\}, \{A\}, \{B\}\}
\end{aligned}
$$

the graph symmetries of the *dumbbell-topologies* can be written as

$$
\begin{aligned}
\{\{k_1\}, \{k_2\}, \{C\}, \{A\}, \{B\}\} &= \{R[\{k_2\}], R[\{k_1\}], R[\{C\}], \{B\}, \{A\}\} \\
&= \{R[\{k_1\}], R[\{k_2\}], \{C\}, \{A\}, \{B\}\} \\
&= \{R[\{k_2\}], \{k_1\}, R[\{C\}], \{B\}, \{A\}\} \\
&= \{\{k_2\}, R[\{k_1\}], R[\{C\}], \{B\}, \{A\}\} \qquad , \qquad (4.2) \\
&= \{\{k_1\}, R[\{k_2\}], \{C\}, \{A\}, \{B\}\} \\
&= \{\{k_2\}, \{k_1\}, R[\{C\}], \{B\}, \{A\}\} \\
&= \{R[\{k_1\}], \{k_2\}, \{C\}, \{A\}, \{B\}\}
\end{aligned}
$$

---

[10] Where we use the abbreviation $R[\{k_i\}] \equiv Reverse[\{k_i\}]$.
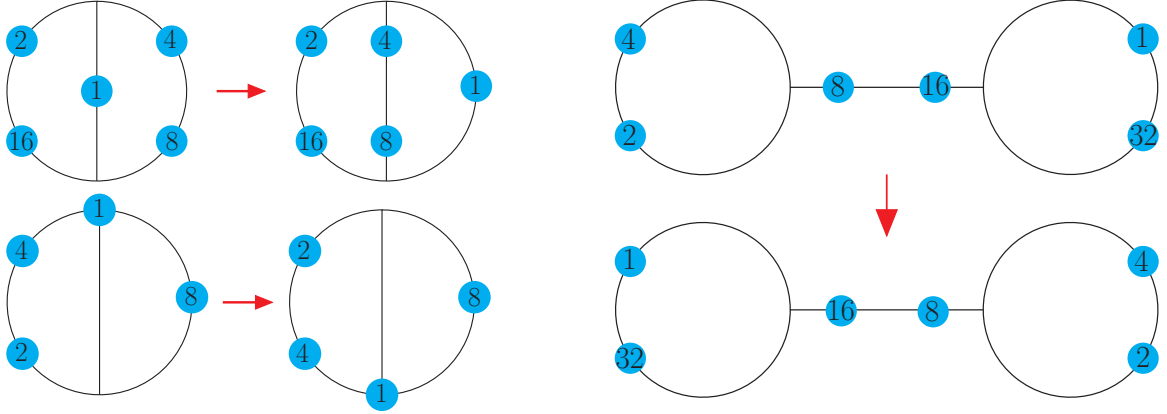
Figure 4.4: Three examples (two thetas in lhs and one dumbbell in rhs) of reordering of the sub-lists in order for the blob containing the particle 1 to be included in a desired sub-list.

and finally, the graph symmetries of the *infinity-topologies* can be formulated as

$$\{\{k_1\}, \{k_2\}\} = \{R[\{k_1\}], R[\{k_2\}]\} = \{R[\{k_1\}], \{k_2\}\} = \{\{k_1\}, R[\{k_2\}]\}$$
$$= \{R[\{k_2\}], \{k_1\}\} = \{\{k_2\}, R[\{k_1\}]\} = \{R[\{k_2\}], R[\{k_1\}]\}. \qquad (4.3)$$
$$= \{\{k_2\}, \{k_1\}\}$$

The ordering that we apply (in all the master topologies) for the sub-lists during the generation of the blob-topologies is the following

$$L_1 \geq L_2 \geq L_3 \geq L_C \geq 0, \quad 0 \leq L_A \leq 1, \quad \text{and} \quad 0 \leq L_B \leq 1, \qquad (4.4)$$

where we denote with $\{L_1, L_2, L_3\}$ the size (length) of the sub-lists $\{\{k_1\}, \{k_2\}, \{k_3\}\}$ and with $\{L_A, L_B, L_C\}$ the size of the sub-lists $\{\{A\}, \{B\}, \{C\}\}$. After the generation[11], wherever is needed, we reorder the sub-lists of the blob-topologies so that the blob containing the particle 1 to be always included in the sub-lists (see Figure 4.4 for examples):

- Thetas: $\{k_1\}$, $\{k_2\}$ or $\{B\}$. Thus when this blob is in $\{k_3\}$ we swap $\{k_3\}$ with $\{k_2\}$, while when it is in $\{A\}$ we swap $\{A\}$ with $\{B\}$ and reverse the blobs of $\{k_1\}$, $\{k_2\}$ and $\{k_3\}$.

- Infinities: $\{k_1\}$. Thus when this blob is in $\{k_2\}$ we swap it with $\{k_1\}$.

- Dumbbells: $\{k_1\}$, $\{A\}$ or $\{C\}$. Thus when this blob is in $\{k_2\}$ or $\{B\}$ we swap $\{k_2\}$ with $\{k_1\}$ and $\{B\}$ with $\{A\}$ and we reverse the order of blobs in $\{C\}$.

Moreover, after the reordering of the blob-topologies the following extra filters are applied in order to remove tadpole, snail, self-energy, and scaleless graphs (assuming that the loop particles are massless):

- Thetas: remove graphs with i) $n_{bl} = 1$, and ii) $n_{bl} = 2$ with the level of one of the blobs equal to 1.

---

[11]This is done for purposes of efficiency throughout the step where the Dyson-Schwinger recursion is applied to the blobs.
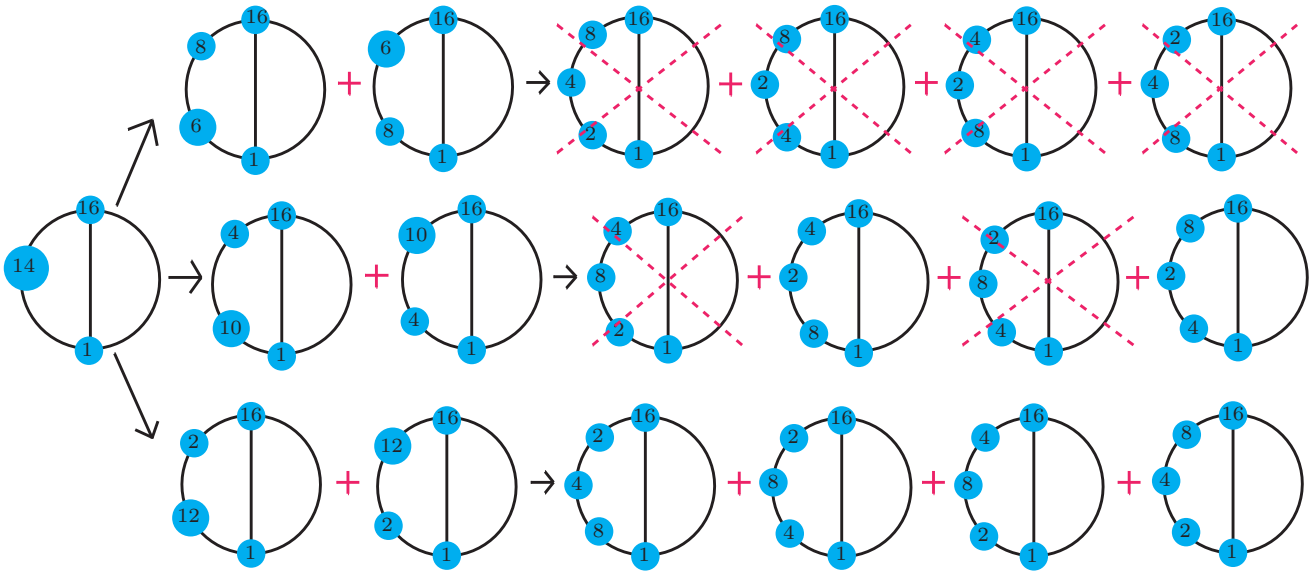
Figure 4.5: Schematic example of how the algorithm in `GENTOOLS` works. Starting from the leftmost higher-sector blob-topology the ones on rhs (lower-sector) are created, where six of them are identical (due to graph symmetries) to the rest ones and thus are removed.

- **Infinities and Dumbbells:** remove graphs with i) $L_{k_1} = 0$ ($L_{k_2} = 0$), and ii) $L_{k_1} = 1$ ($L_{k_2} = 1$) with the level of the blob in $\{k_1\}$ ($\{k_2\}$) being equal to 1.

where n_{bl} is the number of blobs of the topology, defined as

$$n_{bl} = \begin{cases} L_1 + L_2 + L_3 + L_A + L_B, & \text{for theta-topologies} \\ L_1 + L_2, & \text{for infinity-topologies} \\ L_1 + L_2 + L_A + L_B + L_C, & \text{for dumbbell-topologies} \end{cases} \quad (4.5)$$

To ensure that we have accounted for all necessary topologies and have not included any unnecessary ones, we performed an exhaustive comparison of the blob-topologies generated by both methods. Additionally, we compared these results with the graph topologies generated by `QGRAF` [81] for up to six external particles. In all cases we found complete agreement, confirming the consistency of our approach. As anticipated due to be functioning in a low-level programming language (`FORTRAN`), the computational efficiency of `GENTOOLS` surpasses that of `BlobMod`, making it the preferred generator implemented in `HELAC-2LOOP`. To provide a clearer illustration of the procedure outlined earlier, Figure 4.5 presents a schematic example of how `GENTOOLS` generates higher-level topologies from a lower-sector topology, specifically for a *theta-topology*. This visual aid enhances the understanding of the process.

Similar to Feynman graphs, blob-topologies are associated with symmetry factors. In the framework of `HELAC-2LOOP`, these symmetry factors are considered during the computational phase. A comprehensive summary of the symmetry factors corresponding to blob-topologies is provided in Appendix A.
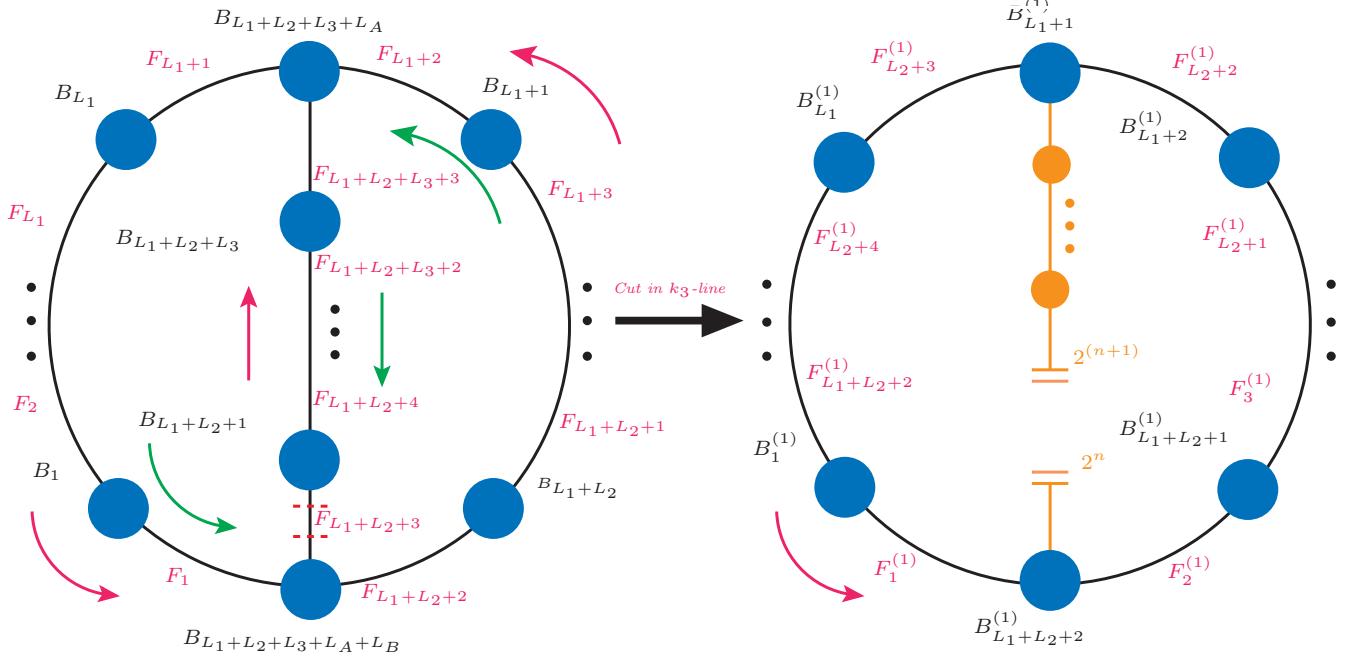
Figure 4.6: A graphical representation of the cutting procedure in a generic *theta-topology*. In lhs we have the two-loop blob-topology and in rhs the resulted one-loop one. The orange part in rhs corresponds to the structure that is stored as extra information when computing the one-loop blobs $B^{(1)}_{L_1+1}$ and $B^{(1)}_{L_1+L_2+2}$. In lhs the cut is represented with a red dashed double line, while the red (green) arrows on both sides (lhs) indicate the flavor (momentum) flow. The blobs $B_1, \ldots, B_{L_1+L_2+L_3+L_A+L_B}$ and the flavors $F_1, \ldots, F_{L_1+L_2+L_3+3}$ are the ones stored in the last line of the numerators in the skeleton.

4.3 Cut - Dress - Cut

As previously stated, after creating the two-loop blob-topologies we cut them, reorder them, and dress with flavor and color the yielded one-loop blob-topologies. The propagator in a two-loop blob-topology, where we apply the first cut depends on which master topology the given blob-topology belongs to. Afterward, we cut the one-loop blob-topologies and obtain tree-level configurations, where, after the reassignment of the colors/anti-color indices of the $n+4$ particles, Dyson-Schwinger recursion is applied respecting their (two-loop) loop-assignment structure. In this section, we will focus on the way that the first cut is committed and we will briefly elaborate the dressing procedure, which is the same as in the one-loop case, and justify the reason why this happens at one-loop level and not directly at two-loop.

4.3.1 From Two-Loop to One-Loop: Theta-Topologies

The general form of a *theta-topology* corresponds to the one illustrated on the lhs of Figure 4.6, where we use B_i, with $i = 1, \ldots, L_1 + L_2 + L_3 + L_A + L_B$, to represent the blobs, and F_i, with $i = 1, \ldots, L_1 + L_2 + L_3 + 3$, to denote the flavors of the loop particles. In our approach, we consistently perform a cut in the first propagator of the k_3 loop-line ascending from the vertex B, specifically meaning the propagator carrying flavor $F_{L_1+L_2+3}$ in Figure 4.6. This leads to the formation of a one-loop blob-topology characterized by a set of blobs, denoted as $B^{(1)}_1, \ldots, B^{(1)}_{L_1+L_2+2}$, and a set of
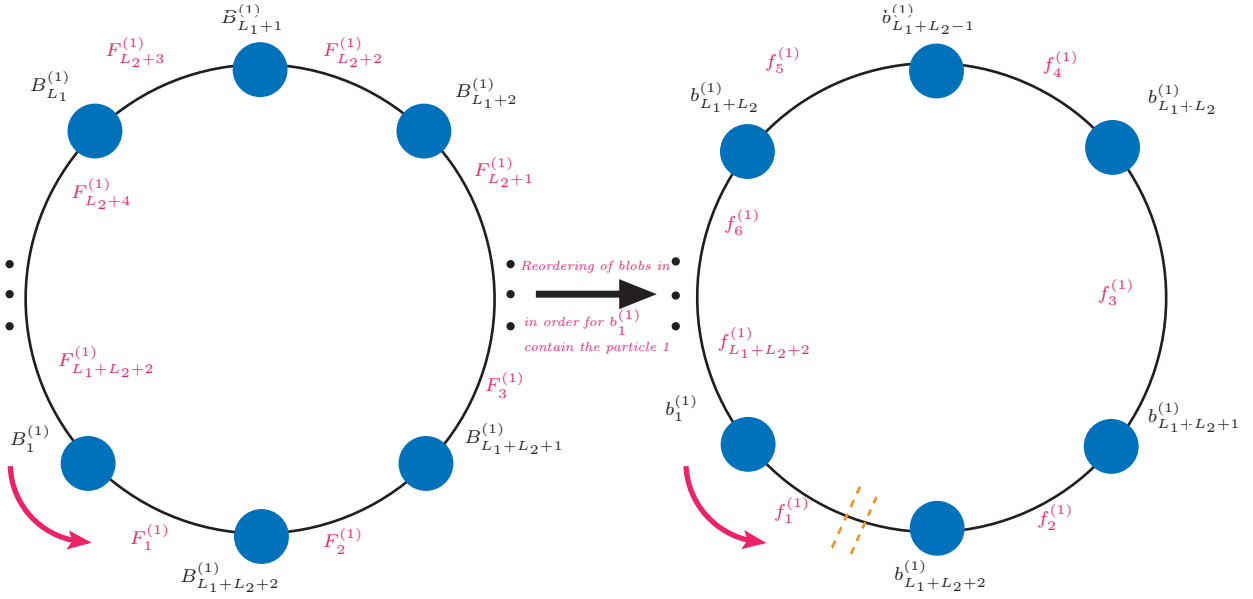
Figure 4.7: Visual depiction of the re-ordering of the blobs of a one-loop blob-topology, originating from a theta-topology. The lhs of this figure is identical to the rhs of Figure 4.6. After the reordering (rhs) the blob containing the particle 1 is $b_1^{(1)}$, and the second cut which drives us to the tree-level configuration is performed in the propagator with flavor $f_1^{(1)}$ (the cut in this picture is represented with the two orange dashed lined).

flavors for the loop particles, denoted as $F_1^{(1)}, \ldots, F_{L_1+L_2+2}^{(1)}$, which are connected to the corresponding two-loop counterparts.

It is crucial during this transition from the two-loop to the one-loop blob-topology that the information pertaining to the structure of the cut loop-line[12] (depicted in orange in Figure 4.6) to be explicitly preserved, and its blobs together with the resulted cut-particles to be included in the definition of the following one-loop blobs

$$
\begin{aligned}
B_{L_1+1}^{(1)} &= 2^{n+1} + B_{L_1+L_2+1} + \cdots + B_{L_1+L_2+L_3} + B_{L_1+L_2+L_3+L_A} \\
B_{L_1+L_2+2}^{(1)} &= 2^n + B_{L_1+L_2+L_3+L_A+L_B}
\end{aligned}
\tag{4.6}
$$

The rest of the one-loop blobs and flavors, are defined algorithmically by the two-loop ones through the relations

$$
\begin{aligned}
&\textcolor{red}{\text{For } 1 \leq i \leq L_1\colon} B_i^{(1)} = B_i,\ F_1^{(1)} = F_1 \text{ and } F_{L_1+L_2+3-i}^{(i)} = F_{i+1} \\
&\textcolor{red}{\text{For } 1 \leq i \leq L_2\colon} B_{L_1+1+i}^{(1)} = B_{L_1+i} \text{ and } F_{L_2+3-i}^{(1)} = F_{L_1+1+i} \text{ (till } L_2+1)
\end{aligned}
\tag{4.7}
$$

Subsequently, as already discussed, the one-loop blob-topology is re-ordered before being dressed with flavor and color, in order for the particle one to be included in first blob of the one-loop topology. In figure 4.7 we present an schematic illustration of how this reordering is done. Assuming that the particle 1 is placed in the blob $B_{i_2}^{(1)}$, the blobs, $b_i^{(1)}$, and the flavors, $f_i^{(1)}$, of the reordered topology are determined from the

---

[12]Meaning the order of the blobs.
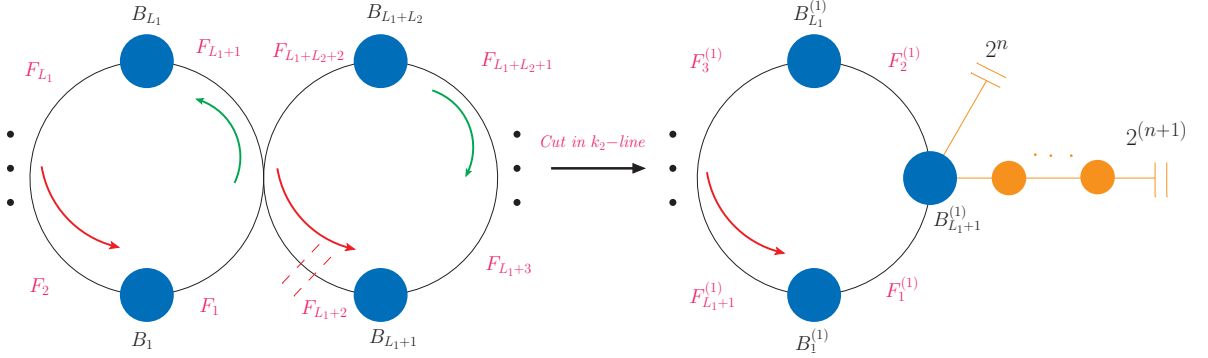
Figure 4.8: A graphical illustration of the cutting process in a generic *infinity-topology*. On the lhs we have the two-loop infinity-topology, while on the rhs we see the resulting one-loop blob-topology. The orange section on the rhs represents the additional structure that is stored when computing the one-loop blob $B^{(1)}_{L_1+1}$. On the lhs, the cut is depicted by red dashed double lines, and the red (green) arrows indicate the flow of flavors (momenta). The blobs $B_1, \ldots, B_{L_1+L_2}$ and the flavors $F_1, \ldots, F_{L_1+L_2+2}$ are the ones stored in the last line of the numerators in the skeleton.

unordered ones using the prescription (for $1 \leq i \leq L_1 + L_2 + 2$)

$$\begin{aligned}
&\text{For } i = 1: b^{(1)}_1 = B^{(1)}_{i_2} \text{ and } f^{(1)}_{i_2} = F^{(1)}_1 \\
&\text{For } i + i_2 - 1 \leq L_1 + L_2 + 2: b^{(1)}_i = B^{(1)}_{i+i_2-1} \text{ and } f^{(1)}_{i+i_2-1} = F^{(1)}_i. \\
&\text{Else: } b^{(1)}_i = B^{(1)}_{i_2+i-L_1-L_2-3} \text{ and } f^{(1)}_{i_2+i-L_1-L_2-3} = F^{(1)}_i
\end{aligned} \tag{4.8}$$

4.3.2 From Two-Loop to One-Loop: Infinity-Topologies

The typical structure of an *infinity-topology* is represented by the lhs of Figure 4.8. In this drawing, we make use of the symbols $B_1, \ldots, B_{L_1+L_2}$ to represent the blobs, and $F_1, \ldots, F_{L_1+L_2+2}$ to indicate the flavors associated with the loop particles. The first cut in an infinity-topology occurs at the first propagator of the k_2 loop-line, specifically, the propagator associated with flavor F_{L_1+2} in Figure 4.8. As a result of this cut, a one-loop blob-topology is formed, which is described by the set of blobs $B^{(1)}_1, \ldots, B^{(1)}_{L_1+1}$ and the set of loop-particle flavors $F^{(1)}_1, \ldots, F^{(1)}_{L_1+1}$.

Once again, in this master blob-topology, details in the structure of the cut loop-line (depicted in orange in Figure 4.8) are explicitly stored, and one-loop blobs and flavors are related to the infinity ones via the equations

$$\begin{aligned}
&\text{For } 1 \leq i \leq L_1: B^{(1)}_i = B_i, \text{ and } F^{(1)}_{L_1+2-i} = F_{i+1} \\
&\text{Else: } B^{(1)}_{L_1+1} = 2^n + 2^{n+1} + B_{L_1+1} + \cdots + B_{L_1+L_2}, \text{ and } F^{(1)}_1 = F_1
\end{aligned} \tag{4.9}$$

where, due to the fact that within SM only gluons interact via a four-particle vertex, we have $F^{(1)}_1 = F_1 = $ gluon.
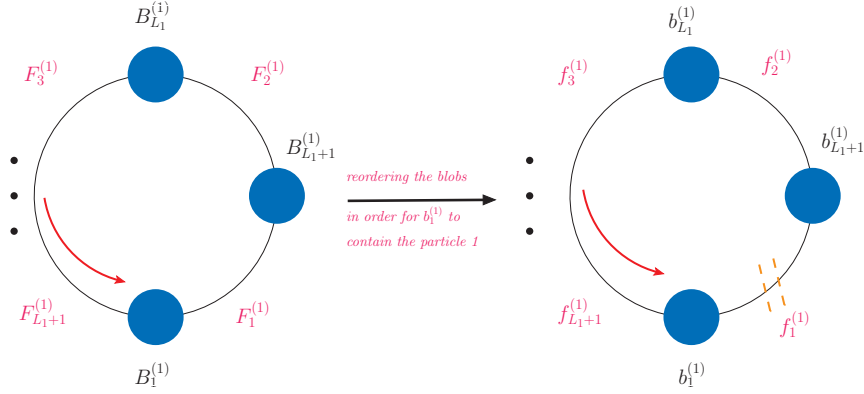
Figure 4.9: This figure provides a visual representation of the re-ordering of the blobs in a one-loop blob-topology derived from an infinity- or dumbbell-topology. The lhs is identical to the rhs of Figures 4.8 and 4.10. After the reordering (rhs), the blob that contains particle 1 is labeled as $b_1^{(1)}$. The second cut, which brings us to the tree-level configuration, is done on the propagator with flavor $f_1^{(1)}$ and is represented by the two orange dashed lines in this figure.

Afterward, the one-loop blob-topology is re-ordered so that the blob containing the particle 1 is the first blob of the topology (see Figure 4.9). By assuming that particle 1 is located in blob $B_{i_2}^{(1)}$, we can determine the blobs $b_i^{(1)}$ and flavors $f_i^{(1)}$ of the reordered topology based on the unordered ones. This can be achieved using the following prescription for $1 \leq i \leq L_1 + 1$

$$
\begin{aligned}
&\text{For } i = 1: b_1^{(1)} = B_{i_2}^{(1)} \text{ and } f_{i_2}^{(1)} = F_1^{(1)} \\
&\text{For } i + i_2 - 1 \leq L_1 + 1: b_i^{(1)} = B_{i+i_2-1}^{(1)} \text{ and } f_{i+i_2-1}^{(1)} = F_i^{(1)}. \\
&\text{Else: } b_i^{(1)} = B_{i_2+i-L_1-2}^{(1)} \text{ and } f_{i_2+i-L_1-2}^{(1)} = F_i^{(1)}
\end{aligned}
\tag{4.10}
$$

4.3.3   From Two-Loop to One-Loop: Dumbbell-Topologies

The lhs of Figure 4.10 showcases the general structure of a dumbbell-topology. As in the other master blob-topologies, we use $B_1, \ldots, B_{L_1+L_2+L_A+L_B+L_C}$ to denote the blobs, and $F_1, \ldots, F_{L_1+L_2+L_C+3}$ to indicate the flavors of the loop particles. The first cut in the dumbbell-topologies is performed (as in the infinity-topologies) in the first propagator of the k_2 loop-line, meaning the one carrying flavor F_{L_1+2} in Figure 4.10. The obtained one-loop topology is characterized by the blobs, $B_1^{(1)}, \ldots, B_{L_1+1}^{(1)}$, and the flavors, $F_1^{(1)}, \ldots, F_{L_1+1}^{(1)}$, which are related to the uncut ones through

$$
\begin{aligned}
&\text{For } 1 \leq i \leq L_1: B_i^{(1)} = B_i, \text{ and } F_{L_1+2-i}^{(1)} = F_{i+1} \\
&\text{Else: } B_{L_1+1}^{(1)} = 2^n + 2^{n+1} + B_{L_1+1} + \cdots + B_{L_1+L_2+L_A+L_B+L_C} \text{ and } F_1^{(1)} = F_1
\end{aligned}
\tag{4.11}
$$

The difference in the dumbbell-topologies with respect to the other master blob-topologies is that except for the structure of the cut k_2 loop-line one needs to explicitly preserve the structure of the whole formation drawn in orange in Figure 4.10, which consists also of the C momentum line and the vertex B. Furthermore, the re-ordering
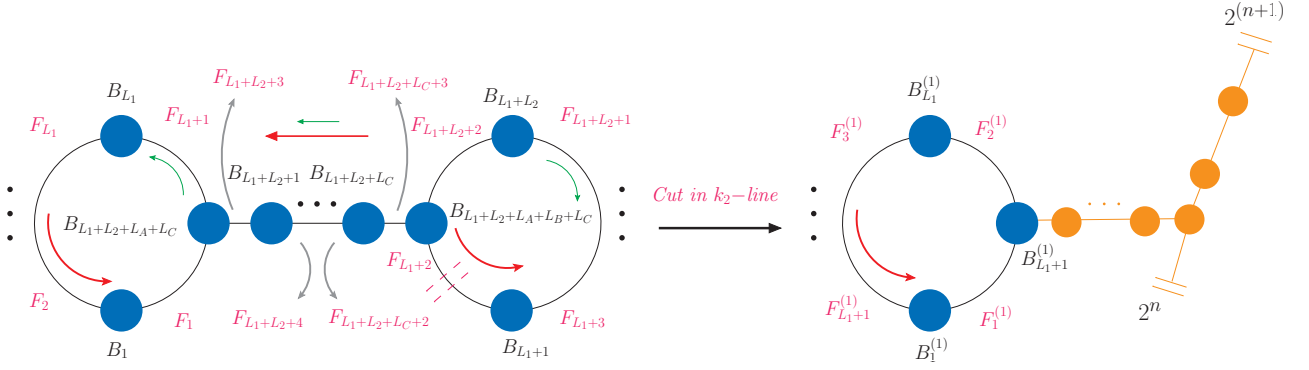
Figure 4.10: Graphical illustration of the cutting procedure in a typical *dumbbell-topology*. On the lhs is depicted the dumbbell topology and on the ths, we have the yielded one-loop blob-topology. The grey arrows indicate to which propagators of the C momentum line the pointed flavors correspond to. The orange section in the rhs denotes the structure that is retained as extra information during the computation of the blob $B_{L_1+1}^{(1)}$ using Dyson-Schwinger recursion. In lhs the cut is represented with a red dashed double line, while the red (green) arrows on both sides (lhs) represent the flavor (momentum) flow. The blobs $B_1, \ldots, B_{L_1+L_2+L_A+L_B+L_C}$ and the flavors $F_1, \ldots, F_{L_1+L_2+L_C+3}$ correspond to the ones stored in the last line of the numerators in the skeleton.

procedure of the blobs after the first cut in the dumbbell-topologies is the same as in the case of the infinity ones, thus for it, we refer to the previous subsection and Figure 4.9.

4.3.4 Flavor/Color Dressing

Regarding the flavor and color dressing of the blob-topologies, which is performed at the one-loop level, the procedure closely resembles the one of `HELAC-1LOOP` [88, 97]. In particular, for a given one-loop blob-topology, we first employ quantum number conservation to identify the flavors and color/anti-color indices of the blobs. Then by assigning a flavor, a color, and an anti-color index to the first propagator[13], and utilizing QCD Feynman rules as well as color conservation (track of color-flow) at each vertex, we are able to determine the flavor and color/anti-color indices of every propagator in the topology.

Besides the propagators of the one-loop topology, we also dress with flavor the propagators of the structure resulting from the first cut and store this information for later use when the Dyson-Schwinger recursion is applied on the higher-level blobs. These propagators are drawn with orange color in Figures 4.6, 4.8, and 4.10. To obtain all viable and contributing configurations, we iterate through all possible values of flavors and color/anti-color indices for the first propagator using three nested `do-loops`. Subsequently, as discussed in detail in the introduction, and as is done in `HELAC-1LOOP` [88, 97], the one-loop configurations constructed with this procedure are cut in the propagator indicated in Figures 4.7 and 4.9, and the color/anti-color indices are re-assigned, tracking the color flow of the one-loop topology, in order to incorporate the color lines introduced by the two extra particles resulted by the second cut.

---

[13]In the one-loop blob-topologies of the Figures 4.7 and 4.9, the first propagator corresponds to the one having flavor $f_1^{(1)}$.
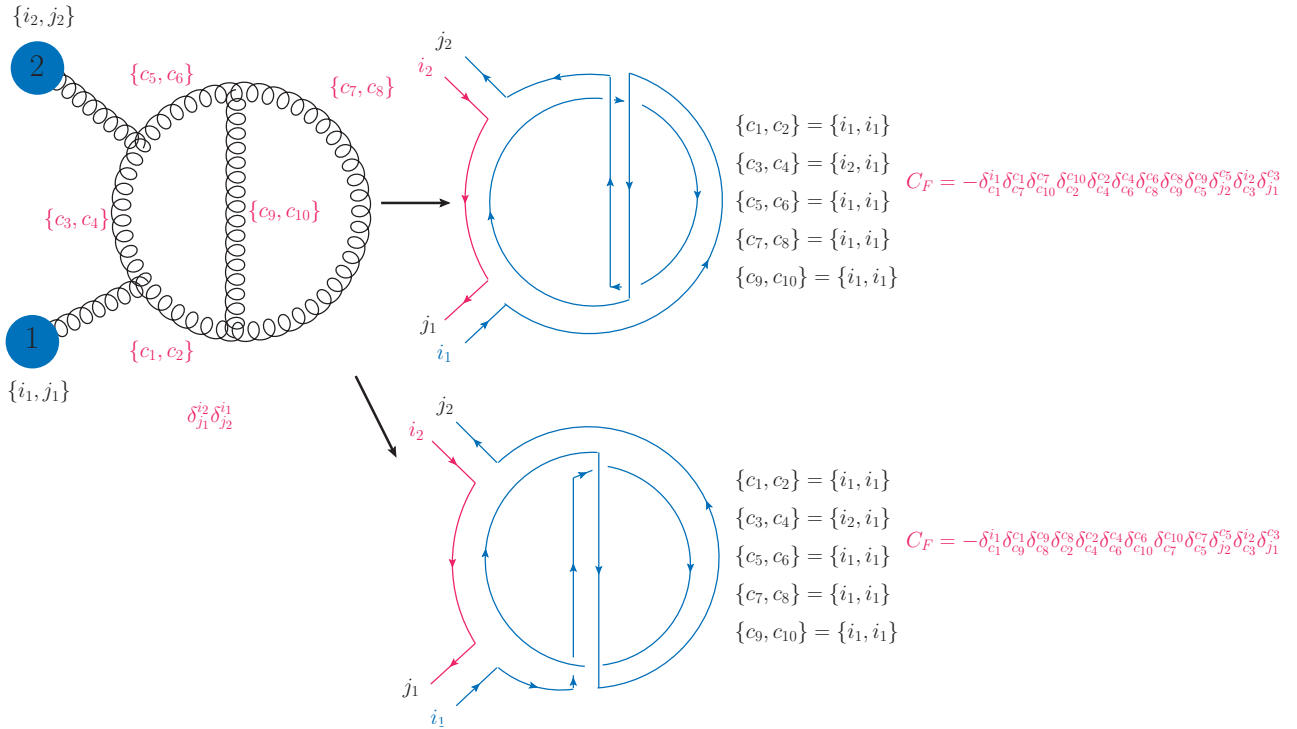
Figure 4.11: Example of two different color configurations that are identical for `HELAC`. Using odd i, we assign the color indices c_i to the loop particles, while even i correspond to the anti-color indices. Moving from the lower propagator of the k_1 loop-line, we encounter $\{c_1, c_2\}$, and as we ascend, we have $\{c_3, c_4\}$ and $\{c_5, c_6\}$ for the subsequent propagators. The color indices $\{c_7, c_8\}$ are associated with the propagator of the k_2 loop-line, while $\{c_9, c_{10}\}$ correspond to the propagator of the k_3 loop-line. The color factor C_F arises from the contraction of the conventional color factor (in the fundamental representation) with a t^a_{ij} matrix for each loop and external gluon. In C_F it is important to note that the repeated c_i indices are left uncontracted (if they were contracted they will result to $\delta^{i_2}_{j_1}\delta^{i_1}_{j_2}$). This is done because by examining the Kronecker's deltas present in C_F, one can trace the flow of color from the external particles through the loop particles and back to the external ones.

In this way of flavor-color dressing, we receive uniquely defined tree-level configurations with four extra particles, which correctly take into account all numerator contributions of the process at hand, when the Dyson-Schwinger recursion is applied.

4.3.5　Comments on Two-Loop Color-Flow Dressing

One might wonder why the flavor and color dressing procedure, in our approach in `HELAC-2LOOP`, is performed at the one-loop level after the first cut, rather than at the two-loop level. As it regards the flavor dressing, this could be equivalently done at the level of two-loop blob-topologies[14]. Concerning the color dressing, the reason why we dress the blob-topologies at one-loop level instead of at two-loop is that at two-loop different color-configurations are identified as identical from the `HELAC` color dressing algorithm and thus it generates only one of them.

---

[14]In practice, this is what is done by dressing with flavor the orange structure resulted by the first cut.
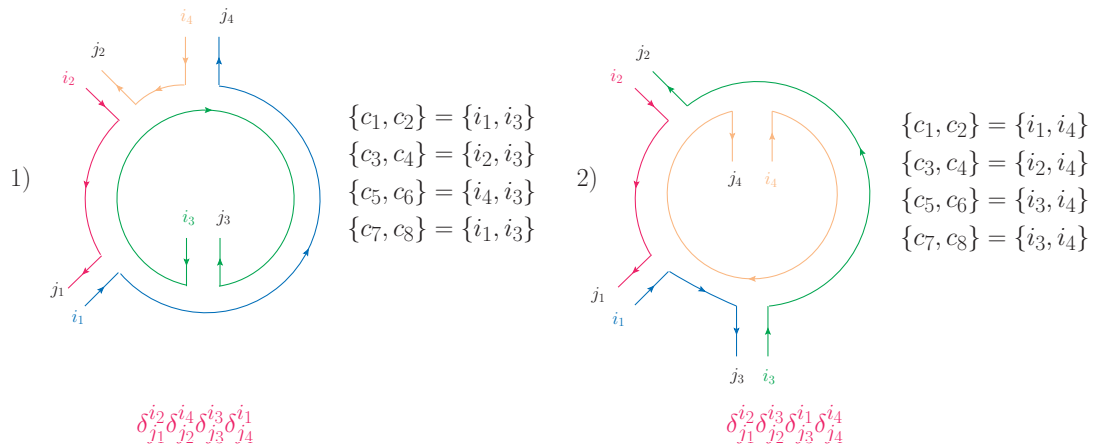
Figure 4.12: The two color configurations resulting from cutting in k_3 loop-line the two configurations of Figure 4.11. The resulted, from the cut, extra color-lines are reassigned with the color (anti-color) indices $\{i_3, i_4\}$ ($\{j_3, j_4\}$). The lhs of this figure corresponds to the upper configuration of Figure 4.11, while the rhs to the lower one. These two one-loop configurations have now different color/anti-color indices for the external and loop particles. From these one can go back to the two-loop ones by applying the constrain that the color (anti-color) index of the one cut-particle is equal the anti-color (color) index of the other cut-particle.

Let us provide a concrete example in order to illustrate this concept. Consider the two-point graph shown on the lhs of Figure 4.11, where all particles (both loop and external) are gluons and the color-state of the external particles is given by $\delta^{i_2}_{j_1}\delta^{i_1}_{j_2}$. Among the various configurations (12 in total) that contribute to this color-state, we choose the two configurations depicted on the rhs of Figure 4.11. From the rhs of Figure 4.11 one can observe that, although the two configurations are different in terms of flow of color (this is clear from the flow of the drawn color lines), all their propagators have the same color and anti-color indices. This is the main problem of HELAC color dressing algorithm as each combination of color/anti-color indices of the propagators is generated only once (per color-state), and (if it survives the color-conservation filters) it corresponds to one only configuration. Thus directly applied at two-loop level, HELAC would have generated only one of the two configurations.

This is a new feature starting from two-loop level due to the existence of the two vertices, A and B, that connect only loop-particles, where at each of them (knowing the color/anti-color indices of the external particles and the incoming propagator) the color can flow in different directions, and hence can lead into different configurations that have the same color/anti-color indices for all their loop and external particles. This contrasts with the one-loop level, where knowing the color/anti-color indices of the external particles and the incoming propagator, the color at each vertex can flow only to one direction. This means that at one-loop, each contributing configuration corresponds to a distinct combination of color/anti-color indices of the loop particles, and thus can be correctly considered by the current algorithm of HELAC.

Cutting in the k_3 loop-line the two two-loop color configurations of Figure 4.11, results to the two one-loop color configurations of Figure 4.12, which can be corresponded

Box	Double-Box	Color-State
0	0	$\delta^{i_1}_{\ j_1}\delta^{i_2}_{\ j_2}\delta^{i_3}_{\ j_3}\delta^{i_4}_{\ j_4}$
0	-4	$\delta^{i_1}_{\ j_1}\delta^{i_2}_{\ j_2}\delta^{i_4}_{\ j_3}\delta^{i_3}_{\ j_4}$
0	2	$\delta^{i_1}_{\ j_1}\delta^{i_3}_{\ j_2}\delta^{i_2}_{\ j_3}\delta^{i_4}_{\ j_4}$
-1	$-N_c$	$\delta^{i_1}_{\ j_1}\delta^{i_4}_{\ j_2}\delta^{i_2}_{\ j_3}\delta^{i_3}_{\ j_4}$
-1	$-N_c$	$\delta^{i_1}_{\ j_1}\delta^{i_3}_{\ j_2}\delta^{i_4}_{\ j_3}\delta^{i_2}_{\ j_4}$
0	-2	$\delta^{i_1}_{\ j_1}\delta^{i_4}_{\ j_2}\delta^{i_3}_{\ j_3}\delta^{i_2}_{\ j_4}$
0	-4	$\delta^{i_2}_{\ j_1}\delta^{i_1}_{\ j_2}\delta^{i_3}_{\ j_3}\delta^{i_4}_{\ j_4}$
2	$6N_c$	$\delta^{i_2}_{\ j_1}\delta^{i_1}_{\ j_2}\delta^{i_4}_{\ j_3}\delta^{i_3}_{\ j_4}$
-1	$-N_c$	$\delta^{i_3}_{\ j_1}\delta^{i_1}_{\ j_2}\delta^{i_2}_{\ j_3}\delta^{i_4}_{\ j_4}$
N_c	N_c^2+2	$\delta^{i_4}_{\ j_1}\delta^{i_1}_{\ j_2}\delta^{i_2}_{\ j_3}\delta^{i_3}_{\ j_4}$
0	2	$\delta^{i_3}_{\ j_1}\delta^{i_1}_{\ j_2}\delta^{i_4}_{\ j_3}\delta^{i_2}_{\ j_4}$
-1	$-N_c$	$\delta^{i_4}_{\ j_1}\delta^{i_1}_{\ j_2}\delta^{i_3}_{\ j_3}\delta^{i_2}_{\ j_4}$

Box	Double-Box	Color-State
-1	$-N_c$	$\delta^{i_2}_{\ j_1}\delta^{i_3}_{\ j_2}\delta^{i_1}_{\ j_3}\delta^{i_4}_{\ j_4}$
0	2	$\delta^{i_2}_{\ j_1}\delta^{i_4}_{\ j_2}\delta^{i_1}_{\ j_3}\delta^{i_3}_{\ j_4}$
0	2	$\delta^{i_3}_{\ j_1}\delta^{i_2}_{\ j_2}\delta^{i_1}_{\ j_3}\delta^{i_4}_{\ j_4}$
-1	$-N_c$	$\delta^{i_4}_{\ j_1}\delta^{i_2}_{\ j_2}\delta^{i_1}_{\ j_3}\delta^{i_3}_{\ j_4}$
2	0	$\delta^{i_3}_{\ j_1}\delta^{i_4}_{\ j_2}\delta^{i_1}_{\ j_3}\delta^{i_2}_{\ j_4}$
0	-4	$\delta^{i_4}_{\ j_1}\delta^{i_3}_{\ j_2}\delta^{i_1}_{\ j_3}\delta^{i_2}_{\ j_4}$
N_c	N_c^2+2	$\delta^{i_2}_{\ j_1}\delta^{i_3}_{\ j_2}\delta^{i_4}_{\ j_3}\delta^{i_1}_{\ j_4}$
-1	$-N_c$	$\delta^{i_2}_{\ j_1}\delta^{i_4}_{\ j_2}\delta^{i_3}_{\ j_3}\delta^{i_1}_{\ j_4}$
-1	$-N_c$	$\delta^{i_3}_{\ j_1}\delta^{i_2}_{\ j_2}\delta^{i_4}_{\ j_3}\delta^{i_1}_{\ j_4}$
0	2	$\delta^{i_4}_{\ j_1}\delta^{i_2}_{\ j_2}\delta^{i_3}_{\ j_3}\delta^{i_1}_{\ j_4}$
0	-4	$\delta^{i_3}_{\ j_1}\delta^{i_4}_{\ j_2}\delta^{i_1}_{\ j_4}\delta^{i_2}_{\ j_3}$
2	0	$\delta^{i_4}_{\ j_1}\delta^{i_3}_{\ j_2}\delta^{i_2}_{\ j_3}\delta^{i_1}_{\ j_4}$

Figure 4.13: Figure consisting of the graphs of gluonic box and double-box, as well as, a table containing the prefactors of the color-states of these graphs.

back to the two-loop ones by contracting their color factors[15] with the deltas $\delta^{j_4}_{i_3}\delta^{j_3}_{i_4}$. As can observed by Figure 4.12, the two one-loop color configurations have different color/anti-color indices for their loop particles and correspond to different color-states. Therefore by generating in `HELAC-2LOOP` all the $(n+2)$-particle color-states and do the color dressing after the first cut (at one-loop level) using the existing algorithm, we are able to produce all the contributing two-loop color configurations for any process at hand.

It is also noteworthy to comment on the behavior of the color-flow representation when moving from one-loop to two-loop problems. To illustrate this, we provide a table in Figure 4.13 showing the coefficients of the color-states for the gluonic box (upper left) and double-box (upper right) topologies. A comparison of the coefficients reveals an increase in the complexity of the color-flow representation when moving from one to two loops. Specifically, there is an expansion in the number of nonzero color states (from 13 in the box to 21 in the double-box) and the multiplicity of their prefactors (from 2 to 6). This expansion results in a greater number of color configurations. Additionally, it is intriguing to note that starting from two loops, the same color-state (e.g., $\delta^{i_4}_{j_1}\delta^{i_1}_{j_2}\delta^{i_2}_{j_3}\delta^{i_3}_{j_4}$) can contribute to different color orders, such as leading color (N_c^2) and sub-sub-leading color (2).

---

[15]These are the red strings of Kronecker's deltas under the graphs of Figure 4.12. Herein we have contracted all the repeated indices related to the loop particles.
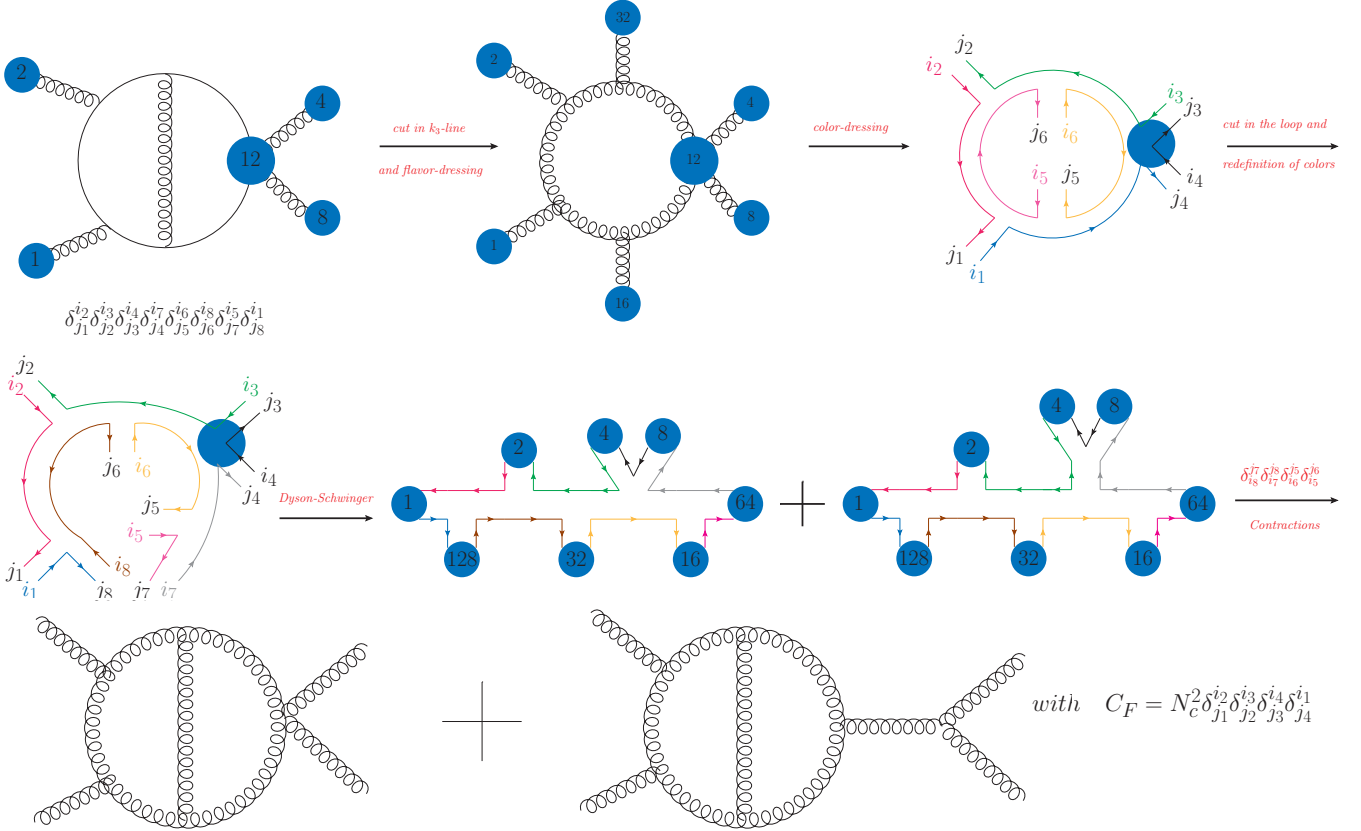
Figure 4.14: In this figure, we present a schematic example of the construction of a two-loop numerator within `HELAC-2LOOP`. We start with the theta-topology $\{\{1, 2\}, \{12\}, \{\}, \{\}, \{\}\}$, and the external particles being all gluons as our input. We also specify the flavor of the first set of cut particles as gluon, and the $(n+2)$-particle state as $\delta^{i_2}_{j_1}\delta^{i_3}_{j_2}\delta^{i_4}_{j_3}\delta^{i_1}_{j_4}\delta^{i_6}_{j_5}\delta^{i_5}_{j_6}$. From the various possible flavors that the first propagator can have, we select the gluon flavor for our example here. After applying the `HELAC-2LOOP` algorithm we obtain one numerator which includes the two depicted graphs with the color factor $N^2_c\delta^{i_2}_{j_1}\delta^{i_3}_{j_2}\delta^{i_4}_{j_3}\delta^{i_1}_{j_4}$.

4.4 An Example of Numerator Construction

After having provided clarification and justification for certain aspects of the algorithm applied within `HELAC-2LOOP` that distinguish it from the existing `HELAC` framework, we will now examine a schematic example in order to illustrate the process of constructing a numerator and how it is stored in the skeleton.

Among the various options available for blob-topologies, flavors of external and cut particles, and $(n+2)$-particle color states, our focus is on the specific scenario depicted in the upper left section of Figure 4.14. In this case, we have as a starting point the flavor of the external and the first set of cut particles being gluon, the $(n+2)$-particle color-state $\delta^{i_2}_{j_1}\delta^{i_3}_{j_2}\delta^{i_4}_{j_3}\delta^{i_1}_{j_4}\delta^{i_6}_{j_5}\delta^{i_5}_{j_6}$, and the theta-like blob-topology $\{\{1, 2\}, \{12\}, \{\}, \{\}, \{\}\}$. In the next step, we cut in the k_3 loop-line the configuration at hand and we dress with flavor and color/anti-color the loop propagators of the corresponding one-loop configuration (see the first line of Figure 4.14). From all the possible flavors that the first propagator can have, in this example, we keep only the gluon case.

Subsequently, we perform the second cut in the propagator connecting the blobs 1 and 16. As previously explained, it is our convention to always perform the cut in the

```
            INFO ==============================================
            INFO COLOR              9 out of          24
            INFO number of nums           0
            INFO ==============================================
            INFO COLOR             10 out of          24
            INFO number of nums         332
            INFO NUM              1  of          332              8
   INFO NUM            110  of          332          7
   INFO =================================
INFO  4  80  35   9  1  1  16  35   5  64  35   7   0   0   0   0   1   2
INFO  4  12  35  10  1  1   4  35   3   8  35   4   0   0   0   0   1   1
INFO  4  92  35  11  1  2  12  35  10  80  35   9   0   0   0   0   1   1
INFO  5  92  35  11  2  2   4  35   3   8  35   4  80  35   9   0   1   5
INFO  4 124  35  12  1  1  32  35   6  92  35  11   0   0   0   0   1   2
INFO  4 126  35  13  1  1   2  35   2 124  35  12   0   0   0   0   1   1
INFO  4 254  35  14  1  1 128  35   8 126  35  13   0   0   0   0   1   2
INFO  6   1  12   1  2  12  35  35  35  35  35  35   0   0   0   0   5   9
```

Figure 4.15: Form, as is stored in the skeleton, of the numerator constructed in Figure 4.14.

propagator of the one-loop blob-topology, ensuring that particle 1 remains the final point of the recursion. Then, in the resulting tree-level configuration we assign the extra color lines introduced by the cut propagator, and by tracking the color flow we rearrange the $(n+2)$-particle color-state $\delta_{j_1}^{i_2}\delta_{j_2}^{i_3}\delta_{j_3}^{i_4}\delta_{j_4}^{i_1}\delta_{j_5}^{i_6}\delta_{j_6}^{i_5}$, into the $(n+4)$-particle one $\delta_{j_1}^{i_2}\delta_{j_2}^{i_3}\delta_{j_3}^{i_4}\delta_{j_4}^{i_7}\delta_{j_5}^{i_6}\delta_{j_6}^{i_8}\delta_{j_7}^{i_5}\delta_{j_8}^{i_1}$. Afterwards, we apply a Dyson-Schwinger recursion on the tree-level configuration, respecting the loop-assignment structure of the topology, which results in the two configurations depicted in the middle line of Figure 4.14, due to the two possible splittings (via SM vertices) of the level-2 blob 12. These correspond to the two graphs depicted in the last section of the same figure with the color factor $C_F = N_c^2 \delta_{j_1}^{i_2}\delta_{j_2}^{i_3}\delta_{j_3}^{i_4}\delta_{j_4}^{i_1}$, identified by reducing via contraction with the product of deltas $\delta_{i_8}^{j_7}\delta_{i_7}^{j_8}\delta_{i_6}^{j_5}\delta_{i_5}^{j_6}$ the $(n+4)$-particle color-state to an n-particle one. In the end, the sub-amplitude structure of the two configurations together with the topological information and the powers of N_c are stored as one numerator to the skeleton of the process at hand.

In Figure 4.15, we provide the representation of the numerator constructed in our example as stored in the skeleton. Similar to `HELAC-1LOOP`, the numerators are organized in the skeleton based on their color-state. For each color-state (24 in our example), there is a corresponding list of numerators labeled as "nums" in Figure 4.15. The structure of each numerator follows the same format as in `HELAC-1LOOP` in all but the last line. Consequently, from the first line to the second-to-last line, there is a sequence of sub-amplitudes accompanied by instructions for their computation. Let us provide a concise explanation of the meaning of each number within a line. Using the first line as our reference, the first number signifies the type of vertex employed for the creation of the output sub-amplitude, the second number represents its ID number, the third number corresponds to its flavor, and the fourth number denotes the rank of the sub-amplitude in the list of constructed sub-amplitudes[16]. The fifth and sixth numbers enumerate the possible methods of constructing the output sub-amplitude using existing sub-amplitudes. For instance, in the third and fourth lines, the sub-amplitude

---

[16]The $n+4$ particles are also counted as sub-amplitudes in this ranking thus the ranking of the output sub-amplitudes starts from 9 in our example.

with ID = 92 can be obtained through two distinct approaches, combining the blobs 80 and 12 via a three-vertex or blobs 80, 4 and 8 via a four-vertex, thus the fifth number takes values from 1 till 2 and the sixth number is equal to 2. Following this, the seventh (tenth) [thirteenth] number corresponds to the ID number of the first (second) [third][17] incoming sub-amplitude, the eighth (eleventh) [fourteenth] number represents its flavor, and the ninth (twelfth) [fifteenth] number denotes its ranking in the list of sub-amplitudes. Subsequently, the sixteenth number indicates the helicity index of the sub-amplitude (taking the values 1 or 2 for fermions and 0 otherwise), the seventeenth number is equal to the sign factor that takes into account the anti-symmetry of the sub-amplitude (defined in Eq. (2.40)), and the last (eighteenth) number specifies the color connection associated with the vertex.

Concerning the last line, the first element is the number of propagators of the blob-topology, and the second element is a number, let's denote it mb, which signifies the master blob-topology to which the numerator corresponds to. The possible values of mb are the following ones

$$mb = \begin{cases} 1, & \text{Theta-topology} \\ 2, & \text{Infinity-topology} \\ 3, & \text{Dumbbell-topology} \end{cases} . \tag{4.12}$$

Then, the third element corresponds to a unique ID per blob-topology, ID_{topo}, defined using a prime number decomposition according to the number of particles included in each sub-list of the blob-topology. More precisely, the definition of ID_{topo} is established through the relation

$$\text{ID}_{topo} = \begin{cases} (2)^{L_1}(3)^{L_2}(5)^{L_3}(7)^{L_A}(11)^{L_B}, & \text{Theta-topology} \\ (2)^{L_1}(3)^{L_2}, & \text{Infinity-topology} \\ (2)^{L_1}(3)^{L_2}(5)^{L_C}(7)^{L_A}(11)^{L_B}, & \text{Dumbbell-topology} \end{cases} . \tag{4.13}$$

After the third element, the blobs of the topology are stored, followed by the flavor of its propagators. The ordering of the blobs and flavors for each master blob-topology is as follows:

- *Theta-topology*: Blobs and flavors are stored starting from the k_1 loop-line ascending from vertex B to A, then continuing with the k_2 loop-line moving from A to B, and concluding with the k_3 loop-line going from B to A. The last recorded blobs correspond to those of A and B, in that particular order.

- *Infinity-topology*: The storage of blobs and flavors starts from the k_1 loop-line using a bottom-up approach, and then is followed by the k_2 loop-line where again a bottom-up approach is used.

- *Dumbbell-topology*: Blobs and flavors are stored starting from the k_1 loop-line using a bottom-up approach, then continuing with the k_2 loop-line using again a bottom-up approach, and concluding with the C momentum-line moving from vertex A to B. The last stored blobs are the ones of A and B (in this order).

---

[17]If there is not third incoming sub-amplitude (three-vertex case), the thirteenth, fourteenth, and fifteenth numbers are left empty, e.g. 0.

Having stored the blobs and the propagator flavors of the blob-topology, the rest of the elements till the penultimate one, if not used, are left empty (0). Then the penultimate element corresponds to an estimation of the rank of the numerator (powers of the loop momenta k_i), and the last number is the prefactor of the n-particle color state ($N_c^2 = 9$ in our example) arising from the projection of the $(n + 4)$-particle one.

4.5   Results and Discussion

In order to get an idea of the complexity and the structure of the skeleton at two-loop level we present in Table 4.1 information about the skeleton of some QCD processes at two-loop, using `HELAC-2LOOP`, and at one-loop, using `HELAC-1LOOP` [88]. These processes consist of gluons (g) and quarks/anti-quarks ($q, \bar{q}$) as external and loop particles, with ghosts/anti-ghosts ($c, \bar{c}$) being also included in the loop, and some of them are studied at leading-color approximation, while others at full-color. Let us discuss now the results presented in Table 4.1.

Process	#	*Loop-Flavors*	*Color*	*Size*	*Crea.Time*	*Nums*
$gg \to gg$	2	$\{g, c, \bar{c}\}$	Lead.	8.9 MB	15.017s	4560
$gg \to gg$	2	$\{g, q, \bar{q}, c, \bar{c}\}$	Full	110.6 MB	6m 54.574s	89392
$gg \to q\bar{q}$	2	$\{g, q, \bar{q}, c, \bar{c}\}$	Full	16.1 MB	3m 14.509s	13856
$gg \to ggg$	2	$\{g, c, \bar{c}\}$	Lead.	300.0 MB	21m 42.609s	81480
$gg \to gg$	1	$\{g, q, \bar{q}, c, \bar{c}\}$	Full	537.8 kB	2.386s	768
$gg \to ggg$	1	$\{g, q, \bar{q}, c, \bar{c}\}$	Full	15.1 MB	8m 53.349s	11496
$gg \to gggg$	1	$\{g, c, \bar{c}\}$	Lead.	394.0 MB	104m 14.95s	19680

Table 4.1: Table containing information for the skeleton of some QCD processes at one- and two-loop. Therein, the column # refers to the number of loops, **Loop-Flavors** denotes the flavor of the particles included in the loops, and **Color** indicates the color order, with Lead. and Full referring to leading- and full-color approximation, respectively. The columns **Size** and **Crea.Time**, indicate the size of the skeleton and the real-time consumed for its construction, respectively. The last column (**Nums**) signifies the number of separate contributions (numerators) to the amplitude. These results have been obtained running 1-core in my personal laptop (i7 processor, 8-core, 24GB RAM).

In the context of the two-loop results, the table above reveals that increasing the number of particles or transitioning from leading-color to full-color leads to an increment in the number of numerators (contributions) and the size of the skeleton. This corresponds to an escalation in the complexity of the amplitude, as anticipated. Additionally, it is worth noting that the construction of the skeleton can sometimes have lengthy timings. However, it is important to emphasize that the skeleton only needs to be created once per process and can then be utilized in its existing form during the computational phase. Furthermore, when comparing the full-color two-loop process of $gg \to gg$ (second line) with the leading-color two-loop process of $gg \to ggg$ (forth line), it becomes apparent that despite the latter having a smaller number of numerators, the former is constructed much faster. This is attributed to the simpler sub-amplitude structure present in the former process, as evidenced by the size of the skeleton.

Upon comparing the full-color $gg \to gg$ process at one-loop (fifth line) with its two-loop counterpart, a notable increase in the number of numerators becomes apparent. Moving from one loop to two loops results in a significant augmentation in the complexity of computing scattering amplitudes, as reflected by the approximately 115-fold increase in the number of numerators in the two-loop case compared to the one-loop case. It is important to note, however, that the large number of numerators at full-color in the two-loop results may be somewhat misleading, as many of these numerators, within the same or different color-states, are either identical or differ by a constant factor. For instance, in the case of the gluonic double-box illustrated in Figure 4.13, the skeleton contains 64 different numerators ($2^{(n+2)}$), which could potentially be consolidated into only 21 distinct contributions, corresponding to the number of non-zero color-states, with the coefficiets of the color-state being included in the last element of the last line of a skeleton numerator. At first glance, this naive and simple reorganization appears to reduce the number of numerators by a factor of three. Therefore, there is still room for further organization and optimization of the skeleton in order to enhance the efficiency of the computational phase in `HELAC-2LOOP`, an aspect that is currently being developed.

One other interesting fact is derived from the Table 4.1, by setting side by side the full-color one-loop $gg \to ggg$ process (sixth line) with the full-color two-loop $gg \to q\bar{q}$ process (third line). More specifically, despite the fact that the two processes are of the same complexity, in terms of the number of numerators and sub-amplitudes (indicated by the size of the skeleton), the skeleton construction time for the latter process is approximately three times faster than that of the former. This improvement is a result of optimizing various aspects of the existing code through extensive profiling. These optimizations are not limited to the two-loop case but will also be implemented in the one-loop scenario. Additionally, ongoing efforts are being made to explore further optimizations and potential parallelization across multiple cores. These measures aim to enhance the efficiency of the initialization phase in `HELAC-2LOOP`.

To validate the correctness of the numerators stored in the skeletons of the processes quoted in Table 4.1, we conducted numerical calculations, in four dimensions and at the integrand level[18], for various numerators, and we cross-checked them with other public packages such as `FeynArts` [82], `FeynCalc` [84], and `FORM` [83]. For completeness, our computations encompassed multiple topologies from each master blob-topology and included all possible QCD flavors ($\{g, q, \bar{q}, c, \bar{c}\}$) for the loop particles. For all cases studied, we found a perfect agreement (in quadruple precission) between our results and those obtained from these packages. For obtaining such numerical computations one should provide in `HELAC-2LOOP` as input, values for the momenta and the polarizations of the external particles together with values for the momenta of the four extra particles[19] resulted from the two cuts performed to the two-loop blob-topologies. The latter are acquired as the loop momenta of the cut propagators. The polarizations of the extra particles, as in the one-loop case, are chosen appropriately in order to reproduce the contractions originally present in the cut propagators, as described by Eq. (2.42).

---

[18]After properly modifying some parts of the computational phase algorithm.

[19]Two momenta should be provided, due to the fact that the two particles yielded from one cut have equal and opposite momentum.

As an illustration, we present the following numerators for configurations involving only gluons as both loop and external particles

1. $N_{\{\{1,2\},\{12\},\{\},\{\},\{\}\}} = 17052219.315419123 + 64639250.888367772i$

2. $N_{\{\{1,2\},\{4,8\},\{\},\{\},\{\}\}} = -12231870819598.090 + 5124375444085.5430i$

3. $N_{\{\{1,2\},\{4\},\{8\},\{\},\{\}\}} = -1268111397619.5310 + 195312105699.88257i$

4. $N_{\{\{2,1\},\{8\},\{\},\{4\},\{\}\}} = -49731029299.352333 + 15599344.440385548i$.

These numerators were computed in the helicity state $-- \rightarrow --$, using for the external and loop momenta the values $p_1 = (250, 0, 0, 250)$, $p_2 = (250, 0, 0, -250)$, $p_3 = (250, 49, -176, -171)$, $k_1 = (0.2, 0.3, 0.5, 0.7)$, and $k_3 = (0.9, 0.11, 0.13, 0.15)$. The first numerator corresponds to the configuration discussed in the previous section (Figure 4.15). The second numerator corresponds to the double-box topology, the third numerator corresponds to the non-planar double-box, and the fourth numerator corresponds to a topology containing a blob in the vertex A.

Chapter 5

Three-loop Integral Families Relevant for Z/H+jet production

In this chapter, we present the analytic computation of the ladder-box and the two tennis-court Feynman integral families, relevant for $2 \to 2$ scattering processes involving one massive external particle and massless particles running on the loops, utilizing the simplified differential equations approach. Our results are expressed in terms of real-valued multiple poly-logarithms of up to transcendental weight six for both Euclidean and physical kinematics, being thus well-suited for phenomenological applications. Furthermore, we present analytic results for two non-planar ladder-box-like families, computed using the standard differential equations method. This chapter is based on novel work presented in the articles [4, 6] and the conference proceedings [5, 7].

5.1 Introduction

The ever-increasing accuracy of the experimental measurements obtained by the current and future runs of LHC, High Luminosity LHC (HL-LHC), and potential new collider experiments, creates a significant demand for equally high-precision theoretical predictions for their interpretation. From a theoretical perspective, achieving high-precision predictions involves the use of perturbative Quantum Field Theory, particularly the use of perturbative QCD for processes concerning strong interactions. Enhancing prediction accuracy entails computing higher-order corrections in the expansion around the coupling constant of the strong interactions. As explored in previous chapters, this computation involves various aspects, including the calculation of multi-loop FIs.

According to estimates, the upcoming High Luminosity upgrade of the LHC is expected to necessitate the computation of numerous scattering processes at next-to-next-to-next-to-leading-order (N³LO) in order to reach a percent level of precision [136]. At this order of perturbative expansion, the calculation of three-loop FIs becomes indispensable, which is a highly challenging task. Notably, all families of FIs with massless internal and external particles have been computed [241, 269–271] and have been applied for the evaluation of three-loop $2 \to 2$ scattering amplitudes for processes such as $q\bar{q} \to \gamma\gamma$ [158], $q\bar{q} \to q\bar{q}$ (with the initial and final state quarks potentially differing in flavor) [159], $gg \to \gamma\gamma$ [160], $gg \to gg$ [161] and $q\bar{q} \to gg$ [162], all of which are of great phenomenological interest.

The next natural progression is to extend these results to processes involving a single massive external particle, such as a vector boson decaying into 3-jets or $gg \to H$+jet via gluon fusion. This extension requires the computation of all four-point integral families involving one massive external particle and massless propagators. Several years ago, progress was made in this direction, by calculating the planar ladder-box topology, which involves massless propagators and one off-shell leg [272]. In this calculation a basis of 85 MIs was obtained, and a canonical DE [227] was derived using Magnus series expansions [234]. In this chapter, we re-calculate this integral family finding a basis of 83 MIs, and we progress even further by conducting a complete analytical computation of the two additional planar three-loop topologies, commonly referred to as the tennis-court topologies. In our computation, we make use of the SDE approach [221] in combination with pure bases of MIs for the studied families, and the solutions are expressed in terms of GPLs [228, 229] in all physical regions of phase-space. Furthermore, we comment for the two tennis-court families on the adjacency conditions that were discovered in [273, 274] regarding the symbol of two-loop and three-loop four-point MIs with one off-shell leg, as these can be represented within the SDE approach. Additionally we compute in terms of GPLs two non-planar ladder-box-like families, using the standard differential equations method [7]. The latter two families have been first calculated in [275]. Our results have been recently used for the computation of planar three-loop QCD helicity amplitudes for V+jet production [163]. We conclude with a discussion of our results.

5.2   Planar Three-Loop Families with One Off-Shell Leg

5.2.1   Integral families

We begin this section by defining the integral families that will be addressed in this chapter. To keep the discussion concise, we will refer to the ladder-box topology as F1 and denote the two tennis-court topologies as F2 and F3, as illustrated in Figure 5.1. We define the corresponding integral families through the following expressions[1]

$$
\begin{aligned}
G_{a_1 \cdots a_{15}}^{F1} \equiv \int \left(\prod_{l=1}^{3} e^{\gamma_E \epsilon} \frac{d^d k_l}{i \pi^{d/2}} \right) & \frac{(k_1 + q_{123})^{-2a_{11}} (k_2 + q_{123})^{-2a_{12}}}{(k_1 + q_{12})^{2a_1} (k_2 + q_{12})^{2a_2} (k_3 + q_{12})^{2a_3} (k_1 - k_2)^{2a_4}} \\
& \times \frac{(k_2 + q_1)^{-2a_{13}} (k_3 + q_1)^{-2a_{14}} (k_1 - k_3)^{-2a_{15}}}{(k_2 - k_3)^{2a_5} (k_3 + q_{123})^{2a_6} k_1^{2a_7} k_2^{2a_8} k_3^{2a_9} (k_1 + q_1)^{2a_{10}}}
\end{aligned}
\tag{5.1}
$$

$$
\begin{aligned}
G_{a_1 \cdots a_{15}}^{F2} \equiv \int \left(\prod_{l=1}^{3} e^{\gamma_E \epsilon} \frac{d^d k_l}{i \pi^{d/2}} \right) & \frac{(k_1 + q_{123})^{-2a_{11}} k_2^{-2a_{12}}}{(k_1 + q_{12})^{2a_1} (k_2 + q_{12})^{2a_2} (k_2 + q_{123})^{2a_3} (k_3 + q_{123})^{2a_4}} \\
& \times \frac{(k_2 + q_1)^{-2a_{13}} (k_3 + q_1)^{-2a_{14}} (k_3 + q_{12})^{-2a_{15}}}{k_3^{2a_5} k_1^{2a_6} (k_1 + q_1)^{2a_7} (k_1 - k_2)^{2a_8} (k_1 - k_3)^{2a_9} (k_3 - k_2)^{2a_{10}}}
\end{aligned}
\tag{5.2}
$$

---

[1]Where we use the abbreviation $q_{12} = q_1 + q_2$ and $q_{123} = q_1 + q_2 + q_3$.
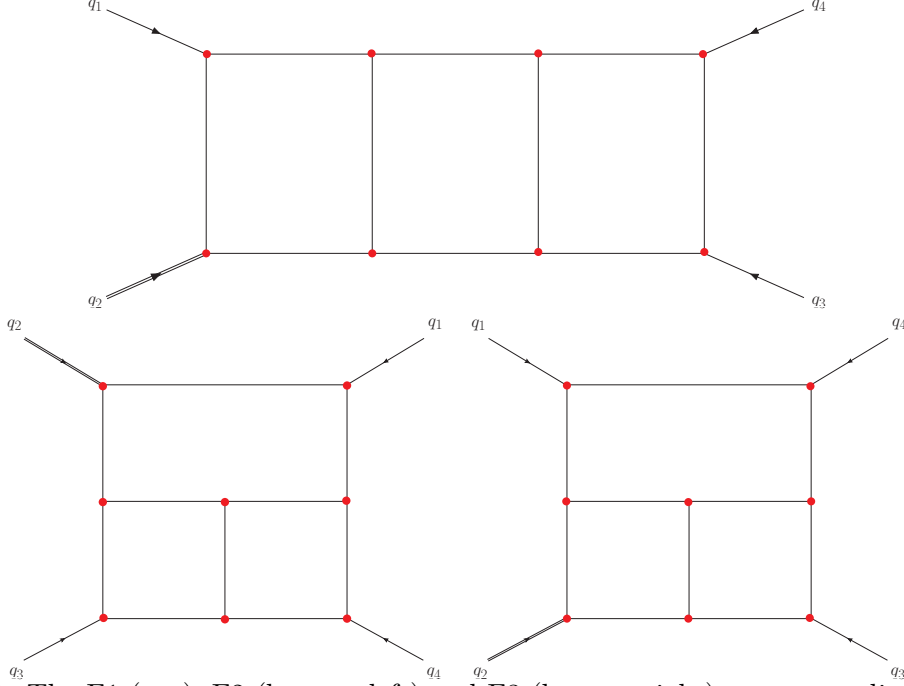
Figure 5.1: The F1 (top), F2 (bottom left) and F3 (bottom right) top-sector diagrams. The double line represents the massive particle and all external momenta are taken to be incoming.

$$
G^{F3}_{a_1 \cdots a_{15}} \equiv \int \left(\prod_{l=1}^{3} e^{\gamma_E \epsilon} \frac{d^d k_l}{i \pi^{d/2}} \right) \frac{(k_1 + q_{12})^{-2a_{11}} \; k_2^{-2a_{12}}}{(k_1 + q_1)^{2a_1} \, (k_2 + q_1)^{2a_2} \, (k_2 + q_{12})^{2a_3} \, (k_3 + q_{12})^{2a_4}}
$$
$$
\times \frac{(k_2 + q_{123})^{-2a_{13}} \; k_3^{-2a_{14}} \, (k_3 + q_1)^{-2a_{15}}}{(k_3 + q_{123})^{2a_5} \, (k_1 + q_{123})^{2a_6} \; k_1^{2a_7} \, (k_1 - k_2)^{2a_8} \, (k_1 - k_3)^{2a_9} \, (k_3 - k_2)^{2a_{10}}}
\tag{5.3}
$$

with a_i being integers. For $i = 11, \ldots, 15$ we have $a_i \leq 0$, corresponding to auxiliary propagators coming from irreducible scalar products. The external momenta ($q_1^2 = q_3^2 = q_4^2 = 0$ and $q_2^2 = m^2$) obey momentum conservation ($\sum_{i=1}^{4} q_i = 0$) and the following kinematics

$$
S_{12} = (q_1 + q_2)^2, \quad S_{23} = (q_2 + q_3)^2, \quad \text{and} \quad S_{13} = m^2 - S_{12} - S_{23}. \tag{5.4}
$$

In order to obtain analytic solutions for these families we utilize the SDE approach [221], where the external momenta are parametrized in terms of a dimensionless parameter, x, with respect to which the DEs are derived. In this case, we choose the following parametrization

$$
q_1 = x p_1, \quad q_2 = p_1 + p_2 - x p_1, \quad q_3 = p_3, \quad \text{and} \quad q_4 = p_4, \tag{5.5}
$$

where the new momenta p_i are all massless ($p_i^2 = 0$). By employing this parametrization, we establish the following mapping for the kinematic invariants between the two momentum configurations

$$
S_{12} = s_{12}, \quad S_{23} = s_{23} x, \quad \text{and} \quad m^2 = s_{12}(1 - x), \tag{5.6}
$$

with $s_{12} = (p_1 + p_2)^2$, $s_{23} = (p_2 + p_3)^2$.

Performing IBP reduction to MIs using modern public packages such as `FIRE6` [58] and `KIRA2` [60], we found for the F1 family a set of 83 MIs (3 at the top-sector[2]) in contrast with [272], where a set of 85 MIs was presented. The two extra MIs contained in the set of 85 MIs were found to be equal from IBP identities with two other integrals of the same set, namely $\mathcal{T}_7 = \mathcal{T}_8$ and $\mathcal{T}_{45} = \mathcal{T}_{46}$ of [272]. These relations can also be verified by checking the solutions for the corresponding basis elements, as presented in [272]. For the F2 and F3 families, using the same IBP packages, we identified a minimal set of 117 MIs (3 at the top-sector) and 166 MIs (4 at the top-sector), respectively.

5.2.2   Scattering kinematics

When addressing the analytical solution of multi-loop FIs in dimensional regularization with the DE method, it is customary to solve them in the Euclidean region, where all MIs of the family are devoid of branch cuts. Subsequently, the obtained results are analytically continued to the physical regions of phase-space. This approach aligns with the methodology we will adopt in our study. By analyzing the second Symanzik polynomial [187] associated with the top-sector integrals of the families F1, F2, and F3 in their Feynman parameter representation, we can identify the Euclidean region in terms of the following specific conditions for the kinematic variables S_{12}, S_{23} and m^2

$$S_{12} < 0, \quad S_{23} < 0, \quad \text{and} \quad m^2 < 0. \tag{5.7}$$

Using basic relativistic kinematics, one can show that for $2 \to 2$ scattering processes involving one massive particle, there exist three physical regions. For ease of reference, we will denote these regions as the s-, t-, and u-channels, respectively

$$
\begin{aligned}
s \text{ - channel} : \quad & m^2 > 0, \quad S_{12} \geq m^2, \quad S_{23} \leq 0, \quad \text{and} \quad S_{13} \leq 0 \\
t \text{ - channel} : \quad & m^2 > 0, \quad S_{12} \leq 0, \quad S_{23} \geq m^2, \quad \text{and} \quad S_{13} \leq 0 \\
u \text{ - channel} : \quad & m^2 > 0, \quad S_{12} \leq 0, \quad S_{23} \leq 0, \quad \text{and} \quad S_{13} \geq m^2.
\end{aligned}
\tag{5.8}
$$

Since we are going to use the SDE approach for solving Eqs. (5.2) and (5.3), it is desirable to express the inequalities of each phase-space region in terms of the variables x, s_{12}, and s_{23}. The mapping provided by Eq. (5.6) enables us to achieve this, however, for reasons that will become apparent later on, we introduce the ratio $y = s_{23}/s_{12}$ and utilize the variables x, y, and s_{12}. Our methodology will thus involve computing all MIs in terms of real-valued GPLs in the Euclidean region

$$0 < x < 1, \quad s_{12} < 0, \quad \text{and} \quad 0 < y < 1, \tag{5.9}$$

and afterwards, using fibration bases techniques implemented in `PolyLogTools` [263] and `HyperInt` [195], analytically continue our solutions to the physical regions

$$
\begin{aligned}
s \text{ - channel} : \quad & 0 < x < 1, \quad s_{12} > 0, \quad \text{and} \quad -1 \leq y \leq 0 \\
t \text{ - channel} : \quad & 1 < x, \quad s_{12} < 0, \quad \text{and} \quad y \leq -1 \\
u \text{ - channel} : \quad & 1 < x, \quad s_{12} < 0, \quad \text{and} \quad y \geq 0.
\end{aligned}
\tag{5.10}
$$

---

[2]By top-sector we mean the FIs with $a_i = 1$ for $i = 1, \ldots, 10$ and $a_i = 0$ for $i = 11, \ldots, 15$ in Eqs. (5.1), (5.2) and (5.3).

5.3 Canonical Differential Equation

Despite the fact that nowadays exist several automated packages and methods for the construction of a pure basis that satisfies a canonical DE, as we have seen in Chapter 3, finding a pure basis for a generic integral family in practice is still a non-trivial task, assuming that such a basis even exists. In our study here for the planar massless three-loop families with one off-shell external leg, for the F1 family, we adopted the pure basis presented within [272], where this family was studied for the first time, while in order to construct pure bases for the families F2 and F3 we used a combined approach, attacking the problem with the different techniques.

One of the methods we employed was the *Magnus exponential method* [234], applied to the matrices of the DEs derived by differentiating with respect to the Mandelstam variables of Eq. (5.4), which we used for a few lower-sector MIs (up to seven propagators). For some intermediate-sector MIs (up to nine propagators) we used the `Mathematica` package `DlogBasis` [241] combined with the SDE parametrization in order to identify appropriate candidates as pure basis elements. More specifically, as we know `DlogBasis` in order to find FIs of d-log form relies on the *spinor-helicity formalism*, which can not be applied when we deal with off-shell external momenta. When one deals with such problems the standard way to proceed is the decomposition of the external massive momentum in terms of two (arbitrary) massless momenta, or the use of the Baikov representation [242, 243]. Another possible way is the use of the SDE notation for the propagators where by definition the external momenta that appear in them for problems with one external massive particle are massless[3] and hence the spinor-helicity parametrization is applicable. Thus while the command [241]

$$\texttt{SetParametrization}[\texttt{SpinorHelicityParametrization}[\{k_1, k_2, k_3\}, \{a, b, c\}, \{q_1, q_2, q_3\}]],$$

doesn't work when one uses the standard notation for the propagators with massive external momenta, it correctly works when one uses the SDE notation for the propagators and the external momenta (Eq. (5.5))

$$\texttt{SetParametrization}[\texttt{SpinorHelicityParametrization}[\{k_1, k_2, k_3\}, \{a, b, c\}, \{p_1, p_2, p_3\}]].$$

The last but most extensively used approach that we applied for the completion of the pure basis is the loop-by-loop *Building-Blocks method* [245]. In our study apart from the standard approach of utilizing one-loop pure basis elements (massless boxes, triangles and bubbles with up to three external massive particles) as building blocks we also used pure basis elements from the massless planar double-box families with up to three external off-shell legs [243, 272, 276]. In intermediate steps we checked that the chosen basis elements were indeed pure by semi-numerical (keeping only x analytic) derivations of the DE. For sectors with multiple MIs where it is difficult to understand which of the chosen basis elements is not UT, a hint was given to us by the `C++` version of `Fuchsia` [237].

---

[3]The same approach can be used for 2-mass problems introducing an extra y parameter beyond x in order to catch the off-shellness of both masses.

Having at hand pure bases for all the families, by differentiating with respect to x we were able to obtain the following DE in canonical form

$$\frac{\partial}{\partial x}\mathbf{g} = \epsilon \left(\sum_{i=1}^{4} \frac{\mathbf{M}_i}{x - l_i} \right) \mathbf{g},\tag{5.11}$$

where $\mathbf{g}$ is the pure basis and $\mathbf{M}_i$ are the residue matrices associated with each letter l_i. The kinematic dependence is encapsulated within the letters l_i, while the matrices $\mathbf{M}_i$ solely contain rational numbers. We have identified an alphabet consisting of four distinct letters

$$l_1 = 0, \quad l_2 = 1, \quad l_3 = \frac{1}{1+y}, \quad \text{and} \quad l_4 = -\frac{1}{y}.\tag{5.12}$$

It is important to note that in this context, we adopt the definition of the alphabet letters as given in [4, 266], which differs from the standard notation [184, 259, 260]. Typically, the $\mathrm{d}\log$ form of a system of canonical DEs is expressed as $\mathrm{d}\mathbf{g}(\vec{x}, \epsilon) = \epsilon \left(\sum_i \mathbf{M}_i \mathrm{d}\log W_i(\vec{x}) \right) \mathbf{g}(\vec{x}, \epsilon)$, where the alphabet $W_i(\vec{x})$ consists of rational or algebraic functions of the independent variables. The standard $\mathrm{d}\log$ form is equivalent to Eq. (5.11) when $W_i(\vec{x}) = x - l_i$. It is also worth mentioning that in all cases where both the standard approach, which involves differentiation with respect to all kinematic invariants, and the SDE approach have been utilized, we have observed a reduction in the number of logarithmic singularities in the canonical SDE. For instance, in the case of the ladder topology, the corresponding canonical DE presented in [272] exhibited six logarithmic singularities, which corresponds to six $W_i(\vec{x})$ functions in the standard $\mathrm{d}\log$ notation. However, when employing the SDE approach, we obtain a canonical DE in terms of x characterized by only four $W_i(\vec{x})$ functions. This decrease in the number of poles in the canonical DE is a consequence of our focus on differentiation with respect to x, while explicitly handling the s_{12} and y dependencies of the MIs through boundary terms. Additionally, the fact that all three-loop planar families with one off-shell leg share the same alphabet is also an intriguing observation.

The simplicity of the alphabet in Eq. (5.12) with respect to x allows for a straightforward solution of Eq. (5.11) in terms of GPLs. The solution can be expressed in a concise form up to weight six as follows:

$$
\begin{aligned}
\mathbf{g} = {}& \epsilon^0 \mathbf{b}_0^{(0)} + \epsilon \left(\sum \mathcal{G}_i \mathbf{M}_i \mathbf{b}_0^{(0)} + \mathbf{b}_0^{(1)} \right) \\
& + \epsilon^2 \left(\sum \mathcal{G}_{ij} \mathbf{M}_i \mathbf{M}_j \mathbf{b}_0^{(0)} + \sum \mathcal{G}_i \mathbf{M}_i \mathbf{b}_0^{(1)} + \mathbf{b}_0^{(2)} \right) \\
& + \epsilon^3 \left(\sum \mathcal{G}_{ijk} \mathbf{M}_i \mathbf{M}_j \mathbf{M}_k \mathbf{b}_0^{(0)} + \sum \mathcal{G}_{ij} \mathbf{M}_i \mathbf{M}_j \mathbf{b}_0^{(1)} + \sum \mathcal{G}_i \mathbf{M}_i \mathbf{b}_0^{(2)} + \mathbf{b}_0^{(3)} \right) \\
& + \ldots \\
& + \epsilon^6 \left(\sum \mathcal{G}_{ijklmn} \mathbf{M}_i \mathbf{M}_j \mathbf{M}_k \mathbf{M}_l \mathbf{M}_m \mathbf{M}_n \mathbf{b}_0^{(0)} + \sum \mathcal{G}_{ijklm} \mathbf{M}_i \mathbf{M}_j \mathbf{M}_k \mathbf{M}_l \mathbf{M}_m \mathbf{b}_0^{(1)} \right. \\
& + \sum \mathcal{G}_{ijkl} \mathbf{M}_i \mathbf{M}_j \mathbf{M}_k \mathbf{M}_l \mathbf{b}_0^{(2)} + \sum \mathcal{G}_{ijk} \mathbf{M}_i \mathbf{M}_j \mathbf{M}_k \mathbf{b}_0^{(3)} + \sum \mathcal{G}_{ij} \mathbf{M}_i \mathbf{M}_j \mathbf{b}_0^{(4)} \\
& \left. + \sum \mathcal{G}_i \mathbf{M}_i \mathbf{b}_0^{(5)} + \mathbf{b}_0^{(6)} \right).
\end{aligned}\tag{5.13}
$$

Here, the GPLs are represented by $\mathcal{G}_{ab\ldots} \equiv \mathcal{G}(l_a, l_b, \ldots; x)$. The terms $\mathbf{b}_0^{(i)}$ correspond to the boundary terms in the $x \to 0$ limit that require determination, with the subscript i denoting the associated weight. These terms consist of Zeta functions $\zeta(i)$ and logarithms $\log(-s_{12})$, $\log(y)$ of weight i. Our results are organized in a manner where

each coefficient of ϵ^i carries a transcendental weight of i. By assigning weight -1 to ϵ, the expression in Eq. (5.13) maintains a uniform degree of transcedentality equal to zero.

5.4 Boundary Conditions

In order to evaluate the required boundary terms $\mathbf{b}_0^{(i)}$ for each pure basis element in Eq. (5.13), we utilize the resummation matrix method at $x = 0$, as described in subsection 3.3.3. Additionally, we introduce a novel approach of utilizing the resummation matrices that significantly simplifies the entire procedure. Our initial step involves exploiting the canonical SDE in the limit $x \to 0$ and defining the resummation matrix

$$\mathbf{R} = \mathbf{S} e^{\epsilon \mathbf{D} \log(x)} \mathbf{S}^{-1}, \tag{5.14}$$

where the matrices $\mathbf{S}$, $\mathbf{D}$ are derived from the Jordan decomposition[4] of the residue matrix corresponding to the letter $l_1 = 0$, $\mathbf{M}_1 = \mathbf{S}\mathbf{D}\mathbf{S}^{-1}$. On the other hand, through IBP reduction, the elements of the pure basis can be related to a set of MIs, say $\mathbf{G}$, via a transformation matrix, meaning

$$\mathbf{g} = \mathbf{T}\mathbf{G}. \tag{5.15}$$

Moreover, by employing the expansion by regions technique [206] implemented in `asy` code bundled with `FIESTA4` [279], we can acquire insights into the asymptotic behavior of MIs in terms of which we express the pure basis (Eq. (5.15)) in the limit $x \to 0$,

$$G_i^{x \to 0} = \sum_j x^{b_j + a_j \varepsilon} G_{i,\mathrm{region}}^{(b_j + a_j \varepsilon)}, \tag{5.16}$$

with a_j and b_j being integer numbers, and $G_{i,\mathrm{region}}^{(b_j + a_j \varepsilon)}$ being the region-integrals of the individual members, G_i, of the basis $\mathbf{G}$ of MIs in Eq. (5.15). Based on this analysis, we can establish the following powerful relation

$$\mathbf{R}\mathbf{b} = \lim_{x \to 0} \mathbf{T}\mathbf{G}\big|_{\mathcal{O}\left(x^{0 + a_j \varepsilon}\right)}, \tag{5.17}$$

where the rhs implies that, apart from the terms $x^{a_i \epsilon}$ coming from Eq. (5.16), we expand around $x = 0$, keeping only terms of order x^0. Eq. (5.17) allows us in principle to determine all the boundary terms $\mathbf{b} = \sum_{i=0}^{6} \varepsilon^i \mathbf{b}_0^{(i)}$.

More specifically, Eq. (5.17) produces two types of relations. The first type, referred to as *pure relations* in [4], takes the form of linear equations with numerical rational coefficients involving boundary conditions $\mathbf{b}$. The second type consists of linear equations that involve both boundary terms $\mathbf{b}$ and region-integrals in the Feynman parameter representation. Applying these relations to families F1, F2, and F3 requires the calculation of several challenging region-integrals with many Feynman parameters to be integrated. To overcome this challenge, we utilize the fact that the limit of our solution in Eq. (5.13) in $x \to 1$ [4] corresponds to the fully massless integral families [4],

---

[4]For an earlier use of the Jordan decomposition method see [277, 278].

which are already known from [270]. Our approach involves exploiting the pure relations between boundary conditions **b**, computing a minimal set of region-integrals, and constructing the complete solution by explicitly retaining the undetermined boundary terms in the final result. Subsequently, we determine the $x \to 1$ limit using the techniques we described in subsection 3.3.3 and use the known analytic results from [270] to fix any remaining unknown boundaries.

As an illustration of this approach, we will now demonstrate the computation of the boundary terms for the F3 family, assuming that we have already solved the families F1 and F2. We begin by constructing equation (5.17) and determining the so-called pure relations. These relations typically determine the boundary terms for the top-sector basis elements, which are the most challenging to compute due to containing complex region-integrals. Specifically, for the F3 family, the pure relations for the four top-sector basis elements are:

$$
\begin{aligned}
b_{163} = & -\frac{371b_1}{132} - \frac{8b_2}{11} + \frac{12b_4}{11} - \frac{637b_5}{33} + 32b_{10} + \frac{64b_{11}}{3} + \frac{37b_{12}}{6} - 15b_{13} + \frac{3b_{15}}{22} - 15b_{18} \\
& + 12b_{19} - \frac{9b_{22}}{4} - \frac{9b_{23}}{2} + 3b_{24} - \frac{15b_{25}}{22} - \frac{b_{26}}{22} + 12b_{29} + 8b_{30} - 6b_{31} + \frac{75b_{35}}{11} + 6b_{36} \\
& - \frac{84b_{38}}{11} + 9b_{43} + 36b_{52} - 18b_{53} - 21b_{54} + 6b_{57} - \frac{6b_{77}}{11} - b_{81} - 12b_{87} + 3b_{88} - 2b_{123} \\
& - 6b_{130} + 2b_{137} + 6b_{144} - 2b_{152} - 2b_{159},
\end{aligned} \tag{5.18}
$$

$$
\begin{aligned}
b_{164} = & -\frac{745b_1}{264} - \frac{13b_2}{66} + \frac{6b_4}{11} - \frac{359b_5}{22} + \frac{92b_{10}}{3} + \frac{52b_{11}}{3} + \frac{31b_{12}}{6} - \frac{89b_{13}}{6} + \frac{51b_{15}}{22} \\
& - \frac{97b_{18}}{6} + 12b_{19} - \frac{9b_{22}}{8} - \frac{9b_{23}}{2} + 3b_{24} - \frac{15b_{25}}{44} + \frac{5b_{26}}{22} + 10b_{29} + \frac{20b_{30}}{3} - 6b_{31} \\
& + \frac{75b_{35}}{22} + 5b_{36} - \frac{42b_{38}}{11} + 9b_{43} + 36b_{52} - 18b_{53} - \frac{33b_{54}}{2} + 6b_{57} - \frac{3b_{77}}{11} - b_{81} \\
& - 12b_{87} + 3b_{88} - 2b_{123} - 6b_{130} + 2b_{137} + 4b_{144} - 3b_{152} - 3b_{159},
\end{aligned} \tag{5.19}
$$

$$
b_{165} = 0, \tag{5.20}
$$

$$
\begin{aligned}
b_{166} = & -\frac{1531b_1}{4752} - \frac{128b_2}{297} + \frac{47b_4}{33} - \frac{1891b_5}{396} + \frac{74b_{10}}{9} + \frac{20b_{11}}{3} + \frac{7b_{12}}{3} - \frac{127b_{13}}{36} - \frac{415b_{15}}{264} \\
& + \frac{13b_{16}}{8} + \frac{10b_{17}}{3} - \frac{47b_{18}}{36} - 2b_{19} + \frac{5b_{20}}{6} - \frac{21b_{22}}{16} - \frac{11b_{23}}{6} + \frac{5b_{24}}{12} - \frac{35b_{25}}{132} - \frac{6b_{26}}{11} \\
& + \frac{16b_{29}}{3} + \frac{32b_{30}}{9} - \frac{10b_{31}}{3} + \frac{581b_{35}}{132} + \frac{29b_{36}}{18} - \frac{197b_{38}}{33} + \frac{3b_{43}}{2} - \frac{14b_{49}}{3} + 7b_{52} \\
& - 5b_{53} - \frac{89b_{54}}{12} + \frac{13b_{57}}{3} - \frac{8b_{60}}{3} - \frac{b_{61}}{6} + 2b_{62} - \frac{7b_{77}}{33} - \frac{b_{81}}{6} + 3b_{83} - \frac{b_{84}}{2} - \frac{13b_{87}}{6} \\
& + \frac{7b_{88}}{12} - \frac{2b_{89}}{3} + \frac{5b_{97}}{6} - \frac{b_{108}}{3} - \frac{2b_{123}}{3} - b_{130} + \frac{2b_{137}}{3} + 2b_{144} - \frac{4b_{152}}{3} - \frac{2b_{159}}{3}.
\end{aligned} \tag{5.21}
$$

Analogous relations are derived for a total of 109 basis elements, leaving the following basis elements undetermined

$$\begin{aligned}
\big\{ &b_1, b_2, b_4, b_5, b_7, b_{10}, b_{11}, b_{12}, b_{13}, b_{15}, b_{16}, b_{17}, b_{18}, b_{19}, b_{20}, b_{22}, \\
&b_{23}, b_{24}, b_{25}, b_{26}, b_{29}, b_{30}, b_{31}, b_{35}, b_{36}, b_{38}, b_{43}, b_{49}, b_{50}, b_{52}, b_{53}, \\
&b_{54}, b_{57}, b_{59}, b_{60}, b_{61}, b_{62}, b_{77}, b_{81}, b_{83}, b_{84}, b_{85}, b_{87}, b_{88}, b_{89}, b_{97}, \\
&b_{108}, b_{116}, b_{123}, b_{130}, b_{135}, b_{137}, b_{144}, b_{151}, b_{152}, b_{157}, b_{159} \big\}.
\end{aligned} \tag{5.22}$$

Among the listed boundary terms, the majority of them can be inferred from either family F1 or family F2. As a result, the only genuinely unknown boundary terms are:

$$\big\{ b_{108}, b_{123}, b_{135}, b_{144}, b_{157}, b_{159} \big\}. \tag{5.23}$$

Furthermore, b_{108} can be computed through a direct integration of the region-integrals that appear in its resulting relation coming from Eq. (5.17),

$$\begin{aligned}
b_{108} = &- 2b_{19} + \frac{3b_{21}}{4} + s_{12}^2 \epsilon^5 G_{111101012000000}^{(-2\epsilon)} + 4 s_{12} \epsilon^4 G_{1022010110-10000}^{(-\epsilon)} \\
&- 3 s_{12}^2 \epsilon^4 G_{112201001000000}^{(-\epsilon)} + 6 s_{12} \epsilon^5 G_{011101012000000}^{(0)}.
\end{aligned} \tag{5.24}$$

From the above relation we observe that the boundary term b_{108} comprises four region-integrals, with the most challenging having seven propagators, i.e requiring the integration of seven Feynman parameters, in general a non-trivial task, but in this case achievable. Hence, we are left with the following five undetermined boundary terms

$$\big\{ b_{123}, b_{135}, b_{144}, b_{157}, b_{159} \big\}. \tag{5.25}$$

Continuing with this approach to determine the remaining undetermined boundary terms would require computing several highly non-trivial region-integrals, involving the direct integration of up to nine Feynman parameters. Performing such computations can be extremely difficult, even if the result of the integration is rather simple. In order to obtain the remaining boundary terms, we exploit a feature of the SDE approach, which is that by taking the $x \to 1$ limit of our results, we retrieve the solution for the families with all the external momenta massless [270], as can be seen from Eqs. (5.5) and (5.6). Our approach entails the following steps:

1. Construct the solution of Eq. (5.13) using a simple ansatz for the unknown boundary conditions, i.e. $b_i = \sum_{k=0}^{6} a(i,k)\epsilon^k$.

2. Construct the resummation matrix from the residue matrix corresponding to the letter $l_2 = 1$, $\mathbf{M}_2$, and using the shuffle properties of GPLs extract the part of the solution in Eq. (5.13) which is regular at $x = 1$. These two ingredients allow us to obtain the $x \to 1$ limit of Eq. (5.13) [4].

3. Map the $x \to 1$ limit of the F3 family, Eq. (5.3), i.e. the massless tennis-court family, to the same family defined in [270].

4. Map the pure basis for the massless tennis-court of [270] to the pure basis that can be obtained from the $x \to 1$ limit of the pure basis of F3 using the techniques we described in subsection 3.3.3 [4].
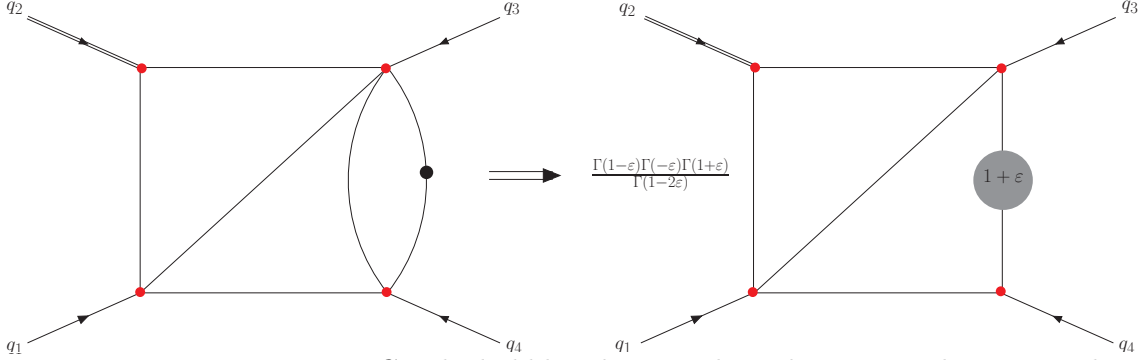
Figure 5.2: Integrating out in G_{32} the bubble sub-integral we obtain a two-loop integral with 5 propagators, where the one related with the bubble sub-integral has its power shifted by ε.

The correspondence between our results and those of [270] reveals that the variable $y = s_{23}/s_{12}$ introduced earlier is equivalent to the dimensionless parameter x employed therein[5]. For the F2 family, the corresponding relation is $y = 1/x$. This illustrates the motivation behind our introduction of the variable y in the first place. The above steps allow us to fix all remaining boundary terms of the F3 family in a purely analytical way.

It is worth mentioning at this point the strategy we employed for the computation of some soft $(x^{-3\varepsilon})$ region-integrals containing bubble sub-graphs, which were necessary for the determination of the boundary conditions of the F1 family. These integrals can be written as a two-loop integral with a bubble insertion. The strategy relies on the Feynman representation of the integrals under consideration, as well as a technique of integrating out bubble sub-integrals. As explained in [270], one can always integrate out bubble sub-integrals and obtain a lower loop integral with some powers shifted by ε. More specifically we have

$$\int \frac{d^d k}{i\pi^{d/2}} \frac{1}{k^{2a_1}(k+p)^{2a_2}} = \frac{\Gamma(a-d/2)\Gamma(d/2-a_1)\Gamma(d/2-a_2)}{\Gamma(a_1)\Gamma(a_2)\Gamma(d-a)}(p^2)^{d/2-a}. \qquad (5.26)$$

where $a = a_1 + a_2$. In the specific cases appearing to the boundary conditions of the F1 family, where $a_1 = 2$ and $a_2 = 1$, the integration of the bubble sub-integral leads to a two-loop integral with a propagator power shifted from 1 to $1 + \varepsilon$. Here, we provide a detailed explanation of the computation of the required region for the integral G_{32} of the F1 family. The computation of other region-integrals involving bubble insertions can be performed following the same procedure. In our notation (Eq. (5.1) after applying the SDE parametrization of Eq. (5.5)), G_{32} is expressed as

$$\int \frac{d^d k_1 d^d k_2 d^d k_3}{(i\pi^{d/2})^3} \frac{e^{3\varepsilon\gamma_E}}{k_2^2(k_1+k_2)^2(k_2+k_3)^2(k_1+p_{12})^2(k_1+xp_1)^2(k_3+p_{123})^4}, \qquad (5.27)$$

and thus its bubble sub-integral is

$$\int \frac{d^d k_3}{i\pi^{d/2}} \frac{1}{(k_2+k_3)^2(k_3+p_{123})^4}. \qquad (5.28)$$

---

[5]Not to be confused with the SDE parameter x.

By performing the shift $k_3 \rightarrow k - p_{123}$, we can rewrite it as shown in Eq. (5.26). Consequently, we are left with a two-loop integral containing five propagators (see Figure 5.2). The distinctive feature, in this case, is that one propagator is raised to the power of $1 + \varepsilon$. When investigating the regions that contribute to the $x \rightarrow 0$ limit of this integral, we find two regions, namely $(x^0, x^{-3\varepsilon})$, which are the same as for the full three-loop integral. Our focus lies on the $x^{-3\varepsilon}$ region, which is notably less complicated compared to the region resulting from the analysis of the complete three-loop integral. After carrying out the necessary integrations, we may assemble the final result by multiplying the outcome of the bubble integration, namely Eq. (5.26) for $a_1 = 2$ and $a_2 = 1$, with the result of the two-loop region, and expand it up to the desired power in the dimensional regulator.

Very interesting is the fact that by observing the boundary conditions of the three planar families we found that the following general ansatz for all the boundary conditions can be constructed

$$
\begin{aligned}
b_i = {} & c(i,0) + \epsilon \log(y) c(i,1) + \epsilon^2 \left(\frac{1}{2} \log^2(y) c(i,2,2) + \frac{1}{6} \pi^2 c(i,2,1) \right) \\
& + \epsilon^3 \left(\frac{1}{6} \log^3(y) c(i,3,2) + \frac{1}{6} \pi^2 \log(y) c(i,3,1) + \zeta(3) c(i,3,3) \right) \\
& + \epsilon^4 \left(\zeta(3) \log(y) c(i,4,4) + \frac{1}{24} \log^4(y) c(i,4,3) + \frac{1}{12} \pi^2 \log^2(y) c(i,4,2) + \frac{1}{90} \pi^4 c(i,4,1) \right) \\
& + \epsilon^5 \Big(\frac{1}{2} \zeta(3) \log^2(y) c(i,5,5) + \frac{1}{120} \log^5(y) c(i,5,3) + \frac{1}{36} \pi^2 \log^3(y) c(i,5,2) \\
& \qquad + \frac{1}{90} \pi^4 \log(y) c(i,5,1) + \zeta(5) c(i,5,6) + \frac{1}{6} \pi^2 \zeta(3) c(i,5,4) \Big) \\
& + \epsilon^6 \Big(\frac{1}{6} \zeta(3) \log^3(y) c(i,6,6) + \log(y) \left(\frac{1}{6} \pi^2 \zeta(3) c(i,6,5) + \zeta(5) c(i,6,8) \right) + \frac{1}{720} \log^6(y) c(i,6,4) \\
& \qquad + \frac{1}{144} \pi^2 \log^4(y) c(i,6,3) + \frac{1}{180} \pi^4 \log^2(y) c(i,6,2) + \zeta(3)^2 c(i,6,7) + \frac{1}{945} \pi^6 c(i,6,1) \Big),
\end{aligned}
\tag{5.29}
$$

where we have multiplied by $(-s_{12})^{(3\epsilon)}$ and expanded up to ϵ^6 to make the ansatz more compact, and the coefficients c are purely rational numbers. Certainly, this represents the most general form that adheres to the scaling properties and universal transcendentality of the boundary conditions. In the scenario where the same alphabet applies to one or more non-planar families, it is plausible to consider obtaining the boundary terms by numerically fitting this ansatz for the remaining integral families. The PSLQ algorithm [280] could be employed for this purpose.

5.5 Results

5.5.1 Analytic continuation

As previously mentioned, our results are presented in the form of GPLs up to weight six, allowing for precise numerical computations using automated tools such as `GinaC` [257] and `HandyG` [262]. The weight W=1,...,6, corresponds to the number of letters l_i in $\mathcal{G}(l_i, \ldots; x)$. For the evaluations to be fast and efficient the GPLs should not contain letters l_i along the integration path connecting the origin and the argument x, i.e. $l_i \notin (0, x)$. While this condition holds true in the Euclidean region, it is no longer

valid in the physical regions. To overcome this problem, we employed fibration-basis techniques [195, 263] for changing appropriately the arguments of GPLs at each physical region and making them real-valued. We followed this procedure using `HyperInt` [195], aiming to obtain results expressed in terms of real-valued GPLs that can be efficiently and accurately evaluated numerically. This renders our solutions highly suitable for various phenomenological applications.

Regions	Letters	Argument	Letters	Argument
Euclidean	$\{0, 1, -1/y, 1/(1+y)\}$	x	$-$	$-$
s-channel	$\{0, 1, -1/y, 1/(1+y)\}$	x	$-$	$-$
t-channel	$\{0, 1, 1+y, -y\}$	$1/x$	$\{0, 1\}$	$-1/y$
u-channel	$\{0, 1, 1+y, -y\}$	$1/x$	$\{0, -1\}$	y

Table 5.1: Structure of GPLs appearing in each of the 4 kinematic regions.

In order to make more clear the form of our solutions, we present in table 5.1 the arguments and the letters of the GPLs in the Euclidean and each of the physical regions after using `HyperInt`. Due to the fact that our GPLs depend on the variables $\{x, y\}$, their analytic continuation resulted into two auxiliary variables $\{\delta_x, \delta_y\}$, which can be equal to ± 1[6]. For verifying the correct sign of the auxiliary variables at each physical region we computed numerically with `FIESTA4` [279] some lower-sector MIs, which include all the GPLs appearing to our results, and we compared them with the numerical values we obtained from the analytic continued results for every possible combination of signs. It is worth noting that before employing fibration-basis techniques, no GPLs with arguments depending on y are present. However, when casting each GPL in a fibration basis, which includes real-valued GPLs along with explicit imaginary terms, GPLs with y-dependent arguments emerge as well.

In table 5.2 we provide an analysis regarding the number of GPLs that appear in each transcendental weight, for every kinematic region. In the same table we quote also the total number of GPLs and the timing (in seconds) required for their numerical evaluation using `GinaC`. For all families except F1, the GPLs are identical in each region. However, the F1 family differs in the Euclidean region and the s-channel, where it contains 42 fewer GPLs, all of them of weight 6. The number of GPLs is the same for the Euclidean and the s-channel due to the fact that the GPLs of the Euclidean region are already real valued in the s-channel and thus their is no need of using fibration-basis techniques for them.

5.5.2   Numerical checks

For the validation of our results we have performed various numerical checks in the Euclidean and the physical regions. More specifically, for the Euclidean region we performed a numerical comparison of every MI in each family with `pySecDec` [199] and `FIESTA4` [279], for the phase-space point

$$s_{12} \to -7, \quad y \to 3/7, \quad \text{and} \quad x \to 1/4. \tag{5.30}$$

---

[6] In `HyperInt` the analytic continuation is performed along a straight path and the result can be ambiguous when this line contains a point where the function is not analytic, thus the auxiliary variables appear to distinguish the branches above and below the real axis

Regions	$W = 1$	$W = 2$	$W = 3$	$W = 4$	$W = 5$	$W = 6$	**Total**	**Timings**
Euclidean	4	14	50	124	367	734	1293	39.0225769
s-channel	4	14	50	124	367	734	1293	39.2172529
t-channel	6	18	58	155	419	603	1259	62.0567800
u-channel	5	16	54	147	403	572	1197	55.1049640

Table 5.2: Number of GPLs per transcendental weight and per kinematic region, and timings (in seconds) for the numerical evaluation of the total of GPLs appearing in all the families. The quoted timings are obtained using the `Ginsh` command of `PolyLogTools`, running 1-core in a personal laptop (i7 processor, 8-core, 25GB RAM). The phase-space points that were used are the ones of Eq. (5.30) for the Euclidean region and the ones of Eqs. (5.31), (5.32) and (5.33) for the corresponding physical regions.

We found that our results exhibited perfect agreement within the numerical accuracy provided by these programs.

Regarding our results for physical regions, obtaining numerical results for all MIs using `pySecDec` or `FIESTA4` can be rather challenging, and in some cases even impossible. To that end, in order to check that the analytic continuation was correct, we determined a specific set of low-sector MIs (with up to 7 propagators), which contained the total set of GPLs at each region and we numerically compared them with `pySecDec` and `Fiesta` for the phase-space points

$$s\text{-channel}: \quad s_{12} \to 2, \quad y \to -1/2, \quad \text{and} \quad x \to 1/4 \tag{5.31}$$

$$t\text{-channel}: \quad s_{12} \to -2, \quad y \to -3/2, \quad \text{and} \quad x \to 5/3 \tag{5.32}$$

$$u\text{-channel}: \quad s_{12} \to -2, \quad y \to 3/2, \quad \text{and} \quad x \to 5/3. \tag{5.33}$$

By carefully selecting the appropriate branch of the analytic continuation, i.e. fixing the values of the auxiliary functions $\{\delta(1/x), \delta(-1/y), \delta(y)\}$ obtained from `HyperInt`, we achieved perfect agreement for every MI that we examined.

5.5.3 Analytic checks

For the MIs of family F1 we verified the correctness of our results by cross-checking them with the analytic results of [272]. For the MIs of families F2 and F3 we performed analytic checks at the limit $x \to 1$ against the results of [270] in the Euclidean region. While the limit $x \to 1$ was utilized to determine certain boundary terms, ensuring that all MIs of families F2 and F3 accurately reproduce the results of [270] in this limit represents a non-trivial confirmation of our calculations.

5.5.4 Ancillary files

The results obtained in our study are accessible in `Mathematica` readable format, and they can be found at the GitHub repository: Planar3loops1mass.git. The repository contains several files, including

- The file `input.m`, which includes essential information for the studied families, such as the propagators described in Eqs. (5.1), (5.2), and (5.3), along with their
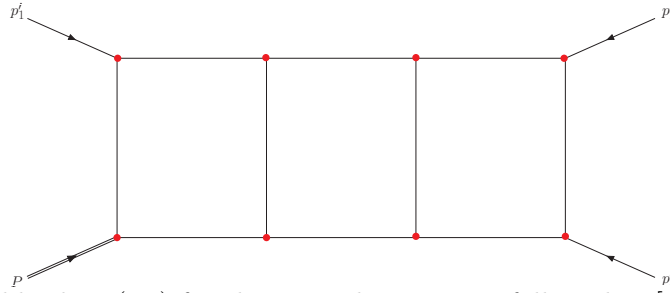
Figure 5.3: The ladder-box (F1) family using the notation followed in [274]. The double line represents the massive particle and all the external momenta are assumed to be incoming.

corresponding kinematic properties. Additionally, the file contains the mapping specified in Eq. (5.6) and the alphabet presented in Eq. (5.12), which remains the same for all the integral families.

- The directories Fi, with $i = 1, 2, 3$, which contain:

  - `Fibasis.m`: the pure basis.
  - `FiDE.m`: the canonical DE.
  - `FiBounds.m`: boundary terms for solving the canonical DE in the Euclidean region.
  - `FiE.m`: the solution in the Euclidean region.
  - `Fis.m`: the solution in the s-channel.
  - `Fit.m`: the solution in the t-channel.
  - `Fiu.m`: the solution in the u-channel.

5.6　Adjacency Conditions in the SDE Approach

In this section, we provide insights into the interpretation of the adjacency conditions identified in [273, 274] within the context of the SDE approach. To accomplish this, firstly, we establish a connection between the conventional DE method and the SDE approach.

For the standard DE method we are going to use the notation used in [274] (see figure 5.3). In this article, the Lorentz invariants are defined as follows

$$z_1 = \frac{2p_1' \cdot p_2'}{P^2}, \quad z_2 = \frac{2p_2' \cdot p_3'}{P^2} \quad \text{and} \quad z_3 = 1 - z_1 - z_2. \tag{5.34}$$

The alphabet of this family (using the standard notation [184, 259, 260]), as it is derived by applying the standard DE method, is

$$\{z_1, z_2, z_3, 1 - z_1, 1 - z_2, 1 - z_3\} \to \{z_1, z_2, 1 - z_1 - z_2, 1 - z_1, 1 - z_2, z_1 + z_2\}, \tag{5.35}$$

and the pure basis of MIs, $\mathbf{g}$, satisfies the DE

$$
\begin{aligned}
\mathrm{d}\mathbf{g} = \epsilon \bigg(& \mathbf{A}_{z_1} \mathrm{d}\log(z_1) + \mathbf{A}_{z_2} \mathrm{d}\log(z_2) + \mathbf{A}_{1-z_1-z_2} \mathrm{d}\log(1 - z_1 - z_2) \\
& + \mathbf{A}_{1-z_1} \mathrm{d}\log(1 - z_1) + \mathbf{A}_{1-z_2} \mathrm{d}\log(1 - z_2) + \mathbf{A}_{z_1+z_2} \mathrm{d}\log(z_1 + z_2) \bigg) \mathbf{g}
\end{aligned}
\tag{5.36}
$$

The C_2 adjacency conditions [274] dictate that the letters $\{1-z_i, 1-z_j\}$ for $i, j = 1, 2, 3$ and $i \neq j$ should never appear next to each other in a symbol, or equivalently (in terms of the residue matrices of the DE), that the residue matrices of the DE should satisfy the following conditions

$$
\mathbf{A}_{1-z_1}\mathbf{A}_{1-z_2} = 0, \quad \mathbf{A}_{1-z_1}\mathbf{A}_{z_1+z_2} = 0 \quad \text{and} \quad \mathbf{A}_{1-z_2}\mathbf{A}_{z_1+z_2} = 0.
\tag{5.37}
$$

As we have already discussed, in our treatment of the massless three-loop planar families with one off-shell leg, we use the notation as is depicted in Figure 5.1, while the kinematic invariants are defined as in Eq. (5.6) with the extra introduction of the ratio $y = s_{23}/s_{12}$. The pure basis elements satisfy the DE of Eq. (5.11), which in more detail can be expressed in the form

$$
\frac{\mathrm{d}}{\mathrm{d}x}\mathbf{G} = \epsilon \left(\frac{\mathbf{M}_0}{x} + \frac{\mathbf{M}_1}{x - 1} + \frac{\mathbf{M}_{-1/y}}{x + 1/y} + \frac{\mathbf{M}_{1/(1+y)}}{x - 1/(1+y)} \right) \mathbf{G}.
\tag{5.38}
$$

From Figures 5.1 and 5.3 (using also Eq. (5.5)) we observe that the momenta in the two different notations are related via the transformation

$$
P \to p_1 + p_2 - xp_1, \quad p_1' \to xp_1, \quad p_2' \to p_4, \quad \text{and} \quad p_3' \to p_3.
\tag{5.39}
$$

Thus replacing Eq. (5.39) in Eq. (5.34) we find that the transformation that takes us from the $\{z_1, z_2\}$ invariants to the $\{x, y\}$ ones, is

$$
z_1 = \frac{xy}{1 - x} \quad \text{and} \quad z_2 = \frac{1}{1 - x},
\tag{5.40}
$$

while the reverse transformation reads

$$
x = \frac{z_2 - 1}{z_2} \quad \text{and} \quad y = \frac{z_1}{z_2 - 1}.
\tag{5.41}
$$

In addition, using Eq. (5.40) the alphabet in Eq. (5.35) can be written in terms of $\{x, y\}$ as (keeping the same ordering for the letters)

$$
\left\{ \frac{xy}{1-x}, \frac{1}{1-x}, \frac{-x(1+y)}{1-x}, -\left(\frac{1+y}{1-x}\right)\left(x - \frac{1}{1+y}\right), \frac{-x}{1-x}, \left(\frac{y}{1-x}\right)\left(x + \frac{1}{y}\right) \right\}.
\tag{5.42}
$$

Having established the connection between the standard DE method and the SDE approach, via the information stated above, we can see now how the adjacency conditions are interpreted within the latter. More specifically, expressing the letters in Eq.

(5.36) via the relation of Eq. (5.42) and differentiating with respect to x we obtain

$$
\frac{\mathrm{d}}{\mathrm{d}x}\mathbf{G} = \epsilon \left(\frac{\mathbf{A}_{1-z_2} + \mathbf{A}_{z_1} + \mathbf{A}_{1-z_1-z_2}}{x} + \frac{\mathbf{A}_{z_1+z_2}}{x + 1/y} + \frac{\mathbf{A}_{1-z_1}}{x - 1/(1+y)} \right.
$$
$$
\left. - \frac{\mathbf{A}_{z_1} + \mathbf{A}_{z_2} + \mathbf{A}_{1-z_1-z_2} + \mathbf{A}_{1-z_1} + \mathbf{A}_{1-z_2} + \mathbf{A}_{z_1+z_2}}{x - 1} \right) \mathbf{G} \qquad (5.43)
$$

Comparing Eqs. (5.38) and (5.43), we find that following relations arise among the residue matrices of the standard DE method and the SDE approach

$$
\begin{aligned}
\mathbf{A}_{1-z_1} &= \mathbf{M}_{1/(1+y)} \\
\mathbf{A}_{z_1+z_2} &= \mathbf{M}_{-1/y} \\
\mathbf{A}_{z_2} &= -\mathbf{M}_0 - \mathbf{M}_1 - \mathbf{M}_{1/(1+y)} - \mathbf{M}_{1/(1+y)} \\
\mathbf{A}_{1-z_2} &= \mathbf{M}_0 - \mathbf{A}_{z_1} - \mathbf{A}_{1-z_1-z_2}
\end{aligned} \qquad (5.44)
$$

From Eq. (5.44) we see that the matrices $\{\mathbf{A}_{1-z_1}, \mathbf{A}_{z_1+z_2}\}$ are completely determined by the residue matrices of SDE, while $\mathbf{A}_{1-z_2}$ remains unknown. Thus the only adjacency relation that can be passed from the DE method to the SDE residue matrices is the

$$
\mathbf{A}_{1-z_1}\mathbf{A}_{z_1+z_2} = 0 \Rightarrow \mathbf{M}_{1/(1+y)}\mathbf{M}_{-1/y} = 0. \qquad (5.45)
$$

Having the residue matrices $\{\mathbf{M}_{1/(1+y)}, \mathbf{M}_{-1/y}\}$ for the families F1, F2, and F3 we checked and we found out that indeed the above relation holds true for all of them[7].

Assuming that (as in the SDE approach) the alphabet of the two tennis-court families is the same as the one of the ladder-box family, one could naively expect that the rest of the adjacency conditions should be valid for the two tennis-court families, as in the ladder-box family. It turns out that this is not the case. Recently the two tennis-court families were computed (together with two non-planar ladder-box-like families depicted in Figure 5.4), using the standard DE method [275]. Therein it was impressively observed that although the tennis-court families indeed share the same alphabet[8] with the ladder-box family, they did not satisfy all the C_2 adjacency conditions. More specifically, for the F3 family, while it was found that the condition

$$
\mathbf{A}_{1-z_2}\mathbf{A}_{z_1+z_2} = 0, \qquad (5.46)
$$

is satisfied, it was also discovered the following violation in the adjacency conditions

$$
\mathbf{A}_{1-z_1}\mathbf{A}_{1-z_2} \neq 0. \qquad (5.47)
$$

5.7   Towards the Non-Planar Families

A natural next step is the calculation in physical kinematics (possibly expressed in terms of GPLs) of the fifteen distinct non-planar massless three-loop FI families with one off-shell leg, which are relevant for making full color phenomenological predictions.

---

[7]For the F1 family this was obvious, as the adjacency conditions have been already studied for this family.

[8]As the alphabet is defined in the standard DE method.
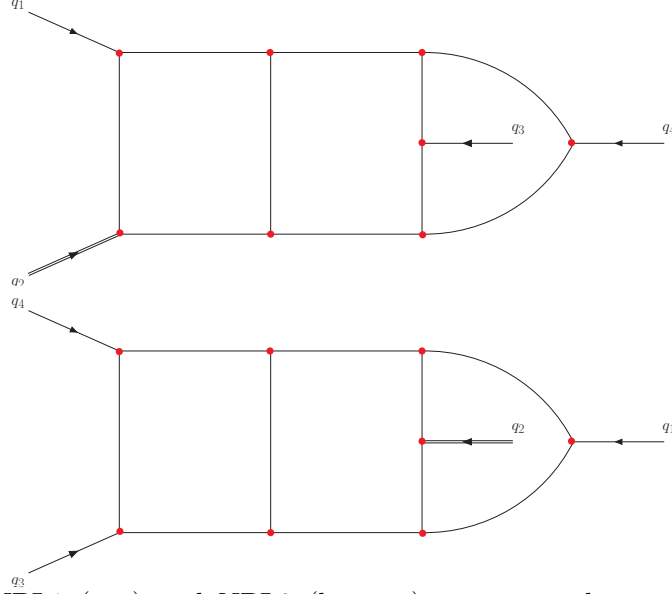
Figure 5.4: The NPL1 (top) and NPL2 (bottom) top-sector diagrams. The double line represents the massive particle and all external momenta are taken to be incoming.

The starting point in this direction is the analysis of the four ladder-box-like families illustrated in Figures 5.4 and 5.5. In fact, there has been already drought attention to these families in the last year, and two of them, the ones pictured in Figure 5.4, have been already computed in Euclidean kinematics using the standard DE method [275], with the results being expressed in terms of GPLs. Independently from this work, we have also computed these families using the standard DE method and a different UT basis. We briefly summarize our results in this chapter. As in the planar case, we define the NPL1 and NPL2 integral families through the following expressions

$$G_{a_1 \cdots a_{15}}^{NPL1} \equiv \int \left(\prod_{l=1}^{3} e^{\gamma_E \epsilon} \frac{d^d k_l}{i \pi^{d/2}} \right) \frac{(k_2 - q_1)^{-2a_{11}} (k_3 - q_1)^{-2a_{12}}}{(k_1)^{2a_1} (k_2)^{2a_2} (k_3)^{2a_3} (k_1 - q_1)^{2a_4} (k_1 - q_{12})^{2a_5}}$$

$$\times \frac{(k_1 - k_2)^{-2a_{13}} (k_1 - k_2 - q_{123})^{-2a_{14}} (k_2 - q_{12})^{-2a_{15}}}{(k_3 - q_{12})^{2a_6} (k_2 - k_3)^{2a_7} (k_2 - k_3 - q_3)^{2a_8} (k_2 - q_{123})^{2a_9} (k_1 - k_3)^{2a_{10}}}$$

$$(5.48)$$

$$G_{a_1 \cdots a_{15}}^{NPL2} \equiv \int \left(\prod_{l=1}^{3} e^{\gamma_E \epsilon} \frac{d^d k_l}{i \pi^{d/2}} \right) \frac{(k_2 - q_3)^{-2a_{11}} (k_3 - q_3)^{-2a_{12}}}{(k_1)^{2a_1} (k_2)^{2a_2} (k_3)^{2a_3} (k_1 - q_3)^{2a_4} (k_1 + q_{12})^{2a_5}}$$

$$\times \frac{(k_1 - k_2)^{-2a_{13}} (k_1 - k_2 - q_1)^{-2a_{14}} (k_2 + q_{12})^{-2a_{15}}}{(k_3 + q_{12})^{2a_6} (k_2 - k_3)^{2a_7} (k_2 - k_3 + q_2)^{2a_8} (k_2 + q_1)^{2a_9} (k_1 - k_3)^{2a_{10}}}$$

$$(5.49)$$

with a_i being integers, and $a_i \leq 0$ for $i = 11, \ldots, 15$. The kinematics are identical to the ones of the planar case (see Eq. (5.4)).

Using FIRE6 [58] and KIRA2 [60] for the IBP reduction, we found for family NPL1

(NPL2) a set of 114 (150) MIs, with 4 (4) of them at the top-sector. Studying independently these two families and constructing pure bases[9] ($\mathbf{g}$) using the techniques we described in section 5.3, we observed that, as in the case of standard DE method, in the SDE approach the family NPL1 shares the same alphabet with the planar families, while NPL2 family extends this alphabet by the following two more letters

$$l_5 = \frac{1+y}{y} \quad \text{and} \quad l_6 = \frac{y}{1+y}. \tag{5.50}$$

Having a canonical DE in the SDE approach, we constructed a system of DEs in the following massless invariants

$$\tilde{x} = S_{12}/m^2, \quad \tilde{y} = S_{13}/m^2 \quad \text{and} \quad \tilde{z} = S_{23}/m^2, \tag{5.51}$$

in order to apply the standard DE method. The canonical DEs have the following form

$$\mathrm{d}\mathbf{g} = \varepsilon \mathbf{A}\mathbf{g} = \varepsilon \sum_i \mathbf{B}_i \mathrm{d}\log(\alpha_i)\mathbf{g}, \tag{5.52}$$

with the matrices $\mathbf{B}_i$ consisting of rational numbers and the letters of the DE (arguments α_i of the dlog forms) being

$$\{\tilde{x}, \tilde{z}, 1 - \tilde{x}, 1 - \tilde{z}, 1 - \tilde{x} - \tilde{z}, \tilde{x} + \tilde{z}, 1 - 2\tilde{x} + \tilde{x}^2 - \tilde{z}, \tilde{x} - \tilde{x}^2 - \tilde{z}\}. \tag{5.53}$$

The last two letters of the above alphabet appear only in NPL2 family, and although they contain a second-order polynomial in $\tilde{x}$, one can obtain an analytic solution for this family in terms of GPLs by first integrating over $\tilde{z}$ and then over $\tilde{x}$. In order to arrive at an analytic solution it is essential to establish boundary conditions for the MIs, which due to their involved analytic structure (branch points at $\{\tilde{z} = 0, \tilde{z} = 1 - \tilde{x}, \tilde{x} = 0\}$) goes beyond the standard regularity constraints. For this reason, we pursued a more universal strategy, investigating the solution of the DEs across all physical and unphysical limits [241, 245]. More specifically, the d log form of Eq.(5.52) allows us to write its solution at the limit $\alpha_i = 0$ as

$$e^{\varepsilon \mathbf{B}_i \log(\alpha_i)} \left.\mathbf{g}\right|_{\alpha_i=0} = \mathbf{C}_i \left.\mathbf{g}\right|_{\alpha_i=0}. \tag{5.54}$$

where the matrices $\mathbf{C}_i$ contain terms of the form $\alpha_i^{n_i\varepsilon}$, with n_i being the eigenvalues of $\mathbf{B}_i$. We proceed by enforcing the condition that the unphysical singularities $\{\tilde{z} = -\tilde{x}, \tilde{z} = 1, \tilde{x} = 1\}$, meaning terms involving $\alpha_i^{n_i\varepsilon}$ with $n_i \neq 0$, must vanish at $\left.\mathbf{g}\right|_{\alpha_i=0}$. This imposition serves as another means of enforcing the conventional regularity conditions. Moreover, for the physical singularities $\tilde{z} = 0, \tilde{z} = 1 - \tilde{x}, \tilde{x} = 0$, we impose that terms involving $\alpha_i^{n_i\varepsilon}$ with $n_i > 0$ must also vanish at $\left.\mathbf{g}\right|_{\alpha_i=0}$. This choice is justified by the absence of UV divergencies in the UT basis and we verified using expansion-by-regions [202–207] that for the specific limits, the scaling in powers of ε never carries a positive sign. This methodology enables us to determine all necessary boundary conditions, yielding analytic results for the two non-planar families of Figure

---

[9]Interesting is the fact that, while the techniques we used for the construction of the pure bases are similar to the ones used in [275] our pure basis elements are different from the ones chosen therein.
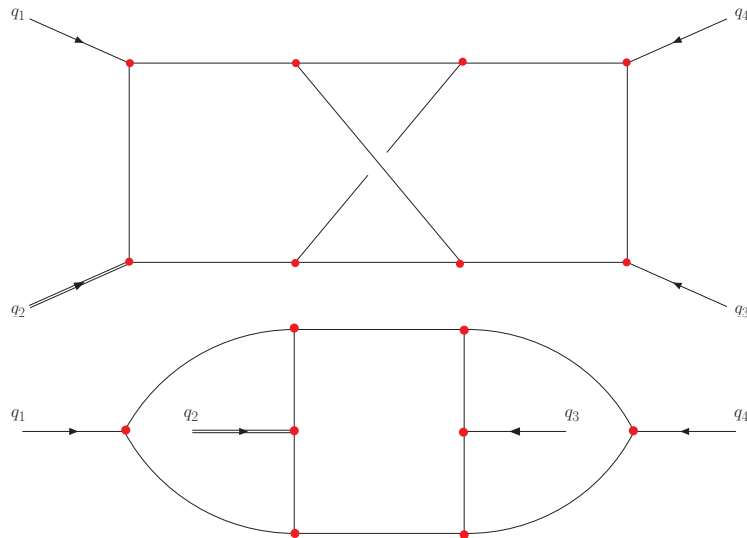
Figure 5.5: The NPL3 (top) and NPL4 (bottom) top-sector diagrams. The double line represents the massive particle and all external momenta are taken to be incoming.

5.4 in terms of GPLs up to transcendental weight six. We have cross checked our findings against [275], finding perfect agreement. Our results are provided in the ancillary files attached to the arxiv submission of [7].

Concluding we would like to make some comments on the two non-planar families depicted in Figure 5.5, where the first of them, NPL3, consists of 173 MIs, 68 of which are new (in the sense that they are not included in the previously studied families), while the second, NPL4, is described by a set of 121 MIs, 9 of which are new. Interesting is the fact that, for the construction of a pure basis for the NPL4 family one comes across with a pure basis element which contains the following square root

$$\text{root} = \sqrt{m^2 S_{12} S_{23} S_{13}}, \tag{5.55}$$

something that is unprecedented for $2 \to 2$ particle kinematics with one external massive particle and massless loop particles, as for the corresponding families at two-loop and one-loop there do not exist square roots nether in the definition of the basis elements nether in the alphabet. Although this square root is rationalizable, allowing for a solution of the relevant canonical differential equations in terms of GPLs, special care has to be taken when considering the analytic continuation to physical regions of phase space. Furthermore, we would like to mention that the most complicated non-planar family, which is a tennis-court-like family, contains 371 MIs, with 19 of them at the top sector, posing a significant challenge in finding a UT basis for this family. Thus the computation of the non-planar massless three-loop families with one off-shell leg holds significant interest not only from a phenomenological perspective but also from a mathematical standpoint due to the new intricate features appearing in their structure.

Chapter 6

Epilogue

This thesis journeyed through the intricate realm of NNLO and N3LO QCD computations. For the former we presented the algorithm implemented within `HELAC-2LOOP` for the recursive construction of two-loop scattering amplitudes for any process at hand, while for the latter we presented the analytic computation of some $2 \to 2$ three-loop Feynman integral families, relevant for processes like $e^+e^- \to \gamma^* \to$ 3jets and $pp \to H/Z+$jet.

Despite the importance of these results, further work and extensions need to be elaborated in the future on both directions. Current experimental data require NNLO accuracy for many $2 \to 3$ QCD processes, and for conducting these computations using `HELAC-2LOOP`, a numerical and applicable at the integrand level, method for the reduction of a generic two-loop scattering amplitude into a basis of two-loop FIs (subsequently to be reduced to MIs using IBPs) is a necessity. Presently, in collaboration with the research group led by the supervisor of this thesis, investigations are underway to explore the feasibility and implementation of such an integrand reduction approach. Furthermore, while for the moment the complete list of all the MIs relevant for two-loop scattering amplitudes is unknown, the development of efficient libraries and routines, akin to pentagon functions, for their computation is imperative for the automation of NNLO QCD computation.

Regarding the N3LO corrections, the extension of the accuracy for $2 \to 2$ processes at this level will be important for comparisons with the results of LHC and future collider experiments. Beyond planar families, there exist 15 non-planar families that need to be computed in order to complete the $4-$point $3-$loop massless MIs with one external massive leg, while the number of families and MIs grows even larger by considering more massive external particles. Beyond the phenomenological interest of these families, of great interest is also their mathematical structure.

Concluding, the growing complexity of the NNLO and N3LO computations, constitutes a great challenge for the already existing techniques and necessitates the development of novel methods and techniques. The key that would lead to the discovery and efficient implementation of such methods is the combination of a better understanding of the mathematical aspects of scattering amplitudes alongside with the adoption of new technologies and developments from Computer Science.

Appendix A

Symmetry Factors

The symmetry factors used for the blob-topologies, within `HELAC-2LOOP`, are the followings (topologies that are not included have weight $W = 1$):
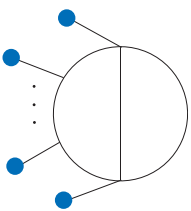
1) : $\begin{cases} \text{i) } L_1 \geq 1, \ L_A = 1, \ L_2 = L_3 = 0, \ \text{and } L_B = 0, 1 \\ \text{ii) } L_1 \geq 1, \ L_B = 1, \ L_2 = L_3 = 0, \ \text{and } L_A = 0, 1 \end{cases} \longrightarrow W = 1/2.$
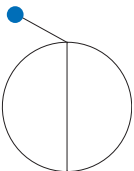
2) : i) $L_1 = L_2 = L_3 = 0, \ \text{and } L_A = L_B = 1 \longrightarrow W = 1/6.$
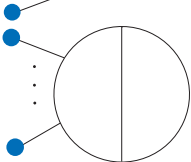
3) : i) $L_1 \geq 2, \ \text{and } L_2 = L_3 = L_A = L_B = 0 \longrightarrow W = 1/2.$
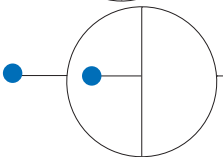
4) : i) $L_1 = L_2 = L_3 = 1, \ \text{and } L_A = L_B = 0 \longrightarrow W = 1/2.$
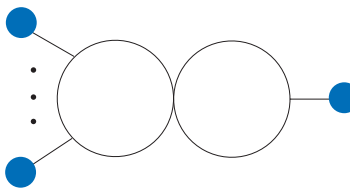
5) : $\begin{cases} \text{i) } L_1 = 1, \ \text{and } L_2 \geq 2 \\ \text{ii) } L_2 = 1, \ \text{and } L_1 \geq 2 \end{cases} \longrightarrow W = 1/2.$
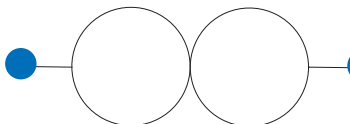
6) : i) $L_1 = L_2 = 1 \longrightarrow W = 1/4.$
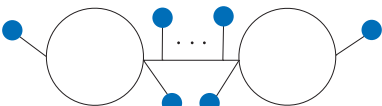
7) : i) $L_1 = 1, \ \text{and } L_A = 1 \longrightarrow W = 1/4$
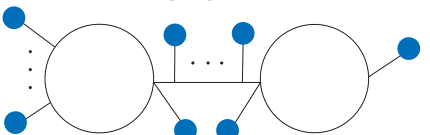
8) : $\begin{cases} \text{i) } L_1 \geq 2, \ \text{and } L_2 = 1 \\ \text{ii) } L_2 \geq 2, \ \text{and } L_1 = 1 \end{cases} \longrightarrow W = 1/2 \ .$

Bibliography

[1] G. Bevilacqua, D. D. Canko, A. Kardos, and C. G. Papadopoulos, "Progress on 2—loop Amplitude Reduction," *J. Phys. Conf. Ser.* **2105** no. 5, (2021) 012010.

[2] G. Bevilacqua, D. Canko, A. Kardos, C. Papadopoulos, A. Smirnov, N. Syrrakos, and C. Wever, "Progress on Multiloop calculations," *PoS* **CORFU2021** (2022) 010.

[3] G. Bevilacqua, D. Canko, and C. Papadopoulos, "Two-Loop Amplitude Reduction with HELAC," in *16th International Symposium on Radiative Corrections: Applications of Quantum Field Theory to Phenomenology.* 9, 2023. `arXiv:2309.14886 [hep-ph]`.

[4] D. D. Canko and N. Syrrakos, "Resummation methods for Master Integrals," *JHEP* **02** (2021) 080, `arXiv:2010.06947 [hep-ph]`.

[5] D. D. Canko, F. Gasparotto, L. Mattiazzi, C. G. Papadopoulos, and N. Syrrakos, "N^3LO calculations for $2 \rightarrow 2$ processes using simplified differential equations," *SciPost Phys. Proc.* **7** (2022) 028, `arXiv:2110.08110 [hep-ph]`.

[6] D. D. Canko and N. Syrrakos, "Planar three-loop master integrals for $2 \rightarrow 2$ processes with one external massive particle," *JHEP* **04** (2022) 134, `arXiv:2112.14275 [hep-ph]`.

[7] N. Syrrakos and D. D. Canko, "Three-loop master integrals for H+jet production at N3LO: Towards the non-planar topologies," *PoS* **RADCOR2023** (2024) 044, `arXiv:2307.08432 [hep-ph]`.

[8] D. D. Canko, I. D. Gialamas, and G. P. Kodaxis, "A simple $F(\mathcal{R}, \phi)$ deformation of Starobinsky inflationary model," *Eur. Phys. J. C* **80** no. 5, (2020) 458, `arXiv:1901.06296 [hep-th]`.

[9] D. D. Canko, C. G. Papadopoulos, and N. Syrrakos, "Analytic representation of all planar two-loop five-point Master Integrals with one off-shell leg," *JHEP* **01** (2021) 199, `arXiv:2009.13917 [hep-ph]`.

[10] D. D. Canko, C. G. Papadopoulos, and N. Syrrakos, "Simplified Differential Equations for Master Integrals at N³LO," *Acta Phys. Polon. B* **52** no. 8, (2021) 879–887.

[11] M. E. Peskin and D. V. Schroeder, *An Introduction to quantum field theory.* Addison-Wesley, Reading, USA, 1995.

[12] M. D. Schwartz, *Quantum Field Theory and the Standard Model.* Cambridge University Press, 3, 2014.

[13] M. Srednicki, *Quantum field theory.* Cambridge University Press, 1, 2007.

[14] J. F. Donoghue, E. Golowich, and B. R. Holstein, *Dynamics of the Standard Model : Second edition*, vol. 2. Oxford University Press, 2014.

[15] **Particle Data Group** Collaboration, R. L. Workman and Others, "Review of Particle Physics," *PTEP* **2022** (2022) 083C01.

[16] P. Skands, "Introduction to QCD," in *Theoretical Advanced Study Institute in Elementary Particle Physics: Searching for New Physics at Small and Large Scales*, pp. 341–420. 2013. arXiv:1207.2389 [hep-ph].

[17] J. Campbell, J. Huston, and F. Krauss, *The Black Book of Quantum Chromodynamics : a Primer for the LHC Era.* Oxford University Press, 2018.

[18] E. P. Wigner, "On Unitary Representations of the Inhomogeneous Lorentz Group," *Annals Math.* **40** (1939) 149–204.

[19] J. C. Romao and J. P. Silva, "A resource for signs and Feynman diagrams of the Standard Model," *Int. J. Mod. Phys. A* **27** (2012) 1230025, arXiv:1209.6213 [hep-ph].

[20] L. D. Faddeev and V. N. Popov, "Feynman Diagrams for the Yang-Mills Field," *Phys. Lett. B* **25** (1967) 29–30.

[21] C. G. Bollini and J. J. Giambiagi, "Dimensional Renormalization: The Number of Dimensions as a Regularizing Parameter," *Nuovo Cim. B* **12** (1972) 20–26.

[22] G. 't Hooft and M. J. G. Veltman, "Regularization and Renormalization of Gauge Fields," *Nucl. Phys. B* **44** (1972) 189–213.

[23] J. C. Collins, *Renormalization: An Introduction to Renormalization, The Renormalization Group, and the Operator Product Expansion*, vol. 26 of *Cambridge Monographs on Mathematical Physics.* Cambridge University Press, Cambridge, 1986.

[24] P. A. Baikov, K. G. Chetyrkin, and J. H. Kühn, "Five-Loop Running of the QCD coupling constant," *Phys. Rev. Lett.* **118** no. 8, (2017) 082002, arXiv:1606.08659 [hep-ph].

[25] F. Herzog, B. Ruijl, T. Ueda, J. A. M. Vermaseren, and A. Vogt, "The five-loop beta function of Yang-Mills theory with fermions," *JHEP* **02** (2017) 090, arXiv:1701.01404 [hep-ph].

[26] T. Luthe, A. Maier, P. Marquard, and Y. Schroder, "Complete renormalization of QCD at five loops," *JHEP* **03** (2017) 020, arXiv:1701.07068 [hep-ph].

[27] T. Luthe, A. Maier, P. Marquard, and Y. Schroder, "The five-loop Beta function for a general gauge group and anomalous dimensions beyond Feynman gauge," *JHEP* **10** (2017) 166, arXiv:1709.07718 [hep-ph].

[28] K. G. Chetyrkin, G. Falcioni, F. Herzog, and J. A. M. Vermaseren, "Five-loop renormalisation of QCD in covariant gauges," *JHEP* **10** (2017) 179, `arXiv:1709.08541 [hep-ph]`. [Addendum: JHEP 12, 006 (2017)].

[29] T. Kinoshita, "Mass singularities of Feynman amplitudes," *J. Math. Phys.* **3** (1962) 650–677.

[30] T. D. Lee and M. Nauenberg, "Degenerate Systems and Mass Singularities," *Phys. Rev.* **133** (1964) B1549–B1562.

[31] R. P. Feynman, "Very high-energy collisions of hadrons," *Phys. Rev. Lett.* **23** (1969) 1415–1417.

[32] J. C. Collins and D. E. Soper, "Parton Distribution and Decay Functions," *Nucl. Phys. B* **194** (1982) 445–492.

[33] J. C. Collins, D. E. Soper, and G. F. Sterman, "Factorization of Hard Processes in QCD," *Adv. Ser. Direct. High Energy Phys.* **5** (1989) 1–91, `arXiv:hep-ph/0409313`.

[34] G. F. Sterman, "Partons, factorization and resummation, TASI 95," in *Theoretical Advanced Study Institute in Elementary Particle Physics (TASI 95): QCD and Beyond*, pp. 327–408. 6, 1995. `arXiv:hep-ph/9606312`.

[35] V. N. Gribov and L. N. Lipatov, "e+ e- pair annihilation and deep inelastic e p scattering in perturbation theory," *Sov. J. Nucl. Phys.* **15** (1972) 675–684.

[36] Y. L. Dokshitzer, "Calculation of the Structure Functions for Deep Inelastic Scattering and e+ e- Annihilation by Perturbation Theory in Quantum Chromodynamics.," *Sov. Phys. JETP* **46** (1977) 641–653.

[37] G. Altarelli and G. Parisi, "Asymptotic Freedom in Parton Language," *Nucl. Phys. B* **126** (1977) 298–318.

[38] A. Vogt, S. Moch, and J. A. M. Vermaseren, "The Three-loop splitting functions in QCD: The Singlet case," *Nucl. Phys. B* **691** (2004) 129–181, `arXiv:hep-ph/0404111`.

[39] S. Moch, J. A. M. Vermaseren, and A. Vogt, "The Three loop splitting functions in QCD: The Nonsinglet case," *Nucl. Phys. B* **688** (2004) 101–134, `arXiv:hep-ph/0403192`.

[40] L. J. Dixon, "Calculating scattering amplitudes efficiently," in *Theoretical Advanced Study Institute in Elementary Particle Physics (TASI 95): QCD and Beyond*, pp. 539–584. 1, 1996. `arXiv:hep-ph/9601359`.

[41] G. 't Hooft, "A Planar Diagram Theory for Strong Interactions," *Nucl. Phys. B* **72** (1974) 461.

[42] A. Kanaki and C. G. Papadopoulos, "HELAC: A Package to compute electroweak helicity amplitudes," *Comput. Phys. Commun.* **132** (2000) 306–315, `arXiv:hep-ph/0002082`.

[43] F. Maltoni, K. Paul, T. Stelzer, and S. Willenbrock, "Color Flow Decomposition of QCD Amplitudes," *Phys. Rev. D* **67** (2003) 014026, `arXiv:hep-ph/0209271`.

[44] R. J. Eden, P. V. Landshoff, D. I. Olive, and J. C. Polkinghorne, *The analytic S-matrix.* Cambridge Univ. Press, Cambridge, 1966.

[45] R. E. Cutkosky, "Singularities and discontinuities of Feynman amplitudes," *J. Math. Phys.* **1** (1960) 429–433.

[46] Z. Bern, L. J. Dixon, D. C. Dunbar, and D. A. Kosower, "One loop n point gauge theory amplitudes, unitarity and collinear limits," *Nucl. Phys. B* **425** (1994) 217–260, `arXiv:hep-ph/9403226`.

[47] Z. Bern, L. J. Dixon, D. C. Dunbar, and D. A. Kosower, "Fusing gauge theory tree amplitudes into loop amplitudes," *Nucl. Phys. B* **435** (1995) 59–101, `arXiv:hep-ph/9409265`.

[48] K. G. Chetyrkin and F. V. Tkachov, "Integration by Parts: The Algorithm to Calculate beta Functions in 4 Loops," *Nucl. Phys. B* **192** (1981) 159–204.

[49] F. V. Tkachov, "A Theorem on Analytical Calculability of Four Loop Renormalization Group Functions," *Phys. Lett. B* **100** (1981) 65–68.

[50] A. V. Smirnov and A. V. Petukhov, "The Number of Master Integrals is Finite," *Lett. Math. Phys.* **97** (2011) 37–44, `arXiv:1004.4199 [hep-th]`.

[51] T. Gehrmann and E. Remiddi, "Differential equations for two loop four point functions," *Nucl. Phys. B* **580** (2000) 485–518, `arXiv:hep-ph/9912329`.

[52] R. N. Lee, "Group structure of the integration-by-part identities and its application to the reduction of multiloop integrals," *JHEP* **07** (2008) 031, `arXiv:0804.3008 [hep-ph]`.

[53] A. G. Grozin, "Integration by parts: An Introduction," *Int. J. Mod. Phys. A* **26** (2011) 2807–2854, `arXiv:1104.3993 [hep-ph]`.

[54] S. Laporta, "High precision calculation of multiloop Feynman integrals by difference equations," *Int. J. Mod. Phys. A* **15** (2000) 5087–5159, `arXiv:hep-ph/0102033`.

[55] J. Usovitsch, "Factorization of denominators in integration-by-parts reductions," `arXiv:2002.08173 [hep-ph]`.

[56] A. V. Smirnov and V. A. Smirnov, "How to choose master integrals," *Nucl. Phys. B* **960** (2020) 115213, `arXiv:2002.08042 [hep-ph]`.

[57] C. Anastasiou and A. Lazopoulos, "Automatic integral reduction for higher order perturbative calculations," *JHEP* **07** (2004) 046, `arXiv:hep-ph/0404258`.

[58] A. V. Smirnov and F. S. Chuharev, "FIRE6: Feynman Integral REduction with Modular Arithmetic," *Comput. Phys. Commun.* **247** (2020) 106877, `arXiv:1901.07808 [hep-ph]`.

[59] R. N. Lee, "LiteRed 1.4: a powerful tool for reduction of multiloop integrals," *J. Phys. Conf. Ser.* **523** (2014) 012059, `arXiv:1310.1145 [hep-ph]`.

[60] J. Klappert, F. Lange, P. Maierhöfer, and J. Usovitsch, "Integral reduction with Kira 2.0 and finite field methods," *Comput. Phys. Commun.* **266** (2021) 108024, `arXiv:2008.06494 [hep-ph]`.

[61] A. von Manteuffel and C. Studerus, "Reduze 2 - Distributed Feynman Integral Reduction," `arXiv:1201.4330 [hep-ph]`.

[62] A. Georgoudis, K. J. Larsen, and Y. Zhang, "Azurite: An algebraic geometry based package for finding bases of loop integrals," *Comput. Phys. Commun.* **221** (2017) 203–215, `arXiv:1612.04252 [hep-th]`.

[63] Z. Wu, J. Boehm, R. Ma, H. Xu, and Y. Zhang, "NeatIBP 1.0, A package generating small-size integration-by-parts relations for Feynman integrals," `arXiv:2305.08783 [hep-ph]`.

[64] J. Gluza, K. Kajda, and D. A. Kosower, "Towards a Basis for Planar Two-Loop Integrals," *Phys. Rev. D* **83** (2011) 045012, `arXiv:1009.0472 [hep-th]`.

[65] R. M. Schabinger, "A New Algorithm For The Generation Of Unitarity-Compatible Integration By Parts Relations," *JHEP* **01** (2012) 077, `arXiv:1111.4220 [hep-ph]`.

[66] A. von Manteuffel and R. M. Schabinger, "A novel approach to integration by parts reduction," *Phys. Lett. B* **744** (2015) 101–104, `arXiv:1406.4513 [hep-ph]`.

[67] K. J. Larsen and Y. Zhang, "Integration-by-parts reductions from unitarity cuts and algebraic geometry," *Phys. Rev. D* **93** no. 4, (2016) 041701, `arXiv:1511.01071 [hep-th]`.

[68] T. Peraro, "Scattering amplitudes over finite fields and multivariate functional reconstruction," *JHEP* **12** (2016) 030, `arXiv:1608.01902 [hep-ph]`.

[69] H. A. Chawdhry, M. A. Lim, and A. Mitov, "Two-loop five-point massless QCD amplitudes within the integration-by-parts approach," *Phys. Rev. D* **99** no. 7, (2019) 076011, `arXiv:1805.09182 [hep-ph]`.

[70] T. Peraro, "FiniteFlow: multivariate functional reconstruction using finite fields and dataflow graphs," *JHEP* **07** (2019) 031, `arXiv:1905.08019 [hep-ph]`.

[71] J. Klappert and F. Lange, "Reconstructing rational functions with FireFly," *Comput. Phys. Commun.* **247** (2020) 106951, `arXiv:1904.00009 [cs.SC]`.

[72] D. Bendle, J. Böhm, W. Decker, A. Georgoudis, F.-J. Pfreundt, M. Rahn, P. Wasser, and Y. Zhang, "Integration-by-parts reductions of Feynman integrals using Singular and GPI-Space," *JHEP* **02** (2020) 079, `arXiv:1908.04301 [hep-th]`.

[73] X. Guan, X. Liu, and Y.-Q. Ma, "Complete reduction of integrals in two-loop five-light-parton scattering amplitudes," *Chin. Phys. C* **44** no. 9, (2020) 093106, `arXiv:1912.09294 [hep-ph]`.

[74] J. Boehm, M. Wittmann, Z. Wu, Y. Xu, and Y. Zhang, "IBP reduction coefficients made simple," *JHEP* **12** (2020) 054, `arXiv:2008.13194 [hep-ph]`.

[75] D. Bendle, J. Boehm, M. Heymann, R. Ma, M. Rahn, L. Ristau, M. Wittmann, Z. Wu, and Y. Zhang, "pfd-parallel, a Singular/GPI-Space package for massively parallel multivariate partial fractioning," `arXiv:2104.06866 [hep-ph]`.

[76] P. Mastrolia and S. Mizera, "Feynman Integrals and Intersection Theory," *JHEP* **02** (2019) 139, `arXiv:1810.03818 [hep-th]`.

[77] H. Frellesvig, F. Gasparotto, S. Laporta, M. K. Mandal, P. Mastrolia, L. Mattiazzi, and S. Mizera, "Decomposition of Feynman Integrals on the Maximal Cut by Intersection Numbers," *JHEP* **05** (2019) 153, `arXiv:1901.11510 [hep-ph]`.

[78] H. Frellesvig, F. Gasparotto, S. Laporta, M. K. Mandal, P. Mastrolia, L. Mattiazzi, and S. Mizera, "Decomposition of Feynman Integrals by Multivariate Intersection Numbers," *JHEP* **03** (2021) 027, `arXiv:2008.04823 [hep-th]`.

[79] V. Chestnov, F. Gasparotto, M. K. Mandal, P. Mastrolia, S. J. Matsubara-Heo, H. J. Munch, and N. Takayama, "Macaulay matrix for Feynman integrals: linear relations and intersection numbers," *JHEP* **09** (2022) 187, `arXiv:2204.12983 [hep-th]`.

[80] G. Fontana and T. Peraro, "Reduction to master integrals via intersection numbers and polynomial expansions," `arXiv:2304.14336 [hep-ph]`.

[81] P. Nogueira, "Automatic Feynman graph generation," *J. Comput. Phys.* **105** (1993) 279–289.

[82] T. Hahn, "Generating Feynman diagrams and amplitudes with FeynArts 3," *Comput. Phys. Commun.* **140** (2001) 418–431, `arXiv:hep-ph/0012260`.

[83] B. Ruijl, T. Ueda, and J. Vermaseren, "FORM version 4.2," `arXiv:1707.06453 [hep-ph]`.

[84] V. Shtabovenko, R. Mertig, and F. Orellana, "FeynCalc 9.3: New features and improvements," *Comput. Phys. Commun.* **256** (2020) 107478, `arXiv:2001.04407 [hep-ph]`.

[85] V. Shtabovenko, R. Mertig, and F. Orellana, "FeynCalc 10: Do multiloop integrals dream of computer codes?," `arXiv:2312.14089 [hep-ph]`.

[86] T. Hahn and M. Perez-Victoria, "Automatized one loop calculations in four-dimensions and D-dimensions," *Comput. Phys. Commun.* **118** (1999) 153–165, `arXiv:hep-ph/9807565`.

[87] A. Cafarella, C. G. Papadopoulos, and M. Worek, "Helac-Phegas: A Generator for all parton level processes," *Comput. Phys. Commun.* **180** (2009) 1941–1955, `arXiv:0710.2427 [hep-ph]`.

[88] G. Bevilacqua, M. Czakon, M. V. Garzelli, A. van Hameren, A. Kardos, C. G. Papadopoulos, R. Pittau, and M. Worek, "HELAC-NLO," *Comput. Phys. Commun.* **184** (2013) 986–997, `arXiv:1110.1499 [hep-ph]`.

[89] S. Actis, A. Denner, L. Hofer, A. Scharf, and S. Uccirati, "Recursive generation of one-loop amplitudes in the Standard Model," *JHEP* **04** (2013) 037, `arXiv:1211.6316 [hep-ph]`.

[90] A. Denner, J.-N. Lang, and S. Uccirati, "Recola2: REcursive Computation of One-Loop Amplitudes 2," *Comput. Phys. Commun.* **224** (2018) 346–361, `arXiv:1711.07388 [hep-ph]`.

[91] G. Ossola, C. G. Papadopoulos, and R. Pittau, "Reducing full one-loop amplitudes to scalar integrals at the integrand level," *Nucl. Phys. B* **763** (2007) 147–169, `arXiv:hep-ph/0609007`.

[92] G. Ossola, C. G. Papadopoulos, and R. Pittau, "Numerical evaluation of six-photon amplitudes," *JHEP* **07** (2007) 085, `arXiv:0704.1271 [hep-ph]`.

[93] F. J. Dyson, "The S matrix in quantum electrodynamics," *Phys. Rev.* **75** (1949) 1736–1755.

[94] J. S. Schwinger, "On the Green's functions of quantized fields. 1.," *Proc. Nat. Acad. Sci.* **37** (1951) 452–455.

[95] J. S. Schwinger, "On the Green's functions of quantized fields. 2.," *Proc. Nat. Acad. Sci.* **37** (1951) 455–459.

[96] F. Caravaglios and M. Moretti, "An algorithm to compute Born scattering amplitudes without Feynman graphs," *Phys. Lett. B* **358** (1995) 332–338, `arXiv:hep-ph/9507237`.

[97] A. van Hameren, C. G. Papadopoulos, and R. Pittau, "Automated one-loop calculations: A Proof of concept," *JHEP* **09** (2009) 106, `arXiv:0903.4665 [hep-ph]`.

[98] G. Ossola, C. G. Papadopoulos, and R. Pittau, "CutTools: A Program implementing the OPP reduction method to compute one-loop amplitudes," *JHEP* **03** (2008) 042, `arXiv:0711.3596 [hep-ph]`.

[99] G. Ossola, C. G. Papadopoulos, and R. Pittau, "On the Rational Terms of the one-loop amplitudes," *JHEP* **05** (2008) 004, `arXiv:0802.1876 [hep-ph]`.

[100] P. Draggiotis, M. V. Garzelli, C. G. Papadopoulos, and R. Pittau, "Feynman Rules for the Rational Part of the QCD 1-loop amplitudes," *JHEP* **04** (2009) 072, `arXiv:0903.0356 [hep-ph]`.

[101] M. V. Garzelli, I. Malamos, and R. Pittau, "Feynman rules for the rational part of the Electroweak 1-loop amplitudes," *JHEP* **01** (2010) 040, `arXiv:0910.3130 [hep-ph]`. [Erratum: JHEP 10, 097 (2010)].

[102] H.-S. Shao, Y.-J. Zhang, and K.-T. Chao, "Feynman Rules for the Rational Part of the Standard Model One-loop Amplitudes in the 't Hooft-Veltman γ_5 Scheme," *JHEP* **09** (2011) 048, `arXiv:1106.5030 [hep-ph]`.

[103] L. M. Brown and R. P. Feynman, "Radiative corrections to Compton scattering," *Phys. Rev.* **85** (1952) 231–244.

[104] D. B. Melrose, "Reduction of Feynman diagrams," *Nuovo Cim.* **40** (1965) 181–213.

[105] G. 't Hooft and M. J. G. Veltman, "Scalar One Loop Integrals," *Nucl. Phys. B* **153** (1979) 365–401.

[106] G. Passarino and M. J. G. Veltman, "One Loop Corrections for e+ e- Annihilation Into mu+ mu- in the Weinberg Model," *Nucl. Phys. B* **160** (1979) 151–207.

[107] W. L. van Neerven and J. A. M. Vermaseren, "LARGE LOOP INTEGRALS," *Phys. Lett. B* **137** (1984) 241–244.

[108] G. J. van Oldenborgh, "FF: A Package to evaluate one loop Feynman diagrams," *Comput. Phys. Commun.* **66** (1991) 1–15.

[109] R. K. Ellis and G. Zanderighi, "Scalar one-loop integrals for QCD," *JHEP* **02** (2008) 002, `arXiv:0712.1851 [hep-ph]`.

[110] A. van Hameren, "OneLOop: For the evaluation of one-loop scalar functions," *Comput. Phys. Commun.* **182** (2011) 2427–2438, `arXiv:1007.4716 [hep-ph]`.

[111] A. Denner, S. Dittmaier, and L. Hofer, "Collier: a fortran-based Complex One-Loop LIbrary in Extended Regularizations," *Comput. Phys. Commun.* **212** (2017) 220–238, `arXiv:1604.06792 [hep-ph]`.

[112] Z. Bern, L. J. Dixon, and D. A. Kosower, "One loop amplitudes for e+ e- to four partons," *Nucl. Phys. B* **513** (1998) 3–86, `arXiv:hep-ph/9708239`.

[113] Z. Bern, L. J. Dixon, and D. A. Kosower, "One loop corrections to five gluon amplitudes," *Phys. Rev. Lett.* **70** (1993) 2677–2680, `arXiv:hep-ph/9302280`.

[114] Z. Bern, L. J. Dixon, and D. A. Kosower, "One loop corrections to two quark three gluon amplitudes," *Nucl. Phys. B* **437** (1995) 259–304, `arXiv:hep-ph/9409393`.

[115] R. Britto, F. Cachazo, and B. Feng, "Generalized unitarity and one-loop amplitudes in N=4 super-Yang-Mills," *Nucl. Phys. B* **725** (2005) 275–305, `arXiv:hep-th/0412103`.

[116] R. Britto, F. Cachazo, B. Feng, and E. Witten, "Direct proof of tree-level recursion relation in Yang-Mills theory," *Phys. Rev. Lett.* **94** (2005) 181602, `arXiv:hep-th/0501052`.

[117] A. Denner and S. Dittmaier, "Reduction of one loop tensor five point integrals," *Nucl. Phys. B* **658** (2003) 175–202, `arXiv:hep-ph/0212259`.

[118] A. Denner and S. Dittmaier, "Reduction schemes for one-loop tensor integrals," *Nucl. Phys. B* **734** (2006) 62–115, `arXiv:hep-ph/0509141`.

[119] C. Anastasiou, R. Britto, B. Feng, Z. Kunszt, and P. Mastrolia, "Unitarity cuts and Reduction to master integrals in d dimensions for one-loop amplitudes," *JHEP* **03** (2007) 111, `arXiv:hep-ph/0612277`.

[120] C. Anastasiou, R. Britto, B. Feng, Z. Kunszt, and P. Mastrolia, "D-dimensional unitarity cut method," *Phys. Lett. B* **645** (2007) 213–216, `arXiv:hep-ph/0609191`.

[121] F. del Aguila and R. Pittau, "Recursive numerical calculus of one-loop tensor integrals," *JHEP* **07** (2004) 017, `arXiv:hep-ph/0404120`.

[122] R. K. Ellis, W. T. Giele, and Z. Kunszt, "A Numerical Unitarity Formalism for Evaluating One-Loop Amplitudes," *JHEP* **03** (2008) 003, `arXiv:0708.2398 [hep-ph]`.

[123] W. T. Giele, Z. Kunszt, and K. Melnikov, "Full one-loop amplitudes from tree amplitudes," *JHEP* **04** (2008) 049, `arXiv:0801.2237 [hep-ph]`.

[124] C. F. Berger, Z. Bern, L. J. Dixon, F. Febres Cordero, D. Forde, H. Ita, D. A. Kosower, and D. Maitre, "An Automated Implementation of On-Shell Methods for One-Loop Amplitudes," *Phys. Rev. D* **78** (2008) 036003, `arXiv:0803.4180 [hep-ph]`.

[125] R. K. Ellis, W. T. Giele, Z. Kunszt, and K. Melnikov, "Masses, fermions and generalized *D*-dimensional unitarity," *Nucl. Phys. B* **822** (2009) 270–282, `arXiv:0806.3467 [hep-ph]`.

[126] P. Mastrolia, G. Ossola, T. Reiter, and F. Tramontano, "Scattering AMplitudes from Unitarity-based Reduction Algorithm at the Integrand-level," *JHEP* **08** (2010) 080, `arXiv:1006.0710 [hep-ph]`.

[127] P. Mastrolia, E. Mirabella, and T. Peraro, "Integrand reduction of one-loop scattering amplitudes through Laurent series expansion," *JHEP* **06** (2012) 095, `arXiv:1203.0291 [hep-ph]`. [Erratum: JHEP 11, 128 (2012)].

[128] T. Binoth, J. P. Guillet, and G. Heinrich, "Reduction formalism for dimensionally regulated one loop N point integrals," *Nucl. Phys. B* **572** (2000) 361–386, `arXiv:hep-ph/9911342`.

[129] J. Alwall, R. Frederix, S. Frixione, V. Hirschi, F. Maltoni, O. Mattelaer, H. S. Shao, T. Stelzer, P. Torrielli, and M. Zaro, "The automated computation of tree-level and next-to-leading order differential cross sections, and their matching to parton shower simulations," *JHEP* **07** (2014) 079, `arXiv:1405.0301 [hep-ph]`.

[130] R. Frederix, S. Frixione, V. Hirschi, D. Pagani, H. S. Shao, and M. Zaro, "The automation of next-to-leading order electroweak calculations," *JHEP* **07** (2018) 185, `arXiv:1804.10017 [hep-ph]`. [Erratum: JHEP 11, 085 (2021)].

[131] F. Cascioli, P. Maierhofer, and S. Pozzorini, "Scattering Amplitudes with Open Loops," *Phys. Rev. Lett.* **108** (2012) 111601, `arXiv:1111.5206 [hep-ph]`.

[132] **OpenLoops 2** Collaboration, F. Buccioni, J.-N. Lang, J. M. Lindert, P. Maierhöfer, S. Pozzorini, H. Zhang, and M. F. Zoller, "OpenLoops 2," *Eur. Phys. J. C* **79** no. 10, (2019) 866, `arXiv:1907.13071 [hep-ph]`.

[133] **GoSam** Collaboration, G. Cullen, N. Greiner, G. Heinrich, G. Luisoni, P. Mastrolia, G. Ossola, T. Reiter, and F. Tramontano, "Automated One-Loop Calculations with GoSam," *Eur. Phys. J. C* **72** (2012) 1889, `arXiv:1111.2034 [hep-ph]`.

[134] **GoSam** Collaboration, G. Cullen *et al.*, "G*OSAM*-2.0: a tool for automated one-loop calculations within the Standard Model and beyond," *Eur. Phys. J. C* **74** no. 8, (2014) 3001, `arXiv:1404.7096 [hep-ph]`.

[135] F. Febres Cordero, A. von Manteuffel, and T. Neumann, "Computational Challenges for Multi-loop Collider Phenomenology: A Snowmass 2021 White Paper," *Comput. Softw. Big Sci.* **6** no. 1, (2022) 14, `arXiv:2204.04200 [hep-ph]`.

[136] A. Huss, J. Huston, S. Jones, and M. Pellen, "Les Houches 2021—physics at TeV colliders: report on the standard model precision wishlist," *J. Phys. G* **50** no. 4, (2023) 043001, `arXiv:2207.02122 [hep-ph]`.

[137] P. Mastrolia, T. Peraro, and A. Primo, "Adaptive Integrand Decomposition in parallel and orthogonal space," *JHEP* **08** (2016) 164, `arXiv:1605.03157 [hep-ph]`.

[138] T. Peraro and L. Tancredi, "Physical projectors for multi-leg helicity amplitudes," *JHEP* **07** (2019) 114, `arXiv:1906.03298 [hep-ph]`.

[139] T. Peraro and L. Tancredi, "Tensor decomposition for bosonic and fermionic scattering amplitudes," *Phys. Rev. D* **103** no. 5, (2021) 054042, `arXiv:2012.00820 [hep-ph]`.

[140] L. Chen, "A prescription for projectors to compute helicity amplitudes in D dimensions," *Eur. Phys. J. C* **81** no. 5, (2021) 417, `arXiv:1904.00705 [hep-ph]`.

[141] R. Bonciani *et al.*, "Two-Loop Four-Fermion Scattering Amplitude in QED," *Phys. Rev. Lett.* **128** no. 2, (2022) 022002, `arXiv:2106.13179 [hep-ph]`.

[142] M. K. Mandal, P. Mastrolia, J. Ronca, and W. J. Bobadilla Torres, "Two-loop scattering amplitude for heavy-quark pair production through light-quark annihilation in QCD," *JHEP* **09** (2022) 129, `arXiv:2204.03466 [hep-ph]`.

[143] A. Broggio *et al.*, "Muon-electron scattering at NNLO," *JHEP* **01** (2023) 112, `arXiv:2212.06481 [hep-ph]`.

[144] H. A. Chawdhry, M. Czakon, A. Mitov, and R. Poncelet, "Two-loop leading-color helicity amplitudes for three-photon production at the LHC," *JHEP* **06** (2021) 150, `arXiv:2012.13553 [hep-ph]`.

[145] H. A. Chawdhry, M. Czakon, A. Mitov, and R. Poncelet, "Two-loop leading-colour QCD helicity amplitudes for two-photon plus jet production at the LHC," *JHEP* **07** (2021) 164, `arXiv:2103.04319 [hep-ph]`.

[146] S. Badger, C. Brønnum-Hansen, H. B. Hartanto, and T. Peraro, "Analytic helicity amplitudes for two-loop five-gluon scattering: the single-minus case," *JHEP* **01** (2019) 186, `arXiv:1811.11699 [hep-ph]`.

[147] S. Badger, D. Chicherin, T. Gehrmann, G. Heinrich, J. M. Henn, T. Peraro, P. Wasser, Y. Zhang, and S. Zoia, "Analytic form of the full two-loop five-gluon all-plus helicity amplitude," *Phys. Rev. Lett.* **123** no. 7, (2019) 071601, `arXiv:1905.03733 [hep-ph]`.

[148] S. Badger, H. B. Hartanto, and S. Zoia, "Two-Loop QCD Corrections to Wbb⁻ Production at Hadron Colliders," *Phys. Rev. Lett.* **127** no. 1, (2021) 012001, `arXiv:2102.02516 [hep-ph]`.

[149] S. Badger, E. Chaubey, H. B. Hartanto, and R. Marzucca, "Two-loop leading colour QCD helicity amplitudes for top quark pair production in the gluon fusion channel," *JHEP* **06** (2021) 163, `arXiv:2102.13450 [hep-ph]`.

[150] S. Badger, C. Brønnum-Hansen, D. Chicherin, T. Gehrmann, H. B. Hartanto, J. Henn, M. Marcoli, R. Moodie, T. Peraro, and S. Zoia, "Virtual QCD corrections to gluon-initiated diphoton plus jet production at hadron colliders," *JHEP* **11** (2021) 083, `arXiv:2106.08664 [hep-ph]`.

[151] S. Badger, H. B. Hartanto, J. Kryś, and S. Zoia, "Two-loop leading-colour QCD helicity amplitudes for Higgs boson production in association with a bottom-quark pair at the LHC," *JHEP* **11** (2021) 012, `arXiv:2107.14733 [hep-ph]`.

[152] B. Agarwal, F. Buccioni, A. von Manteuffel, and L. Tancredi, "Two-loop leading colour QCD corrections to $q\bar{q} \to \gamma\gamma g$ and $qg \to \gamma\gamma q$," *JHEP* **04** (2021) 201, `arXiv:2102.01820 [hep-ph]`.

[153] B. Agarwal, F. Buccioni, A. von Manteuffel, and L. Tancredi, "Two-Loop Helicity Amplitudes for Diphoton Plus Jet Production in Full Color," *Phys. Rev. Lett.* **127** no. 26, (2021) 262001, `arXiv:2105.04585 [hep-ph]`.

[154] H. B. Hartanto, R. Poncelet, A. Popescu, and S. Zoia, "Next-to-next-to-leading order QCD corrections to $Wb\bar{b}$ production at the LHC," *Phys. Rev. D* **106** no. 7, (2022) 074016, `arXiv:2205.01687 [hep-ph]`.

[155] S. Badger, H. B. Hartanto, J. Kryś, and S. Zoia, "Two-loop leading colour helicity amplitudes for $W^{\pm}\gamma + j$ production at the LHC," *JHEP* **05** (2022) 035, `arXiv:2201.04075 [hep-ph]`.

[156] S. Badger, M. Czakon, H. B. Hartanto, R. Moodie, T. Peraro, R. Poncelet, and S. Zoia, "Isolated photon production in association with a jet pair through next-to-next-to-leading order in QCD," *JHEP* **10** (2023) 071, arXiv:2304.06682 [hep-ph].

[157] B. Agarwal, F. Buccioni, F. Devoto, G. Gambuti, A. von Manteuffel, and L. Tancredi, "Five-Parton Scattering in QCD at Two Loops," arXiv:2311.09870 [hep-ph].

[158] F. Caola, A. Von Manteuffel, and L. Tancredi, "Diphoton Amplitudes in Three-Loop Quantum Chromodynamics," *Phys. Rev. Lett.* **126** no. 11, (2021) 112004, arXiv:2011.13946 [hep-ph].

[159] F. Caola, A. Chakraborty, G. Gambuti, A. von Manteuffel, and L. Tancredi, "Three-loop helicity amplitudes for four-quark scattering in massless QCD," *JHEP* **10** (2021) 206, arXiv:2108.00055 [hep-ph].

[160] P. Bargiela, F. Caola, A. von Manteuffel, and L. Tancredi, "Three-loop helicity amplitudes for diphoton production in gluon fusion," *JHEP* **02** (2022) 153, arXiv:2111.13595 [hep-ph].

[161] F. Caola, A. Chakraborty, G. Gambuti, A. von Manteuffel, and L. Tancredi, "Three-Loop Gluon Scattering in QCD and the Gluon Regge Trajectory," *Phys. Rev. Lett.* **128** no. 21, (2022) 212001, arXiv:2112.11097 [hep-ph].

[162] F. Caola, A. Chakraborty, G. Gambuti, A. von Manteuffel, and L. Tancredi, "Three-loop helicity amplitudes for quark-gluon scattering in QCD," *JHEP* **12** (2022) 082, arXiv:2207.03503 [hep-ph].

[163] T. Gehrmann, P. Jakubčík, C. C. Mella, N. Syrrakos, and L. Tancredi, "Planar three-loop QCD helicity amplitudes for V+jet production at hadron colliders," *Phys. Lett. B* **848** (2024) 138369, arXiv:2307.15405 [hep-ph].

[164] H. Ita, "Two-loop Integrand Decomposition into Master Integrals and Surface Terms," *Phys. Rev. D* **94** no. 11, (2016) 116015, arXiv:1510.05626 [hep-th].

[165] S. Abreu, F. Febres Cordero, H. Ita, M. Jaquier, and B. Page, "Subleading Poles in the Numerical Unitarity Method at Two Loops," *Phys. Rev. D* **95** no. 9, (2017) 096011, arXiv:1703.05255 [hep-ph].

[166] S. Abreu, F. Febres Cordero, H. Ita, M. Jaquier, B. Page, and M. Zeng, "Two-Loop Four-Gluon Amplitudes from Numerical Unitarity," *Phys. Rev. Lett.* **119** no. 14, (2017) 142001, arXiv:1703.05273 [hep-ph].

[167] S. Abreu, F. Febres Cordero, H. Ita, B. Page, and M. Zeng, "Planar Two-Loop Five-Gluon Amplitudes from Numerical Unitarity," *Phys. Rev. D* **97** no. 11, (2018) 116014, arXiv:1712.03946 [hep-ph].

[168] S. Abreu, F. Febres Cordero, H. Ita, B. Page, and V. Sotnikov, "Planar Two-Loop Five-Parton Amplitudes from Numerical Unitarity," *JHEP* **11** (2018) 116, arXiv:1809.09067 [hep-ph].

[169] S. Abreu, J. Dormans, F. Febres Cordero, H. Ita, and B. Page, "Analytic Form of Planar Two-Loop Five-Gluon Scattering Amplitudes in QCD," *Phys. Rev. Lett.* **122** no. 8, (2019) 082002, `arXiv:1812.04586 [hep-ph]`.

[170] S. Abreu, J. Dormans, F. Febres Cordero, H. Ita, B. Page, and V. Sotnikov, "Analytic Form of the Planar Two-Loop Five-Parton Scattering Amplitudes in QCD," *JHEP* **05** (2019) 084, `arXiv:1904.00945 [hep-ph]`.

[171] S. Abreu, F. Febres Cordero, H. Ita, B. Page, and V. Sotnikov, "Leading-color two-loop QCD corrections for three-jet production at hadron colliders," *JHEP* **07** (2021) 095, `arXiv:2102.13609 [hep-ph]`.

[172] S. Abreu, F. Febres Cordero, H. Ita, M. Klinkert, B. Page, and V. Sotnikov, "Leading-color two-loop amplitudes for four partons and a W boson in QCD," *JHEP* **04** (2022) 042, `arXiv:2110.07541 [hep-ph]`.

[173] S. Abreu, G. De Laurentis, H. Ita, M. Klinkert, B. Page, and V. Sotnikov, "Two-loop QCD corrections for three-photon production at hadron colliders," *SciPost Phys.* **15** no. 4, (2023) 157, `arXiv:2305.17056 [hep-ph]`.

[174] G. De Laurentis, H. Ita, M. Klinkert, and V. Sotnikov, "Double-Virtual NNLO QCD Corrections for Five-Parton Scattering: The Gluon Channel," `arXiv:2311.10086 [hep-ph]`.

[175] G. De Laurentis, H. Ita, and V. Sotnikov, "Double-Virtual NNLO QCD Corrections for Five-Parton Scattering: The Quark Channels," `arXiv:2311.18752 [hep-ph]`.

[176] S. Abreu, J. Dormans, F. Febres Cordero, H. Ita, M. Kraus, B. Page, E. Pascual, M. S. Ruf, and V. Sotnikov, "Caravel: A C++ framework for the computation of multi-loop amplitudes with numerical unitarity," *Comput. Phys. Commun.* **267** (2021) 108069, `arXiv:2009.11957 [hep-ph]`.

[177] S. Pozzorini, N. Schär, and M. F. Zoller, "Two-loop tensor integral coefficients in OpenLoops," *JHEP* **05** (2022) 161, `arXiv:2201.11615 [hep-ph]`.

[178] S. Pozzorini, H. Zhang, and M. F. Zoller, "Rational Terms of UV Origin at Two Loops," *JHEP* **05** (2020) 077, `arXiv:2001.11388 [hep-ph]`.

[179] J.-N. Lang, S. Pozzorini, H. Zhang, and M. F. Zoller, "Two-Loop Rational Terms in Yang-Mills Theories," *JHEP* **10** (2020) 016, `arXiv:2007.03713 [hep-ph]`.

[180] J.-N. Lang, S. Pozzorini, H. Zhang, and M. F. Zoller, "Two-loop rational terms for spontaneously broken theories," *JHEP* **01** (2022) 105, `arXiv:2107.10288 [hep-ph]`.

[181] V. A. Smirnov, *Analytic tools for Feynman integrals*, vol. 250. Springer, 2012.

[182] J. M. Henn and J. C. Plefka, *Scattering Amplitudes in Gauge Theories*, vol. 883. Springer, Berlin, 2014.

[183] J. M. Henn, "Lectures on differential equations for Feynman integrals," *J. Phys. A* **48** (2015) 153001, `arXiv:1412.2296 [hep-ph]`.

[184] C. Duhr, "Mathematical aspects of scattering amplitudes," in *Theoretical Advanced Study Institute in Elementary Particle Physics: Journeys Through the Precision Frontier: Amplitudes for Colliders*, pp. 419–476. 2015. `arXiv:1411.7538 [hep-ph]`.

[185] S. Abreu, R. Britto, and C. Duhr, "The SAGEX review on scattering amplitudes Chapter 3: Mathematical structures in Feynman integrals," *J. Phys. A* **55** no. 44, (2022) 443004, `arXiv:2203.13014 [hep-th]`.

[186] S. Weinzierl, *Feynman Integrals*. Springer, 1, 2022. `arXiv:2201.03593 [hep-th]`.

[187] C. Bogner and S. Weinzierl, "Feynman graph polynomials," *Int. J. Mod. Phys. A* **25** (2010) 2585–2618, `arXiv:1002.3458 [hep-ph]`.

[188] G. Heinrich, "Collider Physics at the Precision Frontier," *Phys. Rept.* **922** (2021) 1–69, `arXiv:2009.00516 [hep-ph]`.

[189] L. D. Landau, "On analytic properties of vertex parts in quantum field theory," *Nucl. Phys.* **13** no. 1, (1959) 181–192.

[190] A. V. Smirnov and M. N. Tentyukov, "Feynman Integral Evaluation by a Sector decomposiTion Approach (FIESTA)," *Comput. Phys. Commun.* **180** (2009) 735–746, `arXiv:0807.4129 [hep-ph]`.

[191] S. Borowka, G. Heinrich, S. P. Jones, M. Kerner, J. Schlenk, and T. Zirke, "SecDec-3.0: numerical evaluation of multi-scale integrals beyond one loop," *Comput. Phys. Commun.* **196** (2015) 470–491, `arXiv:1502.06595 [hep-ph]`.

[192] H. Cheng and T. T. Wu, *EXPANDING PROTONS: SCATTERING AT HIGH-ENERGIES*. The MIT Press, 1987.

[193] F. Brown, "The Massless higher-loop two-point function," *Commun. Math. Phys.* **287** (2009) 925–958, `arXiv:0804.1660 [math.AG]`.

[194] E. Panzer, "On hyperlogarithms and Feynman integrals with divergences and many scales," *JHEP* **03** (2014) 071, `arXiv:1401.4361 [hep-th]`.

[195] E. Panzer, "Algorithms for the symbolic integration of hyperlogarithms with applications to Feynman integrals," *Comput. Phys. Commun.* **188** (2015) 148–166, `arXiv:1403.3385 [hep-th]`.

[196] M. Bonetti, E. Panzer, V. A. Smirnov, and L. Tancredi, "Two-loop mixed QCD-EW corrections to $gg \to Hg$," *JHEP* **11** (2020) 045, `arXiv:2007.09813 [hep-ph]`.

[197] M. Bonetti, E. Panzer, and L. Tancredi, "Two-loop mixed QCD-EW corrections to $q\bar{q} \to$ Hg, qg $\to$ Hq, and $\bar{q}g \to H\bar{q}$," *JHEP* **06** (2022) 115, `arXiv:2203.17202 [hep-ph]`.

[198] G. Heinrich, "Sector Decomposition," *Int. J. Mod. Phys. A* **23** (2008) 1457–1486, `arXiv:0803.4177 [hep-ph]`.

[199] S. Borowka, G. Heinrich, S. Jahn, S. P. Jones, M. Kerner, J. Schlenk, and T. Zirke, "pySecDec: a toolbox for the numerical evaluation of multi-scale integrals," *Comput. Phys. Commun.* **222** (2018) 313–326, `arXiv:1703.09692 [hep-ph]`.

[200] G. Heinrich, S. P. Jones, M. Kerner, V. Magerya, A. Olsson, and J. Schlenk, "Numerical Scattering Amplitudes with pySecDec," `arXiv:2305.19768 [hep-ph]`.

[201] A. V. Smirnov, N. D. Shapurov, and L. I. Vysotsky, "FIESTA5: Numerical high-performance Feynman integral evaluation," *Comput. Phys. Commun.* **277** (2022) 108386, `arXiv:2110.11660 [hep-ph]`.

[202] M. Beneke and V. A. Smirnov, "Asymptotic expansion of Feynman integrals near threshold," *Nucl. Phys. B* **522** (1998) 321–344, `arXiv:hep-ph/9711391`.

[203] V. A. Smirnov and E. R. Rakhmetov, "The Strategy of regions for asymptotic expansion of two loop vertex Feynman diagrams," *Theor. Math. Phys.* **120** (1999) 870–875, `arXiv:hep-ph/9812529`.

[204] A. Pak and A. Smirnov, "Geometric approach to asymptotic expansion of Feynman integrals," *Eur. Phys. J. C* **71** (2011) 1626, `arXiv:1011.4863 [hep-ph]`.

[205] B. Jantzen, "Foundation and generalization of the expansion by regions," *JHEP* **12** (2011) 076, `arXiv:1111.2589 [hep-ph]`.

[206] B. Jantzen, A. V. Smirnov, and V. A. Smirnov, "Expansion by regions: revealing potential and Glauber regions automatically," *Eur. Phys. J. C* **72** (2012) 2139, `arXiv:1206.0546 [hep-ph]`.

[207] T. Y. Semenova, A. V. Smirnov, and V. A. Smirnov, "On the status of expansion by regions," *Eur. Phys. J. C* **79** no. 2, (2019) 136, `arXiv:1809.04325 [hep-th]`.

[208] G. Heinrich, S. Jahn, S. P. Jones, M. Kerner, F. Langer, V. Magerya, A. Pöldaru, J. Schlenk, and E. Villa, "Expansion by regions with pySecDec," *Comput. Phys. Commun.* **273** (2022) 108267, `arXiv:2108.10807 [hep-ph]`.

[209] P. A. Baikov, "Explicit solutions of the three loop vacuum integral recurrence relations," *Phys. Lett. B* **385** (1996) 404–410, `arXiv:hep-ph/9603267`.

[210] P. A. Baikov, "Explicit solutions of the multiloop integral recurrence relations and its application," *Nucl. Instrum. Meth. A* **389** (1997) 347–349, `arXiv:hep-ph/9611449`.

[211] J. Bosma, K. J. Larsen, and Y. Zhang, "Differential equations for loop integrals in Baikov representation," *Phys. Rev. D* **97** no. 10, (2018) 105014, `arXiv:1712.03760 [hep-th]`.

[212] J. Bosma, M. Sogaard, and Y. Zhang, "Maximal Cuts in Arbitrary Dimension," *JHEP* **08** (2017) 051, arXiv:1704.04255 [hep-th].

[213] H. Frellesvig and C. G. Papadopoulos, "Cuts of Feynman Integrals in Baikov representation," *JHEP* **04** (2017) 083, arXiv:1701.07356 [hep-ph].

[214] G. Chen, J. Liu, R. Xie, H. Zhang, and Y. Zhou, "Syzygies Probing Scattering Amplitudes," *JHEP* **09** (2016) 075, arXiv:1511.01058 [hep-th].

[215] J. Böhm, A. Georgoudis, K. J. Larsen, M. Schulze, and Y. Zhang, "Complete sets of logarithmic vector fields for integration-by-parts identities of Feynman integrals," *Phys. Rev. D* **98** no. 2, (2018) 025023, arXiv:1712.09737 [hep-th].

[216] J. Boehm, D. Bendle, W. Decker, A. Georgoudis, F.-J. Pfreundt, M. Rahn, and Y. Zhang, "Module Intersection for the Integration-by-Parts Reduction of Multi-Loop Feynman Integrals," *PoS* **MA2019** (2022) 004, arXiv:2010.06895 [hep-th].

[217] A. V. Kotikov, "Differential equations method: New technique for massive Feynman diagrams calculation," *Phys. Lett. B* **254** (1991) 158–164.

[218] A. V. Kotikov, "Differential equation method: The Calculation of N point Feynman diagrams," *Phys. Lett. B* **267** (1991) 123–127. [Erratum: Phys.Lett.B 295, 409–409 (1992)].

[219] A. V. Kotikov, "Differential equations method: The Calculation of vertex type Feynman diagrams," *Phys. Lett. B* **259** (1991) 314–322.

[220] E. Remiddi, "Differential equations for Feynman graph amplitudes," *Nuovo Cim. A* **110** (1997) 1435–1452, arXiv:hep-th/9711188.

[221] C. G. Papadopoulos, "Simplified differential equations approach for Master Integrals," *JHEP* **07** (2014) 088, arXiv:1401.6057 [hep-ph].

[222] T. Gehrmann and E. Remiddi, "Two loop master integrals for gamma* —> 3 jets: The Planar topologies," *Nucl. Phys. B* **601** (2001) 248–286, arXiv:hep-ph/0008287.

[223] S. Di Vita, T. Gehrmann, S. Laporta, P. Mastrolia, A. Primo, and U. Schubert, "Master integrals for the NNLO virtual corrections to $q\bar{q} \rightarrow t\bar{t}$ scattering in QCD: the non-planar graphs," *JHEP* **06** (2019) 117, arXiv:1904.10964 [hep-ph].

[224] D. Chicherin, T. Gehrmann, J. M. Henn, N. A. Lo Presti, V. Mitev, and P. Wasser, "Analytic result for the nonplanar hexa-box integrals," *JHEP* **03** (2019) 042, arXiv:1809.06240 [hep-ph].

[225] S. Abreu, H. Ita, F. Moriello, B. Page, W. Tschernow, and M. Zeng, "Two-Loop Integrals for Planar Five-Point One-Mass Processes," *JHEP* **11** (2020) 117, arXiv:2005.04195 [hep-ph].

[226] R. N. Lee, "Modern techniques of multiloop calculations," in *49th Rencontres de Moriond on QCD and High Energy Interactions*, pp. 297–300. 2014. `arXiv:1405.5616 [hep-ph]`.

[227] J. M. Henn, "Multiloop integrals in dimensional regularization made simple," *Phys. Rev. Lett.* **110** (2013) 251601, `arXiv:1304.1806 [hep-th]`.

[228] A. B. Goncharov, "Multiple polylogarithms, cyclotomy and modular complexes," *Math. Res. Lett.* **5** (1998) 497–516, `arXiv:1105.2076 [math.AG]`.

[229] A. B. Goncharov, M. Spradlin, C. Vergu, and A. Volovich, "Classical Polylogarithms for Amplitudes and Wilson Loops," *Phys. Rev. Lett.* **105** (2010) 151605, `arXiv:1006.5703 [hep-th]`.

[230] M. Besier, D. Van Straten, and S. Weinzierl, "Rationalizing roots: an algorithmic approach," *Commun. Num. Theor. Phys.* **13** (2019) 253–297, `arXiv:1809.10983 [hep-th]`.

[231] M. Besier, P. Wasser, and S. Weinzierl, "RationalizeRoots: Software Package for the Rationalization of Square Roots," *Comput. Phys. Commun.* **253** (2020) 107197, `arXiv:1910.13251 [cs.MS]`.

[232] S. Abreu, H. Ita, B. Page, and W. Tschernow, "Two-loop hexa-box integrals for non-planar five-point one-mass processes," *JHEP* **03** (2022) 182, `arXiv:2107.14180 [hep-ph]`.

[233] N. Arkani-Hamed, J. L. Bourjaily, F. Cachazo, and J. Trnka, "Local Integrals for Planar Scattering Amplitudes," *JHEP* **06** (2012) 125, `arXiv:1012.6032 [hep-th]`.

[234] M. Argeri, S. Di Vita, P. Mastrolia, E. Mirabella, J. Schlenk, U. Schubert, and L. Tancredi, "Magnus and Dyson Series for Master Integrals," *JHEP* **03** (2014) 082, `arXiv:1401.2979 [hep-ph]`.

[235] T. Gehrmann, A. von Manteuffel, L. Tancredi, and E. Weihs, "The two-loop master integrals for $q\bar{q} \rightarrow VV$," *JHEP* **06** (2014) 032, `arXiv:1404.4853 [hep-ph]`.

[236] M. Prausa, "epsilon: A tool to find a canonical basis of master integrals," *Comput. Phys. Commun.* **219** (2017) 361–376, `arXiv:1701.00725 [hep-ph]`.

[237] O. Gituliar and V. Magerya, "Fuchsia: a tool for reducing differential equations for Feynman master integrals to epsilon form," *Comput. Phys. Commun.* **219** (2017) 329–338, `arXiv:1701.04269 [hep-ph]`.

[238] R. N. Lee, "Libra: A package for transformation of differential systems for multiloop integrals," *Comput. Phys. Commun.* **267** (2021) 108058, `arXiv:2012.00279 [hep-ph]`.

[239] C. Meyer, "Algorithmic transformation of multi-loop master integrals to a canonical basis with CANONICA," *Comput. Phys. Commun.* **222** (2018) 295–312, `arXiv:1705.06252 [hep-ph]`.

[240] C. Dlapa, J. Henn, and K. Yan, "Deriving canonical differential equations for Feynman integrals from a single uniform weight integral," *JHEP* **05** (2020) 025, `arXiv:2002.02340 [hep-ph]`.

[241] J. Henn, B. Mistlberger, V. A. Smirnov, and P. Wasser, "Constructing d-log integrands and computing master integrals for three-loop four-particle scattering," *JHEP* **04** (2020) 167, `arXiv:2002.09492 [hep-ph]`.

[242] D. Chicherin, T. Gehrmann, J. M. Henn, P. Wasser, Y. Zhang, and S. Zoia, "All Master Integrals for Three-Jet Production at Next-to-Next-to-Leading Order," *Phys. Rev. Lett.* **123** no. 4, (2019) 041603, `arXiv:1812.11160 [hep-ph]`.

[243] C. Dlapa, X. Li, and Y. Zhang, "Leading singularities in Baikov representation and Feynman integrals with uniform transcendental weight," *JHEP* **07** (2021) 227, `arXiv:2103.04638 [hep-th]`.

[244] Z. Bern, E. Herrmann, S. Litsey, J. Stankowicz, and J. Trnka, "Logarithmic Singularities and Maximally Supersymmetric Amplitudes," *JHEP* **06** (2015) 202, `arXiv:1412.8584 [hep-th]`.

[245] P. Wasser, *Analytic properties of Feynman integrals for scattering amplitudes*. PhD thesis, Mainz U., 2018.

[246] J. Chen, X. Jiang, X. Xu, and L. L. Yang, "Constructing canonical Feynman integrals with intersection theory," *Phys. Lett. B* **814** (2021) 136085, `arXiv:2008.03045 [hep-th]`.

[247] J. Chen, X. Jiang, C. Ma, X. Xu, and L. L. Yang, "Baikov representations, intersection theory, and canonical Feynman integrals," *JHEP* **07** (2022) 066, `arXiv:2202.08127 [hep-th]`.

[248] F. Moriello, "Generalised power series expansions for the elliptic planar families of Higgs + jet production at two loops," *JHEP* **01** (2020) 150, `arXiv:1907.13234 [hep-ph]`.

[249] M. Hidding, "DiffExp, a Mathematica package for computing Feynman integrals in terms of one-dimensional series expansions," *Comput. Phys. Commun.* **269** (2021) 108125, `arXiv:2006.05510 [hep-ph]`.

[250] T. Armadillo, R. Bonciani, S. Devoto, N. Rana, and A. Vicini, "Evaluation of Feynman integrals with arbitrary complex masses via series expansions," *Comput. Phys. Commun.* **282** (2023) 108545, `arXiv:2205.03345 [hep-ph]`.

[251] X. Liu, Y.-Q. Ma, and C.-Y. Wang, "A Systematic and Efficient Method to Compute Multi-loop Master Integrals," *Phys. Lett. B* **779** (2018) 353–357, `arXiv:1711.09572 [hep-ph]`.

[252] X. Liu and Y.-Q. Ma, "Multiloop corrections for collider processes using auxiliary mass flow," *Phys. Rev. D* **105** no. 5, (2022) L051503, `arXiv:2107.01864 [hep-ph]`.

[253] Z.-F. Liu and Y.-Q. Ma, "Determining Feynman Integrals with Only Input from Linear Algebra," *Phys. Rev. Lett.* **129** no. 22, (2022) 222001, `arXiv:2201.11637 [hep-ph]`.

[254] X. Liu and Y.-Q. Ma, "AMFlow: A Mathematica package for Feynman integrals computation via auxiliary mass flow," *Comput. Phys. Commun.* **283** (2023) 108565, `arXiv:2201.11669 [hep-ph]`.

[255] M. Caffo, H. Czyz, M. Gunia, and E. Remiddi, "BOKASUN: A Fast and precise numerical program to calculate the Master Integrals of the two-loop sunrise diagrams," *Comput. Phys. Commun.* **180** (2009) 427–430, `arXiv:0807.1959 [hep-ph]`.

[256] M. Czakon, "Tops from Light Quarks: Full Mass Dependence at Two-Loops in QCD," *Phys. Lett. B* **664** (2008) 307–314, `arXiv:0803.1400 [hep-ph]`.

[257] J. Vollinga and S. Weinzierl, "Numerical evaluation of multiple polylogarithms," *Comput. Phys. Commun.* **167** (2005) 177, `arXiv:hep-ph/0410259`.

[258] H. Frellesvig, D. Tommasini, and C. Wever, "On the reduction of generalized polylogarithms to Li_n and $Li_{2,2}$ and on the evaluation thereof," *JHEP* **03** (2016) 189, `arXiv:1601.02649 [hep-ph]`.

[259] C. Duhr, H. Gangl, and J. R. Rhodes, "From polygons and symbols to polylogarithmic functions," *JHEP* **10** (2012) 075, `arXiv:1110.0458 [math-ph]`.

[260] C. Duhr, "Hopf algebras, coproducts and symbols: an application to Higgs boson amplitudes," *JHEP* **08** (2012) 043, `arXiv:1203.0454 [hep-ph]`.

[261] C. W. Bauer, A. Frink, and R. Kreckel, "Introduction to the GiNaC framework for symbolic computation within the C++ programming language," *J. Symb. Comput.* **33** (2002) 1–12, `arXiv:cs/0004015`.

[262] L. Naterop, A. Signer, and Y. Ulrich, "handyG —Rapid numerical evaluation of generalised polylogarithms in Fortran," *Comput. Phys. Commun.* **253** (2020) 107165, `arXiv:1909.01656 [hep-ph]`.

[263] C. Duhr and F. Dulat, "PolyLogTools — polylogs for the masses," *JHEP* **08** (2019) 135, `arXiv:1904.07279 [hep-th]`.

[264] J. L. Bourjaily *et al.*, "Functions Beyond Multiple Polylogarithms for Precision Collider Physics," in *Snowmass 2021*. 3, 2022. `arXiv:2203.07088 [hep-ph]`.

[265] C. G. Papadopoulos, D. Tommasini, and C. Wever, "Two-loop Master Integrals with the Simplified Differential Equations approach," *JHEP* **01** (2015) 072, `arXiv:1409.6114 [hep-ph]`.

[266] C. G. Papadopoulos, D. Tommasini, and C. Wever, "The Pentabox Master Integrals with the Simplified Differential Equations approach," *JHEP* **04** (2016) 078, `arXiv:1511.09404 [hep-ph]`.

[267] N. Syrrakos, "One-loop Feynman integrals for $2 \to 3$ scattering involving many scales including internal masses," *JHEP* **10** (2021) 041, `arXiv:2107.02106 [hep-ph]`.

[268] A. Kardos, C. G. Papadopoulos, A. V. Smirnov, N. Syrrakos, and C. Wever, "Two-loop non-planar hexa-box integrals with one massive leg," *JHEP* **05** (2022) 033, `arXiv:2201.07509 [hep-ph]`.

[269] V. A. Smirnov, "Analytical result for dimensionally regularized massless on shell planar triple box," *Phys. Lett. B* **567** (2003) 193–199, `arXiv:hep-ph/0305142`.

[270] J. M. Henn, A. V. Smirnov, and V. A. Smirnov, "Analytic results for planar three-loop four-point integrals from a Knizhnik-Zamolodchikov equation," *JHEP* **07** (2013) 128, `arXiv:1306.2799 [hep-th]`.

[271] J. M. Henn, A. V. Smirnov, and V. A. Smirnov, "Evaluating single-scale and/or non-planar diagrams by differential equations," *JHEP* **03** (2014) 088, `arXiv:1312.2588 [hep-th]`.

[272] S. Di Vita, P. Mastrolia, U. Schubert, and V. Yundin, "Three-loop master integrals for ladder-box diagrams with one massive leg," *JHEP* **09** (2014) 148, `arXiv:1408.3107 [hep-ph]`.

[273] L. J. Dixon, A. J. McLeod, and M. Wilhelm, "A Three-Point Form Factor Through Five Loops," *JHEP* **04** (2021) 147, `arXiv:2012.12286 [hep-th]`.

[274] D. Chicherin, J. M. Henn, and G. Papathanasiou, "Cluster algebras for Feynman integrals," *Phys. Rev. Lett.* **126** no. 9, (2021) 091603, `arXiv:2012.12285 [hep-th]`.

[275] J. M. Henn, J. Lim, and W. J. Torres Bobadilla, "First look at the evaluation of three-loop non-planar Feynman diagrams for Higgs plus jet production," *JHEP* **05** (2023) 026, `arXiv:2302.12776 [hep-th]`.

[276] J. M. Henn, K. Melnikov, and V. A. Smirnov, "Two-loop planar master integrals for the production of off-shell vector bosons in hadron collisions," *JHEP* **05** (2014) 090, `arXiv:1402.7078 [hep-ph]`.

[277] F. Dulat and B. Mistlberger, "Real-Virtual-Virtual contributions to the inclusive Higgs cross section at N3LO," `arXiv:1411.3586 [hep-ph]`.

[278] P. Mastrolia, M. Passera, A. Primo, and U. Schubert, "Master integrals for the NNLO virtual corrections to μe scattering in QED: the planar graphs," *JHEP* **11** (2017) 198, `arXiv:1709.07435 [hep-ph]`.

[279] A. V. Smirnov, "FIESTA4: Optimized Feynman integral calculations with GPU support," *Comput. Phys. Commun.* **204** (2016) 189–199, `arXiv:1511.03614 [hep-ph]`.

[280] H. Ferguson and D. Bailey, "A polynomial time, numerically stable integer relation algorithm," *Math. Comp.* **68** (1999) 351.